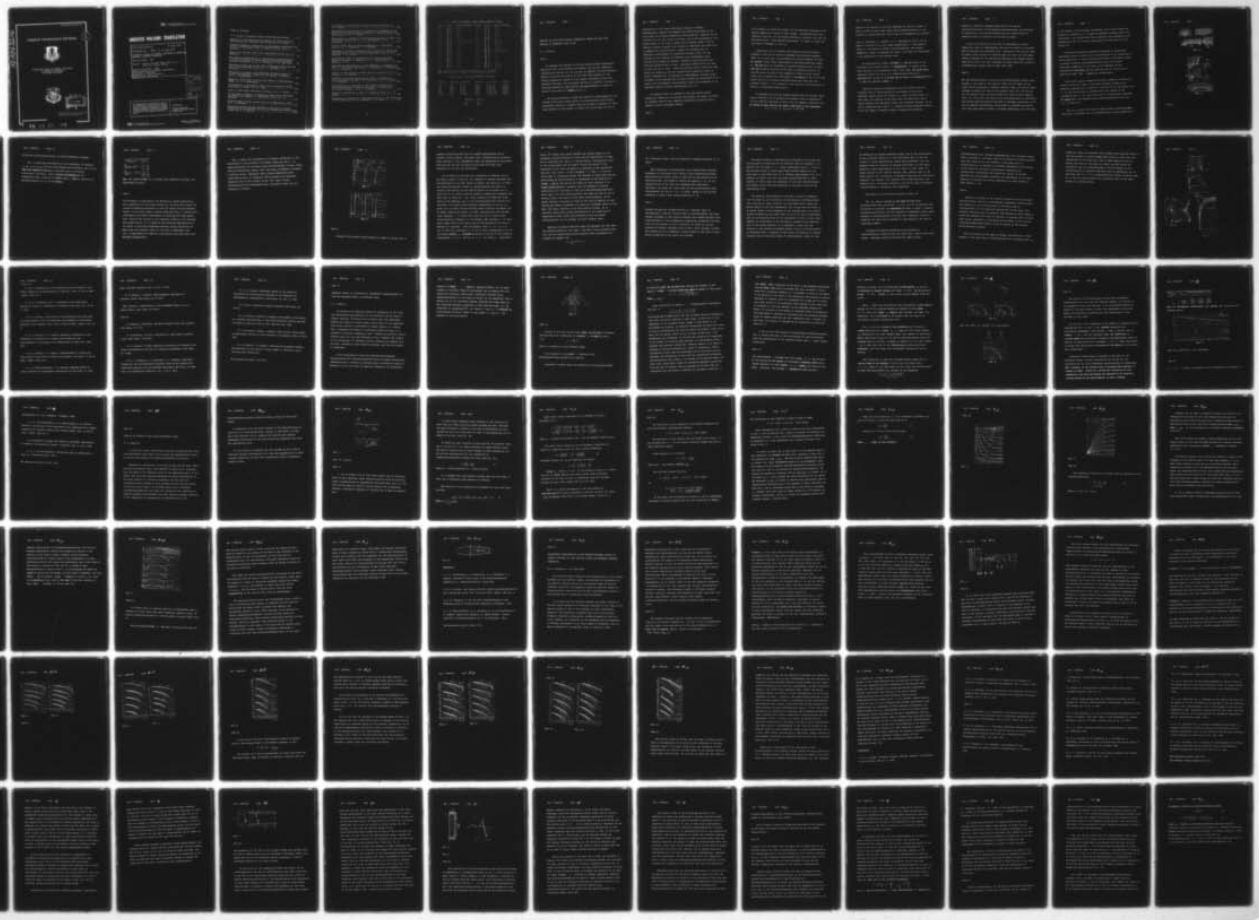
AD-A067 216 FOREIGN TECHNOLOGY DIV WRIGHT-PATTERSON AFB OHIO F/G 20/4
SCIENTIFIC NOTES OF CENTRAL INSTITUTE OF AEROHYDRO DYNAMICS (SE--ETC(U)
JUN 78 A S FONAREV, A G ZAKHAROV

UNCLASSIFIED FTD-ID(RS)T-0679-78 NL

1 OF 5
AD A067216



AD-A062216

FTD-ID(RS)T-0679-78

1

FOREIGN TECHNOLOGY DIVISION

SCIENTIFIC NOTES OF CENTRAL INSTITUTE
OF AEROHYDRO DYNAMICS
(SELECTED ARTICLES)

DDC
RECEIVED
9 APR 1979
E

Approved for public release;
distribution unlimited.

78 12 22 179

UNEDITED MACHINE TRANSLATION

FTD-ID(RS)T-0679-78 21 June 1978

MICROFICHE NR: FTD-78-C-000839

SCIENTIFIC NOTES OF CENTRAL INSTITUTE OF AEROHYDRO DYNAMICS (SELECTED ARTICLES)

English pages: 383

Source: Uchenye Zapiski Tsagi, vol 4, no. 3, 1973, pp. 1-100; 105-158

Country of Origin: USSR

This document is a machine translation.

Requester: FTD/TQTA

Approved for public release; distribution unlimited.

ACCESSION for
NTIS White Section X
DDC Buff Section
UNANNOUNCED
JUSTIFICATION
BY
DISTRIBUTION/AVAILABILITY CODES
Dist. AVAIL. and/or SPECIAL
A

THIS TRANSLATION IS A RENDITION OF THE ORIGINAL FOREIGN TEXT WITHOUT ANY ANALYTICAL OR EDITORIAL COMMENT. STATEMENTS OR THEORIES ADVOCATED OR IMPLIED ARE THOSE OF THE SOURCE AND DO NOT NECESSARILY REFLECT THE POSITION OR OPINION OF THE FOREIGN TECHNOLOGY DIVISION.

PREPARED BY:

TRANSLATION DIVISION
FOREIGN TECHNOLOGY DIVISION
WP-AFB, OHIO.

Table of Contents

U. S. Board on Geographic Names Transliteration System iii

Analysis of Flow About Axially Symmetrical Bodies and Lift Wing Profiles By Transonic Flow of Gas, by A.S. Fonarev 1

Numerical Method of Calculation of Aerodynamic Characteristics of Flat and Nonplanar Wings in Supersonic Flow, by A. G. Zakharov 27

Flow of Gas Through a Wall with Longitudinal Slots, by M. P. Ryabokon'. 39

Experimental Determination of the Pressure Recovery Factors in Conical Diffusers at High Subsonic Speeds and Different Entrance Conditions, by Ya. L. Ginsburg, I. Ye. Idel'chik... 57

Analysis of Slow Ions of the Flow of Rarefied Plasma with the Aid of Multielectrode Probe, by L. V. Nosachev, V. V. Skvortsov 78

Estimation of Change of the Amplitude of Oscillations in a Linear Time-Dependent System with One Degree of Freedom, by V. A. Yaroshevskiy 99

Method of Calculation of the Elastic Waves in Heterogeneous Beams, by I. A. Lyakhovenko..... 120

The Stability of Cylindrical Shell During Compression Under Conditions of Creep, by G. N. Zamul 144

Bulge of Rods Under Conditions of Creep, by V. P. Galkin.... 157

On the Shape of Bodies, in Supersonic Flow Having Resistance and Moment with Respect to Longitudinal Axis, by G. I. Maykapar 173

Some Problems of Plane Vortex Flows of Incompressible Fluid, by V. S. Sadovskiy 176

Temperature Field and Heat Transfer in the Flow of Viscous Incompressible Gas Between Two Parallel Harmonically Oscillating Plates, by Ye. M. Zhmulin 194

One Method of Calculation of Flow in Circular Bearing, by E. N. Sarmin 218

Experimental Investigation of the Effect of Re Number on the Nature of Flow Around Axially Symmetrical Bodies Indented in Nose Section, by V. I. Shustov 239

Application of a Method of Instantaneous Freezing in Flows with Vibrational Relaxation, by V. L. Men'shikova, O. Yu. Polyanskiy 254

Climb of Shock Wave on Wedge Streamlined by a Supersonic Flow, by Yu. F. Makovskiy, F. V. Shygayev 265

Breakaway of Turbulent Boundary Layer During its Interaction with Shock Wave in an Accelerated Supersonic Flow, by A. I. Tolmanov, V. V. Filatov 272

Experimental Study of Axisymmetrically Shaped Supersonic Nozzles with Small re Numbers, by L. I. Kudryavtseva, I.I. Mezhirov, et al 285

Experimental Determination of the Dependence of Intensity of Flow in a Molecular Wind Tunnel on Temperature of Stagnation, by I. D. Vershinin 296

Control of Soft Landing of Space Vehicle on Planet, by E. V. Gaushus, S. N. Maksimov 306

Automatic Device For Measuring the Force of Adhesion of Contacting Heated Solids at Low Pressures, by A. N. Petunin, A. L. Stasenko 322

Derivation of the Equations of the Method of Forces For a Plate Reinforced by a Beam on the Basis of Castigliano's Variation Principle, by Yu. F. Yaremchuk 332

Rational Distribution of Ribs in a Monocoque Wing, by V. N. Semenov 345

Experience in Simulation of Auto-Oscillations of Tall Structures in Wind Tunnels, by A. N. Lugovtsov, G. M. Fomin 363

U. S. BOARD ON GEOGRAPHIC NAMES TRANSLITERATION SYSTEM

Block	Italic	Transliteration	Block	Italic	Transliteration
А а	*А а*	A, a	Р р	*Р р*	R, r
Б б	*Б б*	B, b	С с	*С с*	S, s
В в	*В в*	V, v	Т т	*Т т*	T, t
Г г	*Г г*	G, g	У у	*У у*	U, u
Д д	*Д д*	D, d	Ф ф	*Ф ф*	F, f
Е е	*Е е*	Ye, ye; E, e*	Х х	*Х х*	Kh, kh
Ж ж	*Ж ж*	Zh, zh	Ц ц	*Ц ц*	Ts, ts
З з	*З з*	Z, z	Ч ч	*Ч ч*	Ch, ch
И и	*И и*	I, i	Ш ш	*Ш ш*	Sh, sh
Й й	*Й й*	Y, y	Щ щ	*Щ щ*	Shch, shch
К к	*К к*	K, k	Ъ ъ	*Ъ ъ*	"
Л л	*Л л*	L, l	Ы ы	*Ы ы*	Y, y
М м	*М м*	M, m	Ь ь	*Ь ь*	'
Н н	*Н н*	N, n	Э э	*Э э*	E, e
О о	*О о*	O, o	Ю ю	*Ю ю*	Yu, yu
П п	*П п*	P, p	Я я	*Я я*	Ya, ya

*ye initially, after vowels, and after ъ, ь; e elsewhere.
When written as ё in Russian, transliterate as yё or ё.

RUSSIAN AND ENGLISH TRIGONOMETRIC FUNCTIONS

Russian	English	Russian	English	Russian	English
sin	sin	sh	sinh	arc sh	$\sinh^{-1}$
cos	cos	ch	cosh	arc ch	$\cosh^{-1}$
tg	tan	th	tanh	arc th	$\tanh^{-1}$
ctg	cot	cth	coth	arc cth	$\coth^{-1}$
sec	sec	sch	sech	arc sch	sech^{-1}
cosec	csc	csch	csch	arc csch	csch^{-1}

Russian	English
rot	curl
lg	log

ANALYSIS OF FLOW ABOUT AXIALLY SYMMETRICAL BODIES AND LIFT WING PROFILES BY TRANSONIC FLOW OF GAS.

A. S. Ponarev.

Page 1.

Is examined the problem of the flow around axially symmetrical bodies and lift wing profiles by transonic flow of gas, numerical solutions are carried out with the use of Godunov's finite-difference method. Are given the results of the flow-field analysis of the axially symmetrical bodies of some classes (cylindrical body with spherical blunting, the flat/plane end/face of cylinder), and also of two airfoil/profiles (NACA 64A-410 and spade-shaped) at angles of attack in the range of numbers $M_\infty = 0,7 \div 1,3$.

The application/use of numerical methods of establishment to the problem of the flow around Krylov of airfoil/profiles and axially symmetrical bodies by transonic flow of gas made it possible to solve some problems in this region. In works [1] and [2] with the use of

modification of the finite-difference diagram of Babenko, Voskresenskiy, Lyubimov and Rusanov are solved the problem of the flow around the pointed symmetrical airfoil/profile, comprised of the circular arcs (at zero angle of attack), and of the axisymmetric flow around bodies of the type of sphere and ellipsoid. Works [3-5] by Godunov's method, examines the problem of diffracting the shock wave on symmetrical airfoil/profile, sphere and cylinder with the subsequent establishment of stationary transonic flow. For the solution of the problems of transonic flow, successfully were utilized other numerical methods - method of large particles and different modifications of Lakh - Vendrova's method [6-8]. In work [9] with the use of Lakh - Vendrova's method, was for the first time solved the problem of the flow around curved profile at angle of attack. Together with the methods of establishment, recently began intensely to be developed the iterative methods of calculation of the steady flow of transonic airfoil/profile within the framework of the potential theory of slight disturbances [10, 11].

Is examined below the problem of the flow around axially symmetrical bodies and of carrying wing profile (at angle of attack) by transonic flow of gas, numerical solutions are carried out by Godunov's finite-difference method.

As an example are given the results of the flow-field analyses of the axially symmetrical bodies of some classes - cylindrical body with spherical blunting, the flat/plane end/face of cylinder, and also two airfoil/profiles - NACA 64A-410 and pointed - at angle of attack in the range of numbers $M_\infty = 0,7 \div 1,3$.

Formulation of the problem. The solution of the stationary problem of flow let us obtain as maximum from following unsteady task. Let at zero time the motionless body begin suddenly to travel at constant speed, which corresponds to assigned/prescribed number M_∞. The beginning of rectangular coordinate system xy let us place into the leading edge/nose of the body in question, x-axis it is directed along the axis of the symmetry of body or along airfoil chord. Let us examine the flat/plane or axisymmetric case of the flow around body of the inviscid non-heat-conducting ideal gas with adiabatic index $\gamma = 1.4$, relative to the form of the duct/contour of body of no limitations make let us.

In unsteady flow and the maximum steady flow, are present shock waves; therefore let us proceed from integral laws of conservation for the unsteady equations of Euler [12]. As boundary conditions let us assign on body surface the normal conditions of the nonpassage:

$$p = p_\infty, \quad \rho = \rho_\infty, \quad u = M_\infty a_\infty \cos\alpha, \quad v = M_\infty a_\infty \sin\alpha.$$

normal to the surface of the body component of vector of speed is equal to zero. At zero time (since motion begins suddenly) in all incident to airfoil/profile flow of gas, the parameters are constant:

Here p - pressure, ρ - density, u, v - component of vector of the speed in direction of x and y axes respectively, a - the speed of sound, α - the angle of attack of airfoil/profile (for axially symmetrical bodies is examined the case $\alpha = 0$); index "∞" corresponds to the parameters of the incident flow.

As characteristic linear dimension l_0 let us accept in the flat/plane case airfoil chord, in axisymmetric - a radius of the cross section of the cylindrical part of the body. The given below numerical results are given in a dimensionless form, as p_∞, characteristic values are accepted the parameters of undisturbed flow ρ_∞ and the reference length l_0.

Method of numerical calculation. The flow around bodies of transonic flow is characterized by the presence of the local supersonic zones, which are closed, as a rule, by shock waves. In this case, the position of the sonic line and shock wave, which divide subsonic and supersonic areas, are previously unknown. Let us use in connection with this S. K. Godunov's finite-difference method [12], that makes it possible singly to examine the subsonic,

supersonic and mixed unsteady flows without the special isolation/liberation of nonremovable discontinuities; an experiment in calculation [3-5] already demonstrated its effectiveness in connection with the solution of this type of tasks.

Since no limitations on the form of flat/plane or axially symmetrical body are superimposed, then for the solution of problem must be utilized the calculated grid, versatile to the various forms of bodies. Were utilized the diverse types of grids. For the simple bodies, described by one significant dimension, for example sphere, cube and so forth, the grid consisted of radial lines and concentric circumferences, squares and so forth (Fig. 1a).

Page 3.

For the extended bodies of the type of airfoil/profile (during small changes in the angle of the slope of body) one the family of the lines of grid consisted of parallel vertical lines, the second family repeated as before the form of duct/contour (Fig. 1b). And finally for the bodies of more intricate shape grid could be that combined (Fig. 1c). As a rule, the value of the transverse pitch of calculated grid during removal/distance from body it increases (according to the law of geometric progression), which makes it possible last/latter line (the outer edge of field) to arrange sufficiently far from body,

in the region of the virtually undisturbed flow so that during the solution of problem on it it would be possible to assign either the conditions of the undisturbed flow or equality zero gradients of all parameters of gas in direction from body along the lines of first family [3].

The finite-difference calculation procedure is constructed analogously given in work [12]; the calculation of the parameters of the decomposition of discontinuity/interruption is performed either on precise iterative relationship/ratios [13], or on those linearized, depending on the value of the gradients of the corresponding functions, in this case the type of calculation is selected by EVM [ЭВМ - computer] automatically.

Flow around axially symmetrical bodies. Numerical solution was carried out for two types of the finite bodies: cylinder with spherical blunting with a radius of 1 (length of the cylindrical part L = 3) and the end/face of cylinder with flat (length of the cylindrical part L = 4). The rear portion of both bodies represents by itself flat. Are examined three conditions/modes of the flow: $M_\infty = 0.8$; 1.0; 1.3.

Fig. 2a, b, shows the lines of equal values of pressure about the bodies in question (it is illustrated only the case when $M_\infty = 1$),

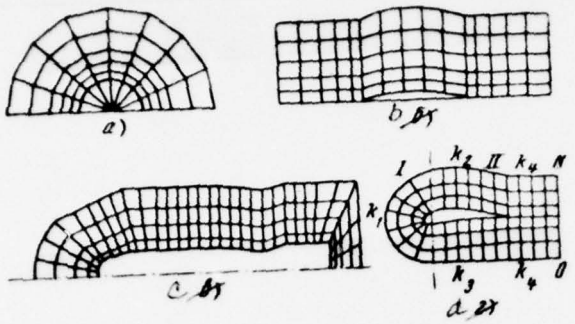


Fig. 1.

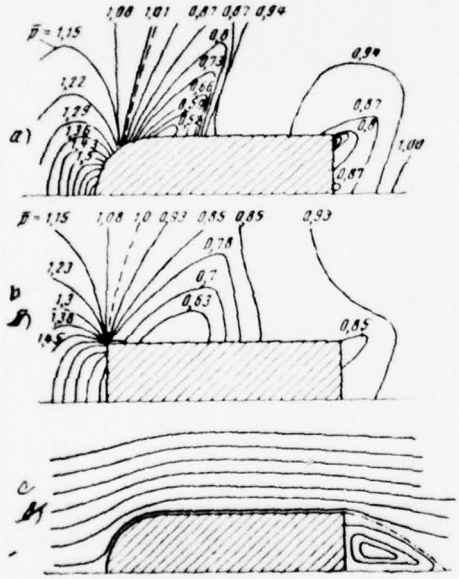


Fig. 2.

Pressure is referred to the static pressure the undisturbed flow. One can see well, as proceeds the acceleration/dispersal of flow from stagnant conditions at critical point before the formation of supersonic region (the sonic line of designation by dotted line) with the emergence of shock wave., in the case of the flow around the end/face of cylinder, the abrupt deceleration of a flow (of type of jump) occurs immediately after expansion at point of inflection, further braking of flow occurs sufficiently smoothly (this one can see well in Fig. 4).

In all examined cases in the rear portion of the bodies after section/shear, is formed the region of recurrent flow. The typical pattern of lines of current is given to Fig. 2c ($M_\infty = 1$). Dot-dash line divides the main flow and the zone of recurrent flow.

Let us make several observations relative to the formation/education of the zones of recurrent flow during the numerical solution of the equations of Euler.

These zones are sufficiently stable and appear independent of the method of the establishment of flow (for example, in the case of acceleration/dispersal with acceleration, during the diffraction of shock wave with the subsequent establishment of flow). The zones of recurrent flow are observed in the case of applying other numerical

methods, for example the method of "large particles" [6]. An experiment in the calculation showed that they are formed in the supersonic and mixed flows (where there are gradients of entropy); in purely subsonic potential flow is realized the nonseparated flow. As a rule, the accuracy/precision of parameter determination in the zones of recurrent flow it is substantially lower than in the main flow; usually with the accuracy/precision of solution in main flow 1-2o/o in the zones of recurrent flow, the error in the value of Bernoulli's constant reaches 5-10o/o.

These zones are qualitatively similar to real separation zones in bottom regions, their value depends on the flow parameters. So, for the bodies in question it was reveal/detected that they increase with an increase in number M_∞. Table gives corrected values of distance along the axis x from bottom section/shear to separation point of flows (in the portions of a radius of the cylindrical part of the body). From these data it follows that the form of the nose section of the bolies in question does not in practice affect the size/dimensions of the zone of recurrent flow.

The formation/education of the zones of recurrent flow during the numerical solution of the equations of Euler represents by itself the recently discovered, generally speaking, paradoxical phenomenon which usually link with the presence of artificial, or circuit, the

ductility/toughness/viscosities in finite-difference diagrams.

Fig. 3, shows the distribution of the coefficient of pressure $\bar{p}=(p-p_\infty)\Big/\frac{1}{2}\gamma M_\infty p_\infty$ in the front/leading and cylindrical part of the body with spherical blunting; along the axis x, is plottel longitudinal coordinate. Small circles plotted/applied the experimental data, obtained in TsAGI [ЦАГИ, - Central Institute of Aerohydrodynamics im. N. Ye Zhukovskiy.

(1) Форма тела	M_∞	Δx
(2) Цилиндр со сферическим затуплением	0,8	1,35
	1,0	1,53
	1,3	1,80
(3) Цилиндр с плоским торцом	0,8	1,41
	0,95	1,56
	1,3	1,80

Key: (1). Form of body. (2). Cylinder with spherical blunting. (3). Flat-topped cylinder.

Page 5.

The agreement of experimental and theoretical values sufficiently good, especially in the forward section of the body where occurs the intense acceleration/dispersal of flow and appear large aerodynamic forces. In the shock region, closing supersonic zone, is observed the sufficiently noticeable disagreement of numerical and experimental data, noted by the authors of all numerical studies of the transonic flow around bodies. It is caused by the essential manifestation of the effect of ductility/toughness/viscosity during interaction of shock wave with boundary layer. In the case of supersonic flow ($M_\infty = 1,3$) the results of numerical calculations will agree well with the data of experiment.

Fig. 4, shows the distribution of pressure coefficient in the duct/contour of the end/face of cylinder, along the axis x - is deposit/postponed the distance along the duct/contour of body. Curves take the sufficiently complex form. The peaks of pressure correspond to salient points. Supersonic region begins immediately after front/leading point of inflection after powerful flow expansion (expansion fan is well visible in Fig. 2b). Small circles plotted/applied the experimental data, obtained in TsAGI for the end/face of cylinier.



Fig. 3.



Fig. 4.

Transonic flow around airfoil/profile at angle of attack. Let us

examine airfoil/profiles from the rounded front/leading and by pointed trailing spaces. Calculated grid, retaining the in principle basic features of the axisymmetric case, has peculiarities associated with the need for the calculation both upper and lower half; therefore let us give its description.

Let us break all the field of calculation by vertical line on two parts: region I (see Fig. 1d), adjacent to leading edge/nose and characterizing by the high values of camber, and region II, in which the slope/inclinations forming of airfoil/profile are small. In region I duct/contour of the airfoil/profile let us break into k_1 parts and let us conduct from the points of separation ray/beams with even pitch on angle $\Delta\theta = \pi/k_1$. After breaking the upper and lower sides of the remaining part of the airfoil/profile and certain axis intercept x of bahind airfoil/profile respectively to k_2, k_3, k_4 parts, let us buckle through dividing points vertical ray/beams. Let us number them (first family of lines), beginning with the extreme right ray/beam n = 0, going down along the axis x, going around airfoil/profile clockwise, to the extreme right ray/beam n = N, which exits upward from x-axis (each point of the separation of x-axis it emerges two ray/beams - down and upward). Thus, $N = k_1 + k_2 + k_3 + 2k_4$. On the first ray/beam (n = 0) let us plot consecutively M of the cuts whose lengths l_m increase according to the law of the geometric progression: $l_m = l_{m-1}q$ (m = 2, 3, 4, ..., M), where q - progression

ratio. The broken line, which connects the initial points of all ray/beams, arranged/located on x-axis and the duct/contour of body, let us call/name zero line m = 0 second family. The remaining lines of the second family let us conduct through the points of the separation of the first ray/beam of in parallel to the appropriate cuts zero line. Line m = M and ray/beams n = 0 and n = N are the outer edges of calculated region. The distance of outer edge from the duct/contour of airfoil/profile is determined by the selection of values l_1 and q, and also by the length of axis intercept it is behind airfoil/profile. Assuming that the boundary is located sufficiently far from body, so that the disturbance/perturbations, which came to it from airfoil/profile, are small and they do not in practice affect the field of flow about airfoil/profile, let us assign boundary conditions of field in the form of equality to zero derived gas-dynamic parameters [3] along the ray/beams, which go from body. The cells, adjacent to the duct/contour of body, let us calculate taking into account satisfaction of the conditions of nonpassage on body, while cells adjacent x-axis are behind airfoil/profile, let us consider as usual internal cells.

Employing procedure described above was designed the flow about the airfoil/profiles of two types - NACA 64A-10 with thickness ratio 10o/o and the spale-shaped airfoil/profile whose coordinates are assigned by formula [14]

$$y = \frac{9}{4\sqrt{3}} c \sqrt{\bar{x}}(1-x)$$

($\bar{c}$ - thickness ratio), with the location of maximum thickness to 1/3 chord.

When conducting of calculations, were selected the following parameters of calculated grid. Region I with alternating/variable beam direction occupied 2.5o/o of chord in the nose section of the airfoil/profile; the number of sectors was equal $k_1 = 21$. In the remaining part of the flow, the ray/beams were constructed vertically. The upper and lower parts of the airfoil/profile were divide/marked off into $k_2 = k_3 = 23$ parts. Number of cuts between ray/beams in region after airfoil/profile $k_4 = 20$.

Page 7.

Extreme ray/beam was arrange/located at a distance, equal to approximately 3 from the trailing edge of airfoil/profile, the space between ray/beams in this region increased with removal/distance from airfoil/profile in the arithmetical progression, beginning from space 0.025. On the surface of airfoil/profile, the space of grid was selected by variable (maximum value of space ~0.05, minimum ~0.0018), was provided as far as possible a smooth change in the value of space during transition of one region into another.

The second family of calculated grid consisted of 38 lines. The initial space of separation on the vertical line (on ray/beam n = 0, see Fig. 1d) was equal to l_1 = 0.002, progression ratio q = 0.18-1.2. The selected values of these quantities provided removing of the outer edge of calculated grid up to distance approximately 5-6. It is possible to expect (and this confirmed calculations) that at this location of outer edges the parameters of flow near airfoil/profile will differ little from the parameters in the case of flow of the unrestricted flow.

The powerful nonuniformity of the space of grid is connected with the need for the calculation of the regions of airfoil/profile with large and by small curvature (in accordance with a sharp and smooth change in the flow parameters). Let us note that the range of an abrupt change of the parameters in the leading edge of an airfoil profile occupies the very small part of chord (~2.5o/o), nevertheless from the accuracy/precision of the calculation of flow in this region depends the correctness of the solution of problem on the remaining part of the airfoil/profile. It is possible to count that the relation of the minimum and maximum spaces of grid on airfoil/profile is determined that in essence, by the radius of curvature of leading edge/nose and by the chord length of airfoil/profile. Space on time

is determined by minimum coordinate space, due to the nonuniformity of the coordinate spaces it in the significant part of the flow (~95o/o of chord) substantially lesser than permissible (for the examined cases the relation of maximum local space on time toward minimum is equal approximately to 25). This, in turn, leads to a sharp increase in the required machine time, several times of the which exceeds time calculation of analogous task with one significant dimension (for example, the transonic flow around cylinder). Was observed also a noticeable increase of the set-up time in transonic conditions/mode in comparison with supersonic.

The results of calculation are given to Fig. 5-7.

Fig. 5a, depicts isobars in the field of flow about airfoil/profile NACA 64A-410 at $M_\infty = 0.72$, $\alpha = 4°$. On pressure side of profile is realized the compression of flow, on upper - powerful evacuation/rarefaction with the formation of supersonic region whose boundary is plotted/applied by dotted line. Supersonic region is closed by the shock wave, presented in curve/graph in the form of thickening isobars.

Pressure distribution according to the surface of airfoil/profile is shown on Fig. 5b: solid line - data of this work, broken - numerical results from work [9], small circles

plotted/applied data, obtained experimentally [15]. Pressure curves, which correspond to the lower side of the surface of airfoil/profile, will well agree by one with another. On the upper side of airfoil/profile, is observed a noticeable difference in the results in the region of the shock configuration, especially are distinguished experimental and theoretical curves. As already mentioned that disagreement (theories and experiment) in the shock position is observed also during calculation by other methods on other bodies [1, 3].

Page 8.

During the solution of the inviscid problem of the flow around airfoil/profile, usually is superimposed Joukowski's condition about the location of rear critical point on the sharp edge of airfoil/profile. In the numerical calculations of this work, this condition specially was not assigned, nevertheless at small angles of attack was obtained flow with the location of critical point on sharp edge, which, apparently, is explained by the effect of the "circuit ductility/toughness/viscosity", which is present in the utilized finite-difference method.

With an increase in the angle of attack, the character of flow changes: on the upper side of airfoil/profile in its central part, is

formed the region of recurrent flow, similar flow described above in the rear portion of axially symmetrical bodies; in this case, the overflowing of flow from lower side to upper does not occur as before. The value of the angle of attack, by which occurs the transition from one conditions/mode of flow to another on the airfoil/profile in question, specially was not determined. Let us note only that at $\alpha = 8^\circ$ is established flow without recurrent zone, at $\alpha = 24^\circ$ this zone occupies the significant part of the upper surface of airfoil/profile.

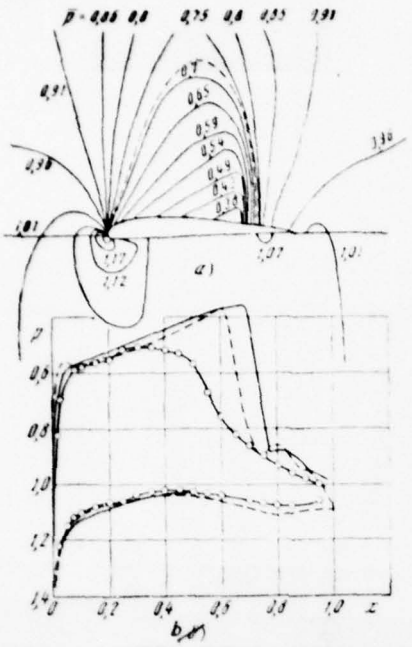


Fig. 5.

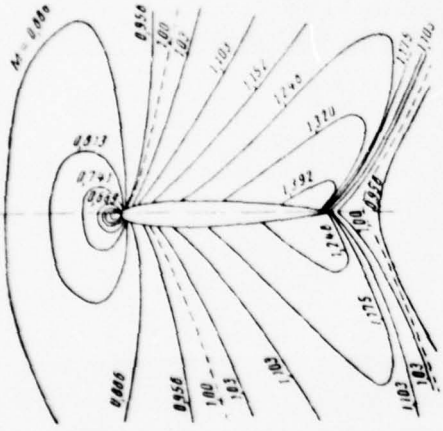


Fig. 6.

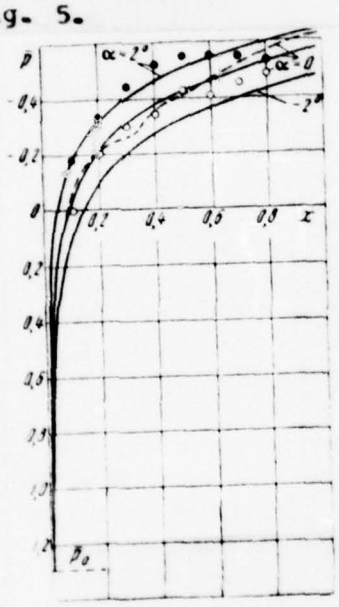


Fig. 7.

Page 9.

Let us give the results of the flow-field analyses of the described above spade-shaped airfoil/profile of thickness $\bar{c}$ = 0.1 with number $M_\infty = 1$.

This airfoil/profile is investigated in detail in work [14], where obtained approximate solution for pressure distribution taking into account ductility/toughness/viscosity by the method, analogous to the method of the local linearization of Spreiter [16]. Furthermore, for it are experimental results. Fig. 6, depicts the lines of equal values of Mach numbers at the angle of attack of the airfoil/profile α = 2°. It is evident that the acceleration/dispersal of flow from the critical point upward over the surface of airfoil/profile occurs very intensely, so that the sonic line, designated by dotted line, is arrange/located near leading edge. By virtue of symmetry of airfoil/profile and smallness of angle of attack on the lower side of airfoil/profile, the flow also is accelerate/dispersed. Shock wave, closing supersonic zone on upper and lower surfaces, is arrange/located on trailing edge, which will agree with the approximate calculated and experimental data.

Fig. 7, depicts the dependence of pressure coefficient on the longitudinal coordinate of airfoil/profile of the angle of attack, equal to zero. Are compared three curves: unbroken curve - a numerical calculation, bright small circles - the experimental data [17] for $M_\infty = 1{,}01$ and the dotted line - approximate analytical solution [14]; should note the fair agreement both of the theoretical data with each other and theoretical data with experimental.

There is shown the distribution of coefficient pressure in airfoil chord at $\alpha = 2°$ and $M_\infty = 1$. Curve with the designation $\alpha = -2°$ corresponds to lower surface. The experimental data (are noted by black small circles) are undertaken from work [17]. As can be seen from the given materials, calculated results satisfactorily will agree with experimental.

In conclusion the author expresses gratitude to V. V. Sichev and A. I. Golubinskiy for the useful discussion of the results of work into V. P. Kolgana after aid when conducting of some numerical calculations.

REFERENCES

1. Yu. B. Lifschitz. On the calculation of the transonic flow around symmetrical airfoil/profile in free jet. "Izv. of the AS USSR - MZhG", 1969, No 1.

2. Yu. M. Lipnitskiy, Yu. B. Lifschitz. On the flow-field analysis of bodies of revolution of transonic flow. PMM. Vol. 34, No 3, 1970.

3. A. S. Fonarev. Calculation of the diffraction of shock wave on airfoil/profile with the subsequent establishment of stationary supersonic and transonic flow. "Izv. of the AS USSR - MZhG", 1071, No 4.

4. A. S. Fonarev, V. P. Kolgan. Numerical calculation of the diffraction of shock wave on sphere and cylinder and the establishment of stationary flow. Transactions of TsAGI iss. 1324, 1971.

5. V. P. Kolgan, A. S. Fonarev. Establishment of steady flow with climb of shock wave to sphere and cylinder. the "publ. of the AS USSR - MZhT" ,1972, No 5.

6. O. M. Belotserkovskiy, S. M. Davidov. Unsteady method of large particles for gas-dynamic calculations by the "jour. of comp.

math. and math. physics", Vol. 11, No 1, 1971.

7. B. Crossman, G. Moretty. Time-dependent calculation of transonic flows. AIAA Paper, No 70-1322.

8. C. P. Kentzer. Computations of time dependent flows on an in finite domain. AIAA Paper, No 70-45.

Page 10.

9. R. Magnus, H. Yoshihara. Inviscid transonic flow over airfoils AIAA Paper, No 70-47.

10. E. M. Murman, J. D. Cole. Calsulation of plan steadu transonic flows. AIAA Paper, No. 70-188.

11. J. L. Steger, H. Lomax. Numerical calculation of transonic flow about two-dimensional airfoils by relaxation prosedures. AIAA Paper, No 71-669.

12. S. K. Godunov, A. V. Zabrodin, G. P. Prokopov. Difference diagram for the two-dimensional unsteady tasks of gas dynamics and flow-field analysis with the detached shock wave. The "jour. of comp. math. and mathematical physics", Vol. 1, No 6, 1961.

13. S. K. Godunov. Difference method of the numerical calculation of discontinuous solutions of the equations of hydrodynamics. "mathematical collection", 47, iss. 3, 1959.

14. R. Truit. Shockless transonic airfoils. AIAA Paper, No 70-187.

15. L. S. Stivers. Effects of subsonic Mach number on the forces and pressure distributions on four NACA 64A-Series airfoil sections at angles of attack as high as 28°. NACA TN 3162, 1954.

16. J. R. Spreiter, Alksne, J Alberta. Thin airfoil theory based on approximate solution of the transonic flow equation. NASA TN 3970, 1957.

17. F. O. Smetana, D. P. Knepper. Predicted ana measured pressure distributions on two airfoils at Mach number 1. AROD-8130, North Carolina State University.

The manuscript entered 1/IX 1972.

Page 11.

NUMERICAL METHOD OF CALCULATION OF AERODYNAMIC CHARACTERISTICS OF FLAT AND NONPLANAR WINGS IN SUPERSONIC FLOW.

A. G. Zakharov.

Is presented the numerical method of calculation of the total and distributed characteristics of the fine/thin lifting wings of complex planform, including with the mixed (sub- and supersonic) leading and subsonic trailing edges, during flow, by the supersonic flow of gas. Method is instituted on linear theory. It is shown, that, increasing the number of calculation points on wing, it is possible to calculate combination wing + housing as fine/thin lifting surface, which has the same planform as wing + housing. The results of the calculations of different lifting surfaces are compared with the data, obtained by other numerical methods, and with the results of experiment.

1. For calculation of total and distributed aerodynamic characteristics both isolated/insulated wings of complex planform and combination wing + housing is utilized series of effective numerical methods [1-3]. On the basis of numerical diagram [1] is developed a

program for ETsVM [digital computer] BESM-6. Let us pause briefly at the basic ideas of this method. Let us examine the flow around the arbitrary, weakly bent, infinitely fine/thin wing, establish/installed at low angle of attack, by the supersonic flow of perfect gas in the coordinate system, connected with wing (Fig. 1). The linearized boundary conditions on wing take the form: $W = -\frac{\partial y}{\partial x}$ (condition of nonpassage $\vec{V} \cdot \vec{n} = 0$), where W = W(x, z) - a component of the disturbed velocity, normal to wing plane; y = y(x, z) - the equation of the wing surface.

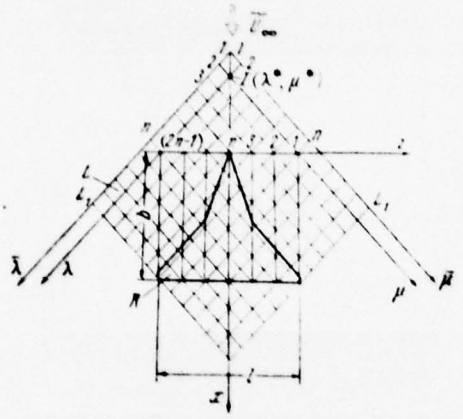


Fig. 1.

Page 12.

Outside of wing and on the vortex sheet (in the case of subsonic trailing edge) the coefficient of pressure c_p is equal to zero, i.e.,

$$c_p = -2\frac{\partial \varphi}{\partial x} = 0,$$

where φ - potential of the disturbed speed.

It is required to calculate c_p on wing at the assigned/prescribed values of $y = y(x, z)$.

According to linear theory the potential of the disturbed speed

in arbitrary point can be expressed through the integral on the domain of effect Σ of the comprising speed W, normal to wing plane:

$$\varphi(x, z) = -\frac{1}{\pi}\iint_{\Sigma'} \frac{W(\xi, \zeta)\, d\xi\, d\zeta}{\sqrt{(x-\xi)^2 - \beta^2(z-\zeta)^2}},$$

where $\beta = \sqrt{M_\infty^2 - 1}$.

After introducing in plane y = 0 characteristic coordinates (see Fig. 1)

$$\lambda = \lambda^* + x - \beta z, \quad \lambda' = \lambda^* + \xi - \beta\zeta,$$
$$\mu = \mu^* + x + \beta z, \quad \mu' = \mu^* + \xi + \beta\zeta$$

with beginning at point $I(\lambda^*, \mu^*)$, let us break wing into rhombiform cells with the sides, parallel to Mach lines. In each cell of the components of the disturbed speed, normal to wing plane, it is set/assumed by constant. Is conducted integration for each cell. Zone of flow is divide/marked off into two zones: the points, which lie on wing, and the points, which lie out of wing. In the first - for determining the downwashes, is utilized the condition of nonpassage, in the second (if trailing edges subsonic or front/leading mixed) - equality zero pressure coefficient. Moreover method [1] it makes it possible to directly determine the values of potentials, without calculating in this case the downwashes out of wing which are not necessary for determining of the total and distributed aerodynamic characteristics. This leads to the savings of the machine memory and count time. Sufficiently simply is realize/accomplished transition from one wing to another. This is provided by the fact that the integration for any wings is conducted on rectangle R (see Fig. 1)

with sides l and b (abscissa of the point of the maximum longitudinal size of wing), into which is entered the wing. In method [1] for wings with transverse symmetry, it is proposed to store in the memory of the machine of the value of the potentials, which belong to entire rectangle R. However, this it is possible not to make and to retain only those values of the potentials which pertain to the right half of rectangle R. This was realized in the developed program for BESM-6. An increase of the number of calculated cells in rectangle R two times makes it possible to calculate only not isolated/insulated wings of complex planform, but also combination wing + housing. In this case, the housing is replaced by its projection on plane xOz (see Fig. 1).

2. Let us give some results of calculations by method presented. Fig. 2, depicts the data of the calculations of load distribution along the spread/scope of two sweptback wings. Wing 1 - swept without contraction.

Page 13.

Load distribution Γ_{ns} on this wing with number $M_\infty = 1{,}2$ is designed by this method and the method of aerodynamic influence coefficients ("panel method") [3] (with number $M_\infty = 1{,}2$ leading and trailing wing edges - subsonic). Derivatives c_y^α designed by these methods,

virtually coincide, and the difference in derivatives m_z^{α} is 5o/o (calculation by "panel" method gave value $c_y^{\alpha}=0{,}0540$, by the proposed method $-c_y^{\alpha}=0{,}0546$, values m_z^{α} were equal to with respect 0.020 and 0.021).

Wing 2 - swept with contraction. The calculation of this wing is carried out by the proposed method and method [4] with number $M_\infty=2{,}6$. With this number M_∞ leading edge subsonic, and rear - is supersonic. From curve/graph it is evident that the results of calculations converge sufficiently well.

Fig. 3, gives an example of the calculation of the wing of complex planform with numbers $M_\infty=1{,}6$ and 2.3. With these numbers M_∞ the wing has the mixed leading edges. The results of calculation show a qualitative change in the law of load distribution along the wingspan with an increase in number M_∞ from 1.6 to 2.3. With number $M_\infty=2{,}3$ the large part of the leading edge of outer wing panel supersonic, and this causes the considerable decrease of load on bracket.

The calculation of wing with deformed median surface let us examine based on the example of delta wing with sweep angle $\chi_{n.\,k}=71{,}5^\circ$ when $M_\infty=2{,}06$. The length of root chord was accepted equal to unit. The wing surface was assigned by the polynomial

$$f(x,\ z)=a_{10}x+a_{11}x|z|+a_{12}xz^2+\\+a_{13}x|z|^3+a_{20}x^2+a_{21}x^2|z|+\\+a_{30}x^3+a_{40}x^4.$$

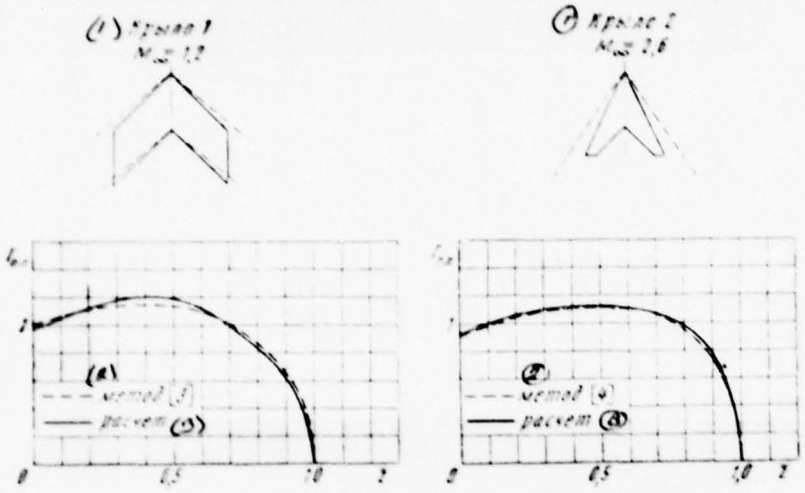


Fig. 2.

Key: (1). Wing. (2). method. (3). calculation.

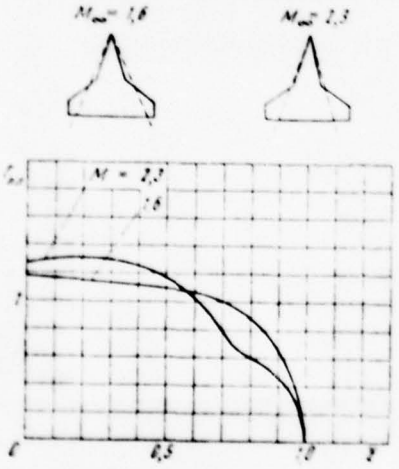


Fig. 3.

Page 14.

The results of the calculations of the total aerodynamic characteristics of this wing for different number n of sections on the semirange of the wing (see Fig. 1) by the proposed method and method [4] are represented in table. The coefficient of pitching moment was determined relatively the wing leading edge in the portions of root chord.

Let us turn to the comparison of the results of calculation with experimental data. In Fig. 4, are compared calculated and experimental aerodynamic coefficients c_y^α and $m_z^{c_y}$ in the range of numbers $1{,}2 \leqslant M_\infty \leqslant 4$ for the sweptback wing. The coefficient of pitching moment was calculated relative to the conditional center of gravity, arrange/located at a distance $\bar{x}_т = 0{,}5$ CAX. From curve/graph is visible the satisfactory convergence of the results of calculation and of experiment.

Program for ETsVM BESM-6, developed on the basis of the described diagram, without modification can be used for the calculation of the total aerodynamic characteristics of combination wing + housing, if the relative area of maximum cross sections of housing is small - order 2o/o. During the calculation of this combination, the wing and housing are replaced by the fine/thin lifting surface of the same planform, as wing + housing.

(1) Аэродинамические коэффициенты	(2) Метод [4]	(3) Расчет предлагаемым методом		
		$n = 69$	$n = 49$	$n = 9$
c_y	0,1	0,0997	0,09966	0,1037
c_x	0,004522	0,00452	0,004557	0,005482
$-m_z$	0,06307	0,063	0,06287	0,06572

Key: (1). Aerodynamic coefficients. (2). Method. (3). Calculation by proposed method.

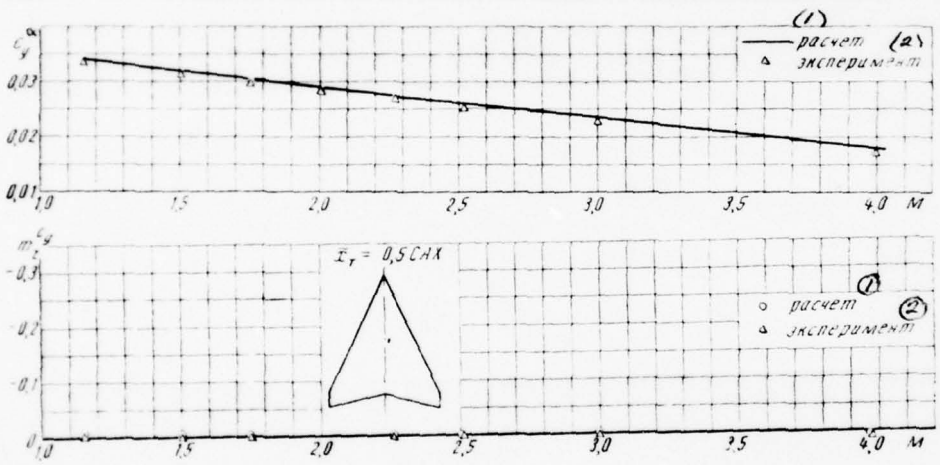


Fig. 4.

Key: (1). calculation. (2). experiment.

Page 15.

On Fig. 5, gives an example of this calculation of the model of

flat/plane wing with housing and is carried out the comparison of obtained values c_y^{α} and $m_z^{c_y}$ with the results of experiment. The coefficient of pitching moment is designed relative to the conditional center of gravity, arrange/located at a distance $\bar{x}_T = 0{,}5\,\text{CAX}$. On this same figure are compared experimental and calculated dependences $c_y = f(c_x - c_{x\,0})$ with number $M_\infty = 2{,}52$. From curve/graph is visible the sufficiently good convergence of experimental and calculation data.

In such a manner, as show calculations, the proposed numerical method is sufficiently effective both for the wings of complex planform and for combination wing + housing.

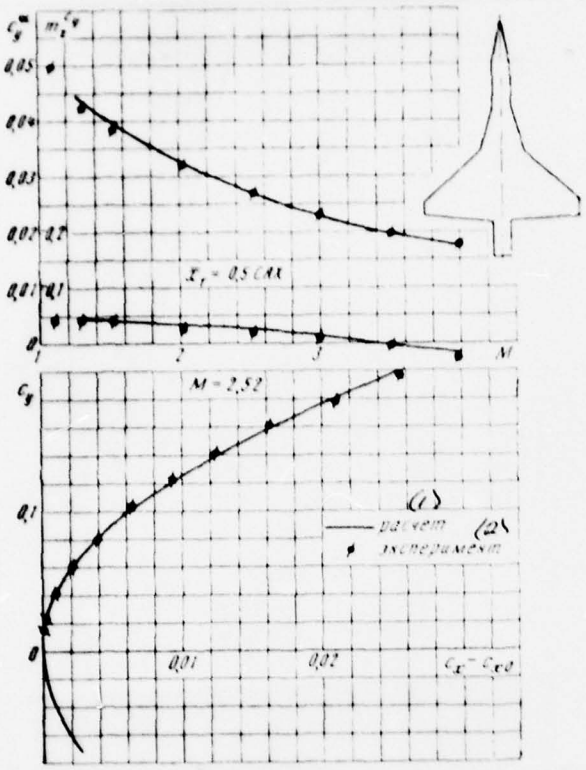


Fig. 5.

Key: (1). calculation. (2). experiment.

REFERENCES

1. M. Fenain, D. Guraud-Vallee. Calcul numerigue des ailes en regime supersonique stationnaire on instaticnnaire. La Recherche

Aerospatiale, No 115, novembere - decembre, 1966.

2. S. M. Belotserkovskiy, N. A. Kudryavtseva, B. N. Fedotov. Method of calculation of the aerodynamic wing characteristics complex planform with subsonic leading and trailing edges. "Izv. of the AS USSR - MZhG", 1969, No 2.

3. F. A. Woodward. Analysis and design of wing-body cimbinations at subsonic and supersonic speeds. J Aircraft, Vol. 5, No 6, 1968.

4. Ye. A. Krasil'shchikova. Finite-span wing in compressible flow. M., Gostekhteorizdat, 1952.

The manuscript entered 10/VII 1972.

Page 16.

FLOW OF GAS THROUGH A WALL WITH LONGITUDINAL SLOTS.

M. P. Ryabokon'.

Is given the theory of the flow of the gas through the wall with the longitudinal slots taking into account the compressibility effect of gas and are examined the leveling properties of this wall.

Questions of interaction of the flow of gas with the wall, which has the longitudinal slots, were examined in work [1] in connection with the study of the leveling action of the penetrated walls. It was shown, that in linear approach/approximation (upon consideration of the first degrees of a velocity increment) the wall with the longitudinal slots behaves as free boundary and the leveling action it does not exert itself. It was shown also, that in nonlinear approach/approximation, but under the condition of the smallness of relative pressure differentials this wall during the proper selection of the coefficient of permeability can decrease from it the

disturbance/perturbations reflected several times (at best eight times).

In connection with the grown interest in the application/use of walls with the longitudinal slots, caused, in particular, by their use in gas ejectors [2], it appeared the need for more precise performance calculation of the flow through the penetrated wall with the longitudinal slots.

In this article is examined the flow through the wall with an arbitrary pressure differential on it and some possibilities of using leveling properties of walls with longitudinal slots at supersonic speeds of flow.

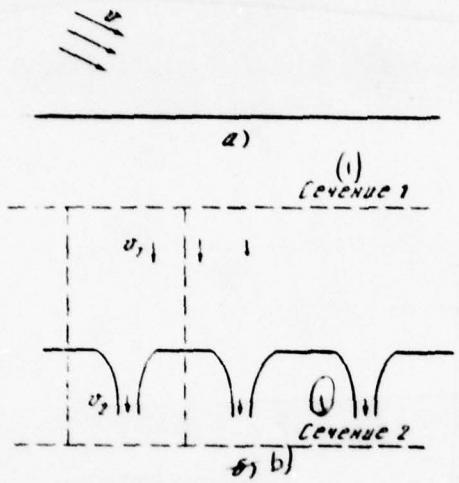


Fig. 1.

Key: (1). Section.

Page 17.

1. Let us examine flow of flow about perfect gas of flat/plane plate of zero thickness, which contains parallel slots of identical width, arrange/located on equidistance from each other (Fig. 1). The ratio of the width of slots to lattice spacing let us designate through k. Peripheral component of velocity let us count to parallel wall.

In ideal fluid composing rates, parallel to the direction of wall, does not affect the flow pattern through the wall. Therefore the task indicated is reduced to the task of determining the flow through the wall with slots when the rate of the undisturbed flow is normal to the wall (see Fig. 1b).

Is known the exact solution of this task for two limiting cases: for $k \to 0$ and $k \to 1$ [3]. Using solutions for these limiting cases, and also by solution for the flow through the Borda mouthpiece [4], let us find approximation for the coefficient of expenditure/consumption through the slots (see Fig. 1b):

$$\mu = \frac{\rho_1 v_1 F_1}{\rho_2 v_2 F_2} = \frac{\rho_1 v_1}{\rho_2 v_2 k}, \qquad (1)$$

where F_1 - lattice spacing, F_2 - width of slots.

It is assumed that each stream is broken away from the edges of slot, and in stagnation zone pressure is constant.

The equation of the conservation of momentum for this flow takes the form:

$$\rho_1 v_1^2 F_1 + p_1 F_1 = \mu \rho_2 v_2^2 F_2 + p_2 F_2 + (p_{cp} - p_2)(F_1 - F_2), \qquad (2)$$

where $p_{cp} = \int_{(F_1 - F_2)} p \frac{dF}{F_1 - F_2}$.

Hence after simple conversions it is possible to obtain expression for μ:

$$\mu = \frac{p_0 - p_2}{\rho_2 v_2^2}\left[1 + \frac{p_0 - p_{cp}}{p_0 - p_2}\left(\frac{F_1}{F_2} - 1\right)\right]\left\{1 - \frac{v_1}{v_2}\left(1 - \frac{p_0 - p_1}{\rho_1 v_1^2}\right)\right\}^{-1} =$$
$$= \frac{1 - p(\lambda_2)}{\varkappa p(\lambda_2) M_2^2}\left[1 + \frac{p_0 - p_{cp}}{p_0 - p_2}\left(\frac{F_1}{F_2} - 1\right)\right]\left\{1 - \frac{\lambda_1}{\lambda_2}\left(1 - \frac{1 - p(\lambda_1)}{\varkappa p(\lambda_1) M_1^2}\right)\right\}^{-1}, \quad (3)$$

where p_0 - stagnation pressure, $p(\gamma)$ - the gas-dynamic function p/p_0.

The value, which stands out of the brackets, represents by itself the compression ratio of flow in Borda mouthpiece:

$$\mu_B = \frac{1 - p(\lambda_2)}{\varkappa p(\lambda_2) M_2^2}\left\{1 - \frac{\lambda_1}{\lambda_2}\left(1 - \frac{1 - p(\lambda_1)}{\varkappa p(\lambda_1) M_1^2}\right)\right\}^{-1}. \quad (4)$$

Therefore formula (3) can be rewritten as follows:

$$\mu = \mu_B\left[1 + \frac{p_0 - p_{cp}}{p_0 - p_2}\left(\frac{F_1}{F_2} - 1\right)\right].$$

Values μ_B with k = 0 ($\lambda_1 = 0$) and change λ_2 from 0 to 1 change from 0.5 to 0.636, whereas the value μ under these conditions according to the data of work [3] (discharge from the container through the slot) they change from 0.611 to 0.745.

With k -> 1, which corresponds to the flow around the isolated/insulated plates, according to the data of work [3], value $\frac{p_{cp}}{p_0 - p_2}$ is changed from 0.88 to 0.91 during change λ from 0 to 1.

All these data can be connected, if we replace expression (4) with the following approximation formula:

$$\mu = \mu_B [1 + 0{,}222(1 - 0{,}23\lambda_2 \sqrt{\bar{\lambda}_2})(1 - 1{,}45k + 0{,}45k^2)].$$

An inaccuracy in this formula does not exceed 0.5o/o with k = 0 and vanishes with k → 1 in all range of subsonic speeds and also at small supersonic speeds.

From expression (1) we obtain

$$k = \frac{1}{\mu} \frac{\rho_1 v_1}{\rho_2 v_2} = \frac{1}{\mu} \frac{q(\lambda_1)}{q(\lambda_2)},$$

where q(λ) - gas-dynamic function $\frac{\rho v}{\rho_* v_*}$.

For the flow through the slots

$$k = \frac{q(\lambda_1)}{\mu_B q(\lambda_2)} [1 + 0{,}222(1 - 0{,}23\lambda_2 \sqrt{\bar{\lambda}_2})(1 - 1{,}45k + 0{,}45k^2)]^{-1}$$

or

$$k[1 + 0{,}222(1 - 0{,}23\lambda_2 \sqrt{\bar{\lambda}_2})(1 - 1{,}45k + 0{,}45k^2)] = \frac{q(\lambda_1)}{q(\lambda_2)} \left\{1 - \frac{\lambda_1}{\lambda_2}\left[1 - \frac{1 - p(\lambda_1)}{\varkappa p(\lambda_1) M_1^2}\right]\right\} \left[\frac{1 - p(\lambda_2)}{\varkappa p(\lambda_2) M_2^2}\right]^{-1}.$$

In the right side the function of values λ_1 and λ_2 confronting represents by itself relative area for the cap/filling by Borda k_B.

The curve/graph of this function is given to Fig. 2. Thus,

$$k_b = k[1 + 0{,}222(1 - 0{,}23\lambda_2\sqrt{\lambda_2})(1 - 1{,}45k + 0{,}45k^2)].$$

These dependences for a series of values k are also represented in Fig. 2. The curve/graph Fig. 2 makes it possible to determine the dependence between λ_1 and λ_2 with the assigned/prescribed coefficient of permeability k. Such dependences for a series of values k are given to Fig. 3.

It should be noted that at each value of k the maximum value λ_1 and, therefore, the maximum air flow rate, according to data Fig. 3, are obtained not when $\lambda_2 = \lambda_{max}$, but with certain comparatively small λ_2 (order 1.3), which contradicts physics of the phenomenon, since the creation of more powerful evacuation/rarefaction behind slotted wall must not lead to the decrease of expenditure/consumption. the presence of maximum is connected with an inaccuracy in formula (2) in the field $\lambda_2 > 1$, which assumes the even distribution of the speeds and pressures in jet in section 2, whereas real distribution must be substantially nonuniform due to the presence of waves. Therefore the data Fig. 3 can be considered valid only to the chutes of maximums λ_1. However, since the range of higher values λ_2 is of interest for further calculations, in Fig. 3, curves are continued further with constant values λ_1 (dotted line).

Using the curve/graph Fig. 3, it is possible to determine the ratio of pressure on wall for each value of k:

$$\frac{p_1}{p_2} = \frac{p(\lambda_1)}{p(\lambda_2)}. \qquad (5)$$

Returning to initial flow, we note that

$$\frac{p_1}{p_2} = \frac{p(\lambda)}{p(\lambda_{cm})}, \qquad (6)$$

where λ_{cm} - speed on free boundary.

Page 19.

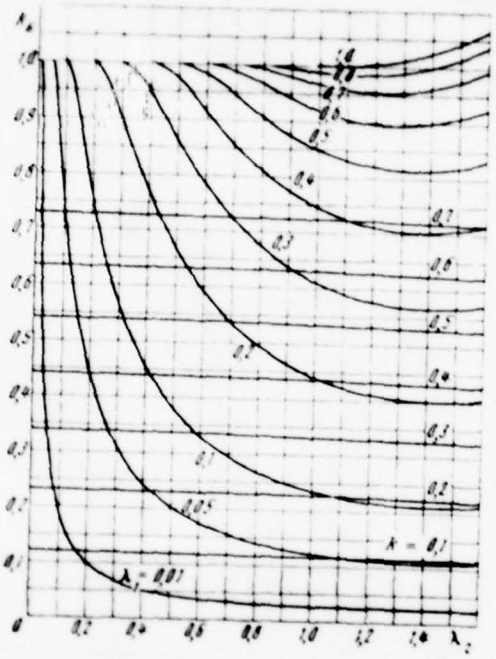


Fig. 2.

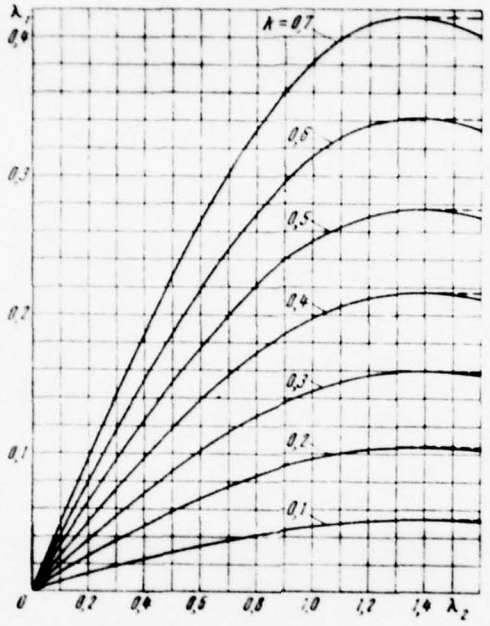


Fig. 3.

Page 20.

The comprising velocities of incident flow are connected by the relationship/ratios:

$$\frac{\lambda_y}{\lambda} = \frac{v_y}{v} = \frac{v_y/a}{v/a} = \frac{M_1}{M}, \qquad (7)$$

$$\lambda_x = \sqrt{\lambda^2 - \lambda_y^2},$$

where $M = f(\lambda)$, $M_1 = f(\lambda_1)$.

Formulas (5) - (7) make it possible to obtain the curves of the hodograph of the speed for the flow through the wall with the longitudinal slots under the condition of absence of pitot losses in the incident flow of gas. With this characteristic of wall $\lambda_y = f(\lambda_x)$ when $\lambda_{cв} = \text{const}$ it will correspond to a constant jump/drop in pressure $p_{cв}/p_0 = p(\lambda_{cв})$.

When pitot losses are present, relationship/ratio (5) - (7) they remain valid, but the characteristic of wall in a constant pressure differential will correspond variable $\lambda_{cв}$ according to formula $\frac{p_{cв}}{p_0} = \nu p(\lambda_{cв})$.

One should, however, ncte that for the range of a change in the direction of the speed in wave to 5° with Mach numbers to 3, i.e., under those conditions which can be of practical interest, pitot losses do not exceed 0.5o/o and therefore they do not virtually affect the characteristics of wall. Wall itself with the longitudinal slots during the flow around it of the steady flow (with $k < \sim 0.7$) does not cause pitot losses unlike wall with the transverse slots or with round opening/apertures. Therefore in further examination of pitot loss be considered they will not be.

2. Let us examine question concerning leveling action of wall with longitudinal slots, through which cccur/flow/lasts flow of gas.

Let the characteristic of wall $\lambda_{cs} = const$ take the form curved AB in Fig. 4. If flow attacks to wall with angle θ_0, the point C of intersection from straight line $\theta = \theta_0$ will be operating point. Let us conduct through point C epicycloid DCE. If in flow is a compression wave with the maximum angle of rotation of flow $\Delta\theta_1$, then its image in Fig. 4 is line CE'. Let us conduct through point E' the epicycloid of the second family E'B'C'. Line CB' corresponds to the wave reflected. Nonuniformity in the wave reflected is characterized by the maximum distance between lines CB' and CE', taken on the ray/beam, passing through pcint O; in this case this of cuttings off B'E".

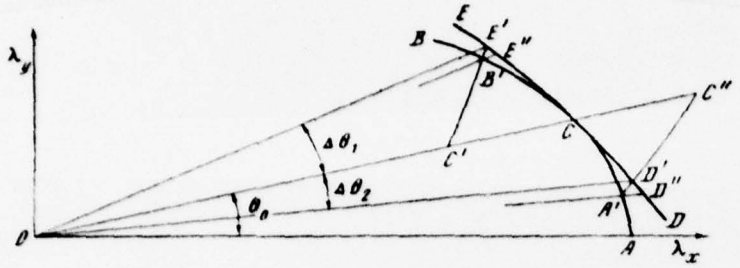


Fig. 4.

Page 21.

Degree of the extinguishing of nonuniformity by the wall is characterized by ratio $\varepsilon = \frac{B'E''}{C'C}$ or $\varepsilon = \frac{B'E''}{2(OC - OE')}$.

In the case of rarefaction wave with the maximum angle of rotation of flow $\Delta\theta_2$ the nonuniformity of flow after reflection is characterized by cut A'D", and the degree of the extinguishing of nonuniformity $\varepsilon = \frac{A'D''}{CC''}$.

To Fig. 5, gives a series of the characteristics of slotted wall with different coefficients of permeability k. For each of the characteristics, is plotted/applied the section of its concerning epicycloid. The analysis of these data shows that the wall with the longitudinal slots with the course through it of flow can provide the

complete equalization of disturbance/perturbations. The field of complete equalization (field of the contact of curves) in the majority of the cases is small. However, during transonic conditions/modes in certain cases of the characteristic of wall, satisfactorily they will agree with epicyclcids over a wide range of the angles of rotation of flow (to 5°). A series of such characteristics is given to Fig. 5. on curve/graphs are shown the ranges of angles and velocities λ in the range of agreement, and also value ε. As is evident, values ε comprise to 2-3o/o, i.e., they are considerably best, than in the case of the flow, parallel to wall, when ε is equal to 12.5o/o (see [1]).

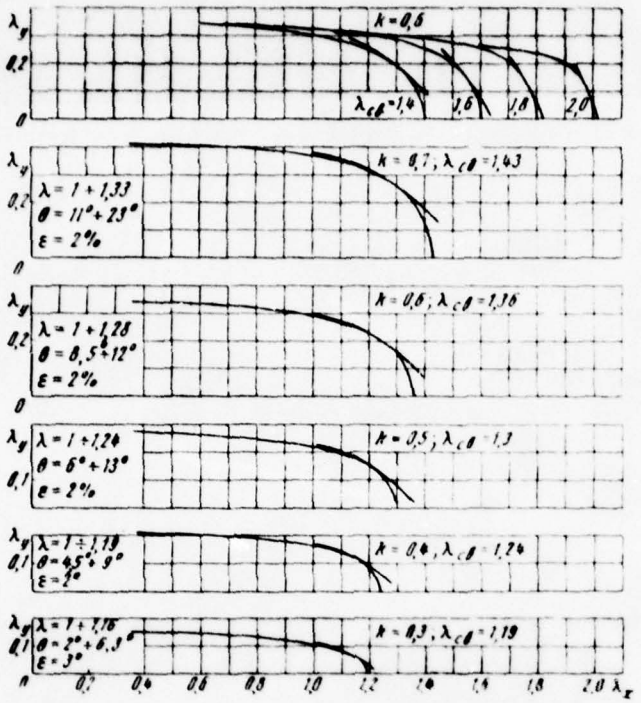


Fig. 5.

Page 22.

3. Slotted walls of examined type can be successfully used in schematic of wind tunnel with small supersonic speeds of flow, if they are establish/installed at certain angle to nozzle liners (Fig. 6).

When assign/prescribed $\lambda_{c\theta}$ the angle of setting the walls of

test section should select in such a way that the operating point would be located in the middle of the field of the adjoining of the characteristic of wall and epicycloid. In this case will be extinguished well the exiting/waste from model compression waves and evacuation/rarefaction whose intensity does not exceed the limits of the field of adjoining.

Test model one should establish/install the system of the waves, exiting/waste from the joint of nozzle and test section. These waves can appear as a result of inaccurate agreement between the nozzle pressure $p = p_0(\lambda)$, the pressure in space after test section $p_{cs} = p_0 p(\lambda_{cs})$ and the angle of setting walls. With the first incidence/drop on the wall of wave, they are extinguished.

The application/use of walls with longitudinal slots, tilted to flow, in wind-tunnel test section is connected with the need for suction from the space, which surrounds test section, the considerable quantity of air, which comprises in the portions of overall expenditure/consumption 10-20o/o and more during the evacuation/rarefaction, which exceeds evacuation/rarefaction by test section. This fact comprises a main deficiency/lack in the application/use of such walls. At the same time the slotted walls, tilted to flow, possess a series of essential advantages in comparison with the usual perforated/punched walls. On the usual

walls there is a boundary layer, which makes the leveling properties worse of walls, whereas on slotted wall it continuously escape/ensues through slots together with the exhausted air. The characteristics of usual walls with inflow and discharge of flow essentially differ from each other, whereas the characteristics of slotted wall with inflow and discharge are the continuation of each other. The usual perforated/punched walls strongly create turbulence flow, whereas slotted walls with the continuous suction through them of air provide conditions for obtaining the low-turbulence flow.

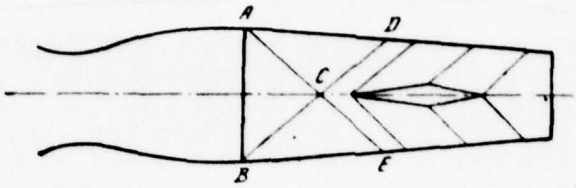


Fig. 6.

REFERENCES.

1. G. L. Grodzovskiy, A. A. Nikol'skiy, G. P. Svishchev, G. I. Taganov. Supersonic flows of gas in the perforated/punched boundaries. M., "machine-building", using 1967.

2. Yu. K. Arkadov. Gas ejector with the nozzle, perforate/punched by the lcngitudinal slots. "Izv. of the AS USSR - MZhG", 1968, No. 2.

3. S. A. Chaplygin. On the gas jets. Moscow-Leningrad, State Publishing House of Technical and Theoretical Literature. 1949.

4. S. A. Khristianovich, V. G. Gal'perin, M. D. Millionshchikov, L. A. Simonov. Applied gas dynamics. M., TsAGI [99sp04 - Central Institute of Aerohydrodynamics im. N. Ye Zhukovskiy, 1948.

The manuscript entered 11/VIII 1972.

EXPERIMENTAL DETERMINATION OF THE PRESSURE RECOVERY FACTORS IN CONICAL DIFFUSERS AT HIGH SUBSONIC SPEEDS AND DIFFERENT ENTRANCE CONDITIONS.

Ya. L. Ginsburg, I. Ye. Idel'chik.

Are given the basic results of the investigations of the conical diffusers at high subsonic speeds. Are obtained the dependences of the pressure recovery factors on the relative speed of flow for different angles and the expansion ratios and relative lengths of direct/straight intake both for the exit cone/diffusers, placed in grid/network and at output/yield from grid/network.

It is known that the diffuser channels are widely accepted in the most varied branches of technology; therefore to the study of the flow of liquid and gas in such channels is given considerable attention. Many questions, connected with flow in the diffuser channels, especially nonseparable, obtained theoretical solution [1-6]; however, the complexity of the phenomenon and the dependence of diffuser performance on the large number of parameters does not make it possible at contemporary level to obtain all these

dependences theoretically. their large part it is necessary to determine only experimentally, but also by this method obtain comprehensive given everything still could not. In the carried out investigations the number of the parameters being investigated remained limited, so that the effect of each of them independent of the remaining parameters not always could be revealed. This relates even to such comparatively extensive studies of the exit cone/diffusers which are presented in works [6-10]. True, for the authors [6] it was possible to the certain degree to determine independently one of another effect of two very important parameters - Re numbers and M. But this concerns only the exit cone/diffusers, working to exhaust, with divergence angles to 30° under constant entrance conditions (uniform airfoil/profile of inlet velocities into the exit cone/diffuser, placed directly after smooth collector/receptacle, and the constant turbulence level of entering flow).

Page 24.

The authors of present article carried out the systematic studies of the conical diffusers (D_1 = 80 mm), of exit cone/diffusers with the square cross sections and of the plane diffusers both in their work on exhaust ($l_2/D_2 = 0$) and in grid/network [1] ($l_2/D_2 = (l_2/D_2)_{opt}$ Fig. 1).

FOOTNOTE [1]. Let us note that in the work of exit cone/diffuser in grid/network must be taken into account not only purely "internal" the losses of pressure in it, but also losses of pressure after it, in direct/straight exit section. These losses are caused by the disturbance/breakdown of flow in exit cone/diffuser itself and by its further equalization on the section indicated. Therefore for the correct determination of the drag coefficient of the exit cone/diffuser, working in grid/network, is required the measurement of the total pressure at this distance after it in the exit section, with which the distribution of speeds virtually already is evenly over section. In our experiments after the experience/tested exit cone/diffusers of the class in question always was establish/installed the direct/straight section (see Fig. 1) with length l_2/D_2, which provided a sufficient uniformity of flow on leaving its in the atmosphere $[l_2/D_2 = (l_2/D_2)_{opt}]$. By virtue of the stated the drag coefficiant, calculated only according to "internal" losses in exit cone/diffuser itself, does not reflect the true (complete) magnitude of losses of pressure in the exit cone/diffuser, working in grid/network. ENDFOOTNOTE.

Here l_2 - length of direct/straight exit section, D_2 - diameter of the wide (exit) section of exit cone/diffuser.

Exit cone/diffusers tested at different divergence angles, taken in limits α = of 4-180° (4°, 6°, 8°, 10°, 14°, 20°, 30°, 45°, 60°, 90°, 120°, 180°), and expansion ratios in the range n = 2-16 (2, 4, 6, 10, 16). Reynolds number was changed within the limits $Re = \frac{w_1 D_1}{\nu}$ = $3 \cdot 10^4$-10^6, but only as a result of changing the speed of the flow (relative speed reached in this case sometimes λ_1 = 0.95). Each exit cone/diffuser tested under the varied conditions of entrance, which were changing by the setting up between smooth inlet manifold and the exit cone/diffuser of direct/straight sections with different relative lengths, undertaken within limits l_1/D_1 = 0-20. By this they were simultaneously changed within the comparatively wide limits (0.5o/o < 2 δ/D_1 < 5.0o/o) both momentum thickness and the turbulence level in inlet boundary layer into exit cone/diffuser.

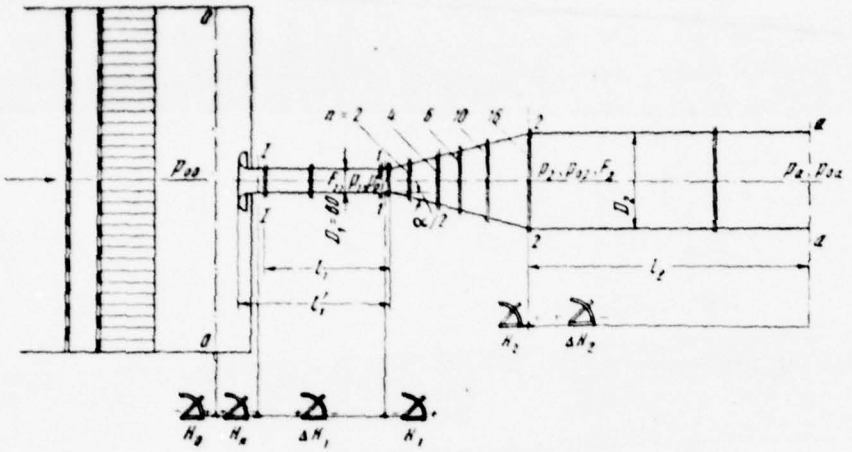


Fig. 1.

Page 25.

It is clear that these experiments possess that deficiency/lack, that in them a change of Re numbers and λ_1 and of the thickness of the "loss of momentum/impulse/pulse" and turbulence levels, occurred simultaneously. However, this is observed in the majority of the cases in practice, in connection with which the obtained results they must, in our opinion, represent sufficiently wide practical interest, especially, if one considers that the experiments made it possible to determine independently of each other the effect of each of such parameters as α, n, δ_1/D_1, δ_2/D_2, the form of section.

The total pressure before the exit cone/diffuser was determined from the total pressure in the preceding exit cone/diffuser camera/chamber of pressurization/supercharging minus of losses to friction ΔH_1 in direct/straight intake:

$$p_{01} = p_{00} - \Delta H_1 = p_a + H_0 - \Delta H_1.$$

This standard method was used not only for simplification in the experimental technique, but also for the increase of their accuracy/precision. It eliminated the need for setting up for section directly before the entrance into the exit cone/diffuser of the meter of pressure. The latter even with very small size/dimensions causes the considerable distortion of flow (aerodynamic shadow) over entire length of exit cone/diffuser, introducing thereby large errors into the determination of true losses in it. Furthermore, supplementary resistance in common/general/total grid/network from the meter of pressure was at high speeds so/such considerable, that under our conditions it sharply decreased the maximum speed of flow λ_1 by the entrance into exit cone/diffuser.

Overpressure H_0 was measured in section by 0-0 according to branch on the wall of the plenum chamber (camera/chamber of pressurization/supercharging, see Fig. 1), in which the speed of flow was virtually equal to zero. Therefore value H_0 can be considered as excess total pressure (stagnation pressure).

Losses of pressure ΔH_1 on section from section 0-0 to section 1-1 before the exit cone/diffuser were determined by preliminary experiments for all values l_1/D_1 [1] in a difference in the total pressures in the sections indicated.

FOOTNOTE [1]. For case $l_1/D_1 = 0$, was accepted $\Delta H_1 \approx$ by 0. ENDFOOTNOTE.

The averaging of the total pressure over section 1-1 was conducted on mass flow rate and the measured fields of the velocities and the total pressures. In this case, the air density was accepted as constant over section, since with $l_1/D_1 = 0\text{-}2$, when exit cone/diffuser was placed directly after smooth collector/receptacle, the distribution of all flow parameters uniform to [2].

FOOTNOTE [2]. Section 1-1 was selected not in entrance itself into exit cone/diffuser, but at a distance of $0.2\ D_1$ in front of it, for purpose of the exception/elimination of the effect of the fracture of wall on the local distribution of speeds and pressures. ENDFOOTNOTE.

At other values l_1/D_1 (more than two) value λ_1 did not exceed 0.7. But with $\lambda_1 < 0.7$, as shown in work [12], by the nonuniformity of distribution over the section of static pressure and density it is

possible to disregard.

In accordance with the observation, made above, the total pressure after the exit cone/diffuser, working in grid/network, was determined from the total pressure at the end of the direct/straight exit section [3] taking into account losses to friction ΔH_2 in this section:

$$p_{02} = p_a + \Delta H_2 = p_a + \zeta_{rp} \frac{\rho_2 w_2^2}{2}.$$

FOOTNOTE [3]. Thereby were considered not only "internal" the diffuser losses, but also the subsequent losses to flattening of flux after it, which, as it was noted, also one should relate to diffuser losses, working in grid/network. ENDFOOTNOTE.

where ζ_{rp} - coefficient of friction drag of direct/straight exit section.

Page 26.

Losses to friction in direct/straight exit section after exit cone/diffuser due to the smallness of speeds are so/such insignificant, which is complete not substantially, on which of their available formulas to calculate. In this article for this, was

utilized the formula, recommended in work [12]:

$$\zeta_{rp} = \frac{\varkappa + 1}{\varkappa - 1} \frac{1}{\lambda_a^2} \left[1 - \left(\frac{p_{0a}}{p_{02}} \right)^{\frac{\varkappa - 1}{\varkappa}} \right] \qquad (\lambda_a \approx \lambda_2).$$

Since

$$p_{0a} = p_a \left(1 - \frac{\varkappa - 1}{\varkappa + 1} \lambda_a^2 \right)^{-\frac{\varkappa}{\varkappa - 1}},$$

that we obtain

$$p_{02} = p_a \left(1 - \frac{\varkappa - 1}{\varkappa + 1} \lambda_a^2 \right)^{-\frac{\varkappa}{\varkappa - 1}} \left(1 - \frac{\varkappa - 1}{\varkappa + 1} \lambda_a^2 \zeta_{rp} \right)^{-\frac{\varkappa}{\varkappa - 1}},$$

where $\varkappa$ - an adiabatic index.

Taking into account the smallness of values ζ_{rp}, $\frac{\varkappa - 1}{\varkappa + 1} \lambda_a^2$ and being limited only to first terms of the expansion of power series, it is possible expression for the total pressure recovery coefficient to lead finally to the following form:

$$\bar{p}_0 = \frac{p_{02}}{p_{01}} = \frac{p_a}{p_{01}} \left[1 + \frac{\varkappa}{\varkappa + 1} (1 + \zeta_{rp}) \lambda_a^2 \right] = \frac{1}{1 + \frac{H_0 - \Delta H_1}{p_a}} \left[1 + \frac{\varkappa}{\varkappa + 1} (1 + \zeta_{rp}) \lambda_a^2 \right],$$

where

$$\lambda_a = \lambda_1 \frac{p_1}{p_a} \frac{1}{n},$$

$$\lambda_1 = \sqrt{\frac{\varkappa + 1}{\varkappa - 1} \left[1 - \left(\frac{p_1}{p_{01}} \right)^{\frac{\varkappa - 1}{\varkappa}} \right]}.$$

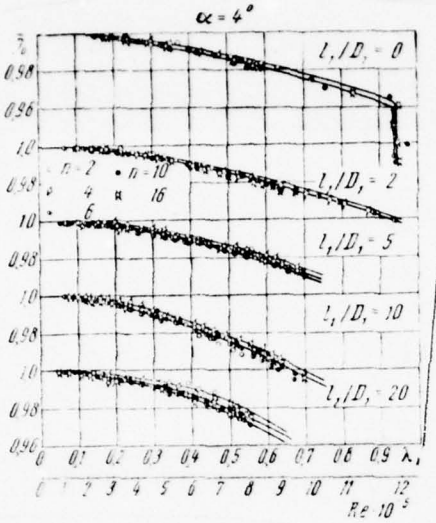


Fig. 2.

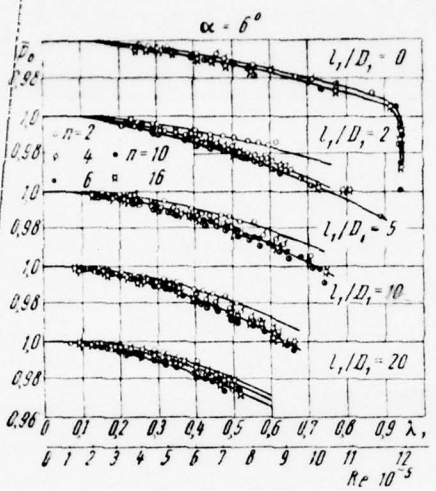


Fig. 3.

Page 27.

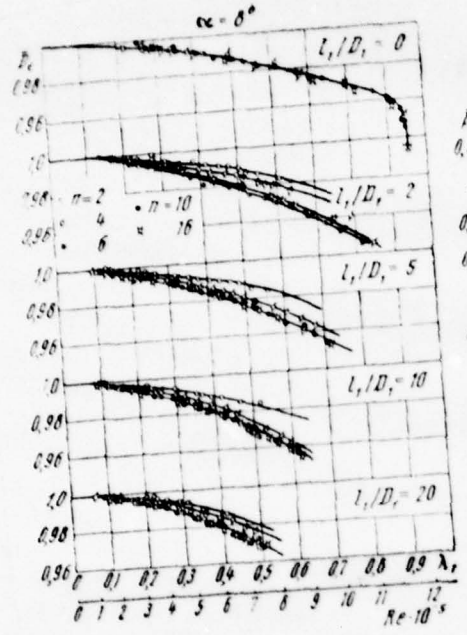

α = 6°
l₁/D₁ = 0
l₁/D₁ = 2
l₁/D₁ = 5
l₁/D₁ = 10
l₁/D₁ = 20
n = 2
4
6
n = 10
16
λ₁
Re·10⁻⁵

Fig. 4.

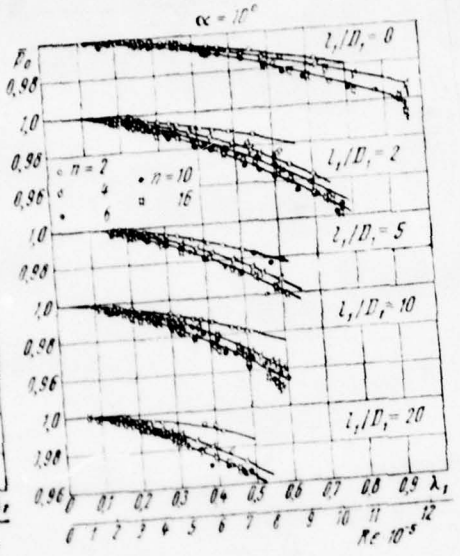

α = 10°
l₁/D₁ = 0
l₁/D₁ = 2
l₁/D₁ = 5
l₁/D₁ = 10
l₁/D₁ = 20
n = 2
4
6
n = 10
16
λ₁
Re·10⁻⁵

Fig. 5.

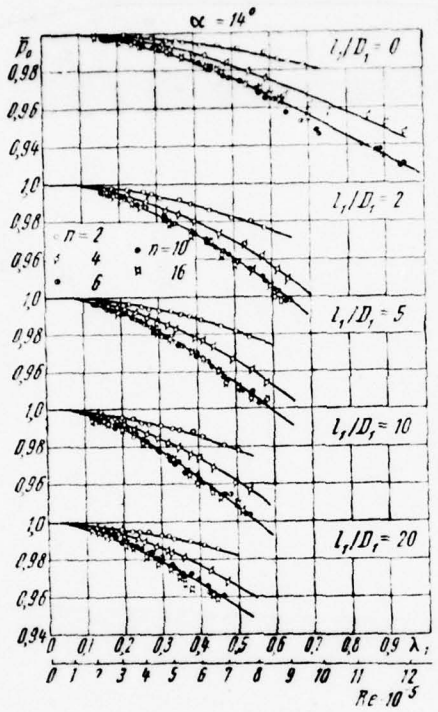


Fig. 6.

Page 28.

In the case of the exit cone/diffusers, working to exhaust, value p_2 was accepted equal to the ambient pressure, so that

$$\bar{p} = \frac{p_2}{p_{01}} = \frac{p_a}{p_{01}} = \frac{1}{1 + \frac{H_0 - \Delta H_1}{p_a}}.$$

The account to an error of measurement of values from which was determined $\bar{p}(\bar{p}_0)$, made it possible to evaluate a relative error in

the determination of values $1-\bar{p}$ and $1-\bar{p}_0$ for the most important velocity band ($\lambda_1 > 0.6$): it render/showed order $\pm$10o/o. Taking into account being inherent in diffuser channels high flow fluctuations, this error one should consider completely acceptable.

The results of experiments in the form of the dependences of coefficients $\bar{p}_0$ and $\bar{p}$ on λ_1 (and Re) of different α, n and l_1/D_1 are given to Fig. 2-6 for the conical diffusers, working in grid/network, and in Fig. 7-11 - for conical exit cone/diffusers, working to exhaust.

Let us note that the decrease of the maximum speed of flow λ_1 at the entrance into exit cone/diffuser with an increase in the relative length l_1/D_1 is explained purely by the technical capabilities of the used by us experimental installation. With an increase in resistance of the experience/tested exit cone/diffusers (as a result of an increase in the length of the direct/straight exit section l_1/D_1) descended the fan capacity, which gave flow into motion, and further increase λ_1 became under our conditions impossible.

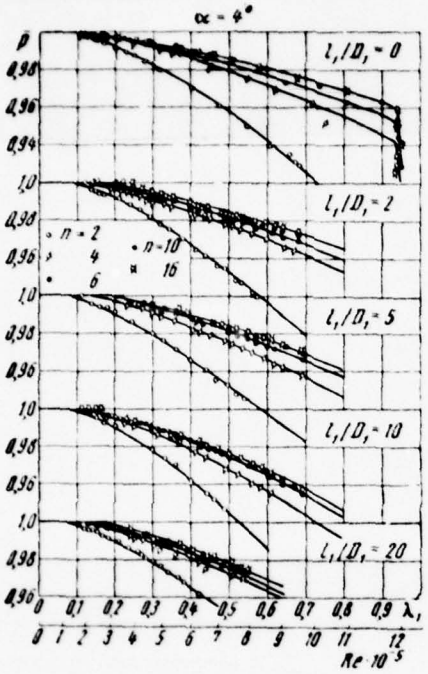

α = 4°
l₁/D₁ = 0
l₁/D₁ = 2
l₁/D₁ = 5
l₁/D₁ = 10
l₁/D₁ = 20
n = 2
4
6
10
16
p̄
λ₁
Re·10⁻⁵

Fig. 7.

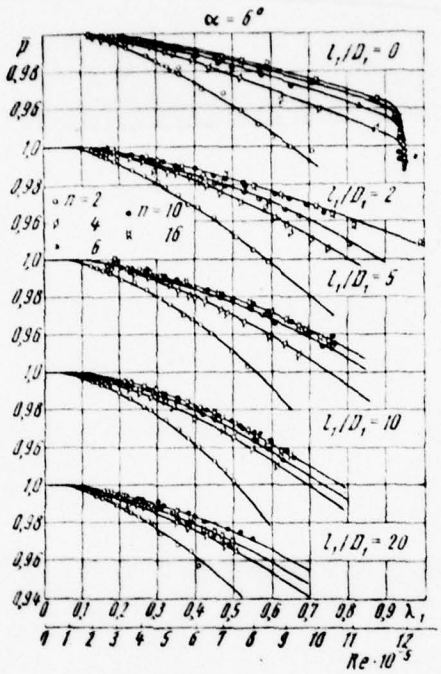

α = 6°
l₁/D₁ = 0
l₁/D₁ = 2
l₁/D₁ = 5
l₁/D₁ = 10
l₁/D₁ = 20
n = 2
4
6
10
16
p̄
λ₁
Re·10⁻⁵

Fig. 8.

Page 29.

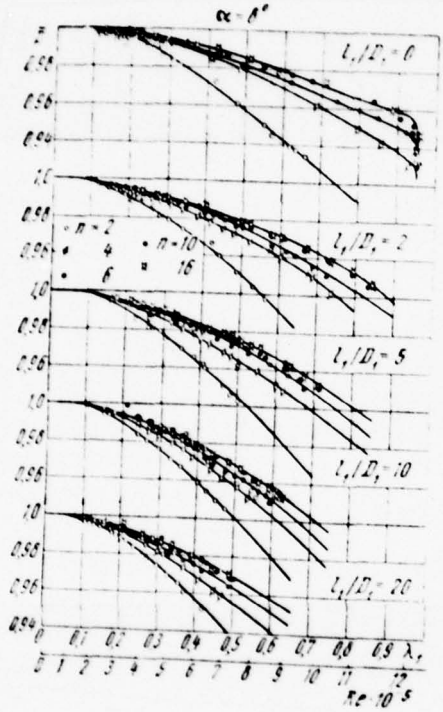


Fig. 9.

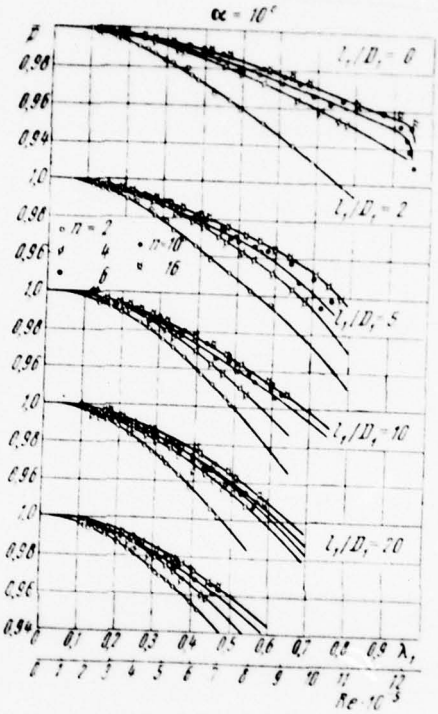


Fig. 10.

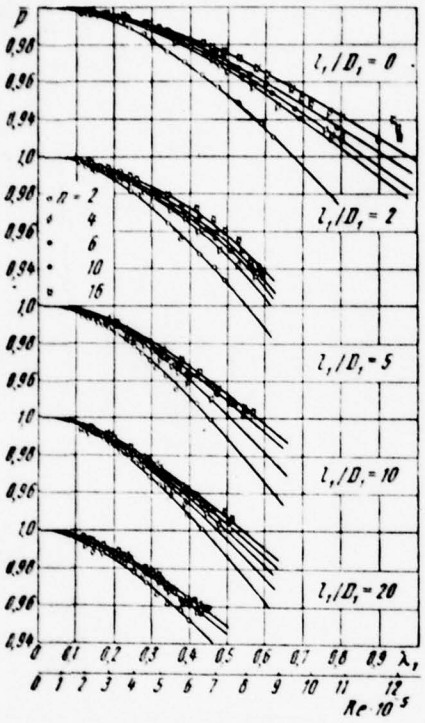


Fig. 11.

Page 30.

The limited volume of article does not make it possible here to dwell on the mechanism of the effect of the conditions of entrance (relative length of straight intake l_1/D_1) for resistance of exit cone/diffusers or, which is the same thing, on the pressure recovery factor $\bar{p}(\bar{p}_0)$ (see [16-18]). Let us point out only that this effect is

caused by two factors: by the increase of thickness and turbulence level of boundary layer in exit cone/diffuser with the elongation of the initial direct/straight section, placed between the very smooth collector/receptacle and the exit cone/diffuser. At small divergence angles α, the first factor (boundary layer growth) the voltage dropping resistor of friction in exit cone/diffuser, and the second (agitation of flow) - raises it. The considerable agitation of flow, which has more powerful effect on resistance of exit cone/diffuser, than boundary layer growth, occur during the initial elongation of direct/straight section approximately to l_1/D_1 = 10-12, with further increase l_1/D_1 agitation is stabilized. The thickening of boundary layer continues with further elongation of direct/straight section (virtually to l_1/D_1 = 20-25). As a result of entire this the drag-rise characteristics (decrease $\bar{p}$ and $\bar{p}_0$) of exit cone/diffusers with small angles α (approximately to 10°) with an increase in the relative length of direct/straight intake occurs within limits $l_1/D_1 \leqslant$ 10-12. With further increase l_1/D_1, value $\bar{p}(\bar{p}_0)$ remains constant or even somewhat grow/rises in comparison with the fact that is obtained with l_1/D_1 = by 10-12.

Until now, as materials for the calculation of exit cone/diffusers at high subsonic speeds, served the data, published in C. C. Stsilard's work [13]. These data figure as almost in all other works, in which are examined analogous questions [12, 14]. Meanwhile

it is missed out of sight, that the investigations indicated are related to exit cone/diffusers only with one ratio of areas ($n \approx 5$) and by the completely specified conditions of the entrance when before exit cone/diffusers are establish/installed supplementary sections (wind-tunnel test section in the form of smooth collector/receptacle with direct/straight section by the common/general/total length $l_1'/D_1 = 3$, or Eiffel's camera/chamber), so that the data [13] are connected both internal resistance of exit cone/diffusers and resistance of these sections. Furthermore, the presence before the exit cone/diffuser of one or the other section additionally raises resistance of this exit cone/diffuser (reduces the pressure recovery factor, which is evident from those given here, and also in the works [15-18] of the results of our investigations). From the aforesaid it follows that the propagation of the results of the investigations of Stsilard for other relations n (especially lesser than five) and other conditions of entrance is incorrect. the true drag coefficient (pressure recovery factor) of exit cone/diffuser will in this case considerably differ from that indicated in work [13].

REFERENCES.

1. A. S. Ginevsiy. Energetic subsonic diffuser channels. "Proceedings of the AS USSR", OTN, No. 3, 1956.

2. A. S. Ginevskiy. Calculation of losses in the expanded and tapering channels. "industrial aerodynamics", iss. 7, TsAGI, 1956.

3. A. S. Ginevskiy. On the calculation of the hydraulic friction of channels with nonseparable and detached flow. "Engineering-Physics journal", Vol. 8, No. 4, 1965.

Page 31.

4. A. S. Ginevskiy, A. V. Kolesnikov. Calculation of initial section and section of the stabilized flow in flat/plane nonseparable exit cone/diffusers. "Proceedings of the AS USSR - MZhG", No. 6, 1969.

5. Ye. Ye. Solodkin, A. S. Ginevskiy. Turbulent nonisothermal flow of viscous compressible gas in the initial sections of the axisymmetric and flat/plane expanding ducts with zero pressure gradient. Transactions of TsAGI, iss. 940, 1964.

6. M. E. Deutsch, A. Ye. Zaryankin. Gas dynamics of exit cone/diffusers and exhaust pipes of turbomachines. M., "energy", 1970.

7. W Kmonicek. Unterschallstromung in Kegeldiffusoren. Acta Technica, 1959, No. 8.

8. W Kmonicek. Zlepsencinnosti diffusoru jednodu chymi zaschy. Strojncky sbornik, 1956, No. 13.

9. F Lippe. Untersuchungen uber den Einfluss des Dralles auf die Stromung in schlanken Kegeldiffusogen. Wissenschaft, Zeitschrift der TN, Dresden, Bd. 8, Nr. 2, 1962.

10. R v Van Devoestine, R W Fox. An experimental investigation on the effect of subsonic inlet Mach number on the performance of conical diffusers. Intern. J of Mech. Scienc., vol. 8, No. 12, 1966.

11. L. I. Sedov. Similarity methods and dimensionality in mechanics. M., "science", 1967.

12. A. Sh. Dorfman, M. M. Nazarchuk, N. I. Pol'skiy, M. I. Saykovskiy. Aerodynamics of exit cone/diffusers and exhaust pipes of turbomachines. Kiev, the publ. of AS UkSSR, 1960.

13. C. C. Stsilard. Study of the wind tunnel diffusers high speeds. TsAGI, "technical notes", No. 160, 1938.

14. G. A. Abramovich. Applied aerodynamics. M., "science", 1969.

15. I. Ye. Idel'chik. On the conditions/modes of detached flows in the shaped pieces of the conduit/manifolds. Coll. of reports during seminar on heat-gas supply and ventilation. Kiev, "Budivel'nik", 1966.

16. I. Ye. Idel'chik, Ya. L. Ginsburg. On the study of the effect of Re number and of the conditions of the entrance on the law governing motion in exit cone/diffusers. Coll. of the reports of the 5th Riga conference on MGD. Institute of physics AN LAT. SSR, 1966. (See also authors's article in the collection of the "problem of ventilation and air conditioning". Minsk, 1969).

17. I. Ye. Idel'chik, Ya. L. Ginsburg. Mechanism of the effect of entrance conditions, the form of section and flow conditions for diffuser performance. Coll. of the reports of the 6th Riga conference on MGD. Institute of physics AN of Lat. SSR, 1968.

18. I. Ye. Idel'chik, Ya. L. Ginsburg. On the mechanism of the effect of entrance conditions for the friction of exit cone/diffusers. "physical engineering journal", Vol. XVI, No. 3, 1969.

The manuscript entered 25/VI 1971.

The reworked version entered 31/V 1972.

Page 32.

ANALYSIS OF SLOW IONS OF THE FLOW OF RAREFIED PLASMA WITH THE AID OF MULTIELECTRODE PROBE.

L. V. Nosachev, V. V. Skvortsov.

Are given the results of the investigations of medium energy and concentration of slow ions, which appeared as a result of overcharging in the flow of rarefied plasma when conducting laboratory experiments in ionospheric aerodynamics. For measurements was applied the multielectrode probe, in which was realize/accomplished the three-dimensional/space separation of the flows of fast and slow ions. It is establish/installed that the medium energy of slow ions can be comparable with the temperature of electrons in flow, and these ion concentration under conditions, typical for experiments in ionospheric aerodynamics, it is more than by an order of the lesser primary ion concentration.

In the flows of the rarefied plasma, utilized in experiments in

ionospheric aerodynamics, together with the primary ions whose energy comprises approximately 100 eV, are present also the ions, which have considerably lower energy and which were being formed, in essence, as a result of the overcharging of high energy ions on neutral atoms of working gas. These ions can affect the structure of the disturbed region about body, if their concentration proves to be commensurable with the accelerated ion concentration of flow.

In works [1] and [2] it is made the attempt to evaluate slow ion concentration in the flows in question from the balance of production and losses of these particles. However, their estimations give only the approximate representation of datum, since loss rate of slow ions in real flows does not yield sufficiently to precise calculation. For purpose of the determination of slow ion concentrations the authors [3] was measured current to the plate, shielded from the direct effect of fast ions, with subsequent processing of results on formula, to Bohm's analogous formula [4], and also was estimated the concentration of electrons (and, therefore, under the assumption of quasi-neutrality/inertness, ion concentration) from the characteristics of Langmuir probe in that region of near trace, into which do not fall fast ions.

However, in the first case before the plate due to the presence of screen, appears shadow zone for primary ions. This leads to the considerable disturbance/perturbation of the adjacent to plate range of plasma, since precisely fast ions give the basic contribution to the concentration of the positively charged particles in the flows in question. As a result the current of slow ions for plate can in terms of uncontrollable form differ from the current, determined on Bohm's usual formula. During the use of the second method, it is necessary to consider that ion concentration in near trace does not coincide with ion concentration in the undisturbed plasma, since in the region of trace it depends also on its geometry and on the existing there electric field in which the ions acquire supplementary speed.

In this work the slow ions, which are in experiments in ionospheric aerodynamics background for a remaining flow, were investigated with the aid of the multielectrode probe whose construction made it possible to isolate slow component and to study its characteristics, without introducing in them essential distortions. In particular, with the aid of multielectrode probe were determined energy of these ions and their concentration in flow at different modes of operation of the source of fast ions and the different pressures residual gas in vacuum chamber.

Conditions of experiment and measuring equipment. Experiments

were carried out in the ionospheric wind tunnel whose schematic diagram was shown on Fig. 1 or was in more detail described in works [5] and [6]. The flow of argon plasma was created with the aid of gas-discharge ionic source 1 with volumetric ionization, equipped with the filament of neutralization with 2. The diameter of flow in the section/shear of source was approximately 80 mm, the half-angle of the solution/opening of flow was equal tc approximately 15°. Energy of primary ions was equal to approximately 150 eV. These ion concentration was varied in the range 10^9-10^5 cm^{-3}.

Vacuum system consisted of metallic vacuum camera/chamber 3 by diameter 500 mm and length 2000 mm, forevacuum and oil-vapor pumps, and also the vapor trap of oil 4, filled by liquid nitrogen. the application/use of liquid nitrogen prevented the appearance of oil films on electrodes and made it possible thereby to improve the conditions of the work of probes and their characteristic.

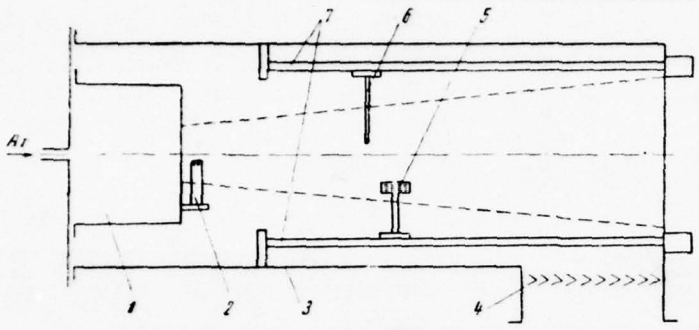


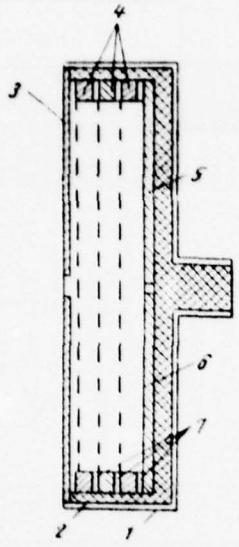
Fig. 1.

Page 34.

The parameters of the flow of the rarefied plasma were measured with the aid of thermal probes by 6 and Langmuir's flat/plane probes. All probes with the aid of coordinate spacer apparatuses 7 could be establish/installed at any point of flow.

In article [6] it was communicated about the results of the investigations of the work of multielectrode probe under conditions of the flow of the synthesized rarefied plasma and were noted the special feature/peculiarities of its characteristics with diagnostics of such flows. However, the multielectrode probe of normal design does not make it possible to measure the parameters of slow ions, since in this case to the collector/receptacle of probe come besides

slow also the fast ions, which give the contribution to the total current approximately to two order greater than slow; as a result low-energy ions virtually cannot be isolated from total current. As already mentioned above, the separation of ion flows out of probe is undesirable and it must be carried out within probe. For this purpose, in this work was used the method of the three-dimensional/space separation at basis of which lie/rests the fact that the fast ions in the multielectrode probe, oriented by their diaphragm in parallel to the axle/axis of flow, can fall only to one half of collector/receptacle 5 (see Fig. 1), if correspondingly is selected the geometry of input diaphragm, the depth of probe and its location with respect to ionic source, whereas slow ions, under the assumption of the approximately Maxwellian distribution of their speeds, must enter approximately evenly both halves. Thus, if collector/receptacle is is cut and is recorded current on that half, on which enter only slow ions, then it is possible to obtain the information about the parameters of this component. It goes without saying that probe in flow must be arrange/located so that to the opening/aperture in its input diaphragm could approach fast ions of all cells of the ion-optical system of the source (otherwise about diaphragm will arise shadow zone), i.e., probe must be located at a distance from the axle/axis of jet not smaller than a radius of the grids of source.



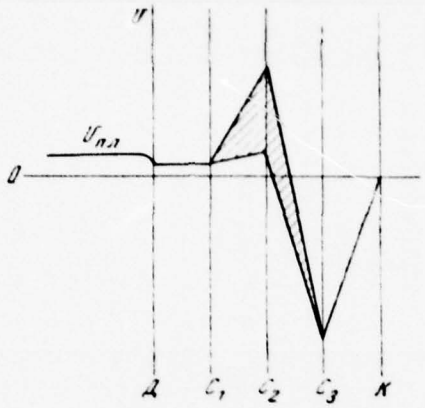


Fig. 2.

Fig. 3.

Page 35.

The construction of the multielectrode probe which was utilized in experiments, is schematically shown on Fig. 2. Probe consisted of metal housing 1, teflon bushing 2, input diaphragm 3, limiting the flow of charged particles inside probe, three flat/plane orthogonal grids 4 with the cells 0.1 x 0.1 mm, two collector/receptacles 5 and 6 and insulating teflon washers 7. Collector/receptacles were made from the stainless steel in the form of the simidiscs, divided

between themselves by clearance 0.2 mm in width. Flat/plane orthogonal grids were manufactured during rings from the tungsten filaments 0.01 mm in diameter. Diaphragm represented by itself fine/thin disk made of the stainless steel 0.5 mm in thickness with the slotted groove 31 x 3.8 m. Slotted groove in diaphragm and the clearance between collector/receptacles were side-by-side to each other. Diaphragm came into contact with grid C_1 (Fig. 3) and it was connected with it electrically, and the distance between the remaining electrodes of probe was 3 mm. The number of grids of probe was selected minimum, necessary for the cutoff of electrons and analysis of ions on energies. The space of cells in these grids was by an order of lesser Debye screening distance in plasma.

During the analysis of the slow ions of flow, was utilized, in essence, the circuit of potential distribution between the electrodes of probe, depicted on Fig. 3. It made it possible to carry out, as showed preliminary experiments, the most effective recording of these ions. On this circuit as zero, is accepted the potential of the wall of vacuum chamber, $U_{пл}$ — potential of plasma. Electronic component was intercept/detached by the electric field, created between grids C_2 and C_3, but the analyzing potential was applied to grid C_2. For the depression of secondary electron emission from collector/receptacle, the latter had the positive potential of relatively nearest electrode.

The electric field of input diaphragm and grid C_1 can substantially affect the penetration of charged particles inside probe, if the potential of given electrodes is different from the potential of plasma which, in turn, is known only approximately. Under these conditions for completely remove/taking the of energy distribution of slow ions, to diaphragm and grid C_1, was supplied the potential, close to the potential of plasma, but knowingly negative with respect to it. The housing of probe was found always under the floating potential. The supply of probe was realize/accomplished from batteries. Since there was an assumption that in the flows of plasma, created with the aid of ionic sources, can be present because of overcharging the slow ions, which have the concentration, comparable with the concentration of fast ions ($\sim 10^8$ cm^{-3}), and temperature, close to room, probe and registering apparatus were designed to that in order with confidence to record slow ions with such parameters.

Multielectrole probe was establish/installed at a distance by 40 mm from the axle/axis of the flow of plasma in such a way that its diaphragm was oriented in parallel to the axle/axis of flow, and long side of slotted groove in diaphragm was arrange/located perpendicular to this axle/axis. This orientation of probe eliminated the formation/education of shadow for fast ions about diaphragm and their

incidence/impingement to the collector/receptacle, arrange/located nearer to gas-discharge ionic source.

Let us examine a question concerning the effect of the geometry of the input electrodes of probe on the form of its volt-ampere characteristic.

Page 36.

In work [7] it was shown, that the input grid of probe does not in practice affect the form of characteristic, if the size/dimensions of its opening/apertures h and the thickness of rod d satisfy condition $h/d \geqslant 2$. In the conducted investigations this sense was equal to 10, and therefore this factor, as final thickness of grid, was not exerted a substantial influence on the results of measurements.

Another factor which can affect the form of voltage-current characteristic of multielectrode probe, is the relationship/ratio between the size/dimension of input diaphragm and collector/receptacle or any other the attract/tightening particles electrode after passage of which they with the probability, close to unit, fall to the collector/receptacle (for example, this electrode in the circuit, given to Fig. 2, is grid C_3). The value of this relationship/ratio determines the particle flux which goes out to the

side walls of probe. Since this flow is caused by the particles, which have the small component of velocity along the axle/axis of probe and considerable that composing speeds across this axle/axis, absence of particles with such components of the speed in flow to collector/receptacle can lead to the distortion of volt-ampere characteristic in the range of values of the analyzing potential, close to the potential of plasma.

If diaphragm fine/thin and the size/dimension of its inlet is small, then the second factor can be taken into account by introduction into formula for flow to the collector/receptacle of the value of the solid angle, at which the collector/receptacle is visible from the opening/aperture of diaphragm. However, in the general case integral transforms for the determination of particle flux must be carried out taking into account the finite dimensions of collector/receptacle and inlet in diaphragm. For the case when diaphragm fine/thin and radius R_0 of collector/receptacle is great in comparison with the sides of slot in diaphragm, these transforms for the flow of the Maxwellian particles to collector/receptacle whose energy, connected with motion along the axle/axis of probe, is more value $e\varphi$, they lead to the following expression:

$$N = n\sqrt{\frac{kT}{2\pi m}}\, S_D e^{-\frac{e\varphi}{kT}}\left(1 - \frac{1}{1+\frac{R_0^2}{z_0^2}}\, e^{-\frac{e\varphi}{kT}\frac{R_0^2}{z_0^2}}\right). \qquad (1)$$

Here m - mass of particles, n - their concentration, T - temperature,

k - Boltzmann constant, S_D — area of opening/aperture in diaphragm, R_0 - radius of collector/receptacle, z_0 - distance between the diaphragm and the collector/receptacle.

As already mentioned that the examined above factors most strongly distort volt-ampere characteristic of probe with the analyzing potentials, close to the potential of plasma, i.e., with $e\phi/kT \approx 0$. Under conditions of experiment this distortion, as show the estimations, carried out according to formula (1), it did not exceed 10o/o, which lie/rests at limits of accuracy of the measurements of the parameters of plasma by probe procedure.

The calculation of slow ion concentrations according to the characteristics of multielectrode probe was performed taking into account the transparency of the grids of probe α, which was determined from the method, described in work [8], and it was equal to 0.5 for the applied geometry of probe and distribution of potentials between its electrodes, and also for typical energy of slow ions.

Page 37.

Results of experiments. For obtaining the reliable information about the parameters of slow ions, were first of all studied the

characteristics of multielectrode probe. Were investigated the curved delays of ion current to the collector/receptacle, recording only slow ions, and to the collector/receptacle, accumulating besides slow also fast ions; were compared the results of the processing by the different methods of volt-amperes characteristic; there was studied the effect of the potentials of input diaphragm and grids of probe on the form of these characteristics.

Fig. 4a, gives on usual scale the characteristic, which shows the dependence of ion current to the collector/receptacle of the multielectrode probe, which accumulates only slow ions, from the analyzing potential U_a for the case when the potential of plasma about probe was equal to approximately 5 V the potential of diaphragm and grid C_1 it was 4 V, and the potential of grid C_3 was equal to -30 V. In Fig. 4b, this same the characteristic is constructed on semilogarithmic scale. Measurements were carried out at a distance of 52 cm from the section/shear of ionic source, pressure in vacuum chamber was approximately $8 \cdot 10^{-3}$ Pa.

As a result of processing voltage-current characteristic, depicted on Fig. 4a, with the potentials U_a, higher than the potential of plasma $U_{пл}$, can be determined, as is known, the values of the medium energy of particles in flow $\bar{E}$ and their concentration n. In the general case these values as follows are expressed through the

parameters, recorded by the multielectrode probe:

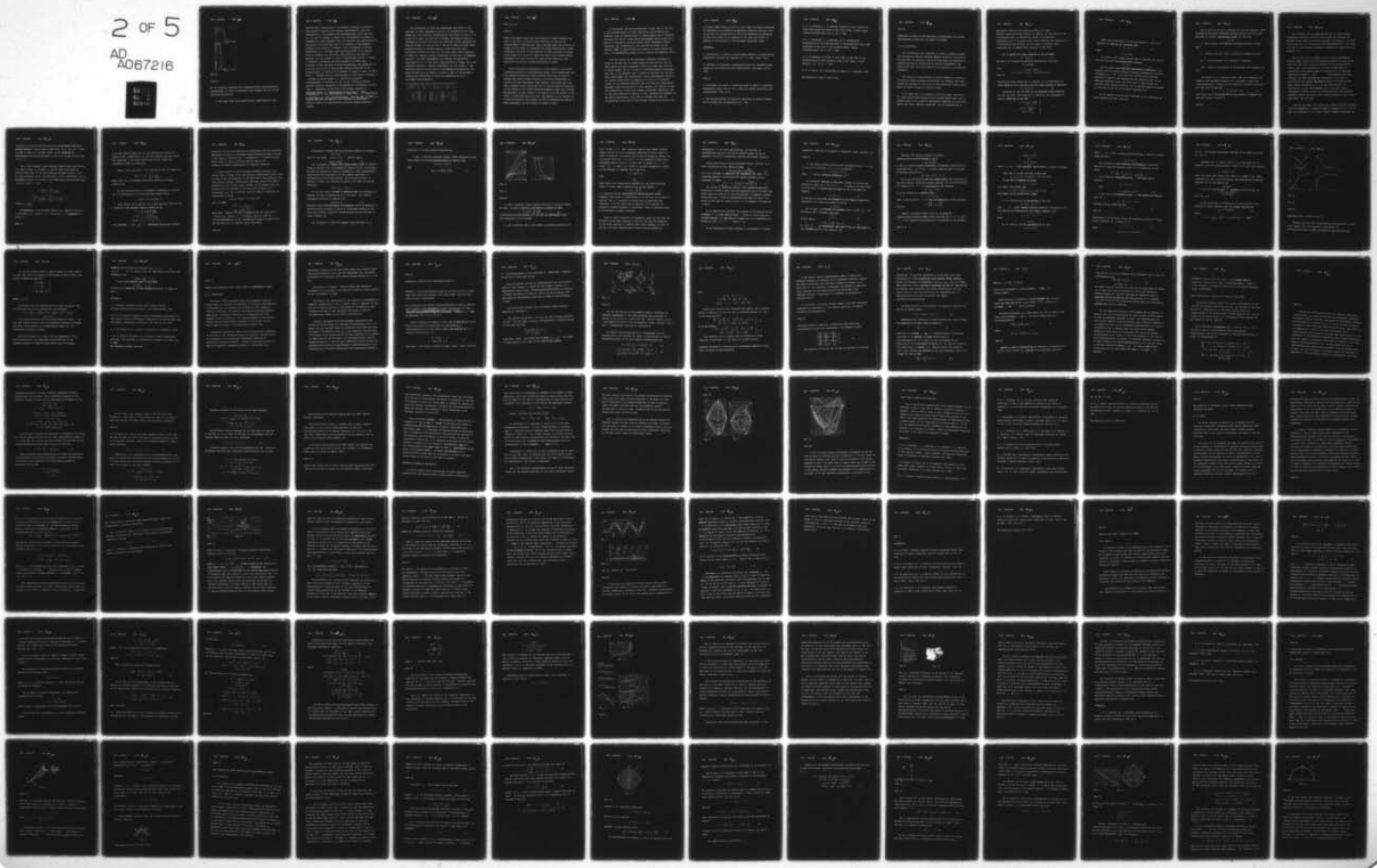
$$\bar{E} = \frac{e}{I_0} \int_0^{I_0} \varphi dI, \tag{2}$$

$$n = \frac{1}{\alpha} \sqrt{\frac{m}{2e^3}} \int_0^{\infty} \frac{dj}{d\varphi} \frac{d\varphi}{\sqrt{\varphi}} = \frac{1}{\alpha} \sqrt{\frac{2m}{e^3}} \int_0^{j'_0} \sqrt{\varphi}\, dj', \tag{3}$$

where I_0 - current to collector/receptacle with the analyzing potential, equal to the potential of plasma; ϕ - potential difference between analyzing electrode and plasma, e - electron charge, m - mass of particle, j - current density of particles for collector/receptacle, $j'_0 = dj/d\phi$ - value of this derivative with $\phi = 0$. In particular, during the Maxwellian distribution $\bar{E} = kT$.

AD-A067 216 FOREIGN TECHNOLOGY DIV WRIGHT-PATTERSON AFB OHIO F/G 20/4
SCIENTIFIC NOTES OF CENTRAL INSTITUTE OF AEROHYDRO DYNAMICS (SE--ETC(U)
JUN 78 A S FONAREV, A G ZAKHAROV
UNCLASSIFIED FTD-ID(RS)T-0679-78 NL

2 OF 5
AD A067216



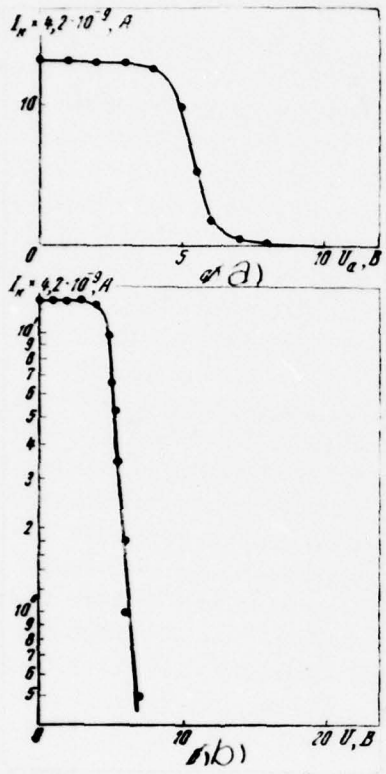


Fig. 4.

Page 38.

In the conducted investigations treatment/working voltage-currents characteristic of probe in accordance with formulas (2) and (3) was conducted graphically.

On the other hand, for determining the concentration of slow

ions and their temperatures it is possible to attempt to utilize a usual method of treating volt-amperes characteristic, since the characteristic, constructed on the semilogarithmic scale (see Fig. 4b), in range of values U_a, higher than the potential of plasma, it represents by itself straight line, and therefore the distribution of the falling into probe slow ions it is possible to approximately describe by the function of Maxwell, which corresponds to certain temperature T. It is logical that this description is not strict, since in actuality the slow ions, which appear in the flows in question, are not located in state of equilibrium; however, it makes it possible to determine the basic parameters of these ions, utilizing a usual procedure of probe measurements. The parameters of slow ions in the flow of the rarefied plasma, determined by the characteristics of probe by both methods, are given in table. In this table z - distance from the section/shear of ionic source to probe, p - pressure in vacuum chamber, A - results of processing characteristics on formulas (2) and (3), V - analogous results, obtained under the assumption of the Maxwellian distribution of slow ions, C - parameters of the flow of the plasma, measured by flat/plane probe, E - medium energy of slow ions, T - their "temperature", n - the concentration of these ions, T_e - temperature of electrons, n_0 - fast ion concentration. From the data of table, it follows that both the method of the treatment of experimental materials lead to the satisfactorily matching between themselves results.

The experiments in which was investigated the effect of the potential of input diaphragm and grid C_1 on recording of slow ions, showed that this potential created barrier for moving the ions, if it proved to be above the potential of plasma. The observed effect is explained by the fact that under the conditions of the experiment the distance between the rods of grid C_1 was by an order of lesser Debye screening distance; therefore electric field about this grid effectively affected the slow ions. In order under these conditions to obtain the complete energy distribution of slow ions, to diaphragm and grid C_1 in basic experiments, was supplied the potential U_D, approximately on 2-3 V the lower, than potential of plasma. As it was establish/installed in special experiments, at such values U_D the saturation current of slow ions for the collector/receptacle of the probe virtually did not depend on value U_D, what is the necessary condition for determining of these ion concentrations from volt-ampere characteristic.

z, см	$p \cdot 10^3$, (1)Па	A		B		C		n/n_e
		$\bar{E}$, К	$n \cdot 10^{-7}$, $см^{-3}$	T_i, К	$n \cdot 10^{-7}$, $см^{-3}$	T_e	$n \cdot 10^{-7}$, $см^{-3}$	
	5,2	16 700	1,2	18 100	1,4	15 300	1,7	~0,08
22	6,8	13 500	1,5	12 100	1,9	16 800	1,74	~0,1
	8,5	14 200	1,6	12 100	2,4	10 600	2,16	~0,1
	10,4	10 300	2,8	9 330	3,7	16 200	3	~0,13
52	8,5	9 100	1,5	8 700	2,2	13 100	1	~0,22

Key: (1). Pa.

Page 39.

These experiments showed that the potential of input diaphragm and grid C_1 does not in practice affect the form of that part of voltage-current characteristic which lie/rests above the potential of plasma and from which is determined the energy distribution of ions. Analogously the value of the potential of grid C_3 during its change in the range 10-50 V did not affect the form of the recorded energy distribution of slow ions and the value of the created by them saturation current the collector/receptacle of probe.

From volt-amperes characteristic of ion current to the second collector/receptacle of multielectrode probe, it was established that this collector/receptacle really receives fast ions, if probe is located near source. During removing it from the section/shear of source up to the sufficiently large distance, with which fast ions fell to probe at small angles and did not reach collector/receptacle, in the circuit of the second collector/receptacle there were recorded approximately the same values of the current as in the circuit of the first, to which fell only slow ions. The symmetry of the location of collector/receptacle with respect to slot in diaphragm was checked in these experiments via the rotation of probe on 180°.

In the present work the concentration of slow ions in the flow of the rarefied plasma and their temperature were measured with different value of pressure basin in vacuum chamber and at different distances from source. Before these measurements were recorded with the aid of flat/plane probe and thermal probe fundamental stream conditions and, in particular, the potential of plasma. In the measured value $U_{пл}$ was selected the potential of input diagram and grid C_1 of multielectrode probe. Grid C_3 usually had potential -30 V.

From the results of the experiments conducted, presented in table, it follows that the medium energy of slow ions in flow two order almost by exceeds analogous value for an inert gas (~0.03 eV) in vacuum chamber and it is close to the medium energy of electrons. This fact, it is probable that it attests to the fact that the slow ions, which appear with overcharging, obtain supplementary energy in the electric field which is present in the flow of the rarefied plasma. It was establish/installed also that slow ion concentration decreases along the axle/axis of flow; however, its relation to fast ion concentration in this case somewhat grow/rises, apparently, due to more rapid decrease of value n_0 in jet, caused by the expansion of jet and by overcharging. From table it follows that slow ion concentration in the flow of the rarefied plasma at the pressure gas

in vacuum chamber below $6.5 \cdot 10^{-3}$ Pa (i.e. under the normal conditions of experiment in ionospheric aerodynamics) comprises less than 10o/o of the fast ion concentration of flow, and therefore the background of slow ions exerts in the majority of the cases weak effect on shaping of the structure of the disturbed range about model.

REFERENCES

1. W.A.Clayden, C.V.Hurdle. An experimental study of a plazma-vehicle interaction. Rarefied Gas Dynamics, N.Y.- L, Acad. Press, 1967.

2. M.Sajben, D.L.Blumental. Experimental study of a rarefied plazma stream and its interaction with simple bodies. AIAA Paper, 69-79, 1969.

3. S.D.Hester, A.A.Sonin. A laboratory study of wakes of ionospheric sattellites. AIAA J vol. 6, No 6. (see also "rocket engineering and astronautics", 1970, No 6).

4. The characteristics of electrical discharges in magnetic fields. Ed. by Guthrie and R.W.Wakerling, N.Y, 1949.

5. V. V. Skvortsov, L. V. Nosachev. Analysis of the structure of trace after spherical models in the flow of the rarefied plasma. "space investigations", Vol. 6, No 2, 1968.

6. V. V. Skvortsov, L. V. Nosachev, Ye. N. Netsvetaylov. Investigation of the characteristics of multielectrode probe under conditions of the flow of the rarefied plasma. "space investigations", Vol. 7, No 3, 1969.

7. I. N. Moskalev. On effect of input grid on the form of the characteristics of the multigrid probe of the "jour. of tech. physics", Vol. 40, No 3, 1970.

8. O. V. Kozlov. The electroprobe in plasma. M., Atomizdat, 1969.

The manuscript entered 31/VIII 1972.

ESTIMATION OF CHANGE OF THE AMPLITUDE OF OSCILLATIONS IN A LINEAR TIME-DEPENDENT SYSTEM WITH ONE DEGREE OF FREEDOM.

V. A. Yaroshevskiy.

Are investigated some properties of linear oscillatory system with alternating/variable hardness. Primary attention is devoted to the case when the asymptotic method of determining the amplitude of oscillations becomes inapplicable in certain intermediate time interval and when the initial phase of oscillations is not strictly determined.

The solution of some problems of flight dynamics is reduced to the study of linear unsteady oscillations. For example, such tasks include the analysis of the motion of noncontrollable flight vehicle about the center of mass in unsteady flight.

It is known that it is possible to find the exact solution of the linear second order equation with variable coefficients only in special cases. If the equation describes the behavior of oscillatory system with slowly changing parameters, for the determination of

approximate solution very effective proves to be the Wentzel-Kramers-Brillouin method [1]. However, the evaluation of the accuracy/precision of VKB-sclution proves tc be difficult, furthermore, not it is always clear, which character has deviation of a VKB-solution from precise. Let us attempt to evaluate these deviations and to examine being inherent in them laws.

Let us examine the linear equation of the 2nd order:

$$y'' + f(t)y = 0. \qquad (1)$$

We search for formally the solution of equation in the form

$$y = A(t)\sin\varphi(t),$$

then

$$y' = A'\sin\varphi + A\cos\varphi\cdot\varphi',$$

$$y'' = A''\sin\varphi + 2A'\varphi'\cos\varphi - A\sin\varphi\cdot\varphi'^2 + A\cos\varphi\cdot\varphi''.$$

Page 42.

Substituting these expressions in equation (1) and equalizing the coefficients of sin φ and cos φ, we will obtain system of equations:

$$A'' - A\varphi'^2 + fA = 0, \qquad (2)$$

$$A\varphi'' + 2A'\varphi' = 0. \qquad (3)$$

Equations (2) and (3) still dc not determine unique solutions for A(t) and φ(t). This ambiguity is removed by the assignment of initial conditions in the form

$$\left.\begin{aligned} A(t_0) &= \sqrt{y^2(t_0) + \frac{y'^2(t_0)}{f(t_0)}}, \\ A'(t_0) &= 0, \\ \operatorname{tg}\varphi(t_0) &= \frac{y(t_0)\sqrt{f(t_0)}}{y'(t_0)}, \\ \varphi'(t_0) &= \sqrt{f(t_0)}. \end{aligned}\right\} \qquad (4)$$

From relationship/ratic (3) we will obtain $\varphi' = C/A^2$, and equation (2) acquires the following form:

$$A'' + fA - \frac{C^2}{A^3} = 0, \tag{5}$$

where

$$C^2 = f(t_0) A^4(t_0).$$

If function f(t) changes slowly, then in equation (5) term A'' can be disregarded and obtained VKB- sclution:

$$\left.\begin{aligned} fA^4 &= C^2, \\ \varphi' &= \sqrt{f}. \end{aligned}\right\} \tag{6}$$

Let us examine such case when applicability condition of the Wentzel-Kramers-Brillouin method on certain intermediate section is disrupted, i.e., f(t) is at first the positive slowly changing function of time, it then changes with the arbitrary form (it can take even negative values) and after this it again becomes the positive slowly changing function. One of the most effective methods in this case is the use of "standard" equations [2].

Let us examine the qualitative character of the difference for exact solution from VKB- sclution.

Let us note the analogy of equation (5) with the equation, which describes three-dimensional/space pendulum cscillations with small amplitude in variable gravitational field. In this case

$$f = \frac{ml}{J} g(t),$$

A - angle between the axle/axis of pendulum and the vertical line,

l - distance from the center of gravity to suspension point,

m, J - mass and moment of the inertia of pendulum,

g(t) - variable acceleration of gravity force (for example, see [3]).

If function f(t) > 0 changes slowly, then for determining the change in the amplitude of angle A it is possible to apply the relationship/ratio, obtained in the "theory of adiabatic invariants" [4] (see also [3] and [5]):

$$I = \int_{A_{min}}^{A_{max}} \frac{dA}{dt}(A)\, dA = \text{const}, \qquad (7)$$

where dA/dt (A) is determined during the solution of equation (5) with the "frozen" value of f.

Let us assume that the pendulum motion is at first regular precession relative to vertical line and that the function f(t) changes slowly. Then, as can easily be seen that integral I is equal to zero and by A it is determined from relationship/ratio (6). Thus, the case of quasi-regular precession corresponds to VKB-solution of equation (1).

Let now term f(t) in equation (5) on certain intermediate section change rapidly, so that relationship/ratio (7) here is not fulfilled. Then the solution of equation (5) on the last/latter section where relationship/ratio (7) again becomes used, it corresponds in the general case to fluctuations A of relatively "equilibrium" value $A_* = \sqrt{\frac{C}{f^{1/2}}}$. This "equilibrium" value coincides with VKB- solution and corresponds to the case of quasi-regular precession. The physical sense of transition from quasi-regular precession ($A = A_*$ on the first section) to oscillations (on the third section) lies in the fact that on intermediate section, during the rapid change f(t), the pendulum seemingly obtains the senses which derive/conclude it from rotation state about vertical line.

From the aforesaid it is clear that A ceases, strictly speaking, to be the "amplitude" of motion changes so rapidly as sin ϕ. Let us show that depending on the initial value of phase ϕ_0 amplitude the

variable y at one and the same value A_0, we can take on the third section different values within limits from $A_{min}(t)$ to $A_{max}(t)$, where A_{min} and A_{max} they are the outer limits, which correspond to oscillations alternating/variable A, and, as it is easy to show that $A_{min} A_{max} = A_0^2$.

Let in the process of quasi-periodic motion on the third section A it reach values A_{min} in point t_1. let us select this value of initial phase $\phi(t_0)$ on the first section, in order to $\phi(t_1) = \pi/2 + \pi n$. Then amplitude y will coincide with A_{min}. It is real/actual, let us determine a change in the phase ϕ for time, when A will increase from A_{min} to A_{max} $(t_1 < t < t_2)$:

$$\Delta\varphi = \int_{t_1}^{t_2} \frac{d\varphi}{dt}\, dt \approx \int_{A_{min}}^{A_{max}} \frac{C}{A^2} \frac{dA}{\frac{dA}{dt}(A)} =$$

$$= \int_{A_{min}}^{A_{max}} \frac{C}{A^2} \frac{dA}{\sqrt{\left(fA_{max}^2 + \frac{C^2}{A_{max}^2}\right) - \left(fA^2 + \frac{C^2}{A^2}\right)}} = \frac{\pi}{2},$$

$\left(\text{since } A_{min}^2 = \frac{C^2}{fA_{max}^2}\right)$.

Consequently, at the greatest value $A = A_{max}$ value $\phi = \pi n$ and $y = 0$, but when $A = A_{min}$ value $\phi = \pi n + \pi/2$, i.e., $y = \pm A_{min}$ depending on parity n.

If we move initial phase $\phi(t_0)$ on $\pi/2$, then we will obtain the opposite case - oscillation y on the third section they will occur with amplitude A_{max}. At other values $\phi(t_0)$ we will obtain the intermediate values of amplitude.

$\Delta\phi(t_0) = \Delta\phi_0$, then $\phi(t_1) = \pi/2 + \Delta\phi_0$ and at the low values $t-t_1$

$$\varphi(A) = \frac{\pi}{2} + \Delta\varphi_0 + \int_{A_{min}}^{A} \frac{C}{A^2} \frac{dA}{\frac{dA}{dt}(A)},$$

where dA/dt (A) is determined during the solution of "frozen" equation (5).

For the determination of the maximum of expression A sin ϕ(A) let us differentiate it on A and will make equal to zero:

$$\sin\varphi(\tilde{A}) + \tilde{A}\cos\varphi(\tilde{A})\frac{d\varphi}{dA}(\tilde{A}) = 0.$$

After solving this equation, let us find values of $\tilde{A}$ and $\tilde{\phi}$, that correspond to the maximum value of value $\tilde{A}$ sin $\tilde{\phi}$:

$$\tilde{A} = \frac{1}{k}\sqrt{\frac{C}{\sqrt{f}}}\sqrt{\frac{k^4 + \mathrm{tg}^2\Delta\varphi_0}{k^2 + \mathrm{tg}^2\Delta\varphi_0}},$$

$$\sin\varphi(\tilde{A}) = \frac{k^4 + \mathrm{tg}^2\Delta\varphi_0}{\sqrt{(k^2 + \mathrm{tg}^2\Delta\varphi_0)(1 + \mathrm{tg}^2\Delta\varphi_0)}},$$

$$\tilde{A}\sin\varphi(\tilde{A}) = \sqrt{\frac{C}{\sqrt{f}}}\frac{\sqrt{k^4\cos^2\Delta\varphi_0 + \sin^2\Delta\varphi_0}}{k}.$$

Here parameter $k = \frac{A_{min}}{A_*} = \frac{A_*}{A_{max}} < 1$ determines the maximum possible

difference for the true amplitude of oscillations from the amplitude, determined according to the Wentzel-Kramers-Brillouin method. During a slow change in function f(t) > 0 parameter k < 1 retains constant value, which is easy to perceive from the rule of the preservation/retention/maintaining of adiabatic invariant.

In many instances, which represent practical interest, the initial value of phase is not the strictly fixed/recorded value. then the task of the determination of the amplitude of oscillations on the third section acquires probabilistic character, since $\tilde{A} \sin \varphi(\tilde{A})$ is determined by the initial value of phase. Let us consider that the values of $\Delta\varphi_0$ are assigned in the range from by zero to $\pi/2$ equiprobable, and let us consider that the values of amplitude are proportional to value

$$\eta_1(\Delta\varphi_0, k) = \frac{\tilde{A}\sin\varphi(\tilde{A})}{A^*} = \frac{\sqrt{k^4\cos^2\Delta\varphi_0 + \sin^2\Delta\varphi_0}}{k}$$

(Fig. 1). Then

$$p(\eta_1) = \frac{2\eta_1}{\pi\sqrt{\eta_1^2 - k^2}\sqrt{\frac{1}{k^2} - \eta_1^2}}, \qquad (8)$$

$$M(\eta) = \frac{2}{\pi k} E(\sqrt{1-k^4}) \geqslant 1,$$

where E(u) - complete elliptic integral of the 2nd kind. With $k \to 1$ value $M(\eta) \to 1$, with $k \to 0$ value $M(\eta) \sim \frac{2}{\pi k}$, i.e., with the disturbance/breakdown of the evenness of a change in function f(t) the amplitude "on the average" always grow/rises.

Analogously is matter with the multipole moments, for example,

$$M(\eta^2) = \frac{1+k^4}{2k^2} \geqslant 1$$

(Fig. 2). For value $\ln \eta (|\ln \eta| \leqslant \ln \frac{1}{k})$ we will obtain

$$M(\ln \eta) = \ln \frac{1+k^2}{2k}. \qquad (9)$$

Let us attempt to examine some characteristic cases of "uneven" change in function f(t) on intermediate section and let us calculate for them the appropriate values of parameter k, which unambiguously characterizes the distribution of the probable amplitudes of oscillations on last/latter section. In principle for this, it suffices to obtain the solutions of equation (5) under the initial conditions

$$A^4(t_0) = \frac{C^2}{f(t_0)}, \quad A'(t_0) = 0.$$

At the same time it is easy to ascertain that the solutions of equation (5) can be expressed by $y_1(t)$ and $y_2(t)$ - the linearly independent solutions of equation (1):

$$A(t) = \sqrt{y_1^2 + y_2^2}. \qquad (10)$$

Therefore during the calculation of parameter k to it is possible or directly utilize an equation (5) or to investigate expression (10) taking into account asymptotic representations for the solutions of linear equation (1).

Let us examine at first the simplest cases for which it is

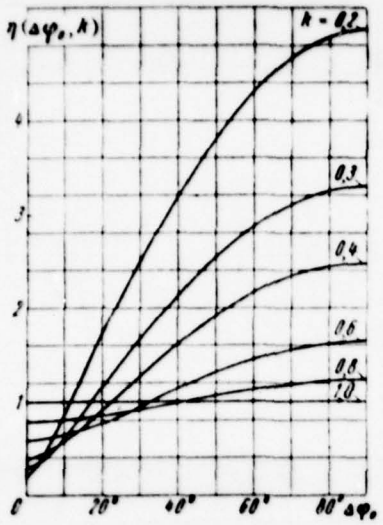
convenient to utilize directly equation (5).

1. F(t) - positive, piecewise smooth, slowly changing function which suffers discontinuity/interruption at certain point

$$f(\tilde{t}-0)=f_1,\ f(\tilde{t}+0)=f_2.$$

Then

$$k(\tilde{t}+0)=\min\left(\sqrt[4]{\frac{f_1}{f_2}},\sqrt[4]{\frac{f_2}{f_1}}\right). \qquad (11)$$



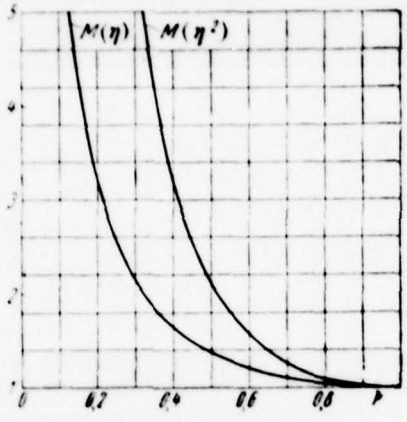


Fig. 1.

Fig. 2.

Page 46.

2. $f(t)$ - positive, slowly changing function, to which at moment of time t is added δ-function, multiplied by constant S. Then

$$\frac{1}{k}, k = \sqrt{1 + \frac{S^2}{4f}} \pm \frac{|S|}{2\sqrt{f}}. \qquad (12)$$

Conclusion/derivation formula (11) and (12) is sufficiently simple and therefore it is not brought.

3. Let us examine case of slow change in variable coefficient of

$f(t) = \omega^2(t)$, $\left|\frac{\omega'}{\omega^2}\right| \ll 1$. when asymptotic method gives almost accurate result, and let us try to determine correction of "first order" to value of amplitude, calculated with the aid of asymptotic method. Let us consider that with $t < t_0$ and $t > t_1$ the asymptotic method gives absolutely correct result (ω = const), but on section $t_0 < t < t_1$, value $\left|\frac{\omega'}{\omega^2}\right|$ is small. As a result of the made assumption we search for the solution of equation (5) in the form

$$A = A_0 + \delta A = \sqrt{\frac{C}{\omega}} + \delta A,$$

where

$$\left|\frac{\delta A}{A_0}\right| \ll 1.$$

Substituting this expression in equation (5) and reject/throwing smalls of higher order relative to δA, we will obtain

$$\delta A'' + 4\omega^2 \delta A = -\left(\sqrt{\frac{C}{\omega}}\right)''. \qquad (13)$$

i.e. functions δA are characteristic oscillation with double frequency with respect to oscillations y. By the way, on the basis of equation (13) it is possible to assume that δA grow/rises most intensely, if in the right side of equation (13) is present the harmonic of double frequency 2ω (resonance). This is confirmed based on the example of Mathieu functions.

Since is above introduced the assumption about the fact that the deviation of the exact solution of equation (5) from the asymptotic is low value, solution of equation with double frequency in terms of the fact will more insignificantly differ from the asymptotic.

Consequently, in the first approximation, the solution of nonhomogeneous equation (13) can be obtained during the use of asymptotic solution of homogeneous equation and Duhamel integral.

Taking into account initial conditions $\delta A(t_0) = \delta A'(t_0) = 0$, after integration we will obtain in parts

$$\delta A \approx \sqrt{\frac{C}{\omega(t)}} \int_{t_0}^{t} \cos\left[2\int_{\tau}^{t}\omega(u)\,du\right] \frac{\frac{d\omega}{d\tau}(\tau)}{2\omega(\tau)}\,d\tau. \qquad (14)$$

It is not difficult to ascertain that expression (14) with $t > t_1$ determines harmonic oscillations with double frequency 2ω and amplitude δA_m, where

$$\frac{\delta A_m}{\sqrt{\frac{C}{\omega(t)}}} \approx 1 - k = \left| \int_{t_0}^{t_1} \exp\left[2i\int_{\tau}^{t_1}\omega(u)\,du\right] \frac{\frac{d\omega}{d\tau}(\tau)}{2\omega(\tau)}\,d\tau \right|. \qquad (15)$$

As a result we obtain the formula, which characterizes small deviation of accurate result from the asymptotic and at the same time which gives the criterion of the applicability of asymptotic method [right side (15) it must be considerably less than the unit]. In a series of the cases of value t_0 and t_1, it is possible to replace by $-\infty$ and ∞.

If we describe the "slowness" of a change in the function by the parameter $\varepsilon = |f - f(\varepsilon t)|$, then with decrease ε value 1-k will vanish for analytic function $f(\varepsilon t)$ this tendency toward zero it is determined by a formula of type $A\exp(-B\varepsilon^{-n})$, where $n > 0$.

In the examination of other examples, it is possible to utilize

asymptotic properties of standard (" standard") linear equations [2].

Page 47.

4. Let slowly changing function f(t) be positive with $t < t_1$ and $t > t_2$, but in interval $t_1 < t < t_2$, is negative:

$$f(t) = \tilde{f}(\varepsilon t)(t - t_1)(t - t_2),$$

where ε — series expansion parameter, $\tilde{f}(\varepsilon t) > 0$.

As "standard" equation in this case, usually is utilized the equation of weber [1] $\tilde{y}'' + (\tilde{t}^2 - a^2)\tilde{y} = 0$. In exactly the same manner it is possible to utilize here for equation (5) as standard the equation

$$A'' + (\tilde{t}^2 - a^2)A = \frac{1}{A^3}. \tag{16}$$

of solution of which they are expressed as the linearly independent solutions of the equation of weber $\tilde{y}_1$ and $\tilde{y}_2$:

$$A = \sqrt{\tilde{y}_1^2 + \tilde{y}_2^2}.$$

Let us make a replacement of variables: $A(t) = u\tilde{A}(\tilde{t})$, $vdt = d\tilde{t}$. Selecting u and v in such a way, that

$$u^4 v^2 = C^2,$$

$$\frac{f}{v^2} = \tilde{t}^2 - a^2, \tag{17}$$

we will obtain:

$$\tilde{A}'' + \left[\tilde{t}^2 - a^2 + \frac{u'v'}{uv} + \frac{u''}{u}\right]\tilde{A} = \frac{1}{\tilde{A}^3}. \tag{18}$$

If $\left|\frac{u'v'}{uv} + \frac{u''}{u}\right|$ is considerably less than $\tilde{t}^2$ and a^2, then equation (18) transfer/converts into equation (16).

Equation (17) makes it possible to obtain communication/connection between t and $\tilde{t}$:

$$v = \frac{d\tilde{t}}{dt} = \sqrt{\frac{f(t)}{\tilde{t}^2 - a^2}}.$$

So that the radicand would be positive, is necessary satisfaction of conditions $\tilde{t}(t_1) = -a$, $\tilde{t}(t_2) = a$. These conditions make it possible to determine constant a:

$$\int_{t_1}^{t_2} \sqrt{-f(\tau)}\, d\tau = \int_{-a}^{a} \sqrt{a^2 - \tilde{\tau}^2}\, d\tilde{\tau} = \frac{\pi a^2}{2}.$$

It is not difficult to see that coefficients k for equations (5) and (18) coincide. Examining standard equation (16), we find solution of $\tilde{A}$ which with $\tilde{t} \longrightarrow \infty$ is determined by the formulas:

$$\tilde{A}(\tilde{t}) \approx \frac{1}{\sqrt[4]{\tilde{t}^2}}, \quad \tilde{A}'(\tilde{t}) \approx 0.$$

It is not difficult to ascertain that

$$\tilde{A} = \sqrt{\tilde{y}_1^2 + \tilde{y}_2^2},$$

where $\tilde{y}_1$ and $\tilde{y}_2$ with $\tilde{t} \longrightarrow \infty$ they are determined by VKB- solutions:

$$\tilde{y}_1 = \frac{\cos\frac{\tilde{t}^2}{2}}{\sqrt[4]{\tilde{t}^2}}, \quad \tilde{y}_2 = \frac{\sin\frac{\tilde{t}^2}{2}}{\sqrt[4]{\tilde{t}^2}}.$$

Page 48.

Further, utilizing Stokes' rule [1], we establish communication/connection between VKB- solutions with $\tilde{t} \longrightarrow \infty$ and $\tilde{t} \longrightarrow -\infty$. This communication/connection is determined by the formulas:

with $\tilde{t} \longrightarrow -\infty$

$$\tilde{y}_1 = \frac{K\cos\frac{\tilde{t}^2}{2} + L\sin\frac{\tilde{t}^2}{2}}{\sqrt[4]{\tilde{t}^2}},$$

$$\tilde{y}_2 = \frac{M\cos\frac{\tilde{t}^2}{2} + N\sin\frac{\tilde{t}^2}{2}}{\sqrt[4]{\tilde{t}^2}},$$

where K, L, M, N - some constants, which depend on Stokes' constants.

After this it is not difficult to show that

$$\frac{1}{k^2} = \frac{K^2 + L^2 + M^2 + N^2 + \sqrt{(K^2 + M^2 - L^2 - N^2)^2 + 4(KL + MN)^2}}{2}.$$

In the case in question we obtain

$$\frac{1}{k},\ k = \sqrt{1 + e^{\pi a^2}} \pm e^{\frac{\pi a^2}{2}}, \tag{20}$$

or, taking into account (19),

$$\frac{1}{k},\ k = \sqrt{1 + \exp\left[2\int_{t_1}^{t_2}\sqrt{-f(\tau)}\,d\tau\right]} \pm \exp\left[\int_{t_1}^{t_2}\sqrt{-f(\tau)}\,d\tau\right]. \tag{21}$$

Analogously let us examine other cases.

5. Let function f(t) be represented in the form

$$f(t) = \tilde{f}(\varepsilon t)\,[(t - t_*)^2 + b^2],$$

where $\tilde{f}(\varepsilon t)$ - slowly changing positive function. Coefficient k for this equation is determined by the formula, analogous (20):

$$\frac{1}{k},\ k = \sqrt{1 + e^{-\pi a^2}} \pm e^{-\frac{\pi a^2}{2}},$$

where

$$a^2 = b^2\sqrt{\tilde{f}(\varepsilon t_*)}.$$

6. Let function f(t) be represented in the form

$$f(t) = a^2 + e^{2bt}\,\tilde{f}(\varepsilon t),$$

where $\tilde{f}(\varepsilon t)$ — slowly changing positive function. Standard equation takes the form

$$\tilde{A}'' + (a^2 + e^{2bt})\tilde{A} = \frac{1}{\tilde{A}^3}$$

The solutions of this equation are expressed as the Bessel functions of apparent/imaginary order [3]. In summation, we will obtain

$$\frac{1}{k},\ k = \sqrt{1 + \frac{1}{\exp\left(\frac{2\pi a}{b}\right) - 1}} \pm \frac{1}{\sqrt{\exp\left(\frac{2\pi a}{b}\right) - 1}}.$$

7. Let f(t) at intermediate point t_* turn into zero or infinity:

$$f(t) = \tilde{f}(\varepsilon t)\,|t - t_*|^{2q-2},\ q > 0.$$

Then

$$\frac{1}{k} = \max\left\{\operatorname{ctg}\frac{\pi}{4q},\ \operatorname{ctg}\frac{\pi q}{4}\right\}. \tag{22}$$

8. Let f(t) at intermediate point t_* have symmetrical fracture (Fig. 3):

$$f(t) = \tilde{f}(\varepsilon t)\,\{a + b\,|t - t_*|\},\ b > 0,\ a \geq 0.$$

Standard equation takes the form

$$\tilde{A}'' + [c + |\tilde{t}|]\,\tilde{A} = \frac{1}{\tilde{A}^3}. \tag{23}$$

Page 49.

Coefficient k can be found, mating the solutions, calculated through Airy's functions [1], at point $\tilde{t} = 0$:

$$\frac{1}{k},\ k = \sqrt{1 + p^2} \pm p. \tag{24}$$

where

$$p = \pi\,[Ai(-c)\,Ai'(-c) + Bi(-c)\,Bi'(-c)],$$

Ai, Bi - the linearly independent solutions of the equation of Airy $w'' - tw = 0$.

Dependence $k(c)$ is given to Fig. 3. It is not difficult to ascertain that with large positive c value $k \approx 1$, with large negative c

$$\frac{1}{k} \approx 2 \exp\left[\int_{t_1}^{t_2} \sqrt{-f(\tau)}\, d\tau\right],$$

which will agree with formula (21); with c = 0 value $k = \frac{1}{\sqrt{3}}$, which coincides with (22). during transition from equation (5) to standard equation (23) we will obtain that

$$c = \frac{a\,[\tilde{f}(\varepsilon t_*)]^{1/3}}{b^{2/3}}.$$

9. Let f(t) have at point t_* asymmetric fracture (Fig. 4):

$$f(t) = \tilde{f}(\varepsilon t)\,|a - b(t - t_*)| \text{ при } t < t_*,$$
$$f(t) = \tilde{f}(\varepsilon t)\, a \text{ при } t > t_*$$
$$(a > 0, \quad b > 0).$$

Key: (1). with.

In this case value k is determined via the coupling of the solution of Airy's equation with the harmonic oscillations

$$\frac{1}{k}, \quad k = \frac{\sqrt{u+2} + \sqrt{u-2}}{2}, \tag{25}$$

where

$$u = \sqrt{c}\, z^2(c) + \frac{1}{\sqrt{c}\, z^2(c)} + \frac{z'^2(c)}{\sqrt{c}}, \quad z(c) = \sqrt{\pi\,[Ai^2(c) + Bi^2(c)]}, \quad c = \frac{a f(\varepsilon t_*)^{1/3}}{b^{2/3}}.$$

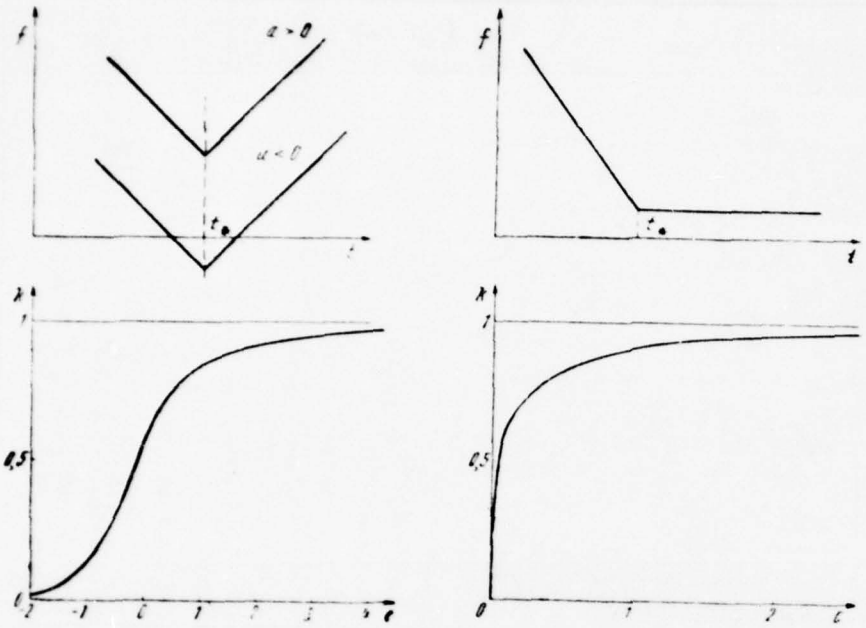


Fig. 3.

Fig. 4.

Page 50.

Dependence k(c) is given to Fig. 4.

Formulas (24) and (25) can be used for the estimation of error, which appears with the inaccurate approximation of alternating/variable hardness (piecewise-linear approximation.)

10. Let f(t) undergo series of abrupt changes at random moment of time. then after the passage of these jumps we obtain taking into account formulas (9) and (11):

$$\left.\begin{aligned} \ln\frac{A}{A_*} &= \sum_{i=1}^{n}\ln r_{ki}, \\ \left(\ln\frac{A}{A_*}\right)_{\max} &= \sum_{i=1}^{n}\ln\frac{1}{k_i}, \\ M\left(\ln\frac{A}{A_*}\right) &= \sum_{i=1}^{n}\ln\frac{1+k_i^2}{2k_i}. \end{aligned}\right|$$

where $\frac{1}{k_i}=\sqrt[4]{\frac{f_{\max i}}{f_{\min i}}}$.

If function f(t) vary monotonically and jumps are small, then the extracted sums can be replaced with the integrals:

$$\left(\ln\frac{A}{A_*}\right)_{\max}=\sum_{i=1}^{n}\ln\frac{1}{k_i}\approx\frac{1}{4}\sum_{i=1}^{n}\ln\left(1+\frac{\Delta f_i}{f_i}\right)\approx\frac{1}{4}\sum_{i=1}^{n}\frac{\Delta f_i}{f_i}\approx\frac{1}{4}\int\frac{df}{f}=\frac{1}{4}\ln\frac{f_{\max}}{f_{\min}},$$

$$M\left(\ln\frac{A}{A_*}\right)\approx 0.$$

It is logical that the law of the distribution of value r_{ki} in this case differs from the law of distribution, described by formula (8). With a large quantity of "commensurable" jumps, the law distribution is close to normal.

From the aforesaid it is clear that the replacement of the smooth function f(t) the determining change hardness, to the piecewise constant can lead to large errors. Let, for example,

function f(t) monotonically decrease from $f_{max}(t = t_0)$ to $f_{min}(t = t_1)$. Let us consider that the true solution coincides with asymptotic. Then

$$\ln \frac{A(t_1)}{A(t_0)} = \ln \frac{A_+(t_1)}{A(t_0)} = \frac{1}{4} \ln \frac{f_{max}}{f_{min}}$$

Stepped approximation leads to the result

$$\left| \ln \frac{A(t_1)}{A(t_0)} \right|_{max} = \frac{1}{2} \ln \frac{f_{max}}{f_{min}},$$

although the probability of this deviation is small, if jumps are small.

REFERENCES

1. J. Kheding. introduction into phase integral method (Wentzel-Kramers-Brillouin method) . M., "peace/world", 1965.

2. A. A. Dorodnitsyn. Asymptotic laws of eigenvalue distribution for some special forms of differential equations of the second order. The "successes of mathematical sciences", Vol. VII, iss. 6, 1952.

4. L. D. Landau, Ye. M. Lifschitz. Mechanics. M., Fizmatgiz, 1958.

5. V. M. Volosov. Averaging in the systems cf usual differential equations. The "successes of mathematical sciences", Vol. XVII, iss. 6, 1962.

The manuscript entered 1/IX 1972.

Page 51.

METHOD OF CALCULATION OF THE ELASTIC WAVES IN HETEROGENEOUS BEAMS.

I. A. Lyakhovenko.

For tasks of the transverse waves in heterogeneous along the length beams, are obtained the equations of the type of the equations of Timoshenko and is described the algorithm of their numerical solution on the basis of method of characteristics during different combinations of boundary conditions. As illustration are given examples of the calculation of the hinged supported on two supports conical beam and uniform beam, supported at one end and free on other, under the effect of the distributed dynamic load.

Transverse vibrations of beams are investigated most frequently on the basis of the engineering theory of curvature, moreover during the derivation of the fundamental differential equation of oscillations (equations bernulli - EyleraZ in the cross sections of beam are eliminated compliance/pliability to shift/shear and

longitudinal inertial forces. With sufficiently long flexural waves the factors indicated do not play the significant role, but during the decrease of wavelength, their effect becomes deciding [1] - [3], [9].

Deficiencies in Bernulli - Euler's theory were removed by Timoshenko via the account of the shearing strains and rotary inertia of the cell/elements of beam.

The field of the applicability of the equations of Timoshenko is inspected theoretically by Ye. S. Sorokin and A. S. Arkhipov [4] with the aid of precise equations of the theory of the elasticity (was considered the task of free transverse vibrations of beam as two-dimensional problem of the theory of elasticity).

Reliable experiments with high-frequency oscillations were carried out by the method of holographic interferometry [5]. It is shown, that the obtained forms and frequencies will agree well with the theory of Timoshenko's beam up to the lengths of the half-waves of the order of the height/altitude of beam. Therefore it is possible to expect that and for the beams of alternating/variable section, examine/considered in this article, Timoshenko's theory provides the acceptable for practical target/purposes accuracy/precision of the determination of internal effort/forces and displacement/movements.

Fundamental equations for heterogeneous beams [1].

FOOTNOTE [1]. Under heterogeneous beams, as in work [6], let us imply beams with alternating/variable over their length rigid and mass characteristics. ENDFOOTNOTE.

Let us designate the complete sagging/deflection of beam in section with coordinate x at the moment of time t through w(x, t), that comprises sagging/deflection from bending - through $w_u(x, t)$, and from shift/shear - through $w_\tau(x, t)$. then we can write: $w(x, t) = w_u(x, t) + w_\tau(x, t)$.

angle β between the tangent to bent axle of beam and the X-axis without the account of shift/shear is defined as $\partial w_u/\partial x$. Relationship/ratios for the bending moment and shearing force in section x take form [1, 7]:

$$\left.\begin{aligned} M &= EI(x)\frac{\partial \varphi}{\partial x}, \\ Q &= -kGF(x)\left(\frac{\partial w}{\partial x} - \beta\right). \end{aligned}\right| \qquad (1)$$

Here EI(x) - the flexural rigidity of beam; kGF(x) - shear stiffness

(G - the module/modulus of the 2nd kind); k - coefficient, depending on the form of structural section.

Work [8] examines the task of determination k for the different forms of cross section. It turned out that values k lie/rest at a comparatively narrow range. Indeterminancy/uncertainties in selection k, consist the authors of work [8], not at all are so serious with that degree of approximation which has the model of the shift/shear of beam.

It will be here accepted that k is certain weakly-changing function of coordinate x.

For positive directions x, w, M, Q, q*, let us accept indicated in Fig. 1 (in left upper to angle). The equations of equilibrium take in this case the form

$$\left.\begin{aligned} \frac{\partial Q}{\partial x} + m(x)\frac{\partial^2 w}{\partial t^2} = q^*(x, t), \\ \frac{\partial M}{\partial x} - Q - I_\rho \frac{\partial^2 \beta}{\partial t^2} = 0. \end{aligned}\right| \qquad (2)$$

Here $m(x) = \rho F(x)$ - the linear mass of beam; $I_\rho(x) = \rho I(x)$ - the moment of mass inertia of the layer of the beam of unit length.

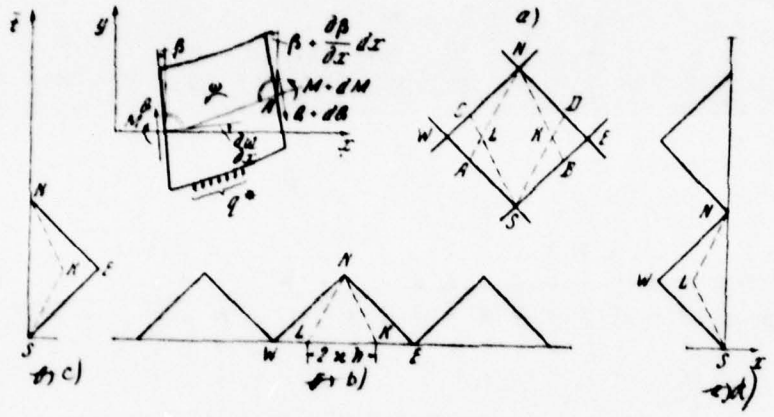


Fig. 1.

Page 53.

For the calculation of heterogeneous beams is convenient to represent expressions of the cross-sectional area and moment of inertia in the form $F(x) = F_0 f(x)$ and $I(x) = I_0 i(x)$, where F_0 and I_0 - some amplitude values of the corresponding values (constant), but f and i - dimensionless functions of coordinate x.

We convert relationship/ratios for torque/moment and the shearing force, also equation (2) after the substitution in them of relationship/ratios (1) to the following dimensionless form:

$$\bar{M} = i(\bar{x})\frac{\partial\beta}{\partial\bar{x}}, \quad \bar{Q} = -\varkappa^2(\bar{x}) f(\bar{x})\left(\frac{\partial\bar{w}}{\partial\bar{x}} - \beta\right); \tag{3}$$

$$\left.\begin{aligned} &\frac{\partial}{\partial\bar{x}}\left[\varkappa^2(\bar{x}) f(\bar{x})\left(\frac{\partial\bar{w}}{\partial\bar{x}} - \beta\right)\right] - f(\bar{x})\frac{\partial^2\bar{w}}{\partial\bar{t}^2} = -\bar{q}^*(\bar{x}, \bar{t}); \\ &\frac{\partial}{\partial\bar{x}}\left[i(\bar{x})\frac{\partial\beta}{\partial\bar{x}}\right] + \varkappa^2(\bar{x}) f(\bar{x})\left(\frac{\partial\bar{w}}{\partial\bar{x}} - \beta\right) - i(\bar{x})\frac{\partial^2\beta}{\partial\bar{t}^2} = 0. \end{aligned}\right| \tag{4}$$

Here

$$\bar{w} = \frac{w}{r_0}; \quad \bar{x} = \frac{x}{r_0}; \quad \bar{t} = \frac{t}{\tau_0};$$
$$\bar{M} = \frac{M}{EI_0/r_0}; \quad \bar{Q} = \frac{Q}{EI_0/r_0^2}; \quad \bar{q}^* = \frac{q^*}{EI_0/r_0^3};$$
$$r_0 = \sqrt{\frac{I_0}{F_0}}; \quad \tau_0 = \frac{r_0}{c_0}; \quad c_0 = \sqrt{\frac{E}{\rho}}; \quad \varkappa^2(\bar{x}) = \frac{k(\bar{x})\,G}{E}.$$

Omitting the feature above dimensionless symbols, let us present system of equations (4) for the case of continuous change of f and i in the following form:

$$\left.\begin{aligned} \frac{\partial^2 w}{\partial x^2} - \frac{1}{\varkappa^2(x)}\frac{\partial^2 w}{\partial t^2} &= \frac{\partial \beta}{\partial x} - A(x)\left(\frac{\partial w}{\partial x} - \beta\right) - \frac{1}{\varkappa^2(x)} P(x, t); \\ \frac{\partial^2 \beta}{\partial x^2} - \frac{\partial^2 \beta}{\partial t^2} &= -C(x)\left(\frac{\partial w}{\partial x} - \beta\right) - B(x)\frac{\partial \beta}{\partial x}. \end{aligned}\right| \quad (5)$$

It is here marked

$$\left.\begin{aligned} A(x) &= \frac{1}{f(\bar{x})}\frac{df(\bar{x})}{\partial x} + \frac{2}{\varkappa(\bar{x})}\frac{\partial \varkappa(\bar{x})}{\partial \bar{x}}, \quad B(x) = \frac{1}{i(\bar{x})}\frac{\partial i(\bar{x})}{\partial \bar{x}}, \\ C(x) &= \varkappa^2(\bar{x})\frac{f(\bar{x})}{i(\bar{x})}, \quad P(x, t) = \frac{\bar{q}^*(\bar{x}, \bar{t})}{f(x)}. \end{aligned}\right| \quad (6)$$

From equations (4) as special case are obtained the known equations of Timoshenko for the beams of constant section.

NUMERICAL ALGORITHM OF THE SOLUTION OF FUNDAMENTAL EQUATIONS ON THE BASIS OF METHOD OF CHARACTERISTICS.

In the general case for heterogeneous beams, to obtain the analytical solution of equations (5) is impossible; therefore appears the task of developing the algorithm of numerical solution. As is known [for 1], the equations of Timoshenko are related to hyperbolic type; therefore for the construction of the algorithm of the numerical solution of equations it is possible to use method of characteristics.

It is logical to consider unknown values w and β the continuous functions of coordinates x, t the derived which they can undergo discontinuity/interruptions.

Page 54.

For those ranges of planes xt, in which the first particular derivatives of w and β are continuous, it is possible to press

$$\left.\begin{aligned} d\left(\frac{\partial w}{\partial x}\right) &= \frac{\partial^2 w}{\partial x^2}\,dx + \frac{\partial^2 w}{\partial x \partial t}\,dt; \\ d\left(\frac{\partial w}{\partial t}\right) &= \frac{\partial^2 w}{\partial x \partial t}\,dx + \frac{\partial^2 w}{\partial t^2}\,dt; \\ d\left(\frac{\partial \beta}{\partial x}\right) &= \frac{\partial^2 \beta}{\partial x^2}\,dx + \frac{\partial^2 \beta}{\partial x \partial t}\,dt; \\ d\left(\frac{\partial \beta}{\partial t}\right) &= \frac{\partial^2 \beta}{\partial x \partial t}\,dx + \frac{\partial^2 \beta}{\partial t^2}\,dt. \end{aligned}\right\} \qquad (7)$$

Six Equations (5) and (7) can be used for definition six second

derivatives, if functions themselves w, β and their first-order derivatives are assign/prescribed along certain curved. However, during the assignment of functions w, β, $\partial w/\partial x$, $\partial w/\partial t$, $\partial\beta/\partial x$, $\partial\beta/\partial t$ along some directions of the solution of equations (5) and (7) they will be not defined. Such directions are called characteristic, and the lines, which go along such directions, by characteristics. On characteristics the second derivatives can undergo discontinuity/interruptions.

On characteristics the determinant Δ of system of equations (5) and (7) is equal to zero:

$$\Delta = (dt^2 - dx^2)\left(dt^2 - \frac{1}{x^2}\,dx^2\right) = 0. \qquad (8)$$

Equalizing zero expression in first brackets (8), we will obtain the equations of straight lines on plane xt:

$$\frac{dx}{dt} = \pm 1, \qquad (9)$$

which let us call/name c_1^+ and c_1^- - characteristics. Along these directions it is possible to obtain characteristic relationship/ratios, if we equate to zero determinant of the matrix/die of the coefficients of system (5), (7) with the column of the coefficients of unknown $\partial^2\beta/\partial x^2$, substituted for the column of right sides. Opening the obtained in this way determinant taking into account (9), let us find

$$d\left(\frac{\partial\beta}{\partial t}\right) \mp d\left(\frac{\partial\beta}{\partial x}\right) \pm R_1\,dx = 0, \qquad (10)$$

where $R_1 = -C(x)\left(\frac{\partial w}{\partial x} - \beta\right) - B(x)\frac{\partial \beta}{\partial x}$.

upper signs correspond to characteristic c_1^+, lower - to characteristic c_1^-.

Equalizing zero expression in second brackets (8), we will obtain the equations of the curves $dx/dt = \pm \varkappa(x)$, which let us call/name c_2^+ and c_2^- - characteristics.

Determining further $\partial^2 w/\partial x^2$ from system (5), (7), we obtain, that along characteristics c_2^+ and c_2^- are valid respectively the relationship/ratios

$$d\left(\frac{\partial w}{\partial t}\right) \pm \varkappa d\left(\frac{\partial w}{\partial x}\right) \mp \varkappa R_2\, dx = 0, \tag{11}$$

where

$$R_2 = \frac{\partial \beta}{\partial x} - A(x)\left(\frac{\partial w}{\partial x} - \beta\right) - \frac{1}{\varkappa^2} P(x, t).$$

Page 55.

Equality to zero of denominators and numerators in solutions for $\partial^2 w/\partial x \partial t$, $\partial^2 w/\partial t^2$, $\partial^2 \beta/\partial x \partial t$, $\partial^2 \beta/\partial t^2$ reduces to the equations, identical

(10) and (11). Since are examined only continuous w and β, then the relationship/ratios

$$\left.\begin{aligned} dw &= \frac{\partial w}{\partial x}\,dx + \frac{\partial w}{\partial t}\,dt, \\ d\beta &= \frac{\partial \beta}{\partial x}\,dx + \frac{\partial \beta}{\partial t}\,dt \end{aligned}\right| \qquad (12)$$

are valid along any direction of plane xt. In those ranges of planes xt, in which the first derivatives of w and β are continuous, relationship/ratios (10)-(12) represent by themselves system of equations and can be used for the determination of six unknowns w, β, $\partial w/\partial x$, $\partial w/\partial t$, $\partial \beta/\partial x$, $\partial \beta/\partial t$, if are assign/prescribed the corresponding boundary and initial conditions.

For the numerical solution of this system, let us construct on plane xt the grid of characteristics. Since we deal with the family of four one-parameter families of lines - the characteristics of positive and negative slope/inclination, then, generally speaking, it is possible the grid of two performance characteristics to construct independently one of another. Then the values of the unknown functions in mesh points are determined with the aid of complex interpolations that it leads, in the final analysis, to the loss of the accuracy/precision of results. Is expedient therefore on plane xt to first construct the grid of characteristics $dx = \pm dt$ with space h, and then characteristics $dx = \pm \varkappa dt$ to enter in basic grid, set/assuming in this case within the limits of one cell $\varkappa$ of constant ^{1}.

FOOTNOTE 1. Since on the sections of a continuous change in structural section value k and, consequently, also x they are little affected, the adopted assumption does not lead to essential errors. ENDFOOTNOTE.

Then interpolation formulas are single for all cells.

Calculation formulas taking into account recalculation let us find for the arbitrary cell ESWN (see Fig. 1A). Segments of the lines WN and SE - characteristic of the first family, NE and SW - characteristic of the second family. Through points N and S, let us conduct by the dotted lines of characteristic of third (AN and SD) and fourth (CS and NB) families.

Let us introduce designations $\partial w/\partial x = p$, $\partial w/\partial t = q$, $\partial\beta/\partial x = u$, $\partial\beta/\partial t = v$ and let us rewrite in the following form of the system characteristics and the corresponding to them relationship/ratios along the characteristics:

$$\left.\begin{aligned}
&\frac{dx}{dt} = 1, \quad dv - du = [C(x)(p-\beta) + B(x)u]\,dt, \quad d\beta = (v+u)\,dt;\\
&\frac{dx}{dt} = -1, \quad dv + du = [C(x)(p-\beta) + B(x)u]\,dt, \quad d\beta = (v-u)\,dt;\\
&\frac{dx}{dt} = \varkappa, \quad dq - \varkappa dp = -\varkappa^2\left[u - A(x)(p-\beta) - \frac{1}{\varkappa^2}P(x,t)\right]dt,\\
&\qquad\qquad dw = (q+\varkappa p)\,dt;\\
&\frac{dx}{dt} = -\varkappa, \quad dq + \varkappa dp = -\varkappa^2\left[u - A(x)(p-\beta) - \frac{1}{\varkappa^2}P(x,t)\right]dt,\\
&\qquad\qquad dw = (q-\varkappa p)\,dt.
\end{aligned}\right| \qquad (13)$$

Page 56.

Differential relationship/ratios (13) along the appropriate characteristics one should replace with the approximate difference expressions. From the obtained thus system of the algebraic equations are determined the unknowns u, p, v, β, q and w at point N through the values of these functions (with the use of linear interpolation) in assemblies W, S and E of the cell of the basic grid of characteristics. Let us note in this case that in the process of the composition of the difference expressions, which replace differential (13), the values of quantities, which stand in brackets in the right sides of relationship/ratios (13), on the appropriate cuts of characteristics are replaced mean arithmetic from the extreme values on these cuts. This procedure of obtaining calculation formulas is equivalent to the recalculation which, as is known [for 10], raises

accuracy/precision by one order. Omitting cumbersome algebraic calculations, let us extract final calculation formulas for the arbitrary internal (field) point of the range of variables (x, t):

$$u_N = u_S + v_E - v_W;$$
$$p_N = p_S + q_E - q_W;$$
$$v_N = \frac{1}{1+\frac{C_S h^2}{4}}\left\{v_S - \frac{C_S h^2}{4}(v_S + v_W + v_E) + \right.$$
$$+ \frac{C_S h}{2}(p_N + p_S - 2\beta_S) + u_E - u_W + \frac{h}{2}[B_S(u_N + u_S) +$$
$$\left. + C_E(p_E - \beta_E) + C_W(p_W - \beta_W) + B_E u_E + B_W u_W]\right\};$$
$$\beta_N = \beta_S + \frac{h}{2}(v_N + v_W + v_S + v_E);$$
$$q_N = q_S + \varkappa^2[p_E - \beta_E - (p_W - \beta_W)] + \frac{h}{2}\{P_N + P_S +$$
$$+ P_W + P_E + A_S[q_E - q_W - (\beta_N - \beta_S)] + A_E(p_E - \beta_E) + A_W(p_W - \beta_W);$$
$$w_N = w_S + \frac{h}{2}(q_N + q_S + q_W + q_E).$$

Let us extract formulas for the points of boundary of the region xt. Let us examine at first half-cell WNE, which adjoins boundary of t = 0 (see Fig. 1b). Let at the initial moment the beam rest and the voltage/stresses in it were equal to zero. In this case

$$w = \frac{\partial w}{\partial x} = \frac{\partial w}{\partial t} = \beta = \frac{\partial \beta}{\partial x} = \frac{\partial \beta}{\partial t} = 0. \qquad (14)$$

After replacing relationship/ratios (13) along the appropriate characteristics by difference expressions and after solving taking into account (14) obtaining in this way algebraic system of equations, let us find:

$$u_N = p_N = v_N = \beta_N = 0;$$
$$q_N = \frac{h}{2}\left(P_N + \frac{P_W + P_E}{2}\right);$$
$$w_N = \frac{h}{2}\, q_N.$$

Let us extract the formulas, valid on the left and right boundaries of the region of the variables xt. Fig. 1c, d, depicts half-cells SEN and SWN, which adjoin the appropriate boundaries.

Page 57.

Let us examine the case of the hinged support of beam on both ends and the case when one end of the beam is supported, another is free. On tip bearings the shift, speed and the bending moment are equal to zero, therefore,

$$w_S = q_S = u_S = w_N = q_N = u_N = 0. \qquad (15)$$

Representing in the difference form of relationship/ratio (13) along the appropriate characteristics and solving taking into account (15) that obtaining in this way algebraic system of equations, let us find for the points of the left boundary

$$p_N = p_S + 2q_E;$$

$$v_N = v_S + \frac{1}{1+\frac{C_S h^2}{4}}\left\{2u_E + h[C_E(p_E - \beta_E) + B_E u_E] + C_S h(p_S + q_E - \beta_S) - \frac{C_S h^2}{4}(v_E + v_S)\right\};$$

$$\beta_N = \beta_S + \frac{h}{2}(v_N + v_S + 2v_E).$$

Analogous formulas for the points of the right boundary:

$$p_N = p_S - 2q_W;$$

$$v_N = v_S + \frac{1}{1+\frac{C_S h^2}{4}}\left\{-2u_W + h[C_W(p_W - \beta_W) + B_W u_W] + \right.$$

$$\left. + C_S h(p_S - q_W - \beta_S) - \frac{C_S h^2}{2}(v_W + v_S)\right\};$$

$$\beta_N = \beta_S + \frac{h}{2}(v_N + v_S + 2v_W).$$

Let us extract finally formulas for the case when the right end of the beam ($x = \lambda$) is free. At free end the torque/moment and the shearing force are equal to zero, therefore,

$$u_N = u_S = p_N - \beta_N = p_S - \beta_S = 0. \qquad (16)$$

Utilizing equality (16) and relationship/ratios (13), written in difference form along the appropriate characteristics, let us find:

$$v_N = v_S - 2u_W + h[C_W(p_W - \beta_W) + B_W u_W];$$

$$\beta_N = \beta_S + \frac{h}{2}(v_N + v_S + 2v_W);$$

$$p_N = \beta_N;$$

$$q_N = q_S + \varkappa^2(p_N - 2p_W + p_S) - \varkappa^3 h[u_W - A_W(p_W - \beta_W)] +$$

$$+ \varkappa^3 h P_W + \frac{\varkappa^2 h}{2}(2-\varkappa)(P_N + P_S);$$

$$w_N = w_S + \frac{\varkappa h}{2}\left[p_N - p_S + 2q_W + \frac{2-\varkappa}{\varkappa}(q_N + q_S)\right].$$

Analogously can be obtained formulas also for other forms of boundary conditions.

The derived formulas make it possible step by step to find at each point N of the grid of characteristics on plane the alternating/variable xt six unknown functions u, p, v, β, q, w. In this case, dimensionless the torque/moment and the shearing force at point N are determined from formulas (3).

On the basis that presented for ETsVM BESM-6, is comprised the program of the calculation of strains and stresses in heterogeneous beams under the action of dynamic loads.

Page 58.

Initial data tasks, such as load, rigid and mass characteristics, are assigned in the form of tables for the specific number of sections.

The intermediate values of the corresponding values are calculated with the aid of interpolation. The space of integration is selected at programmer's discretion, which makes it possible by changing the space and repeated calculation to estimate the accuracy/precision of numerical solution. This estimation can be carried out on the formulas, indicated in work [10].

Let us designate through λ_n the elongation of half-wave (if λ - elongation of entire beam, n - number of half-waves into which is divide/marked off the beam during transverse vibrations with n half-waves, then $\lambda_n = \frac{\lambda}{n}$). The space of integration must be sufficient small in comparison with the length of the half-wave of the high of the harmonics, that contributes to the total effect of waves the significant contribution. It is possible to show that for the correct account of harmonic with the length of the half-wave, equal to λ_n, the assigned/prescribed space h must be less λ_n approximately to one order. Since minimum value λ_n is equal approximately to the height/altitude of beam, then it is possible to restrict from below initial space by the value of the order of tenths r.

EXAMPLES OF NUMERICAL CALCULATION.

1. Let us examine forced oscillations of hinged supported truncated cone with aperture angle 2α under action of distributed

load. The origin of coordinates is accepted in the center of larger basis/base, and X-axis is directed along the axis of cone. The area and the moment of the inertia (dimensionless) of cross section with coordinate x are expressed in this case by the following formulas:

$$f(x) = (1 - x \operatorname{tg} \alpha)^2, \quad i(x) = (1 - x \operatorname{tg} \alpha)^4.$$

Further, utilizing (8), we will obtain

$$A(x) = -\frac{2 \operatorname{tg} \alpha}{1 - x \operatorname{tg} \alpha}, \quad B(x) = -\frac{4 \operatorname{tg} \alpha}{1 - x \operatorname{tg} \alpha}, \quad C(x) = \frac{x^2}{(1 - x \operatorname{tg} \alpha)^2}.$$

In calculation it is accepted λ = by 20, tg α = 0.04 which corresponds to value l/L = 0.4 (l - height/altitude of truncated cone, L - height/altitude of complete cone); load on time builds up linearly to value of t = 20, further instantly is removed (time of action of load comprises approximately 0.06 periods of the first tone of oscillations). The amplitude of load (dimensionless value) is accepted equal to unit, parameter x - equal to 0.7.

Calculation is carried out for three different values of space h (0.2; 0.1; 0.05), also, on findings with the aid of Runge's method [10] is made extrapolation to zero space. The results of calculation are represented in the form of curve/graphs.

Fig. 2 for different torque/moments of time t, shows deflection curves, for the maximum amplitudes of the form of deflection curves,

are very close to the forms of the natural oscillations of truncated cone in the first tone, and the difference in the values of time, which corresponds to the maximum deviations of beam to opposite sides, virtually coincides with the half-period of natural oscillations in the first tone. a maximum error in the calculation during period does not exceed 1o/o.

Fig. 3, depicts the diagram/curves of the bending moments for different moments of time. From the behavior of curves, it follows that and under the effect of the evenly distributed load in beam are excited the high tones of oscillations with considerable amplitude, if the time of load change is sufficiently small.

Page 59.

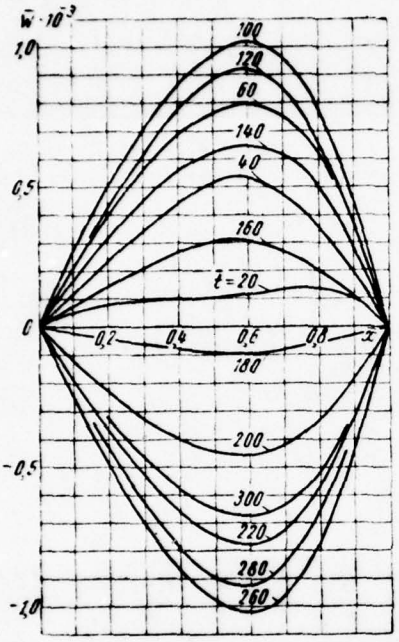


Fig. 2.

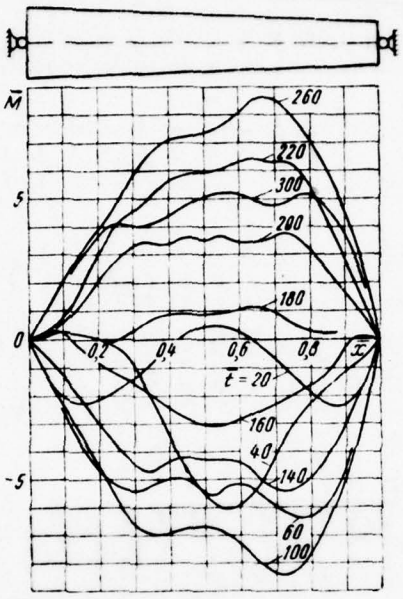


Fig. 3.

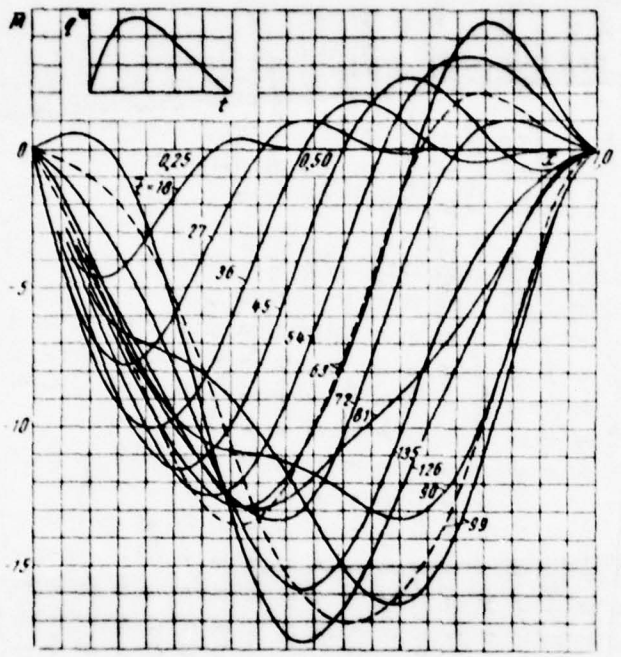


Fig. 4.

Page 60.

2. Let us examine forced oscillations of supported on one and free at other end uniform beam with elongation $\lambda = 30$ under effect of distributed dynamic load. load on time was assigned in form curved, depicted on Fig. 4 (in upper left to angle). Rise time of load to the maximum was taken equal to 0.3 from the common/general/total duration of its action. Period of loading was accepted in the calculation of the equal to 45 that comprises approximately 0.12 periods of the

first tone of natural oscillations.

Fig. 4 depicts the diagram/curves of the bending moments for the different values of time. For an example in question according to bernulli - Euler's theory, there is exact sclution in the form of a series on the forms of natural oscillations. This solution in the form of the curve/graphs of the bending moment is represented in Fig. 4 (dotted lines) for two characteristic values of time (t = 63 and 99). An essential quantitative difference in the solutions of this problem in the theories of bernulli - Euler and Timoshenko completely explicable on the basis that presented is higher.

REFERENCES.

1. S. D. Ponomarev, V. L. Biderman, K. K. Likhorev, V. M. Makushin, N. N. Malinii, V. I. Feodos'yev. Stress analyses in machine-building. T. III, Mashgiz [99sp07 - State Scientific and Technical Publishing House of Literature on Machinery Manufacture], 1959.

2. P E Duwez, D S Clark and N F Bohnenblust. The behavior of long beams under impact loading. J of Appl. Mech., 17, No. 1, 1950. (See also coll. "mechanics". M., publ. foreign lit., 1950).

3. L. I. Slepyan. Unsteady elastic waves. L., "ship-building", 1972.

4. A. S. Arkhipov, Ye. S. Sorokin. Study of free transverse vibrations of beam as two-dimensional problem of the theory of elasticity. In the collection "structural mechanics". M., Stroyizdat, 1966.

5. R Aprahamian, D A Evensen. Applications of holography to dynamics: high-frequency vibrations of beams. J of Appl. Mech., vol. 37, series E, No 2, 1970. (See also "applied mechanics", 1970, No. 2).

6. L. I. Balabukh, K. S. Kolesnikov, V. S. Zarubin, N. A. Alfutov, V. I. Usyukin, V. F. Chizhov. Bases of structural mechanics of rockets. M., "higher school", 1969.

7. I. A. Lyakhovenko. The transverse waves in the split beams. Transactions of TsAGI, No. 1085, 1967.

8. R D Mindlin and H Deresiewicz. Timoschenko's shear coefficient for fluxural vibrations of beams. Proceedings of the Second U.S. National Congress of Applied Mechanics, ASME, 1954.

9. J M Garrelick, J E Benveniste. Comparison of beam impact models. AIAA J, No. 4, 1970. (See also "rocket engineering and astronautics",

Vol. 8, No. 4, 1970).

10. A. I. Zhukov. Applicatien/use of a method of characteristics to the numerical solution of the one-dimensional tasks of gas dynamics. Transactions of math. institute to them. V. A. Glass-Va, No. 58. M, 1960.

The manuscript entered 7/VIII 1972.

THE STABILITY OF CYLINDRICAL SHELL DURING COMPRESSION UNDER CONDITIONS OF CREEP.

G. N. Zamul.

By method, proposed in article [1], is investigated the stability of imperfect cylindrical shell during compression under conditions of creep under different forms of initial sagging, different laws of the creep of the material and change in the load with time.

In article [1] is presented the numerical method of the solution of the problems of the stability of circular cylindrical shells under conditions of creep taking into account the real character of loading and attachment of the end/faces of shell, instantaneity of initial state, initial inaccuracies. Is shown the possibility of the loss of stability (branching of the forms of equilibrium) of ideal shell, by the compressed constant axial force and by evenly heated, in the zone of the development of the edge effect, caused by lateral expansion during compression and by the attachment of end/faces. For an imperfect shell with periodic initial sagging/deflection, are

obtained the results, close to those found approximately in work [2]. Below method indicated is used for the investigation of effect on the stability of the shell of the form of initial sagging, degree of the nonlinearity of the law of the creep of the material and law of a change in the load with time. Shell is assumed to be sufficiently long, evenly heated and that compressed in axial direction, hinged supported on end/faces in the heated to temperature shells rigid diaphragms.

1. Effect of initial sagging/deflections of different view of stability of elastic shells during axial compression is is sufficiently well studied. This does not pertain to the question concerning the effect of the form of initial sagging on the stability of shells under conditicns cf creep, which represents special interest. The value of the amplitude of initial sagging/deflection can be approximately determined by testings for stability of elastic shells, after which becomes possible theoretical stability analysis under conditions of creep [1] with the assigned/prescribed form of initial sagging. Remains unclear the degree of the effect of the form of initial sagging on the obtained thus dependence of ultimate strain of shell on load with the amplitudes of initial sagging, which ensure one and the same critical lcad of elastic shell.

Fig. 1 in a dimensionless form, gives the results of the numerical calculation accordingly [1] of the dependence of critical load of elastic shell on amplitude $\bar{N}_0$ of the axisymmetric initial sagging (symmetrical relative to middle x = L/2 shell), of the assigned/prescribed in the form [3]

$$\bar{\omega}_0(\bar{x}) = \bar{\omega}_0 \exp\left[\lambda\left(\bar{x} - \frac{\bar{L}}{2}\right)\right]\left[\sin(2m-1)\pi\frac{\bar{x}}{\bar{L}} + \frac{\lambda\bar{L}}{(2m-1)\pi}\cos(2m-1)\pi\frac{\bar{x}}{\bar{L}}\right], \quad (1)$$

$$\bar{x} \leqslant \frac{\bar{L}}{2},$$

and ensuring during change parameter λ transition from periodic initial deflection (λ = 0) to local dent (λ ≈ 1). The dimensionless parameters take form [1]

$$\bar{N} = \sqrt{3(1-\nu^2)}\,\frac{R}{h}\,\frac{N}{Eh}, \quad \bar{\omega} = \sqrt{12(1-\nu^2)}\,\frac{\omega}{h},$$

$$\bar{x} = \sqrt[4]{12(1-\nu^2)}\,\frac{x}{\sqrt{Rh}}, \quad \bar{L} = \sqrt[4]{12(1-\nu^2)}\,\frac{L}{\sqrt{Rh}},$$

where x, N - longitudinal coordinate and compressive force in shell, E - modulus of elasticity, ν - Poisson ratio, L, R, h - length, radius and thickness of shell, moreover it is accepted $\nu = 0{,}3$, $\bar{L} = 38$, $\bar{l}/\pi \approx 2m-1 = 11$.

With considerable initial sagging/deflections the critical load is close to that obtained in [3] for a long elastic shell without the account of edge effect of supports. During decrease $\bar{\omega}_0$, it approaches

the critical load of the ideal hinged supported shell, taken with consideration of nonlinear edge effect.

Fig. 2 gives the results of the sclution of the corresponding problem of stability under conditicns of the creep of the material according to the law

$$p = A\sigma^{\mu} \qquad (2)$$

with $\mu = 3$, where σ, p designate the intensities of stresses and rates of creep strains respectively.

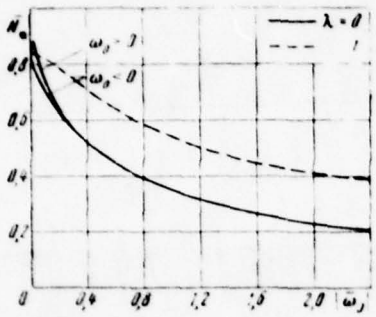


Fig. 1.

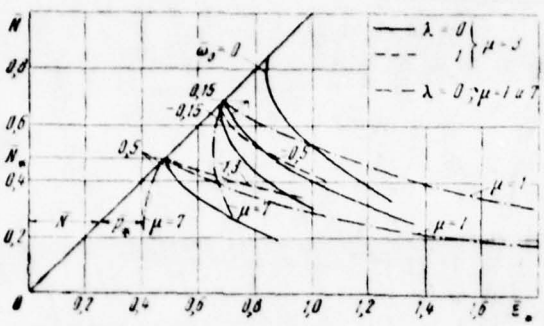


Fig. 2.

Page 63.

Along the axis of abscissas, is deposit/postponed dimensionless ultimate strain of the shell

$$\bar{\varepsilon}_* = \sqrt{3(1-\nu^2)}\,\frac{R}{h}\,\varepsilon_* = \bar{N} + \bar{p}_* = \bar{N}\,(1 + \bar{N}^{\mu-1}\,\bar{\tau}_*), \qquad (3)$$

where $\varepsilon_* = \frac{\sigma}{E} + p_* = \frac{N}{Eh} + A\,\frac{N^\mu}{h^\mu}\,\tau_*$ - ultimate strain of the shortening of zero moment shell; $\tau,\ \bar{\tau} = \frac{E^\mu h^{\mu-1} A\tau}{[\sqrt{3(1-\nu_0)}]^{\mu-1} R^{\mu-1}}$ - dimensional and dimensionless time. The amplitudes of the initial sagging/deflections of imperfect shell were selected in this case according to Fig. 1 so as to ensure the identical values of the critical loads of elastic shell with periodic sagging and with local dent. As we see, the obtained dependences of ultimate strain on load differ with the various forms of initial sagging, moreover with the local character of initial sagging/deflection shell is more stable. Hence becomes

clear the need at least for qualitative evaluation of the forms of initial sagging during the analysis of stability of real shells.

2. Let us examine effect of degree of nonlinearity μ of law of creep of the material (2) on stability of imperfect shell with periodic initial sagging/deflection, which are described by formula (1) with $\lambda = 0$. For the case of the incompressible $(\nu = 0{,}5)$ linear viscoelastic material ($\mu = 1$) neglecting of edge effect it is possible to obtain the analytical solution of problem with the use of data Fig. 1. Variable on coordinate $\bar{x}$ comprising of the dimensionless sagging/deflection of shell retains in this case periodic form (1) $(2m - 1 = \bar{L}/\pi)$

$$\bar{\omega} = \frac{\bar{\omega}_0}{1 - \bar{N}} \exp\left(\frac{\bar{N}}{1 - \bar{N}}\bar{\tau}\right) \sin \bar{x} \qquad (4)$$

with circumferential forces $\bar{N}_y = \sqrt{3(1-\nu^2)}\,\frac{R}{h}\,\frac{N_y}{Eh}$ and curvature $\frac{\partial^2 \bar{\omega}}{\partial \bar{x}^2} = R\frac{\partial^2 \omega}{\partial x^2}$, that have the form

$$\bar{N}_y = -\frac{\bar{N}\bar{\omega}_0}{2(1-\bar{N})} \exp\left(\frac{\bar{N}}{1-\bar{N}}\bar{\tau}\right) \sin \bar{x}, \quad \frac{\partial^2 \bar{\omega}}{\partial \bar{x}^2} = -\frac{\bar{\omega}_0}{1-\bar{N}} \exp\left(\frac{\bar{N}}{1-\bar{N}}\bar{\tau}\right) \sin \bar{x}. \quad (5)$$

Characteristics (5) of initial state determine the stability of shell and at each moment of time $\bar{\tau}$ formally correspond to the characteristics of elastic shell ($\bar{\tau} = 0$) with the amplitude of initial sagging/deflection $\bar{\omega}_0 \exp(\bar{N}/1-\bar{N}\bar{\tau})$. If we designate dependence on the load of the amplitude of initial sagging, required for an elastic loss of stability, according to Fig. 1 as $\bar{\omega}_0 = f(\bar{N}_*)$,

then the condition, which determines critical time $\bar{\tau}_*$ of loss of stability, it takes the form

$$\bar{\omega}_0 \exp\left(\frac{\bar{N}}{1-\bar{N}}\bar{\tau}_*\right) = f(\bar{N}) \text{ или } \bar{\tau}_* = \frac{1-\bar{N}}{\bar{N}} \ln \frac{f(\bar{N})}{f(\bar{N}_*)}. \qquad (6)$$

whence for ultimate strain we obtain the expression

$$\bar{\varepsilon}_* = \bar{N} + \bar{p}_* = \bar{N}(1+\bar{\tau}_*) = \bar{N}\left[1 + \frac{1-\bar{N}}{\bar{N}} \ln \frac{f(\bar{N})}{f(\bar{N}_*)}\right]. \qquad (7)$$

Fig. 2, gives the results of the numerical solution of the task of the stability of shell with the parameters, indicated in p. 1, at two values of the amplitude of periodic initial sagging/deflection $\bar{\omega}_0$ = 0.15 and 0.5 when μ = 1, 3, 7. In the case μ = 1, numerical solution virtually coincides with analytical.

Page 64.

The effect of the degree of the nonlinearity of the law of creep on the dependence of ultimate strain from load proves to be very essential. With μ = 7 and the larger values ultimate strain can be lesser obtained on criterion ultimate strain. The results of calculation for the cases $\bar{\omega}_0$ = + 0.15 and -0.15 with μ = 3 noticeable are distinguished which is explained by the effect of edge effect of supports, opposite in these two cases. With $\bar{\omega}_0$ = 0.5 this effect already virtually is absent, which is evident also from Fig. 1. The results obtained when μ = 7 qualitatively will agree with the

experimental results of work [4], that differ from those given in article [5]. One of the possible explanaticns of the difference indicated lies in the fact that in work [5] as axial deformation ε in expression (3) is accepted the measured in experiment deformation of the shortening of the shell which affects the instantaneity of initial state. Fig. 3, depicts an example of the calculated distribution of circumferential force and curvature of shell, in Fig. 4 - change in the time of axial deformation $\bar{\varepsilon}$ of shell and stresses $\bar{\sigma}_{x,y} = \sqrt{3(1-\nu^2)}\frac{R}{h}\frac{\sigma_{x,y}}{E}$ in its middle x = L/2 (z - coordinate according to the thickness of shell). As we see, ultimate strain of moment shell can considerably exceed ultimate strain of zero moment shell, moreover increase give not only flexural deformations in moment shell, but also the connected with them increase of stress intensities and acceleration of creep.

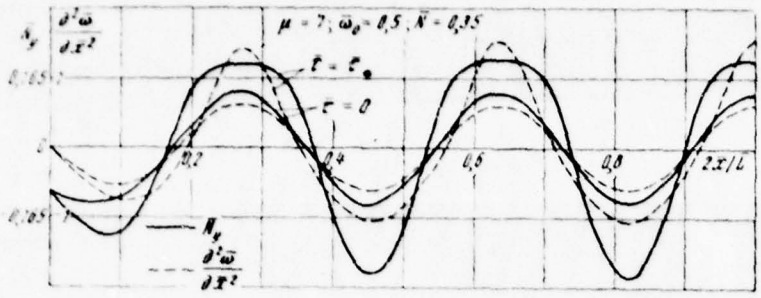


Fig. 3.

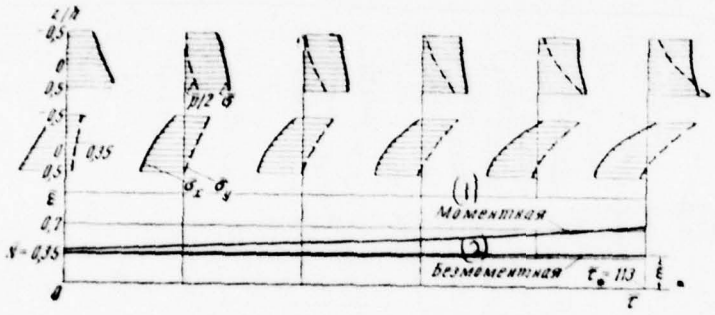


Fig. 4.

Key: (1). Moment. (2). Zero moment.

Page 65.

3. Until now, was examined stability during creep of shell, "instantly" that loaded to constant load and by that heated to constant temperature. Furthermore data Fig. 2 indicate the dependence of ultimate strain on the law of load change and the temperatures in

time. Let us examine, in particular, a very important virtually question concerning effect on residual "instantaneous" critical load $\bar{N}_{*0}$ of the shell of its preliminary delay under conditions of creep at constant temperature and load $\bar{N} < \bar{N}_*$ for a certain period of time $\bar{\tau}_0 < \bar{\tau}_*(\bar{N})$. Under the linear law of the creep of the material ($\mu = 1$) a change in the axisymmetric periodic sagging/deflection, circumferential forces and the curvatures of shell is described at the stage of delay by formulas (4), (5) and the condition of loss of stability (6) takes the form

$$\bar{\omega}_0 \exp\left(\frac{\bar{N}}{1-\bar{N}}\bar{\tau}_0\right) = f(\bar{N}_{*0}) \text{ или } \bar{\tau}_0 = \frac{1-\bar{N}}{\bar{N}} \ln \frac{f(\bar{N}_{*0})}{f(\bar{N}_*)}. \qquad (8)$$

If we introduce as the characteristic of delay accumulated creep strain of zero moment shell $\bar{p}_н = \bar{N}^\mu \bar{\tau}_0$, then of (8) we obtain when $\mu = 1$

$$\bar{p}_н = (1-\bar{N}) \ln \frac{f(\bar{N}_{*0})}{f(\bar{N}_*)}. \qquad (9)$$

The example of calculated accordingly (9) dependence $\bar{N}_{*0}$ on $\bar{p}_н$ is represented by unbroken curve in Fig. 5, there is given the result of the numerical solution of task with nonlinear law of creep ($\mu = 7$). As we see, in the case $\mu = 1$, this dependence is close to linear and differs little from that obtained according to formula (7) and Fig. 2 under the assumption $\bar{N} = \bar{N}_{*0}$, $\bar{p}_* = \bar{p}_н$ (dot-dash curves in Fig. 2 and 5). This means that the law of a change in the load with time has weak effect on critical combination of load and accumulated

creep strain, and stability is determined only by their values at the moment of loss of stability according to the universal curves of interaction Fig. 2 and 5. In the case of nonlinear creep this assumption, as can be seen from Fig. 5, it leads to considerably larger error.

Fig. 5.

REFERENCES.

1. G. N. Zamul. Stability analysis circular cylindrical shells under conditions of creep. "scientific notes of TsAGI", Vol. II, No. 6, 1971.

2. E. I. Grigolyuk, Yu. V. Lipovtsev. On the criteria of the bulge of shells under conditions of creep. "engineering journal", 1966, No. 3.

3. V. K. Kuznetsov, Yu. V. Lipovtsev. Effect of local inadequacies on the stability of cylindrical shell during axial compression. "Izv. of the AS USSR - MTT", 1970, No. 1.

4. A. P. Kuznetsov, N. M. Yungerman. Experimental analysis of stability of shells under conditions of creep. PMTF, 1965, No. 4.

5. A. N. Baranov, M. A. Morozov. Experimental study of ultimate strain of cylindrical shells under conditions of creep. "Izv. of the AS USSR - MTT", 1971, No 1.

The manuscript entered 23/VI 1972.

Page 66.

BULGE OF RODS UNDER CONDITICNS OF CREEP.

V. F. Galkin.

Is examined the task of the determination of the changing in the course of time stressed and state of strain of the compression member of rectangular cross section with initial sagging/deflection under conditions of creep. The results of calculation are compared with the results of experiment. Findings make it possible to compare different calculation methods.

Some elements of airframe structures work as compression members at elevated temperatures. In this case they can be developed the processes of creep, are accumulated defcrmations and upon expiration of certain time occurs the destruction of cell/elements.

During design it is necessary to know the time, during which this element of construction it will exhaust its bearing capacity, or

the time, for which will be achieve/reached the specific level of deformation. Therefore it is necessary to know how to determine stressed and the states of strain of rod depending on time under conditions of creep. To this question is dedicated vast literature, are created several calculation methods; however, some of them give the decreased values of critical time, others need experimental check. It must be noted that there is extremely few experimental data, which correspond to the circuit, accepted in the calculation method.

In this article is set forth the method of calculation of the stressed and state of strain of rod depending on time under conditions of creep on the basis of variation theorem [1], is given the procedure of the test of rods with the hinged support of ends and is given the comparison of results of calculation with the results of experiment.

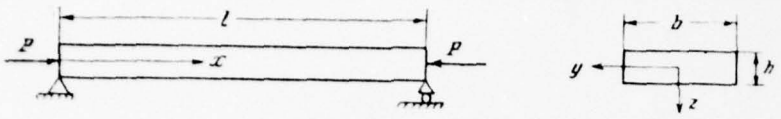


Fig. 1.

Page 67.

1. Variation theorem [1], formulated in nonlinear setting [2] for rates of change of stresses and strains, says, that for body, which is found under conditions of creep, variation equation $\delta J = 0$, where

$$J = \int_V \left[\dot{\sigma}_{ij} \dot{\varepsilon}_{ij} + \frac{1}{2} \sigma_{ij} \dot{u}_{k,i} \dot{u}_{k,j} - \frac{1}{2} (\dot{\varepsilon}'_{ij} + 2\dot{\varepsilon}''_{ij}) \dot{\sigma}_{ij} \right] dV - \\ - \int_{S_S} \dot{\bar{T}}_i \dot{u}_i \, dS - \int_{S_d} \dot{T}_i (\dot{u}_i - \dot{\bar{u}}_i) \, dS \qquad (1)$$

and δu_i, $\delta \sigma_{ij}$ - arbitrary variations, it has as equations of Euler relationship/ratios between stresses and strains and equations of equilibrium, but as natural (Eulerian) boundary conditions, boundary conditions for stresses and boundary conditions for deformations. In equation (1) σ_{ij}, ε_{ij}, ε'_{ij}, ε''_{ij} - tensors respectively of stresses, strains, instantaneous elastoplastic strains, creep strains; T_i - surface effort/forces; u_i - displacement vector; $\bar{T}_i$ - assigned/prescribed surface forces on the part of the body surface S_S; $\bar{u}_i$ - assigned/prescribed displacement vector on the part of the body surface S_d. The points above letters indicate the differentiation of the corresponding values with respect to time. It is assumed that

$\dot{\varepsilon}_{ij}$ are expressed through displacement/movements and the speeds, $\dot{\varepsilon}'_{ij}$ - through stresses and rates of change in the stresses, $\dot{\varepsilon}''_{ij}$ - through stresses. The elasto-plastic part of the strain must satisfy condition [3] $\dot{\sigma}_{ij}\, d\dot{\varepsilon}'_{ij} = \dot{\varepsilon}'_{ij}\, d\dot{\sigma}_{ij}$.

2. Let us examine bulge as a result of creep of uniform hinged supported rod of rectangular cross section, compressed by axial force P (Fig. 1).

Let us select the relationship/ratio between the stresses and strains in the following form:

$$\dot{\varepsilon} = \frac{\dot{\sigma}}{E} + \lambda p\, t^{p-1} \sigma^m,$$

where λ, p, m - empirical constants, t - time. The plastic part of the strain we disregard.

Let us assign the axial displacement u and axial strain respectively in the form

$$u = U - z\frac{\partial W}{\partial x},$$

$$\varepsilon = \frac{\partial U}{\partial x} - z\frac{\partial^2 W}{\partial x^2} + \frac{1}{2}\left(\frac{\partial W}{\partial x}\right)^2,$$

where U and W - displacement of the average/mean layer of rod.

In this case into expressions for J_* will remain the following terms:

$$\dot{\sigma}_{ij}\dot{\varepsilon}_{ij} = \dot{\sigma}\left(\frac{\partial \dot{U}}{\partial x} + \frac{\partial \dot{W}}{\partial x}\frac{\partial \dot{W}}{\partial x} - z\frac{\partial^2 \dot{W}}{\partial x^2}\right),$$

$$\frac{1}{2}\sigma_{ij}\dot{u}_{k,i}\dot{u}_{k,j} = \frac{1}{2}\sigma\left(\frac{\partial \dot{W}}{\partial x}\right)^2$$

[term $\frac{1}{2}\sigma\left(\frac{\partial \dot{u}}{\partial x}\right)^2$ we disregard as a result of its smallness]

$$\frac{1}{2}\left(\dot{\varepsilon}'_{ij} + 2\dot{\varepsilon}''_{ij}\right)\dot{\sigma}_{ij} = \frac{\dot{\sigma}^2}{2E} + \lambda p t^{p-1}\sigma^m\dot{\sigma},$$

$$\int_{S_\sigma}\dot{\bar{T}}_i\dot{u}_i\,dS = -\dot{P}\dot{U}(l, t) = 0, \quad P = \text{const}, \quad \dot{U}(0, t) = 0.$$

Page 68.

Thus, functional J takes the following form:

$$J = \int_V\left[\dot{\sigma}\left(\frac{\partial \dot{U}}{\partial x} + \frac{\partial \dot{W}}{\partial x}\frac{\partial \dot{W}}{\partial x} - z\frac{\partial^2 \dot{W}}{\partial x^2}\right) + \frac{1}{2}\sigma\left(\frac{\partial \dot{W}}{\partial x}\right)^2 - \right.$$
$$\left. - \frac{\dot{\sigma}^2}{2E} - \lambda p\, t^{p-1}\sigma^m\dot{\sigma}\right]dV. \qquad (2)$$

It is known that the distribution of the stresses over the section of rod under conditions of creep will not follow linear law. Let us assume that a change in the stresses in rod occurs as follows:

$$\sigma(x, z, t) = \begin{cases}\dfrac{P}{F}\left[\left(\sigma_0 + \dfrac{z}{h}\sigma_1\right)\sin\dfrac{\pi x}{l} - 1\right] & \text{при } -\dfrac{h}{2} \leqslant z \leqslant 0, \\ \dfrac{P}{F}\left[\left(\sigma_0 + \dfrac{z}{h}\sigma_2\right)\sin\dfrac{\pi x}{l} - 1\right] & \text{при } 0 \leqslant z \leqslant \dfrac{h}{2}\end{cases} \qquad (3)$$

Key: (1). with.

(F - cross-sectional area of rod). Stresses we consider positive with elongation. The dependence of displacements on coordinate x we take

in the form

$$U = U_0 x,$$
$$W = h W_0 \sin \frac{\pi x}{l}. \qquad (4)$$

Values σ_0, σ_1, σ_2, U_0, W_0 in the right sides of expressions (3) and (4) are the functions only of time. Substituting (3) and (4) in functional (2) and fulfilling integration, we will obtain (for m = 3)

$$J = c_1 U_0 \left(2\sigma_0 + \frac{\sigma_2 - \sigma_1}{4}\right) + c_2 W_0 W_0 \left(\sigma_0 + \frac{\sigma_2 - \sigma_1}{8}\right) +$$
$$+ c_3 W_0 (\sigma_2 + \sigma_1) + c_4 W_0^2 f_1 - c_5 \left[\sigma_0^2 + \frac{\sigma_0}{4}(\sigma_2 - \sigma_1) + \frac{1}{24}(\sigma_2 + \sigma_1)\right] -$$
$$- f_0 (\sigma_0 f_2 - \sigma_1 f_3 + \sigma_2 f_4).$$

Are here introduced the following designaticns:

$$c_1 = \frac{Pl}{\pi}, \quad c_2 = \frac{2P}{3\pi l}(h\pi)^2, \quad c_3 = \frac{P}{48l}(h\pi)^2,$$
$$c_4 = \frac{P}{2l}(h\pi)^2, \quad c_5 = \frac{P^2 l}{4EF},$$
$$f_0 = \frac{P^4 l}{F^3} \lambda p t^{p-1},$$
$$f_1 = \frac{2}{3\pi}\left(\sigma_0 + \frac{\sigma_2 - \sigma_1}{8}\right) - \frac{1}{2},$$
$$f_2 = \frac{3}{64}\left[8\sigma_0^3 + 3\sigma_0^2(\sigma_2 - \sigma_1) + \sigma_0(\sigma_2^2 + \sigma_1^2) + \frac{\sigma_2^3 - \sigma_1^3}{8}\right] -$$
$$- \frac{1}{\pi}\left[4\sigma_0^2 + \sigma_0(\sigma_2 - \sigma_1) + \frac{\sigma_2^2 + \sigma_1^2}{6}\right] + \frac{3}{2}\left(\sigma_0 + \frac{\sigma_2 - \sigma_1}{8}\right) - \frac{2}{\pi},$$
$$f_3 = \frac{3}{64}\left(\sigma_0^3 - \sigma_0^2\sigma_1 + \frac{3}{8}\sigma_0\sigma_1^2 + \frac{\sigma_1^2}{32}\right) - \frac{1}{\pi}\left(\frac{\sigma_0^2}{2} - \frac{\sigma_0\sigma_1}{3} + \frac{\sigma_1^2}{16}\right) +$$
$$+ \frac{3}{16}\left(\sigma_0 - \frac{\sigma_1}{3}\right) - \frac{1}{4\pi},$$
$$f_4 = \frac{3}{64}\left(\sigma_0^3 + \sigma_0^2\sigma_2 + \frac{3}{8}\sigma_0\sigma_2^2 + \frac{\sigma_2^2}{32}\right) - \frac{1}{\pi}\left(\frac{\sigma_0^2}{2} + \frac{\sigma_0\sigma_2}{3} + \frac{\sigma_2^2}{16}\right) +$$
$$+ \frac{3}{16}\left(\sigma_0 + \frac{\sigma_2}{3}\right) - \frac{1}{4\pi}.$$

Equalizing to zero particular derivatives of functional J on each of the values with point, we will obtain the system of the nonlinear differential equations:

$$\left.\begin{aligned} 8\dot{\sigma}_0 + \dot{\sigma}_2 - \dot{\sigma}_1 &= 0, \\ f_5(\dot{\sigma}_2 + \dot{\sigma}_1) + \dot{W}_0 &= 0, \\ 2c_1\dot{U}_0 + c_2 W_0 \dot{W}_0 - 2c_5\dot{\sigma}_0 - \frac{c_5}{4}(\dot{\sigma}_2 - \dot{\sigma}_1) - f_6 &= 0, \\ f_8\dot{W}_0 - \frac{c_1}{4}\dot{U}_0 + \frac{c_5}{4}\dot{\sigma}_0 - \frac{c_5}{12}\dot{\sigma}_1 - f_7 &= 0, \\ f_{10}\dot{W}_0 + \frac{c_1}{4}\dot{U}_0 - \frac{c_5}{4}\dot{\sigma}_0 - \frac{c_5}{12}\dot{\sigma}_2 - f_9 &= 0. \end{aligned}\right\} \qquad (5)$$

where

$$f_5 = \frac{c_3}{2c_4 f_1},$$

$$f_6 = f_0\left\{\frac{3}{8}\left[\sigma_0^3 + \frac{3}{8}\sigma_0^2(\sigma_2 - \sigma_1) + \frac{\sigma_0}{8}(\sigma_2^2 + \sigma_1^2) + \frac{1}{64}(\sigma_2^3 - \sigma_1^3)\right] - \right.$$
$$\left. - \frac{4}{\pi}\left[\sigma_0^2 + \frac{\sigma_0}{4}(\sigma_2 - \sigma_1) + \frac{1}{24}(\sigma_2^2 + \sigma_1^2)\right] + \frac{3}{2}\left[\sigma_0 + \frac{1}{8}(\sigma_2 - \sigma_1)\right] - \frac{2}{\pi}\right\},$$

$$f_7 = f_0\left[\frac{3}{64}\left(-\sigma_0^3 + \sigma_0^2\sigma_1 - \frac{3}{8}\sigma_0\sigma_1^2 + \frac{1}{20}\sigma_1^3\right) + \right.$$
$$\left. + \frac{1}{\pi}\left(\frac{\sigma_0^2}{2} - \frac{\sigma_0\sigma_1}{3} + \frac{\sigma_1^2}{8}\right) - \frac{3}{16}\left(\sigma_0 - \frac{\sigma_1}{3}\right) + \frac{1}{4\pi}\right],$$

$$f_8 = c_3 - \frac{c_2}{8}W_0,$$

$$f_9 = f_0\left[\frac{3}{64}\left(\sigma_0^3 + \sigma_0^2\sigma_2 + \frac{3}{8}\sigma_0\sigma_2^2 + \frac{\sigma_2^3}{20}\right) - \right.$$
$$\left. - \frac{1}{\pi}\left(\frac{\sigma_0}{2} + \frac{\sigma_0\sigma_2}{3} + \frac{\sigma_2^2}{8}\right) + \frac{3}{16}\left(\sigma_0 + \frac{\sigma_2}{3}\right) - \frac{1}{4\pi}\right],$$

$$f_{10} = c_3 + \frac{c_2}{8}W_0.$$

Let the rod before the load application have initial sagging in the form $h\Delta\sin\frac{\pi x}{l}$, where Δ - amplitude of initial sagging/deflection $W_н$, divided into the thickness of rod. Then initial conditions for the dimensionless parameters after the load application at elastic instantaneous deformations they will be:

$$W_0(0) = \frac{\Delta}{1 - \frac{P}{P_c}},$$

$$\sigma_0(0) = 0,$$

$$\sigma_1(0) = \sigma_2(0) = \frac{12\Delta}{1 - \frac{P}{P_c}},$$

$$U_0(0) = -\frac{P}{EF},$$

where P_c - critical force for a rod.

Page 70.

For the solution of the system of nonlinear differential equations (5) was comprised the program in language ALGOL-60 for computer BESM-6. In this case, was utilized kutt - Merson's procedure with the automatic calling sequence of integration for providing the assigned/prescribed accuracy in the integration 10^{-6}.

Fig. 2-4, depicts the results of the numerical computation of the coefficient of sagging/deflection W_0, of the stresses in the mean section of rod and strain of the filaments, arrange/located in the center of gravity of section, of the following values of the parameters:

$$\lambda = 5 \cdot 10^{-12},$$
$$p = 1,\ m = 3,$$
$$E = 0{,}39 \cdot 10^{11}\ H/\text{м}^2,\ P = 4900\ H,$$
$$\frac{P}{P_c} = 0{,}67,\ h = 8\ \text{мм},$$
$$b = 20\ \text{мм},\ l = 214\ \text{мм}.$$

Such values of the parameters are selected for that target/purpose so that it would be possible tc compare the obtained results with the data of calculation according to other methods, presented in [4]. The parameters λ, p, m, E indicated correspond to the characteristics of material D 16A-T at temperature of 300°C.

Calculated curves of axial strain in Fig. 4 are constructed according to the formula

$$\varepsilon = U_0 - \frac{1}{2l}\int_0^l \left(\frac{\partial W}{\partial x}\right)^2 dx.$$

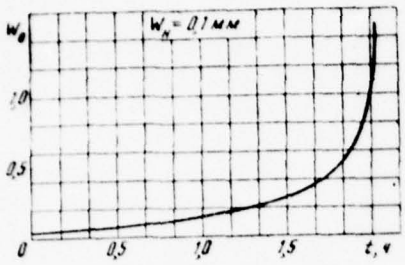


Fig. 2.

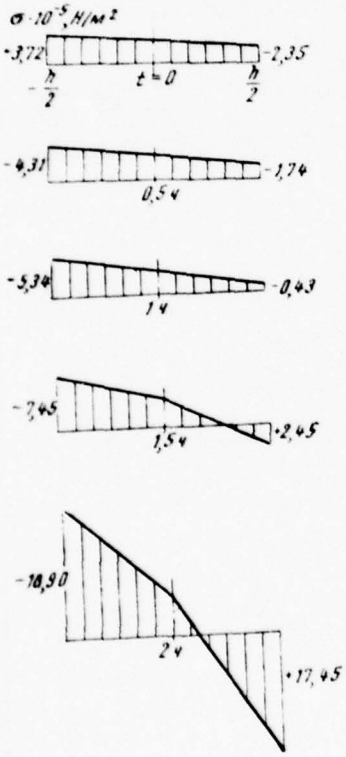


Fig. 3.

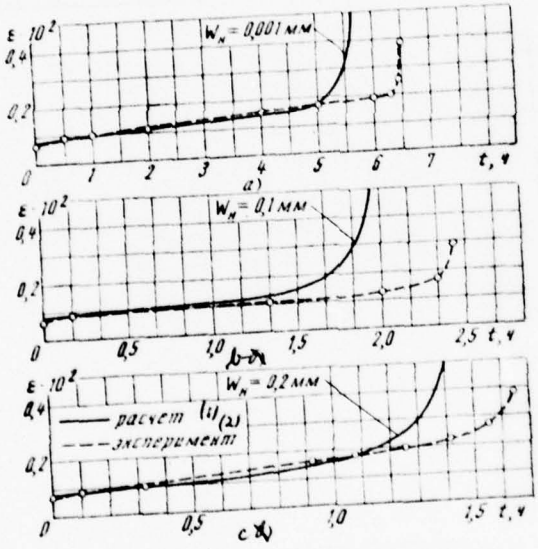


Fig. 4.

Fig. 5, depicts the dependence of critical time on the ratio of initial sagging/deflection to the thickness of rod, moreover for critical was accepted time from the torque/moment of the load application to that torque/moment when $W \to \infty$.

3. For checking results of calculation, it was tested for creep during compression of eight rods from material D16A-T at temperature of 300°C. For providing the hinged support of the ends of the rod, were made two tip bearings (Fig. 6), making it possible to obtain the fixing coefficient, equal to one.

Since during the experimental investigation of the phenomenon of the bulge of rods under conditions of creep is observed the large spread in the values of critical time [5], for the determination of initial sagging/deflection and to centering of rods it was directed special attention. Initial sagging/deflection was determined from the formula

$$W_0 = h_{\max} - \frac{1}{2}\left(h_{cp} + h_2 + \frac{h_1 - h_2}{2}\right),$$

where h_1, h_2, h_{cp} - thickness of rod at ends and in the middle part; h_{max} - great distance from the plane on which lie/rests the rod concave-down, to the upper surface of rod.

Centering of rods was realize/accomplished as follows. On the

supporting/reference pad of tip bearing with accuracy/precision on the order of 0.02 mm, were located the rotational axes. On rods with the same accuracy/precision, were deposited the risks. During the installation of rod into support, the risks on the surface of rod were combined with rotational axes, then the end of the rod was record/fixed by special fixers. Thus was realize/accomplished sufficiently precise centering and was eliminated the displacement of rod relative to rotational axes. This centering render/showed more precisely than centering with the aid of the sensors of strain DK-25.

Rod in tip bearings was placed into the furnace of testing machine and was heated to temperature of 300°C for 1.5 hours. Then to rod was applied compressive force 4900 H by the natural load through the lever of testing machine. In the process of testings with the aid of indicators, were measured axial strains with accuracy/precision 0.01 mm. For critical time was accepted the time from the torque/moment of the load application to the torque/moment of the exhaustion of the bearing capacity of rod. Test results are shown by circles on Fig. 5.

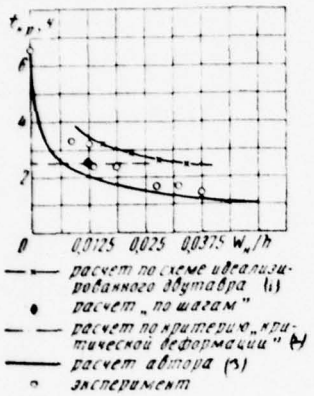


Fig. 5.

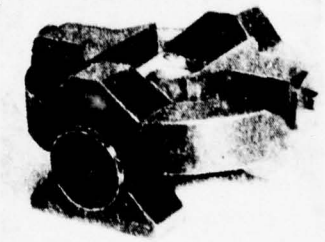


Fig. 6.

Key: (1). calculation according to the circuit of the idealized double T calculation "according to spaces". (2). calculation according to criterion "of ultimate strain". (3). calculation of author. (4). experiment.

Page 72.

Fig. 4, gives the theoretical and experimental curves of the axial strain of middle filament for the rods whose critical time is most close to computed value. Fig. 4a, depicts the curve of axial strain, obtained during rod testing with the initial sagging/deflection, which does not exceed the accuracy/precision of its measurement 0.01 mm. For a comparison is given calculated curve of axial strain for a rod with initial sagging/deflection $W_n = 0{,}001$ mm.

During testing of the rod the curves of creep of which are given to Fig. 4b, in time interval from 20 min to 1 h of 30 min, the temperature was understated on 4-5°C.

In the process of testing, was conducted the visual observation after the sagging/deflection of rods. For this purpose in the reheating furnace before the rod, was secured metallic rule, and through inspection window in furnace it was possible to control the sagging/deflection of rod. In this case, the accuracy of observation was 0.1-0.2 mm. As a result of visual observations, it was noticed that the rod with the initial sagging/deflection, in effect equal to zero, has critical sagging/deflection $W_{кр} = 2{,}5$ mm, i.e., 0.31 h. Under critical we understand such sagging/deflection after achievement of which the rod is destroyed during 2-3 s. For rods with initial sagging/deflection 0.1 mm value $W_{кр} = 4$ mm or 0.5 h, with $W_{н} = 0{,}3$ mm value $W_{кр} = 8$ mm or h.

Comparing data, presented in Fig. 4 and 5, we note that the results of calculation will agree well with the results of experiment. The voltage distribution in the mean section of the rod (see Fig. 3) is close to voltage distribution, obtained by the calculation method "according to spaces" and given to Fig. 6.13 in work [4].

In Fig. 5, are plotted the values of critical time, presented in [4] and calculated according to the criterion "ultimate strain", by method "according to spaces" and according to the circuit of the idealized double T. Moreover in method "on spaces" is noted the time, which corresponds to sagging/deflection $W = 2r_i = 0{,}46$ cm, where r_i - a radius of inertia of the section of rod. In experiment this value of sagging/deflection is reached at the very moment of destruction. If we in the torque/moment of the exhaustion of the bearing capacity accept that torque/moment when $W \to \infty$, then it is possible to obtain the high value of critical time.

The criterion of ultimate strain is simple in use, it gives good and reliable results; however, it is applicable with the insignificant initial sagging/deflections (in our case are less than 0.0125 h). The propagation of this criterion for large initial sagging/deflections requires supplementary investigations. The calculation method according to the circuit of the idealized double T gives the high values of critical time.

REFERENCES

1. J. L. Sanders, Kh. G. Mak-Komb, poppy-combination, F. R. Shlente. Variation theorem for creep with application/appendices to plates and rods. "mechanics", 1965, No 6.

2. V. V. Novozhilov. Theory of elasticity. L., Sudpromgiz, 1958.

3. R. Hill. Mathematical theory of plasticity. M., the State Technical Press, 1965.

4. A. S. Vol'mir. Stability of the systems being deformed. M., "science", 1967.

5. A. P. Kuznetsov. Stability of the compression members from Duralumin under conditions of creep. PMTF, 1961, No 6.

The manuscript entered 15/VI 1972.

ON THE SHAPE OF BODIES, IN SUPERSONIC FLOW HAVING RESISTANCE AND MOMENT WITH RESPECT TO LONGITUDINAL AXIS.

G. I. Maykapar.

Is given an example of the pyramidal body, which possesses in the supersonic flow the moment with respect to of longitudinal axis at zero angle of attack.

The rotation of the flying body of its relatively longitudinal axis is utilized for different target/purposes and can be created by artificial means. For supersonic flight speed, it is possible to indicate, however, the form of the unrotated pyramidal body, which ensures the initial moment with respect to of longitudinal axis at zero angle of attack. Besides force component in the direction of longitudinal axis (resistance), the remaining force component and torque/moments will be in this case equal to zero. The surface of this body is formed by the planes of the current of flow after the step shocks of packing/seal and undisturbed flow. [91] Plane ABCD - plane of jump with angle of the slope θ to the rate of undisturbed flow $u_н$ (Fig. 1), angle δ - angle of the slope of velocity vector after jump. Let us determine that comprise in the direction of X-axis of the torque/moment, which acts on the dihedral angle, formed by planes ORP and ORD.

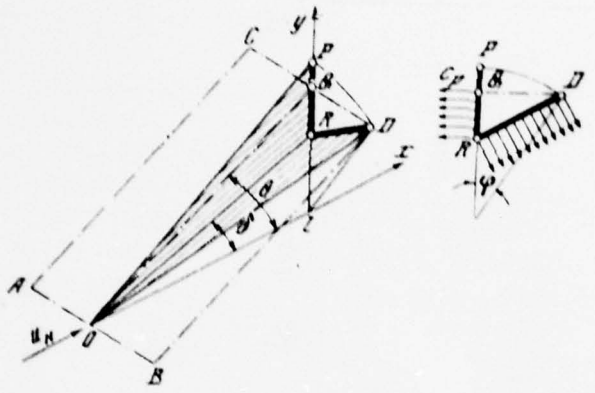


Fig. 1.

Page 74.

Pressure gas on surface ORQ and ORD identical is equal to pressure after jump, pressure on surface OQP is equal to pressure in undisturbed flow; therefore unknown comprising of the torque/moment

$$M_x = c_p q_n \sigma_y \frac{l}{3} \operatorname{tg}\theta \operatorname{tg}\varphi,$$

where $c_p = \frac{4}{\gamma+1}\left(\sin^2\theta - \frac{1}{M_n^2}\right)$, $q_n = \frac{1}{2}\rho_n u_n^2$,

l - the length of body, φ - the angle between the meridian planes, which consist step shock, M - Mach number, ρ - air density, γ - specific heat ratio, σ_y - the projection of surface ORD on the

plane, perpendicular to axle/axis y, index „∞" is related to undisturbed flow. Value σ_y is equal to

$$\sigma_y = \frac{l^2}{2} \operatorname{tg}\theta \operatorname{tg}\varphi,$$

therefore

$$M_x' = \frac{l^3}{6} c_p q_\infty \operatorname{tg}^2\theta \operatorname{tg}^2\varphi.$$

If angle $\varphi = \frac{2\pi}{n}$, n - integer, then of dihedral angles it is possible to comprise the surface of the pyramidal body whose cross section will have a form of 2n-angle (Fig. 2), for which will act the torque/moment

$$M_x = n \frac{l^3}{6} c_p q_\infty \operatorname{tg}^2\theta \operatorname{tg}^2 \frac{2\pi}{n}.$$

Are different from zero only force component and torque/moment, that act on body surface in the direction of X-axis.

Torque/moment decreases, when body rotates around axle/axis in positive direction.

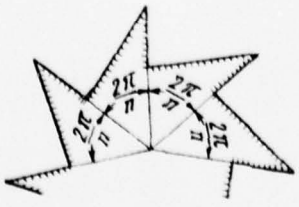


Fig. 2.

The manuscript entered 18/XII 1972.

SOME PROBLEMS OF PLANE VORTEX FLOWS OF INCOMPRESSIBLE FLUID.

V. S. Sadovskiy.

Are obtained in an explicit form the exact solutions of the task of the eddy of the incompressible ideal fluid in circle for the case of vorticity distribution Ω according to the laws: $\Omega = \omega$ sign y, $\Omega = \omega$ sign (xy). where ω = const. Is examined the case of the evenly vortex flow in half-fringe.

1. As is known, besides irrotational flow of incompressible fluid complete equations of nav'ye - Stokes satisfies even class of Vikhrev of flows, which have constant value of eddy/vortex (in flat/plane case). From this point, any exact solutions of this type of the motion of the incompressible fluid are of certain interest. It is necessary to note that the solutions of the problems of the evenly vortex flow in finite domains can be used in the theory of elasticity, since there appear identical boundary-value problems, and also for the investigation of the course of viscous fluid in the channel of the corresponding cross section.

The constancy of eddy/vortex in all flow leads to essential simplifications during the solution of problems, since it makes it possible to utilize the well developed apparatus of the theory of complex variable functions (TFKP). For the first time the methods of TFKP for the study of vortex motions of liquid were used by S. A. Chaplygin [1, 2] and subsequently one way or another is won acceptance in foreign and Soviet literature.

In this work the methods of TFKP are used for obtaining some exact solutions of two-dimensional stationary Vikhrev the motions of the incompressible fluid.

2. Let us examine the flow of ideal fluid in the range, which represents by itself circle with a radius of R. Let the eddy/vortex Ω be distributed according to the law $\Omega = \omega \operatorname{sign} y$, where $\omega = \text{const}$ isolating only upper (lower) part of the circle, we obtain the flow of the mentioned above class $\Omega = \text{const}$. (Let us note that the known exact solution of Chaplygin [3] it is given for the case when eddy/vortex is proportional to the function of current). Let us relate all linear dimensions to value R. In that case the zone of flow in plane z is limited by unit circle (Fig. 1). The function of current $\Psi(x, y)$. introduced in the usual way, satisfies, as is known, the equation of Poisson $\Delta\Psi = -\Omega R^2$, where Δ - operator of Laplace in the coordinates, in reference to a radius R. In view of the obvious

symmetry of flow relative to X-axis, is logical subsequently to examine solution only for the upper part of the circle AOBCA, where Ω = ω.

Page 76.

Function $\Psi(x, y)$ let us search for in the form

$$\Psi = \psi - \omega R^2 r^2/4 \quad (r^2 = x^2 + y^2), \tag{2.1}$$

where ψ - to be determined harmonic function. Set/assuming $\Psi(x, y)$ equal to zero on the boundary of semicircle, from (2.1) we find:

$$\psi_s = \begin{cases} \omega R^2/4 = \text{const}, & z \in ACB, \\ \omega R^2 r^2/4, & z \in AOB. \end{cases} \tag{2.2}$$

Thus, the task of determining the flow is brought to the known boundary-value problem of the Dirichlets - to determination of harmonic function $\psi(x, y)$ in its known value (2.2) on boundary.

It is resolvable the interior of semicircle AOBCA of plane z to the upper part of the plane ζ with the aid of the function of Joukowski

$$\zeta = -\frac{1}{2}\left(z + \frac{1}{z}\right). \tag{2.3}$$

In this case, points A, C, B, O transfer/convert respectively in ζ = 1; 0; -1; ∞ (Fig. 2), and the value of function ψ on boundary

proves to be, as it is not difficult to test that equal to

$$\psi_s = \begin{cases} \frac{1}{4}\omega R^2(-\xi - \sqrt{\xi^2-1})^2, & \xi \leqslant -1, \\ \omega R^2/4, & -1 \leqslant \xi \leqslant 1, \\ \frac{1}{4}\omega R^2(-\xi + \sqrt{\xi^2-1})^2, & \xi \geqslant 1. \end{cases} \tag{2.4}$$

For determination $\psi(\xi, \eta)$ we will use now known Poisson integral for the upper half-plane (for example, see [4]). As a result the unknown function ψ can be written in the form

$$\psi(\xi_0, \eta_0) = \frac{1}{\pi}\int_{-\infty}^{\infty} \psi_s \frac{\eta_0\, d\xi}{(\xi-\xi_0)^2 + \eta_0^2}, \tag{2.5}$$

where $\zeta = \xi_0 + i\eta_0$ - certain fixed/recorded point of upper half-plane, ζ, and ψ_s is given by expression (2.4). It is convenient (2.5) to present in the form

$$\left.\begin{aligned} \psi &= \frac{\omega R^2}{4\pi}(I_1 + I_2 + I_3), \quad I_2 = \int_{-1}^{1} \frac{\eta_0\, d\xi}{(\xi-\xi_0)^2 + \eta_0^2}, \\ I_1 &= \eta_0 \int_{-\infty}^{-1} \frac{(-\xi - \sqrt{\xi^2-1})^2}{(\xi-\xi_0)^2 + \eta_0^2}\, d\xi, \quad I_3 = \eta_0 \int_{1}^{\infty} \frac{(-\xi + \sqrt{\xi^2-1})^2}{(\xi-\xi_0)^2 + \eta_0^2}. \end{aligned}\right\} \tag{2.6}$$

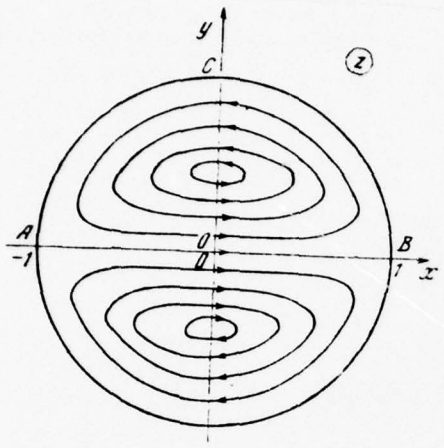


Fig. 1.

Page 77.

Integral I_2 is calculated immediately:

$$I_2 = \operatorname{arctg}\frac{1-\xi_0}{\eta_0} + \operatorname{arctg}\frac{1+\xi_0}{\eta_0}.$$

From (2.3) it is obtained

$$\xi_0 = -\frac{1+r^2}{2r}\cos\theta, \quad \eta_0 = \frac{1-r^2}{2r}\sin\theta,$$

therefore I_2 takes the final form

$$I_2(r,\theta) = \operatorname{arctg}\frac{2r+(1+r^2)\cos\theta}{(1-r^2)\sin\theta} + \operatorname{arctg}\frac{2r-(1+r^2)\cos\theta}{(1-r^2)\sin\theta}. \qquad (2.7)$$

The determination of integrals I_1 and I_3 is connected with the

specific technical difficulties. For an example let us calculate I_3.

Let us pass in I_3 from plane ζ into plane z. This to the equivalently following replacement of variable in the integrand: $t = -\xi + \sqrt{\xi^2 - 1}$, whence

$$\xi = -\frac{1+t^2}{2t}\,dt, \quad d\xi = \frac{1-t^2}{2t^2}\,dt. \tag{2.8}$$

The variable t indicates the sliding point of integration on cut [-1, 0] of plane z. Expression in denominator I_3 can be converted taking into account the fact that from (2.3)

$$\zeta - \zeta_0 = -\frac{1}{2}\left(t - z + \frac{1}{t} - \frac{1}{z}\right).$$

We have:

$$(\xi - \xi_0)^2 + r_0^2 = |\zeta - \zeta_0|^2 = \frac{(t^2 r^2 - 2tx + 1)(t^2 - 2tx + r^2)}{4t^2 r^2}. \tag{2.9}$$

After substitution (2.8) and (2.9) into I_3 and some transforms we obtain:

$$I_3 = r\sin\theta \int_{-1}^{0} \left[\frac{t^2}{t^2 - 2tx + r^2} - \frac{t^2}{t^2 r^2 - 2tx + 1}\right] dt. \tag{2.10}$$

Integral (2.10) is tabular and easily it is taken in an explicit form.

By analogous form is calculated I_1.

Omitting all intermediate mathematical lining/calculations, let us give the resultant expression for functicning the current $\Psi(r, \theta)$:

$$\Psi(r, \theta) = \frac{\omega R^2}{4\pi}\left[\operatorname{arctg}\frac{2r + (1+r^2)\cos\theta}{(1-r^2)\sin\theta} + \operatorname{arctg}\frac{2r - (1+r^2)\cos\theta}{(1-r^2)\sin\theta} - \right.$$
$$- 2\frac{1-r^2}{r}\sin\theta - \frac{1}{2}\frac{1-r}{r^2}\sin 2\theta \ln\frac{1-2r\cos\theta + r^2}{1+2r\cos\theta + r^2} +$$
$$+ r^2\cos 2\theta\left(\operatorname{arctg}\frac{1-r\cos\theta}{r\sin\theta} + \operatorname{arctg}\frac{1+r\cos\theta}{r\sin\theta}\right) -$$
$$\left. - \frac{\cos 2\theta}{r^2}\left(\operatorname{arctg}\frac{r-\cos\theta}{\sin\theta} + \operatorname{arctg}\frac{r+\cos\theta}{\sin\theta}\right) - \pi r^2\right]. \qquad (2.11)$$



Fig. 2.

Page 78.

As an example let us give another expression for distributing the rate according to radius r when $\theta = \pi/2$, which is obtained by substitution $\theta = \pi/2$ in (2.11) and by its subsequent differentiation with respect to r:

$$\frac{1}{\omega R}\frac{\partial W}{R\,dr} = \frac{1+r^2}{\pi r^2} - \frac{1}{\pi r}\left(r^2 \operatorname{arctg}\frac{1}{r} + \frac{1}{r^2}\operatorname{arctg} r\right) - \frac{1}{2}r \qquad (2.12)$$

Fig. 3, depicts the velocity profile with x = 0 in portions ωR, designed on relationship/ratio (2.12). Velocity in points O and C (see Fig. 1) is equal to respectively

$$u_O = 0{,}424; \quad u_C = 1 - \frac{2}{\pi} = 0{,}363.$$

3. Let us examine now flow in circle with a radius of R in the case when eddy/vortex Ω is distributed according to the law Ω = ω

sign (xy), ω = const. During this vorticity distribution, the flow proves to be symmetrical both relative to the y axis and relative to X-axis (Fig. 4). Therefore subsequently is examined only the first quadrant of the circle of AOBCA, where $\omega = \omega$

As earlier, let us relate linear dimensions to the value of radius R, and the function of current ψ to search for in the form (2.1). For the value of the unknown function ψ on boundary, remains valid relationship/ratio (2.2).

Let us represent region AOBCA consecutively to the interior of the semicircle of plane t (Fig. 5), and then to the upper part of the plane ζ (see Fig. 2) respectively by the functions

$$t = \alpha + i\beta = \sigma^2, \quad \zeta = \xi + i\eta = -\frac{1}{2}\left(t + \frac{1}{t}\right).$$

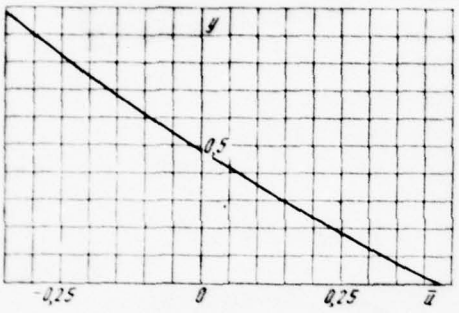


Fig. 3.

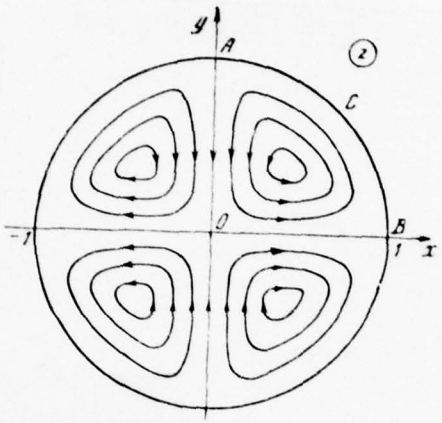


Fig. 4.

Page 79.

In this case the value of function ψ on boundary $\eta=0$ proves to be equal to:

$$\psi_s = \begin{cases} \frac{1}{4}\omega R^2(\xi - \sqrt{\xi^2-1}), & \xi > 1, \\ \frac{1}{4}\omega R^2 = \text{const}, & 1 \geqslant \xi \geqslant -1, \\ \frac{1}{4}\omega R^2(-\xi - \sqrt{\xi^2-1}), & \xi < -1. \end{cases} \tag{3.1}$$

Integral of Poisson (2.5) when ψ_s expressed by relationship/ratios (3.1), also is conveniently written in the form of three integrals (2.6), from which I_2 (on the cutting off [-1, 1]) it is taken immediately. Other two integrals

$$I_1 = \eta_0 \int_{-\infty}^{-1} \frac{(-\xi - \sqrt{\xi^2-1})\,d\xi}{(\xi-\xi_0)^2 + \eta_0^2}; \qquad I_3 = \eta_0 \int_{1}^{\infty} \frac{(-\xi + \sqrt{\xi^2-1})\,d\xi}{(\xi-\xi_0)^2 + \eta_0^2}$$

also are taken in an explicit form, if we in integrands pass from plane ζ to plane t. For example, for I_3 this equivalently to the replacement of a variable of type (2.8) and (2.9), after which for an integral is obtained the expression, almost analogous (2.10). Omitting very cumbersome, but elementary intermediate calculation, let us give the resultant expression for functioning the current $\Psi(r, \theta)$, that describes flow in the first quadrant of the circle (see Fig. 4):

$$\Psi(r, \theta) = \frac{\omega R^2}{4\pi}\left[\operatorname{arctg}\frac{2r^2+(1+r^4)\cos 2\theta}{(1-r^4)\sin 2\theta} + \operatorname{arctg}\frac{2r^2-(1+r^4)\cos 2\theta}{(1-r^4)\sin 2\theta} - \right.$$
$$- 2r^2 \ln r^2 \sin 2\theta - \frac{1-r^4}{2r^2}\sin 2\theta \ln(1-2r^4\cos 4\theta + r^8) -$$
$$- \frac{1-r^4}{r^2}(\pi - 4\theta)\cos 2\theta - r^2\cos 2\theta\left(\operatorname{arctg}\frac{1+r^2\cos 2\theta}{r^2\sin 2\theta} - \operatorname{arctg}\frac{1-r^2\cos 2\theta}{r^2\sin 2\theta}\right) -$$
$$\left. - \frac{\cos 2\theta}{r^2}\left(\operatorname{arctg}\frac{r^2-\cos 2\theta}{\sin 2\theta} - \operatorname{arctg}\frac{r^2+\cos 2\theta}{\sin 2\theta}\right) - \pi r^2\right]. \qquad (3.2)$$

For obtaining the solution, for example, in the second quadrant, it suffices in (3.2) to carry out a transform of the rotation of plane to angle $\pi/2$ and to change sign of eddy/vortex ω. In other words, is sufficient in (3.2) to make the replacement: $\omega \to -\omega$, $\theta \to \theta - \frac{\pi}{2}$.

It is not-without-interest to determine the form of solution (3.2) with $r \to 0$, i.e., to find the asymptotic behavior of solution. Expanding all terms (3.2) in a series on r and being limited only by the members of order r^2, we obtain:

$$\Psi = -\frac{\omega l^2}{2\pi}\bar{r}^2\left[\ln \bar{r}^2 \sin 2\theta - \left(\frac{\pi}{2} - 2\theta\right)\cos 2\theta + \frac{\pi}{2}\right] + \frac{\omega l^2}{2\pi}\bar{r}^2\left(\ln \bar{R}^2 + \frac{3}{2}\right)\sin 2\theta. \quad (3.3)$$

Here the line above the letter means that the corresponding value is referred to certain arbitrary size/dimension l, not connected with R.

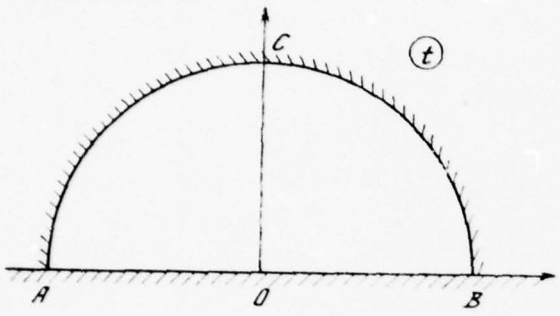


Fig. 5.

Page 80.

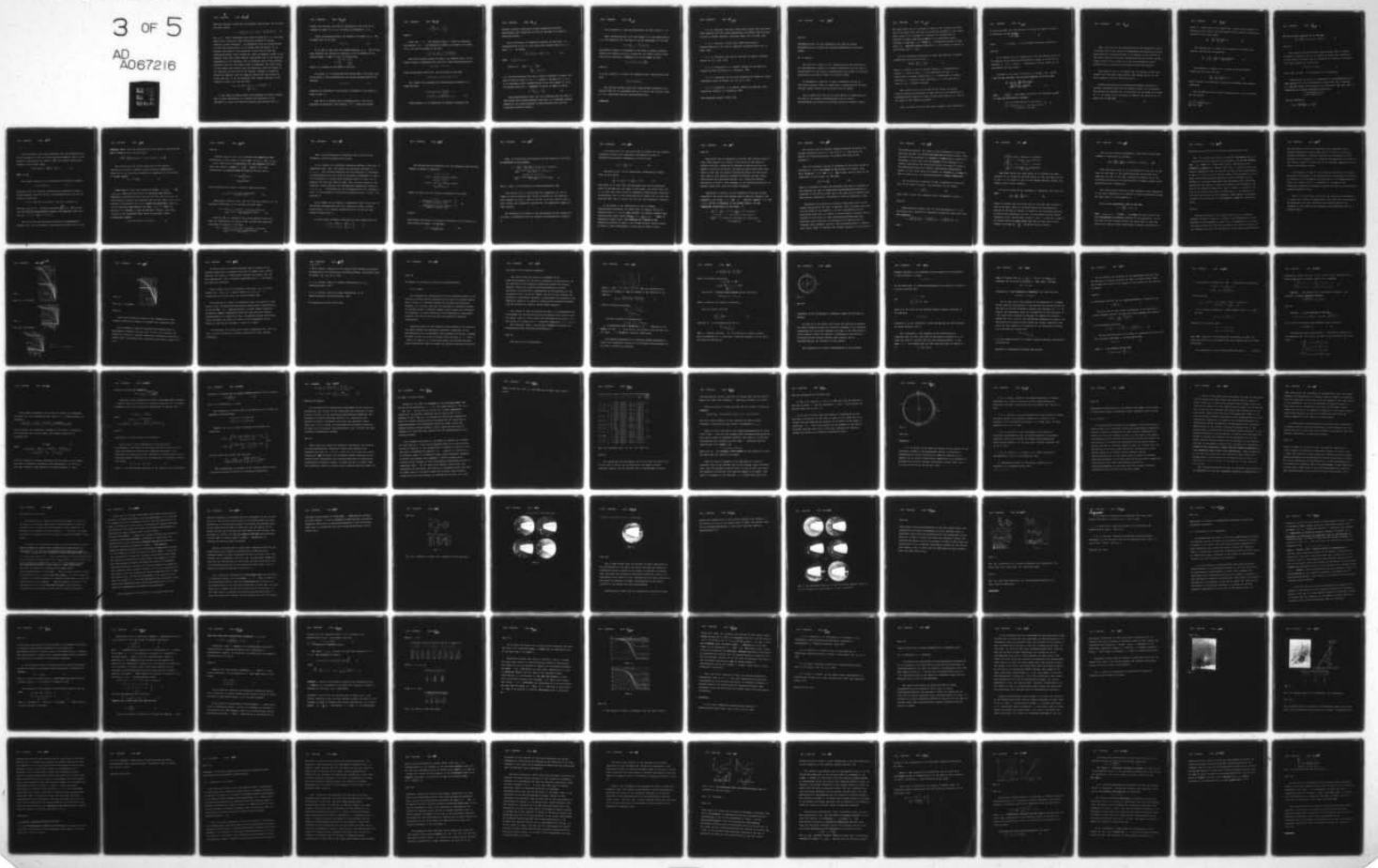
As one would expect that asymptotic behavior is defined "purely" vortex/eddy solution obtained earlier in work [5], and by certain addition, which satisfies, as it is not difficult to test and also in accordance with [5], to the equation of Laplace.

In conclusion let us note still one fact. First term in (3.3) gives the asymptotic form of the solution of vortex flow in the vicinity of the apex/vertex of right angle without the account of the curvature of the flow lines, which form right angle. The effect of the curvature of flow line can be revealed from solution (2.11), if it are examined, for example, in the vicinity of critical point A (see Fig. 1). For this, it suffices to decompose this solution in the vicinity of point z = of -1. This process/operation was made.

AD-A067 216 FOREIGN TECHNOLOGY DIV WRIGHT-PATTERSON AFB OHIO F/G 20/4
SCIENTIFIC NOTES OF CENTRAL INSTITUTE OF AEROHYDRO DYNAMICS (SE--ETC(U)
JUN 78 A S FONAREV, A G ZAKHAROV

UNCLASSIFIED FTD-ID(RS)T-0679-78 NL

3 OF 5
AD A067216



Omitting extremely cumbersome and numerous calculations, let us write the final result:

$$\Psi = -\frac{\omega l^2}{2\pi}\bar{\rho}^2\left[\ln\bar{\rho}^2\sin 2\varphi - \left(\frac{\pi}{2} - 2\varphi\right)\cos 2\varphi + \frac{\pi}{2}\right] + \frac{\omega\rho^2}{2\pi}\ln\frac{4\bar{R}^2}{e}\sin 2\varphi. \qquad (3.4)$$

Here ρ, φ - polar coordinates with focus at point A(-1, 0); the lines above R and ρ mean that these values are referred to certain arbitrary linear dimension l. In expression (3.4) are reject/thrown all the terms whose order on ρ is higher than the second. As is evident, the effect of the curvature of flow line AC with the accuracy/precision, which exceeds ρ^2, does not manifest itself in the dominant term, which gives "purely" vortex/eddy part of the solution (expression in the brackets), but is exhibited only in the potential addition, which has the higher order of smallness, than first term. In this vortex flow differs from the potential, where the effect of the curvature of flow line on the velocity gradient is exhibited already in dominant term. For example, during the flow around the circle (see Fig. 1) by the potential flow complex potential in the vicinity of point A it has the form:

$$W(z) \equiv V_\infty\left(z + \frac{R^2}{z}\right) = 2V_\infty\left[-R + (z+R) + \frac{(z+R)^2}{2R} + \cdots\right],$$

$$\frac{d^2W}{dz^2} \approx \frac{2V_\infty}{R}.$$

4. Let range of evenly vortex flow represent by itself triangle OAB, in which apex/vertex O is distant into infinity, cut AB lie/rests on y axis, and side BO coincides with positive part of

X-axis. Let, further, the task be calibrated so that side AB of triangle is equal to π, i.e., to point A corresponds $z = \pi i$.

Unlike preceding/previous, the function of current $\Psi(x, y)$ let us search for in the form

$$\Psi = \psi - \omega y^2/2. \tag{4.1}$$

It is easy to test that the unknown function $\psi(x, y)$ and in this case satisfies the equation of Laplace. If we on boundary of the region assume $\Psi = 0$, then of (4.1) it follows that

$$\psi_s = \begin{cases} \frac{\omega\pi^2}{2} = \text{const}, & z \in AO, \\ \frac{\omega r^2}{2}, & z \in ACB, \\ 0, & z \in BO \end{cases}$$

(point C is located on the middle of cut AB).

As earlier, it is resolvable half-fringe OABO to the upper part of the plane ζ. This representation is realize/accomplished by the function

$$\zeta \equiv \xi + i\eta = \operatorname{ch} z, \tag{4.2}$$

moreover the conformity of the points of boundary of the region is shown on Fig. 2.

From (4.2) it follows that on boundary ACB $r = \arccos \xi$; therefore on axle/axis ξ the function $\psi(\xi, \eta)$ takes the values:

$$\psi_s = \begin{cases} \omega\pi^2/2, & \xi \leqslant -1, \\ \frac{1}{2}\,\omega \arccos^2 \xi, & -1 \leqslant \xi \leqslant 1, \\ 0, & 1 \leqslant \xi. \end{cases}$$

Page 81.

Since when $\xi \to \infty$ the boundary value ψ_s does not grow/rise, the function $\psi(\xi, \eta)$ is determined as before by integral of Poisson (2.5), who can be written in the form

$$\psi = \frac{\omega}{2\pi}\left[\pi^2 \int_{-\infty}^{-1} \frac{\eta_0\, d\xi}{(\xi - \xi_0)^2 + \eta_0^2} + \int_{-1}^{1} \frac{\eta_0 \arccos^2 \xi\, d\xi}{(\xi - \xi_0)^2 + \eta_0^2}\right].$$

The first integral easily is taken in an explicit form. In the second integral denominator with the aid of the relationship/ratios

$$\xi_0 = \operatorname{ch} x \cos y, \quad \eta_0 = \operatorname{sh} x \sin y,$$

those escape/ensue from (4.2), can be written in the form

$$(\xi - \xi_0)^2 + \eta_0^2 = \xi^2 - 2\xi \operatorname{ch} x \cos y + (\operatorname{sh}^2 x + \cos^2 y).$$

As a result the expression for functioning the current $\Psi(x, y)$ takes the form

$$\Psi(x, y) = \frac{\omega}{2\pi}\left(\pi^2 \operatorname{arcctg} \frac{1 + \operatorname{ch} x \cos y}{\operatorname{sh} x \sin y} - \pi y^2 + \right.$$
$$\left. + \operatorname{sh} x \sin y \int_{-1}^{1} \frac{\arccos^2 \xi\, d\xi}{\xi^2 - 2\xi \operatorname{ch} x \cos y + \operatorname{sh}^2 x + \cos^2 y}\right). \qquad (4.3)$$

Unfortunately, it is impossible to express in brackets the

definite integral confronting through elementary functions. Nevertheless some properties of flow all the same it is easy to establish/install.

Let us determine the asymptotic behavior of flow when $x \to \infty$. Differentiating (4.3) on y and taking into account that $\operatorname{sh} x \sim \operatorname{ch} x \to \infty$ when $x \to \infty$, we obtain

$$u = \frac{\partial \Psi}{\partial y} \approx \frac{\omega}{2\pi}\left(\pi^2 \operatorname{cth} x + A\frac{\cos y}{\operatorname{sh} x} - 2\pi y\right), \tag{4.4}$$

where $A = \int_{-1}^{1} \arccos^2 \xi \, d\xi = \pi^2 - 4.$

Since $\operatorname{cth} x \to 1$ when $x \to \infty$, that

$$\left.\frac{\partial \Psi}{\partial y}\right|_{x=\infty} = \omega\left(\frac{\pi}{2} - y\right),$$

i.e. the airfoil/profile of rate of flow at infinity is linear. The rate of flow on walls y = 0, y = π proves to be equal to $u_\infty = \pm \omega\pi/2$. It is analogous, after differentiation (4.3) with respect to x for the maximum value of y - component of vector of speed we obtain

$$v = -\left.\frac{\partial \Psi}{\partial x}\right|_{\substack{x\to\infty \\ y=\pi/2}} = -\frac{2\omega}{\pi \operatorname{sh} x}. \tag{4.5}$$

Relationship/ratios (4.4) and (4.5) indicate that the eddy in half-fringe with removal/distance from wall x = 0 extremely rapidly emerges to the conditions/mode of plane-parallel flow with the rectilinear velocity profile.

Is of interest to find the distribution of rate on wall y = 0.

After differentiation (4.3) with respect to y and substitution y = 0, the expression for rate u(x, 0) can be represented in the form

$$u(x, 0) = \frac{\partial \psi}{\partial y}\Big|_{y=0} = -\frac{\omega \operatorname{sh} x}{\pi} \int_0^{\pi} \frac{y\, dy}{\cos y - \operatorname{ch} x}.$$

Last/latter integral is expressed in the form of infinite function series (for example, see [6], of page 451, No 3.794), which in this case can be simplified. Expression for a rate takes the form

$$u(x, 0) = \frac{2\omega}{\pi} \left(x \ln \operatorname{cth} \frac{x}{2} + \int_0^{\pi} \frac{t\, dt}{\operatorname{sh} t} \right).$$

Page 82.

It is not difficult to obtain now expression for a derivative of the rate:

$$\frac{\partial u}{\partial x}(x, 0) = \frac{2\omega}{\pi} \ln \operatorname{cth} \frac{x}{2}.$$

The velocity gradient along wall render/showed expressed in an explicit form and in accordance with [5] it has at the critical point x = of 0 logarithmic special feature/peculiarity.

REFERENCES

1. S. A. Chaplygin. The flow, which flows around with continuous rates sampling with the formation/education of constant eddy/vortices in front is behind sampling. Collected works, Vol. II OGIZ, 1948.

2. S. A. Chaplygin. Vortex flow, which flows around barrier/obstacle in the form of sampling. Collected works, Vol. II OGIZ, 1948.

3. S. A. Chaplygin. One Case of the eddy of liquid. Collected works, Vol. II, OGIZ, 1948.

4. M. A. Lavrentyev, B. V. Shabat. Methods of the theory of complex variable functions, M., "science", 1965.

5. V. S. Sadovskiy. On the local properties of Vikhrev of flows. "scientific notes of TsAGI", Vol. II, No 4, 1971.

6. I. S. Gradstein, I. M. Ryzhik. Tables of integrals, sums, series and products. M., Fizmatgiz, 1963.

The manuscript entered 10/III 1972.

Page 83.

TEMPERATURE FIELD AND HEAT TRANSFER IN THE FLOW OF VISCOUS INCOMPRESSIBLE GAS BETWEEN TWO PARALLEL HARMONICALLY OSCILLATING PLATES.

Ye. M. Zhmulin.

Are given the results of the investigation of the solution of the nonhomogeneous equation of thermal conductivity for the case of viscous motion of the viscous incompressible gas between the parallel harmonically oscillating plates of infinite length.

Is determined a quantity of heat, transferred through the oscillating surface, when its temperature is maintained by constant, and heat supply through the motionless plate is absent.

Let us examine the task of the distribution of temperature for the case of the laminar one-dimensional flow of viscous incompressible gas between two parallel plates of infinite length.

The lower plate (let us call/name it plate 2) let us place on x-axis and let us assume that the rate of its motion is equal to zero. Upper plate (plate 1) is arranged at a distance of h from x-axis in parallel to plate 2 and let us assign to it oscillatory motion according to the law $u_1 = u_0 e^{i\omega t}$, where u_1 - instantaneous speed of upper plate, u_0 - amplitude value of velocity, ω - the angular frequency of oscillations and t - time.

For the formulated conditions of task, the equation of thermal conductivity will take the form:

$$\rho c g A^2 \frac{\partial T}{\partial t} = \lambda \frac{\partial^2 T}{\partial y^2} + \frac{\mu}{I}\left(\frac{\partial u}{\partial y}\right)^2, \qquad (1)$$

where ρ - density of gas (a constant value), g - acceleration of gravity c - specific heat, T - the temperature in flow, λ - a coefficient of thermal conductivity, μ - a coefficient of dynamic viscosity, I - mechanical heat equivalent, u - a gas velocity in flow, $\bar{y} = y/h$ - relative ordinate.

Heat source in flow is the work of the forces of viscous friction (besides introduction to heat flow via its transmission in boundaries) which depends, as this follows from equation (1), then of the square of the velocity gradient.

Work [1] shows, that for the case in question the distribution

of the rate within the flow between two plates in complex variables is determined by the formula

$$u = u_0 e^{i\omega t} \frac{\operatorname{sh} \delta y}{\operatorname{sh} \delta h}. \qquad (2)$$

where $\delta = (1+i)\sqrt{\frac{\omega}{2\nu}}$, $\nu = \mu/\rho$ – a kinematic viscosity coefficient.

Page 84.

Let us assume that the temperature of the gas between plates in the absence of disturbance/perturbations is equal to T_0 and let us designate $T = T_0 + \tau$, where τ - temperature in flow, caused by the oscillations of upper plate.

Determining the value of velocity u, derived $\partial u/\partial \bar{y}$ in the field of real variable, let us write equation (1) in the form

$$\frac{\partial \tau}{\partial t} = \frac{\nu}{h^2 \operatorname{Pr}} \frac{\partial^2 \tau}{\partial \bar{y}^2} + \frac{\nu u_0^2 \gamma^2}{gcJh^2} \frac{\operatorname{sh}^2 \gamma\bar{y} + \cos^2 \gamma\bar{y}}{\operatorname{sh}^2 \gamma + \sin^2 \gamma} + \\ + \frac{\nu u_0^2 \gamma^2}{gcJh^2} \frac{\vartheta(\bar{y}) \cos 2\omega t + \Theta(\bar{y}) \sin 2\omega t}{(\operatorname{sh}^2 \gamma + \sin^2 \gamma)^2}, \qquad (3)$$

where $\gamma = h\sqrt{\frac{\omega}{2\nu}}$, the number of Prandtl, and function $\vartheta(\bar{y})$ and $\Theta(\bar{y})$ they are determined as follows:

$$\left.\begin{aligned} \vartheta(\bar{y}) &= \frac{1}{4}[(1-\bar{b})\operatorname{sh} 2\gamma\bar{y} \cdot \sin 2\gamma\bar{y} + \bar{a}(1 + \operatorname{ch} 2\gamma\bar{y} \cdot \cos 2\gamma\bar{y})], \\ \Theta(\bar{y}) &= \frac{1}{4}[\bar{a} \operatorname{sh} 2\gamma\bar{y} \cdot \sin 2\gamma\bar{y} - (1-\bar{b})(1 + \operatorname{ch} 2\gamma\bar{y} \cdot \cos 2\gamma\bar{y})], \\ \bar{a} &= \operatorname{sh} 2\gamma \cdot \sin 2\gamma, \quad \bar{b} = \operatorname{ch} 2\gamma \cdot \cos 2\gamma. \end{aligned}\right\} \qquad (4)$$

Thus, the tasks of the determination of the temperature profile in laminar flow of the viscous incompressible gas between two plates whose motion is determined above, it is brought to the solution of the linear equation of thermal conductivity for the uniform stream of single section with a length of h with heat-insulated lateral surfaces and the internal, continuously acting heat sources.

From equation (3) it is evident that the sources of heat were divided into two forms: being steady, that depend only on $\bar{y}$, and being unsteady, that are function $\bar{y}$ and t.

Without specifying the preliminarily boundary conditions, a question concerning which will be examined below, let us determine the solution of equation (3). In this case, let us assume that number Pr = 1. By virtue of the linearity of equation (3) solution let us search for in the form

$$\tau = \tau' + \tau''. \tag{5}$$

where τ' - temperature of disturbed flow, caused by the presence of stationary heat sources and determined from the ordinary differential equation of the second order

$$\frac{d^2\tau'}{d\bar{y}^2} + \frac{u_0^2\gamma^2}{cgl}\,\frac{\mathrm{sh}^2\gamma\bar{y} + \sin^2\gamma\bar{y}}{\mathrm{sh}^2\gamma + \sin^2\gamma} = 0. \qquad (6)$$

The temperature τ'', caused by the presence of unsteady heat sources, will satisfy the equation:

$$\frac{\partial\tau''}{\partial t} = \frac{\nu}{h^2}\,\frac{\partial^2\tau''}{\partial\bar{y}^2} + \frac{\nu u_0^2\gamma^2}{cgh^2}\,\frac{\vartheta(\bar{y})\cos 2\omega t + \Theta(\bar{y})\sin 2\omega t}{(\mathrm{sh}^2\gamma + \sin^2\gamma)^2}. \qquad (7)$$

The solution of equation (6) is found by direct/straight integration and takes the form

$$\tau' = -\frac{u_0^2}{8cgl}\cdot\frac{\mathrm{ch}\,2\gamma\bar{y} - \cos 2\gamma\bar{y}}{\mathrm{sh}^2\gamma + \sin^2\gamma} + \bar{c}\bar{y} + \bar{c}_1, \qquad (8)$$

where $\bar{c}$ and $\bar{c}_1$ - the arbitrary constants, determined from boundary conditions.

Let us determine the solution of equation (7). Let us designate for the brevity

$$\frac{\nu}{h^2} = M \quad \text{и} \quad \frac{\nu u_0^2\gamma^2}{cgh^2(\mathrm{sh}^2\gamma + \sin^2\gamma)^2} = N$$

Key: (1). and.

and let us write equation (7) in the form

$$\frac{\partial \tau''}{\partial t} = M \frac{\partial^2 \tau''}{\partial \bar{y}^2} + N\vartheta(\bar{y}) \cos 2\omega t + N\Theta(\bar{y}) \sin 2\omega t. \qquad (7a)$$

Page 85.

Since within flow act the heat sources whose power is changed according to harmonic law, it is logical to assume that temperature τ'' will follow this same law [2]. Therefore the solution of equation (7a) let us search for in the form

$$\tau'' = P(\bar{y}) \cos 2\omega t + Q(\bar{y}) \sin 2\omega t, \qquad (9)$$

where $P(\bar{y})$ and $Q(\bar{y})$ - the functions, to be determined.

Substituting the value τ'', determined by relationship/ratio (9), into equation (7a) and by accumulating terms with $\cos 2\omega t$ and $\sin 2\omega t$, we will obtain for determining the functions $P(\bar{y})$ and $Q(\bar{y})$ the system of the ordinary differential equations:

$$\left.\begin{aligned} -2\omega P(\bar{y}) &= MQ''(\bar{y}) + N\Theta(\bar{y}), \\ 2\omega Q(\bar{y}) &= MP''(\bar{y}) + N\vartheta(\bar{y}). \end{aligned}\right\} \qquad (10)$$

Are here designated

$$P''(\bar{y}) = \frac{d^2 P(\bar{y})}{d\bar{y}^2} \text{ and } Q''(\bar{y}) = \frac{d^2 Q(\bar{y})}{d\bar{y}^2}.$$

Differentiating twice second equation (10) and substituting for to the derivative $Q''(\bar{y})$ its value from first equation (10), we will obtain for determining the function $P(\bar{y})$ the ordinary differential equation of the fourth order:

$$P^{IV}(\bar{y}) + 4m^4 P(\bar{y}) = -\frac{2\omega N}{M^2}\Theta(\bar{y}) - \frac{N}{M}\vartheta''(\bar{y}). \qquad (11)$$

where $m^4 = \frac{\omega^2}{M^2}$.

The general solution of the homogeneous differential equation

$$P^{IV}(\bar{y}) + 4m^4 P(\bar{y}) = 0, \qquad (11a)$$

coinciding with the equation, describing the curvature of beam on elastic support under the action of concentrated force [3], can be written in the form:

$$P_1(\bar{y}) = c_1 \operatorname{ch} m\bar{y}\cdot\cos m\bar{y} + c_2 \operatorname{ch} m\bar{y}\cdot\sin m\bar{y} + c_3 \operatorname{sh} m\bar{y}\cdot\cos m\bar{y} + c_4 \operatorname{sh} m\bar{y}\cdot\sin m\bar{y}, \quad (12)$$

where c_1, c_2, c_3, c_4 - arbitrary constants, and $m = \gamma\sqrt{2}$. Let us note that the roots of characteristic equation for equation (11a) they will be $r_{1,2} = m(1 \pm i)$ and $r_{3,4} = -m(1 \pm i)$.

Let us find now the particular solution of nonhomogeneous equation (11). Let us examine in more detail the right side of this

equation, which after the substitution of the values of function $\vartheta(\bar{y})$ and $\vartheta(\bar{y})$ from (4) will take the form

$$\left(\frac{2\gamma^2 N}{M} - \frac{\omega N}{2m^2}\right)[\bar{a}\,\mathrm{sh}\,2\gamma\bar{y}\cdot\sin 2\gamma\bar{y} - (1-\bar{b})\,\mathrm{ch}\,2\gamma\bar{y}\cdot\cos 2\gamma\bar{y}] + (1-\bar{b})\,\frac{\omega N}{2M^2}.$$

The last/latter term of the right side of the equation represents by itself a constant value; therefore immediately we obtain one of the particular solutions of equation (11) in the form of "static shift":

$$P_2 = (1-\bar{b})\,\frac{\omega N}{8M^2m^4}. \qquad (13)$$

First term of right side contains products $\mathrm{sh}\,2\gamma\bar{y}\cdot\sin 2\gamma\bar{y}$ and $\mathrm{ch}\,2\gamma\bar{y}\cdot\cos 2\gamma\bar{y}$. Utilizing expressions of hyperbolic and circular functions in exponential form, and also the fact that the roots of characteristic equation for equation (11a) are not equal to 2γ, it is possible in accordance with [3] to search for particular solutions for the remaining right side in the form $A_n e^{\pm 2\gamma(1\pm i)\bar{y}}$, where the unknown it is constant A_n. Let us determine, however, particular solution in the equivalent form, which considerably reduces calculations, namely:

$$P_3(\bar{y}) = K\,\mathrm{ch}\,2\gamma\bar{y}\cdot\cos 2\gamma\bar{y} + L\,\mathrm{sh}\,2\gamma\bar{y}\cdot\sin 2\gamma\bar{y}. \qquad (14)$$

Constant values K and L are located by the equating of the coefficients of the products of functions $\mathrm{ch}\,2\gamma\bar{y}\cdot\cos 2\gamma\bar{y}$ and $\mathrm{sh}\,2\gamma\bar{y}\cdot\sin 2\gamma\bar{y}$ after substitution of expression (14) into equation (11) with right side without constant $(1-\bar{b})\frac{\omega N}{2M^2}$. Carrying out these calculations and opening values of M and N, we will obtain:

$$K=(1-\bar{b})\frac{u_0^2}{48\,cgl\,(\mathrm{sh}^2\gamma+\sin^2\gamma)^2},$$

$$L=-\bar{a}\frac{u_0^2}{48\,cgl\,(\mathrm{sh}^2\gamma+\sin^2\gamma)^2},$$

which determines the value of function $P_3(\bar{y})$ in the form

$$P_3(\bar{y})=\frac{u_0^2[(1-\bar{b})\,\mathrm{ch}\,2\gamma\bar{y}\cdot\cos 2\gamma\bar{y}-\bar{a}\,\mathrm{sh}\,2\gamma\bar{y}\cdot\sin 2\gamma\bar{y}]}{48\,cgl\,(\mathrm{sh}^2\gamma+\sin^2\gamma)^2}. \qquad (14a)$$

Summarizing solutions (12), (13) and (14a) and carrying out the necessary transforms, let us determine function $P(\bar{y})$:

$$P(\bar{y})=c_1\,\mathrm{ch}\,m\bar{y}\cdot\cos m\bar{y}+c_2\,\mathrm{ch}\,m\bar{y}\cdot\sin m\bar{y}+c_3\,\mathrm{sh}\,m\bar{y}\cdot\cos m\bar{y}+c_4\,\mathrm{sh}\,m\bar{y}\cdot\sin m\bar{y}+$$
$$+\frac{u_0^2}{48\,cgl}\frac{(1-\bar{b})(3+\mathrm{ch}\,2\gamma\bar{y}\cdot\cos 2\gamma\bar{y})-\bar{a}\,\mathrm{sh}\,2\gamma\bar{y}\cdot\sin 2\gamma\bar{y}}{(\mathrm{sh}^2\gamma+\sin^2\gamma)^3}. \qquad (15)$$

Function $Q(\bar{y})$ is determined from second equation (10), also, after the substitution of values $P''(\bar{y})$ and $\vartheta(\bar{y})$ and conducting conversions is reduced to the form

$$Q(\bar{y})=-c_1\,\mathrm{sh}\,m\bar{y}\cdot\sin m\bar{y}+c_2\,\mathrm{sh}\,m\bar{y}\cdot\cos m\bar{y}-c_3\,\mathrm{ch}\,m\bar{y}\cdot\sin m\bar{y}+c_4\,\mathrm{ch}\,m\bar{y}\cdot\cos m\bar{y}+$$
$$+\frac{u_0^2}{48\,cgl}\frac{(1-\bar{b})(\mathrm{sh}\,2\gamma\bar{y}\cdot\sin 2\gamma\bar{y}+\bar{a}(3+\mathrm{ch}\,2\gamma\bar{y}\cdot\cos 2\gamma\bar{y})}{(\mathrm{sh}^2\gamma+\sin^2\gamma)^3}. \qquad (16)$$

Thus, the determination of functions $P(\bar{y})$ and $Q(\bar{y})$ stated problem is solved in general form to end.

Let us examine now a question concerning boundary conditions. In expressions (8), (15), (16) enters six arbitrary constants: $\bar{c}$, $\bar{c}_1$, c_2, c_3, c_4. For boundary conditions for the function τ'', determined by relationship/ratio (9), would be satisfying independent of time t, it is necessary to require their execution with $\bar{y} = 0$ and 1 it is separate for functions $P(\bar{y})$ and $Q(\bar{y})$. This will give system of four algebraic linear equations for determination unknown the constants c_1, c_2, c_3, c_4. Analogously for the determination of the constants $\bar{c}$ and $\bar{c}_1$ it is necessary to satisfy the condition with $\bar{y} = 0$ and 1 for function τ'.

As an example let us examine a temperature field in the flow of the viscous incompressible gas and a quantity of heat, isolated through plate 1, at constant temperature T_0 on it and zero heat current through plate 2.

In other words, boundary conditions for this example will be:

$$\left.\begin{array}{llll} \bar{y}=0, & \dfrac{\partial \tau'}{\partial \bar{y}}=0, & \dfrac{dP(\bar{y})}{d\bar{y}}=0, & \dfrac{dQ(\bar{y})}{d\bar{y}}=0; \\ \bar{y}=1, & \tau'=0, & P(\bar{y})=0, & Q(\bar{y})=0. \end{array}\right\} \qquad (17)$$

The satisfaction of conditions (17) for functions $P(\bar{y})$ and $Q(\bar{y})$ reduces to system of equations:

$$c_2 + c_3 = 0; \quad c_2 - c_3 = 0;$$

$$c_1 \operatorname{ch} m \cos m + c_2 \operatorname{ch} m \sin m + c_3 \operatorname{sh} m \cos m + c_4 \operatorname{sh} m \sin m + \frac{u_0^2 (3 - \bar{a}^2 - 2\bar{b} - \bar{b}^2)}{48 c g l (\operatorname{sh}^2 \gamma + \sin^2 \gamma)^2} = 0;$$

$$-c_1 \operatorname{sh} m \sin m + c_2 \operatorname{sh} m \cos m - c_3 \operatorname{ch} m \sin m + c_4 \operatorname{ch} m \cos m + \frac{4 \bar{a} u_0^2}{48 c g l (\operatorname{sh}^2 \gamma + \sin^2 \gamma)^2} = 0,$$

whence we obtain for the arbitrary constants of the value:

$$\left.\begin{aligned} c_2 &= c_3 = 0; \\ c_1 &= -\frac{u_0^2 [4 \bar{a} \operatorname{sh} m \sin m - (3 - \bar{a}^2 - 2\bar{b} - \bar{b}^2) \operatorname{ch} m \cos m]}{48 c g l (\operatorname{sh}^2 \gamma + \sin^2 \gamma)^2 (\operatorname{sh}^2 m + \cos^2 m)}; \\ c_4 &= -\frac{u_0^2 [4 \bar{a} \operatorname{ch} m \cos m + (3 - \bar{a}^2 - 2\bar{b} - \bar{b}^2) \operatorname{sh} m \sin m]}{48 c g l (\operatorname{sh}^2 \gamma + \sin^2 \gamma)^2 (\operatorname{sh}^2 m + \cos^2 m)}. \end{aligned}\right\} \quad (18)$$

Page 87.

Analogously satisfaction of boundary conditions (17) for function r' gives values of $\bar{c}$ and $\bar{c}_1$, in the form

$$\bar{c} = 0, \quad \bar{c}_1 = \frac{u_0^2}{8 c g l (\operatorname{sh}^2 \gamma + \sin^2 \gamma)}. \quad (18a)$$

Thus, the temperature distribution over the section of flow will be determined by the formula:

$$T = T_0 + \frac{u_0^2}{4cgl}\left(1 - \frac{\mathrm{sh}^2\gamma\bar{y} + \sin^2\gamma\bar{y}}{\mathrm{sh}^2\gamma + \sin^2\gamma}\right) + \left[c_1\,\mathrm{ch}\,m\bar{y}\cdot\cos m\bar{y} + c_4\,\mathrm{sh}\,m\bar{y}\cdot\sin m\bar{y} + \right.$$
$$\left. + \frac{u_0^2}{48cgl}\,\frac{(1-\bar{b})(3+\mathrm{ch}\,2\gamma\bar{y}\cdot\cos 2\gamma\bar{y}) - \bar{a}\,\mathrm{sh}\,2\gamma\bar{y}\cdot\sin 2\gamma\bar{y}}{(\mathrm{sh}^2\gamma + \sin^2\gamma)^2}\right]\cos 2\omega t -$$
$$- \left[c_1\,\mathrm{sh}\,m\bar{y}\cdot\sin m\bar{y} - c_4\,\mathrm{ch}\,m\bar{y}\cdot\cos m\bar{y} - \right.$$
$$\left. - \frac{u_0^2}{48cgl}\,\frac{(1-\bar{b})\,\mathrm{sh}\,2\gamma\bar{y}\cdot\sin 2\gamma\bar{y} + \bar{a}(3+\mathrm{ch}\,2\gamma\bar{y}\cdot\cos 2\gamma\bar{y})}{(\mathrm{sh}^2\gamma + \sin^2\gamma)^2}\right]\sin 2\omega t, \qquad (19)$$

where c_1 and c_4 are determined by relationship/ratios (18).

From formula (19) it follows that the temperature of flow is summed up from stationary part, which is function $\bar{y}$, and unsteady, which depends on $\bar{y}$ and t. When in cos 2ωt or sin 2ωt receive zero or equal values, the temperature profiles for the appropriate moments of time coincide.

We investigate the effect on the distribution of the temperature of value γ, considering that its changes are determined by frequency ω.

It is known that for the steady flow of Couette and the boundary conditions accepted the temperature distribution in flow is determined by quadratic dependence on $\bar{y}$ of the form

$$T_* = T_0 + \frac{u_0^2}{2cgl}(1-\bar{y}^2). \qquad (20)$$

Calculating lim T of the temperature, determined by formula (19), we will obtain

$$\lim_{\gamma\to 0} T = T_0 + \frac{u_0^2}{4cgl}(1-\bar{y}^2) + \frac{u_0^2}{4cgl}(1-\bar{y}^2)\cos 2\omega t. \qquad (21)$$

from which it is clear that the stationary part and the amplitude value of unsteady part are equal to each other, but within limit with $\omega = 0$, both these parts form the temperature distribution, determined by dependence (20) for the steady motion of Couette. Let us note that function $Q(\bar{y})$, that is factor with sin $2\omega t$, with decrease γ vanishes.

At low values γ, the temperature of flow is changed simultaneously throughout the whole depth of channel, taking the minimum value of $T = T_0$ on upper boundary and maximum values at any fixed/recorded point within flow y_*, $T = T_0 + \frac{u_0^2}{2cgl}(1-\bar{y}_*^2)$. equal to temperature steady flows. The frequency of a change in the temperature profile is equal to the doubled angular traffic density of plate 1, phase displacement in this case is equal to zero.

Physically this is explained by the fact that thermal energy in flow, which appears as a result of the action of the forces of internal friction, caused by the presence of motion and does not depend on direction of motion. Oscillating plate, being moved from state of rest into the point of maximum deviation and vice versa, will cause in flow shearing stresses of friction and heat fluxes twice during one oscillatory period, i.e., during the harmonic oscillation of plate 1 with frequency ω, the isolation/liberation of thermal energy must occur with double frequency.

Expressing in formula (19) the hyperbolic functions through exponential and taking into account that at the high values of the parameter γ by values $e^{-\gamma\sqrt{2}}$ and $e^{-2\gamma}$, and also canoes $e^{-\gamma\sqrt{2}(1+\bar{y})}$ and $e^{-2\gamma(1+\bar{y})}$ can be disregarded, we will obtain formula for the temperature distribution in flow when $\gamma\to\infty$:

$$\lim_{\gamma\to\infty} T = T_0 + \frac{u_0^2}{4cgl}\left[1 - e^{-2\gamma(1-\bar{y})}\right] + \frac{u_0^2}{12cgl}\left[e^{-\gamma\sqrt{2}(1-\bar{y})}(\cos m\cos m\bar{y} + \sin m\sin m\bar{y}) - e^{-2\gamma(1-\bar{y})}(\cos 2\gamma\cos 2\gamma\bar{y} + \sin 2\gamma\sin 2\gamma\bar{y})\right]\cos 2\omega t - \frac{u_0^2}{12cgl}\left[e^{-\gamma\sqrt{2}(1-\bar{y})}(\cos m\sin m\bar{y} - \sin m\cos m\bar{y}) - e^{-2\gamma(1-\bar{y})}(\sin 2\gamma\cos 2\gamma\bar{y} - \cos 2\gamma\sin 2\gamma\bar{y})\right]\sin 2\omega t. \quad (22)$$

Let us note that the obtained formula satisfies accurately the boundary conditions with $\bar{y} = 1$, but with $\bar{y} = 0$ - with which the greater the accuracy/precision, the greater the value of the parameter γ.

With the unlimited increase of frequency at the finite values of difference $1 - \bar{y} \neq 0$ are member in the brackets of formulas (22), which depend on $e^{-\gamma(1-\bar{y})}$ and $e^{-2\gamma(1-\bar{y})}$, they vanish, and the value of the temperature in this range - to the limit

$$\lim_{\gamma \to \infty} T = T_0 + \frac{u_0^2}{4cgl}. \qquad (22a)$$

Hence it is possible to make the conclusion that with an increase in the frequency the zone of temperature disturbance/perturbations is displaced to the side of driver and at the same time is expanded zone from constant temperature, determined in value by expression (22a).

Physically this process is explained sufficiently well by the dynamic properties of the flow in question. Work [1] shows, that with the low values of the parameter γ of flow disturbance from the oscillating plate they are spread to entire depth of channel. With an increase in the values γ, these disturbance/perturbations near motionless plate decrease, and beginning with certain value of frequency they disappear entirely. Near motionless plate is formed a dead region, which is expanded with further increase γ to the side of

the positive values $\bar{y}$. The range of flow disturbance in this case ever more and more is concentrated near the oscillating plate. Since the zone of the gradients of velocity $\partial u/\partial y$, determining a quantity of isolatable in heat flow, with an increase in the parameter γ is reduced, approaching the oscillating plate, the range of change in the temperature also it is reduced, approaching a perturbation source. In the region where the gradient of velocity $\partial u/\partial \bar{y}$ is equal to zero or close to it, is establish/installed constant temperature.

Let us calculate a quantity of heat, transferred through the unit of the length of plate 1 and determined by the formula

$$q_1 = -\frac{\lambda}{h}\left(\frac{\partial T}{\partial \bar{y}}\right)_1. \qquad (23)$$

where index 1 means that parameter value corresponds to plate 1.

Page 89.

Differentiating formula (19) on $\bar{y}$ and set/assuming $\bar{y} = 1$, we will obtain for a quantity of isolatable through the upper plate heat the expression

$$q_1 = \frac{\lambda \gamma a_0^2}{4 cgh} \frac{\operatorname{sh} 2\gamma + \sin 2\gamma}{\operatorname{sh}^2 \gamma + \sin^2 \gamma} + \frac{\lambda}{h}\left[\frac{dP(\bar{y})}{d\bar{y}}\right]_1 \cos 2\omega t - \frac{\lambda}{h}\left[\frac{dQ(\bar{y})}{d\bar{y}}\right]_1 \sin 2\omega t, \quad (24)$$

where

$$\left[\frac{dP(\bar{y})}{d\bar{y}}\right]_1 = \gamma\sqrt{2}\left[(c_1+c_4)\,\mathrm{sh}\,m\cos m-(c_1-c_4)\,\mathrm{ch}\,m\sin m\right]+$$
$$+\frac{\gamma u_0^2}{24\,cgl}\,\frac{(1-\bar{b}-\bar{a})\,\mathrm{sh}\,2\gamma\cos 2\gamma-(1-\bar{b}+\bar{a})\,\mathrm{ch}\,2\gamma\sin 2\gamma}{(\mathrm{sh}^2\gamma+\sin^2\gamma)^2};$$
$$\left[\frac{dQ(\bar{y})}{d\bar{y}}\right]_1 = \gamma\sqrt{2}\left[(c_1+c_4)\,\mathrm{ch}\,m\sin m+(c_1-c_4)\,\mathrm{sh}\,m\cos m\right]-$$
$$-\frac{\gamma u_0^2}{24\,cgl}\,\frac{(1-\bar{b}-\bar{a})\,\mathrm{ch}\,2\gamma\sin 2\gamma+(1-\bar{b}+\bar{a})\,\mathrm{sh}\,2\gamma\cos 2\gamma}{(\mathrm{sh}^2\gamma+\sin^2\gamma)^2}.$$

Heat flux through the upper plate, as it follows from (24), consists of the steady and unsteady parts, in this case when cos2 ωt or sin 2 ω t are equal to zero or will humble identical values, the values of heat fluxes coincide.

At the low values of the parameter γ, expression (24) takes the form

$$\lim_{\gamma\to 0}\varphi_1=\frac{\lambda u_0^2}{2\,cgIh}+\frac{\lambda u_0^2}{2\,cgIh}\cos 2\omega t, \qquad (24a)$$

whence it follows that the steady part of the heat flux is equal to half of the heat, which is isolated through the driving/moving surface in the flow of Couette. A change in the isolatable quantity of heat as the temperature in flow, in time occurs with the double frequency of the oscillations of plate 1. For ω = 0 we have a case of the steady motion of upper plate, the value of heat flux is here constant and equal to $\frac{\lambda u_0^2}{cgl}$, as in the flow of Couette.

For the high values of parameter γ, heat flux through upper boundary is determined as follows:

$$\lim_{\gamma \to \infty} q_1 = \frac{\lambda u_0^2 \gamma}{2 cgh} + \frac{\lambda u_0^2 \gamma}{12 cgh} \left[(2 - \sqrt{2}) \cos 2\omega t - (2 + \sqrt{2}) \sin 2\omega t \right]. \qquad (24b)$$

From expression (24b) it is not difficult to see that in this case, as with small γ, the steady-state part of the heat flux comprises the half of the heat, isolated in Couette's flow. The isolation/liberation of the unsteady part of thermal energy occurs periodically with frequency 2ω.

The characteristic feature of heat release at high frequencies is the linear dependence of a quantity of heat, transferred through the upper plate, on the parameter γ.

After giving expressions (24b) to the form

$$q_{1,\infty} = \frac{\gamma \lambda u_0^2}{2 cgl} [1 + \cos(2\omega t + \varepsilon)],$$

where $\varepsilon = \operatorname{arcctg}(3 + \sqrt{2})$. a index ∞ it means that the value of heat flux corresponds to unlimited increase of the parameter γ, let us note that the heat release through the upper plate in this case occurs with constant phase displacement, caused by interaction of

inertial forces and forces of internal friction within flow.

Fig. 1-4, depicts the curves of relative temperature $\frac{T-T_0}{u_0^2/4cgl} = f(\bar{y})$ for the different values of the parameter γ and of the relative time $\bar{t} = t/T^*$, where T* - oscillatory period. Calculations were conducted on computers on formula (19). Fig. 1, gives the curves of relative temperature over the section of flow for the torque/moments of time $\bar{t}$ = 0; 0.5; 1.0. At the low values of the parameter $\gamma \leqslant 0.5$, these curves have parabolic character, with an increase in the parameter γ, relative temperature near moticnless plate decreases, approaching one. With $\gamma > 2$ with an increase in the frequency, the zone of the relative temperature, equal to unity, is spread to the side of the oscillating plate, reaching when $\gamma = 10$ ordinates $\bar{y}$ = 0.7. With an increase in the parameter γ there occurs considerable increase in the gradients of temperature $\partial\theta/\partial y$ near the oscillating plate.

Page 90.

Through the fourth of the period (see Fig. 2) is observed somewhat different picture of a change in the temperature in flow depending on the parameter γ. When $\gamma \leqslant 0.2$ temperatures is constant over entire section of flow and is equal to T_0. With an increase in the frequency ($\gamma > 0.2$) in all points of flow, occurs simultaneously

the continuous increase of temperature. Near motionless plate relative temperature reaches unity with $\gamma = 2$ and it is retained constant independent of further increase in the parameter γ. The increase of the parameter $\gamma > 2$ leads to the expansion of the zone of the constant, equal to unity value of the relative temperature to the side of perturbation source.

At the moment of time $\bar{t} = 1/3$ (see Fig. 3) with $\gamma \leq 0.5$ occurs initially the decrease of the temperature in all section of flow with an increase in the frequency, and then when $\gamma > 0.5$ temperatures in flow it is raised. When $\gamma > 2$ character of a change in the temperature depending on frequency remains the same as for previously examined moments of time.

With $\bar{t} = 0.6$ (see Fig. 4) and the low values of the parameter γ it occurs the increase of temperature in all flow with an increase in the frequency, and then, beginning with certain value of the parameter γ, the decrease of temperature near motionless wall to a constant value.

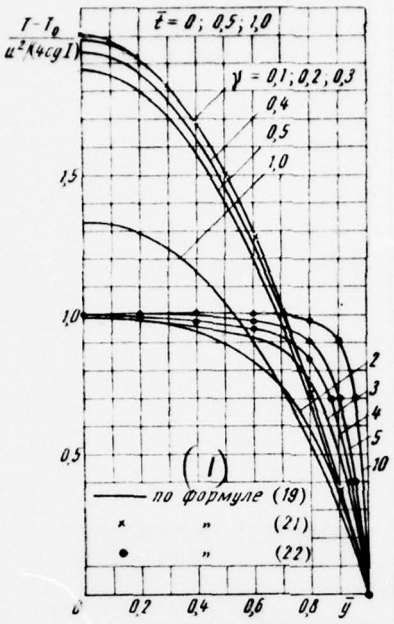


Fig. 1.

Key: (1). on formula.

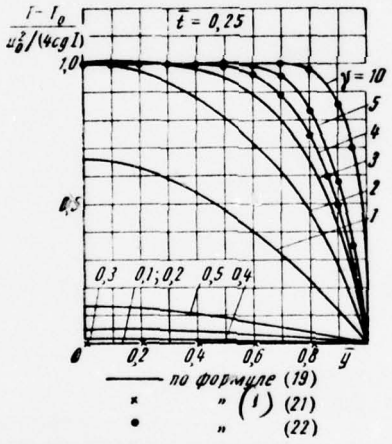


Fig. 2.

Key: (1). on formula.

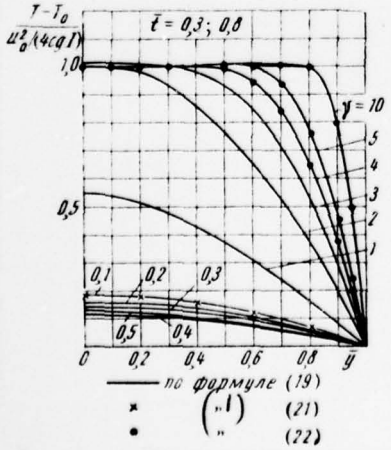


Fig. 3.

Key: (1). on formula.

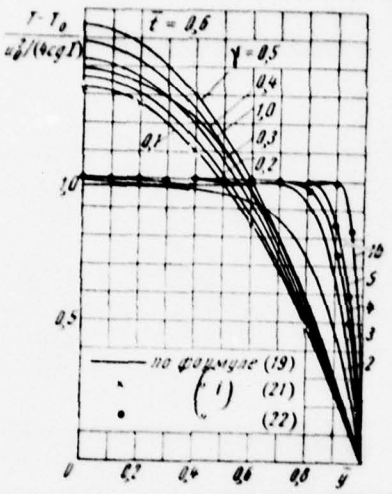


Fig. 4.

Key: (1). on formula.

Page 91.

Given the distribution curves of the temperature in flow visually confirm the analysis of formula (19), presented above.

Let us examine a question concerning the applicability of approximation formulas (21) and (22). In Fig. 1-4 to curves, are plotted the values of relative temperature, calculated according to formula (21), sufficiently well coinciding with precise values for $\gamma \leq 0.1$.

To these figures are plotted/applied also the values of the relative temperature, calculated according to formula (22). Results show that the values of temperatures, obtained on precise (19) and that approximated (22) to formulas, beginning with $\gamma = 4$ and above, are virtually identical.

Thus, formula (21) it is possible to use with $\gamma \leqslant 0.1$, and by formula (22) - with $\gamma \geqslant 4$. Within limits of $0.1 \leqslant \gamma \leqslant 4$ calculations one should carry out through formula (19).

The distribution curves of temperature over the section of flow, given to Fig. 1-4, give the sufficiently demonstrative representation of derivatives $\partial T/\partial \bar{y}$, and consequently, of heat fluxes within the oscillating liquid. Expressions (24a) and (24b) give the complete representation of a quantity of heat, transferred through oscillating plate. Therefore are given the curves of the dependences of heat fluxes on time and the parameter γ there is no need.

In conclusion let us note that, having expressions (8), (15) and (16), it is not difficult to obtain solutions for other boundary conditions.

REFERENCES

1. Ye. M. Zhmulin. Dynamics of the viscous fluid between two parallel driving/moving and harmonically oscillating plates. "scientific notes of TsAGI", Vol. III, No 2, 1972.

2. G. S. Karslou. Theory of thermal conductivity, M. -L., Gostekhteorizdat, 1947.

3. V. I. Smirnov. Course of higher mathematics. T. II Moscow-Leningrad, Gostekhtecrizdat, 1940.

The manuscript entered 16/IX 1972.

Page 92.

One Method of calculation of flow in circular bearing

E. N. Sarmin.

Are estimated the characteristics of one iterative method of the solution of Navier-Stokes equations for the case of circular bearing when is small the clearance between the rotating and motionless surfaces. It is shown, that with the decrease of clearance increase the allowed values of Reynolds numbers, which ensure the convergence of iterations. Is given evaluation of the deviation of approximate solution from precise and are given the results of numerical calculations.

Iterative method of the solution of the problem of the motion of the liquid between two noncoaxial cylinders, instituted on the introduction of the low parameter under boundary conditions, examined in works [1] and [2]. Work [2] shows, which in space $W_2^{l+1/2}$, where l - whole, is equal or it is more than three, this method converges during sufficiently small Re number and certain restriction placed on

the value of the iterative parameter.

The case of bearing, which is an example of the application/appendix of the task in question, is characteristic by the smallness of the clearance between motionless and rotating surfaces. Using this special feature/peculiarity, we define concretely the limitations, superimposed on the parameters of the calculation (see [2]) and Re number, and let us also estimate the deviation of approximate solution, in particular the solution of the simplified equation, in which are reject/thrown convective members, from the solution of complete Navier-Stokes equation.

The content of task is clarified by Fig. 1. Is investigated the flow between the circular motionless pin/journal, with center O and the radius, equal to unity, and by the rotating pin by radius $r < 1$ with center O'. Distance $OO' = e$ satisfies inequality $e < 1 - r \ll 1$.

The rotational speed - the unknown constant V_0 provides the assigned/prescribed expenditure/consumption W_0.

Page 93.

With the aid of transformation

$$\left.\begin{aligned} x &= \frac{1}{\xi}\,\frac{\left(\frac{1}{\xi}-\xi\right)\rho\sin\varphi}{\frac{1}{\xi^2}+\rho^2-2\frac{\rho}{\xi}\cos\varphi}, \\ y &= -\frac{1}{\xi}\,\frac{(1+\rho^2)-\left(\frac{1}{\xi}+\xi\right)\cos\varphi}{\frac{1}{\xi^2}+\rho^2-2\frac{\rho}{\xi}\cos\varphi}, \end{aligned}\right\} \qquad (1)$$

where $\varepsilon = 0.5\left[e+\frac{1-r^2}{e}-\sqrt{\left(e+\frac{1-r^2}{e}\right)^2-4}\right]$, and the introduction to function of current Ψ task is reduced to the solution of the equation

$$\Delta H_\rho^{-2}\Delta\Psi = \frac{\mathrm{Re}}{\rho}\left(\frac{\partial H_\rho^{-2}\Delta\Psi}{\partial\rho}\frac{\partial\Psi}{\partial\varphi}-\frac{\partial H_\rho^{-2}\Delta\Psi}{\partial\varphi}\frac{\partial\Psi}{\partial\rho}\right) \qquad (2)$$

with the boundary conditions

$$\Psi|_{\Gamma_1}=0,\quad \Psi|_{\Gamma_0}=1,$$

$$\frac{\partial\Psi}{\partial n}\Big|_{\Gamma_1}=0,\quad -H_\rho^{-1}\frac{\partial\Psi}{\partial\rho}\Big|_{\Gamma_0}=V_{\rho_0},$$

$$\int_{\Gamma_0}\frac{\partial H_\rho^{-2}\Delta\Psi}{\partial n}\,dl=0.$$

Are here accepted the designations:

$$H_\rho=\left(\frac{1}{\xi^2}-1\right)\Big/\left(\frac{1}{\xi^2}+\rho^2-\frac{2\rho}{\xi}\cos\varphi\right);$$

Γ_0 - circumference with a radius $\rho_0 = \frac{r}{1-\xi r}$, the form of the surface of pin; Γ_1 - unit circle, the surface of pin/journal; $\mathrm{Re} = \frac{V_0}{\nu}$, where ν - a kinematic viscosity coefficient.

The examine/considered by us iterative method represents by itself the consecutive solution of two boundary-value problems. In the first is solved the equation

$$\Delta\Omega_i = \frac{\mathrm{Re}}{\rho}\left(\frac{\partial\Omega_{i-1}}{\partial\rho}\frac{\partial\Psi_{i-1}}{\partial\varphi} - \frac{\partial\Omega_{i-1}}{\partial\varphi}\frac{\partial\Psi_{i-1}}{\partial\rho}\right)$$

under the boundary conditions

$$\Omega_i = \alpha H_\rho^{-1}\frac{\partial\Psi_{i-1}}{\partial n} + \Omega_{i-1} \text{ on } \Gamma_1,$$

$$\Omega_i = \alpha\left(H_\rho^{-1}\frac{\partial\Psi_{i-1}}{\partial n} - V_{0,i-1}\right) + \Omega_{i-1} \text{ on } \Gamma_0,$$

$$\int_{\Gamma_0}\frac{\partial\Omega_i}{\partial n}\,dl = 0.$$

The second - boundary-value problem of the Dirichlets:

$$\Delta\Psi_i = H_\rho^2\Omega_i, \quad \Psi_i|_{\Gamma_0} = 1, \quad \Psi_i|_{\Gamma_1} = 0.$$

Index i indicates the number of iteration.

Work [2] shows, that with

$$-2\left(\frac{\frac{1}{\xi}-1}{\frac{1}{\xi}+1}\right)^2 \|K_\varepsilon\|^{-1} < \alpha < 0 \qquad (3)$$

(operator K_ε is introduced there) and at

$$\mathrm{Re} < \frac{c}{\|\bar{\Psi}_0\|_{W_2^{\frac{1}{2}+\frac{1}{2}}(S)}},$$

where c - certain constant, $\bar{\Psi}_0$ - the solution of initial problem, which corresponds Re = 0 (see [1]), iterations converge, and is shown the speed of convergence.

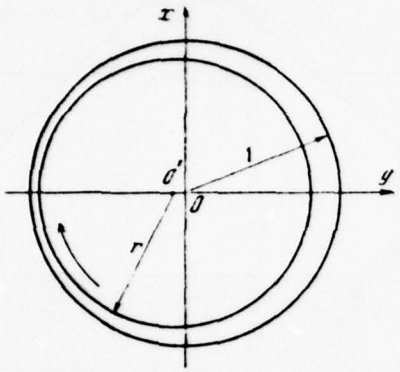


Fig. 1.

Page 94.

CONDITIONS OF THE CONVERGENCE OF NUMERICAL METHOD FOR THE CASE OF BEARING.

In work [3] it was shown, that during the solution of problem for simply connected region the iterative parameter α was inversely proportional to the linear dimension of range. In our case values α and Re numbers, affect two factors: a difference in the radii of cylinders and the distance between their centers. Let us establish/install the character of this effect.

The consequence of a small size/dimension of the clearance

between cylinders is the smallness of the interval of the variation in the coordinate ρ, since

$$1-\rho_0=h\leqslant 1-r.$$

On the other hand, by expansion/decomposition in a series in terms of h we are convinced that

$$1-r=h+O(h^2)$$

and

$$\left(\frac{\frac{1}{\xi}+1}{\frac{1}{\xi}-1}\right)^2=M[1+O(h)],$$

where M is the ratio of the greatest distance between cylinders to the smallest:

$$M=\frac{1-r+e}{1-r-e},$$

therefore to us are sufficient to give estimations the which interest us values through M and h.

Let us estimate α. The expansion of the coefficients of equations (9b) and (9c) from work [2] according to degrees of h, it gives the right to confirm that with any fixed/recorded k > 0 and when $h\to 0$ the maximum form of these equations does not depend on k:

$$\lambda_k^2-\frac{2}{3}h\lambda_k+\frac{h^2}{12}=0.$$

Hence it follows that $\bar{\lambda}_k^{(1)} \underset{h\to 0}{\to} h/2$, $\bar{\lambda}_k^{(2)} \underset{h\to 0}{\to} h/6$. For k = 0 value $\bar{\lambda}_0 \underset{h\to 0}{\to} h/2$, therefore for the norm of operator K_c with small h we have

$$\| K_c \| = \frac{h}{2} + O(h^2).$$

Consequently, lower boundary in inequality (3) takes the form

$$-4/(hM^2) = \alpha_1, \quad \alpha_1 + O(1) \leqslant \alpha < 0.$$

Let us turn now to the estimate of the magnitude of Re number. During numerical calculations it was noticed that allowed values Re, for which the method converges, increase with decrease of 1 - r. To explain this phenomenon helps the introduction of new coordinate $\bar{\rho}$: $\rho = h\bar{\rho}$. After this transform in equation (2) appears new Reynolds number: $\overline{Re}$ = Re h, and all the significant dimensions of range S and the entering the equation terms become the values, comparable with unity. To this equation it is possible to use the results of works [2], from which it follows that

$$\operatorname{Re} hM \leqslant \frac{\bar{c}}{\| \Psi_0 \|_{W_2^l + \frac{3}{2}(S)}},$$

i.e. the allowed values of Re number increase inversely proportional to product Mh.

DEVIATION OF APPROXIMATE SOLUTION FROM PRECISE.

Let us estimate the deviation of any approximate solution from the solution of complete equation (2) when h is sufficiently small. Let us make this based on the example of the solution of the equation of Stokes.

Page 95.

Is decomposed solution (2) in a series according to degrees of Re:

$$\Psi = \sum_{j=0}^{\infty} \Psi_j \mathrm{Re}^j. \qquad (4)$$

The zero term of this series corresponds to the solution of linear equation with Re = 0, and those follcw satisfy the equation

$$\Delta H_\rho^{-2} \Delta \Psi_j = \frac{1}{\rho} \sum_{k+i=j-1} \frac{D(H_\rho^{-2} \Delta \Psi_k, \Psi_i)}{D(\rho, \varphi)} \qquad (5)$$

and the boundary conditions

$$\Psi_j\Big|_\Gamma = \frac{\partial \Psi_j}{\partial n}\Big|_{\Gamma_1} = 0, \quad H_\rho^{-1} \frac{\partial \Psi_j}{\partial n}\Big|_{\Gamma_0} = V_j, \quad \int_{\Gamma_0} \frac{\partial H_\rho^{-2} \Delta \Psi_j}{\partial n} dl = 0. \qquad (6)$$

For the determination of the radius of convergence of series (4) let us present each term Ψ_j in the form of sum

$$\Psi_j = \tilde{\Psi}_j + c_j f_1, \qquad (7)$$

where $\tilde{\Psi}_j$ - the solution of the task

$$\Delta H_\rho^{-2} \Delta \tilde{\Psi}_j = F_j, \quad \tilde{\Psi}_j\Big|_\Gamma = \frac{\partial \tilde{\Psi}_j}{\partial n}\Big|_\Gamma = 0,$$

F_j - right side of equation (5), and χ_1 satisfies the conditions

$$\Delta H_\rho^{-2}\Delta\chi_1 = 0, \quad \chi_1\Big|_\Gamma = \frac{\partial\chi_1}{\partial n}\Big|_{\Gamma_1} = 0,$$

$$H_\rho^{-1}\frac{\partial\chi_1}{\partial n}\Big|_{\Gamma_0} = \text{const}, \quad \int\limits_{\Gamma_0}\frac{\partial H_\rho^{-2}\Delta\chi_1}{\partial n}\,dl = 1;$$

χ_1 has the form

$$\chi_1 = \left(\frac{1}{\xi^2} - 1\right) H_\rho \frac{[(2\ln\rho_0 + 1 - \rho_0^2)\rho^2 - (2\rho_0^2\ln\rho_0 + 1 - \rho_0^2)]\ln\rho - (1-\rho_0^2)\ln\rho_0(\rho^2-1)}{8\pi\left(\frac{2\ln\rho_0 + 1 - \rho_0^2}{\xi^2} - 2\rho_0^2\ln\rho_0 - 1 + \rho_0^2\right)}.$$

Let us estimate function $\tilde{u}_j$, after writing it as $\tilde{u}_j = H_\rho u_j$. For u_j we have

$$\Delta\Delta u_j = H_\rho F_j, \quad u_j\Big|_\Gamma = \frac{\partial u_j}{\partial n}\Big|_\Gamma = 0.$$

Therefore for any right side

$$\|u_j\|_{L_2(S)} \leq \frac{1}{\lambda_1}\|H_\rho F_j\|_{L_2(S)},$$

$$\|\Delta u_j\|_{L_2(S)} \leq \frac{1}{\lambda_1^2}\|H_\rho F_j\|_{L_2(S)},$$

where λ_1 - smallest of the eigenvalues of operator Δ^2 above the functions, which turn on boundary into zero together with its normal derivatives.

The investigation of the latter shows that when $h \to 0$ values λ

increase not slower than π/h, i.e., $\lambda \leqslant \pi/h + O(1)$. Therefore for a bearing from Green's formula, easily it is obtained

$$\left.\begin{aligned} &\left\| \frac{1}{\rho}\frac{\partial u_j}{\partial \varphi}\right\|_{L_2} \leqslant \frac{h^4}{\pi^3}\| H_\rho F_j\|_{L_2}, \quad \left\|\frac{\partial u_j}{\partial \rho}\right\|_{L_2} \leqslant \frac{h^3}{\pi^3}\| H_\rho F_j\|_{L_2}, \\ &\left\|\frac{\partial \Delta u_j}{\partial \rho}\right\|_{L_2} \leqslant \frac{h}{\pi}\| H_\rho F_j\|_{L_2}, \quad \left\|\frac{1}{\rho}\frac{\partial \Delta u_j}{\partial \varphi}\right\|_{L_2} \leqslant \frac{h^2}{\pi}\| H_\rho F_j\|_{L_2}. \end{aligned}\right| \qquad (8)$$

Constant c_j in equality (7) is determined through $\tilde{\Psi}_j$ and therefore it can be expressed through F_j:

$$c_j = -\int_{\Gamma_0} \frac{\partial H_\rho^{-2}\Delta\tilde{\Psi}_j}{\partial n}\, dl = \frac{1}{\chi_0|_{\Gamma_1}}\iint_S \chi_0 F_j\, ds.$$

Page 96.

Function χ_0 is the solution of the task

$$\Delta H_\rho^{-2}\Delta\chi_0 = 0, \quad \chi_0\left|_{\Gamma_1} = \frac{\partial\chi_0}{\partial n}\right|_{\Gamma} = 0, \quad \chi_0|_{\Gamma_0} = \text{const}, \quad \int_{\Gamma_0}\frac{\partial H_\rho^{-2}\Delta\chi_0}{\partial n}\, dl = 1$$

and is taken on boundary great absclute value. Therefore

$$|c_j| \leqslant \sqrt{2\pi h}\,\| F_j\|_{L_2}. \qquad (9)$$

Decompose/expanding coefficients χ_0 according to degrees of h and comparing (7), (8) and (9), we come to the conclusion that with small h

$$\left\|\frac{1}{\rho}\frac{\partial\Psi_j}{\partial\varphi}\right\|_{L_2} \leqslant h^4\| F_j\|_{L_2}\left(\frac{M^{1/2}}{\pi^3} + \frac{M}{6}\right) + O(h^5),$$

$$\left\|\frac{\partial\Psi_j}{\partial\rho}\right\|_{L_2} \leqslant h^3\| F_j\|_{L_2}\left(2 + \frac{M^{1/2}}{\pi^3}\right) + O(h^4),$$

$$\left\|\frac{1}{\rho}\frac{\partial H_\rho^{-2}\Delta\Psi_j}{\partial\varphi}\right\| \leqslant h^2\| F_j\|_{L_2}\frac{M^{1/2}}{\pi} + O(h^3),$$

$$\left\|\frac{\partial H_\rho^{-2}\Delta\Psi_j}{\partial\rho}\right\| \leqslant h\| F_j\|_{L_2}\left(\frac{M^{1/2}}{\pi} + \sqrt{\frac{3}{2}}\right) + O(h^2).$$

Using these estimations, let us find the radius of convergence of series (4). If we require so that each of Ψ_j it would satisfy the inequality

$$\max\left\{\left\|\frac{1}{\rho}\frac{\partial\Psi_j}{\partial\varphi}\right\|_{L_2},\ \left\|\frac{1}{\rho}\frac{\partial\Psi_j}{\partial\rho}\right\|_{L_2}h,\ \left\|\frac{1}{\rho}\frac{\partial H_\rho^{-2}\Delta\Psi_j}{\partial\varphi}\right\|_{L_2}h^2,\ \left\|\frac{\partial H_\rho^{-2}\Delta\Psi_j}{\partial\rho}\right\|_{L_2}h^3\right\}\leqslant\frac{Aq^j}{(j+1)^2},$$

and to conduct the reasonings, analogous to the proof of inequality (11) from work [4], we will obtain the results: series (4) it converges with

$$\mathrm{Re}<\frac{1}{4AKh}. \tag{10}$$

where

$$A=\max\left\{\left\|\frac{1}{\rho}\frac{\partial\Psi_0}{\partial\varphi}\right\|_{L_2},\ \left\|\frac{\partial\Psi_0}{\partial\rho}\right\|_{L_2}h,\ \left\|\frac{1}{\rho}\frac{\partial H_\rho^{-2}\Delta\Psi_0}{\partial\varphi}\right\|_{L_2}h^2,\ \left\|\frac{\partial H_\rho^{-2}\Delta\Psi_0}{\partial\rho}\right\|_{L_2}h^3\right\},$$

$$K=\max\left\{\frac{M}{6}+\frac{M^{1/2}}{\pi},\ \frac{M^{1/2}}{\pi^3}+2,\ \frac{M^{1/2}}{\pi}+\sqrt{\frac{3}{2}}\right\}.$$

Since the terms of a series, beginning with the first, do not exceed the terms of geometric progression with dencminator q = 4 AK Re h, the under condition (10) deviation of Stokes solution Ψ_0 from

precise satisfies the inequality

$$\|\Psi - \Psi_0\|_{W_2^3(S)} \leqslant \frac{2\,\mathrm{Re}\,K h \|\Psi_0\|_{W_2^3(S)}}{1 - 4\,A K h\,\mathrm{Re}}.$$

Similarly, after presenting an error in any approximate solution Ψ in the form of the "tail" of a series of type (4), it is possible to evaluate this error through the discrepancy of equation (2):

$$\|\Psi - \bar{\Psi}\|_{W_2^3(S)} \leqslant \frac{BKh}{1 - \mathrm{Re}\,A_1 K h},$$

where

$$B = \left\| \Delta H_\rho^{-2} \Delta \bar{\Psi} - \frac{\mathrm{Re}}{\rho} \frac{D(H_\rho^{-2} \Delta \bar{\Psi},\ \bar{\Psi})}{D(\rho,\ \varphi)} \right\|_{L_2},$$

$$A_1 = 4 \max \left\{ \left\| \frac{1}{\rho} \frac{\partial \bar{\Psi}}{\partial \varphi} \right\|_{L_2},\ \left\| \frac{\partial \Psi}{\partial \rho} \right\|_{L_2} h,\ \left\| \frac{1}{\rho} \frac{\partial H_\rho^{-2} \Delta \bar{\Psi}}{\partial \varphi} \right\|_{L_2} h^2,\ \left\| \frac{\partial H_\rho^{-2} \Delta \Psi}{\partial \rho} \right\|_{L_2} h^3 \right\}.$$

Page 97.

Calculation of forces, which act on bearing.

Let us turn to the determination of the forces and torque/moment, with which the lubricant film acts on pin. If into those interesting us stress-tensor component from work [5] to substitute the expression of the components of velocity from [1], to consider boundary conditions and the equations of continuity, then we will obtain

$$p_{\rho\rho} = -p, \quad p_{\rho\varphi} = -\mu\left(\Omega + 2\frac{V_0}{r}\right). \tag{11}$$

where p - the hydrodynamic pressure on the surface of pin, determined

according to equation for an angular velocity from [1] by the formula

$$p = \mu\rho_0 \int_0^{\varphi} \frac{\partial\Omega}{\partial\rho}\Big|_{r_0} d\varphi, \tag{12}$$

and Ω - an eddy/vortex, $\Omega = H_\rho^{-2}\Delta\Psi$.

The knowledge of solution makes it possible for us to obtain the components resultant force

$$F_x = \int_{l_0} (p_{\rho\rho}\cos(\rho, x) + p_{\rho\varphi}\cos(\varphi, x))\, dl,$$
$$F_y = \int_{l_0} (p_{\rho\rho}\cos(\rho, y) + p_{\rho\varphi}\cos(\varphi, y))\, dl.$$

Formulas (1) and (11) make it possible to calculate the integrands:

$$\left.\begin{aligned} F_x &= \rho_0\left(\frac{1}{\xi^2} - 1\right)\int_0^{2\pi} \frac{p\left(\frac{1}{\xi^2} - \rho_0^2\right)\sin\varphi + \mu\Omega\left[\left(\frac{1}{\xi^2} + \rho_0^2\right)\cos\varphi - 2\frac{\rho_0}{\xi}\right]}{\left(\frac{1}{\xi^2} + \rho_0^2 - 2\frac{\rho_0}{\xi}\cos\varphi\right)^2} d\varphi, \\ F_y &= \rho_0\left(\frac{1}{\xi^2} - 1\right)\int_0^{2\pi} \frac{-p\left[\left(\frac{1}{\xi^2} + \rho_0^2\right)\cos\varphi - 2\frac{\rho_0}{\xi}\right] + \mu\Omega\left(\frac{1}{\xi^2} - \rho_0^2\right)\sin\varphi}{\left(\frac{1}{\xi^2} + \rho^2 - 2\frac{\rho_0}{\xi}\cos\varphi\right)^2}. \end{aligned}\right\} \tag{13}$$

Is here taken into account the fact that

$$\int_0^{2\pi} \frac{\sin\varphi d\varphi}{\left(\frac{1}{\xi^2} + \rho_0^2 - 2\frac{\rho_0}{\xi}\cos\varphi\right)^2} = \int_0^{2\pi} \frac{\left(\frac{1}{\xi^2} + \rho_0^2\right)\cos\varphi - 2\frac{\rho_0}{\xi}}{\left(\frac{1}{\xi^2} + \rho_0^2 - 2\frac{\rho_0}{\xi}\cos\varphi\right)^2} d\varphi = 0.$$

The torque/moment of tangents to the rotating surface forces relative to center of rotation is calculated analogously:

$$M = r\int_{\Gamma_0} p_{p\varphi}\,dl = -\mu r\int_0^{2\pi}\left(\Omega + \frac{2V_0}{r}\right)\frac{\left(\frac{1}{\xi^2}-1\right)\rho_0}{\frac{1}{\xi^2}+\rho_0^2-2\frac{\rho_0}{\xi}\cos\varphi}\,d\varphi =$$

$$= -2\mu r V_0 - \mu r^2\left(\frac{1}{\xi^2}-\rho_0^2\right)\int_0^{2\pi}\frac{\Omega d\varphi}{\frac{1}{\xi^2}+\rho_0^2-2\frac{\rho_0}{\xi}\cos\varphi}. \qquad (14)$$

ANALYSIS OF RESULTS.

Let us describe now computational experiment and the results of calculations. The circuit of the construction of iterations is shown in works [1] and [2], and successive approximations themselves were calculated by finite-difference method, i.e., derivatives were replaced by central differences and result was obtained in mesh points (ρ_0 + h/L k, 2wi/N). The approximation of boundary conditions is given in [2]. Integrals from duct/contour (12), (13) and (14) were calculated from Simpson's method.

Page 98.

Table gives the results of difference calculation. For checking its accuracy/precision, difference solution was compared with analytical for case of r = 0.9, e = 0.05, Re = 0. On the grid, which contains 20 x 20 points, the difference between solutions did not exceed 0.01o/o. Apparently, this accuracy/precision for engineering calculations is surplus; however, in table we give in certain cases five significant digits in order to more visually trace the effect of

Re number on final results.

Results in the table are groupped in the following order: for the set of the parameters τ = (r, e, Re) are given value V_0/Ψ_0, $F_x/\mu\Psi_0$, $F_y/\mu\Psi_0$ and $M/\mu\Psi_0$. but at the end of the row, is made observation relative to the presence recurrent flow (" there are") or its absences (" no"). Then in τ is changed the last/latter component Re until its further increase makes it possible for 100 iterations to establish/install five significant digits of result. After this changes distance between centers e and is given the new group of results, etc. Some data were omitted from the considerations of the savings of place.

Let us observe the effect of Re number on results. It is noted [6] that with Re = 0 total force component which act on the rotating surface of bearing, to the perpendicular of centers of circle. In our case this is expressed by equality $F_y = 0$ with Re = 0. With Re $\neq$ 0 in equation, appear the convective terms, which contribute asymmetry v.tecenie, and appears that comprise F_y, which increases with increase in Re. However, it does not comprise considerable portion in comparison with F_x on all range of Re numbers, which ensure the convergence of iterations. The results of calculations show also that Re number does not virtually change the velocity, which realizes single fluid flow rate between the surfaces of bearing, i.e., with

small h value $V_\theta \approx V_0(r, \theta)$. The same can be said, also, about F_r and M.

r	e	Re	V/Ψ_0	$F_x/\mu\Psi_0$	$F_y/\mu\Psi_0$	$M/\mu\Psi_0$	Возвратное течение (1)
		0	21,070	$0,1002\cdot10^4$	0	$-0,11021\cdot10^4$	Нет (2)
0,9	0,015	10	21,070	$0,5006\cdot10^4$	$0,3251\cdot10^3$	$-0,11021\cdot10^4$	.
		35	21,072	$0,5052\cdot10^4$	$0,1134\cdot10^4$	$-0,11022\cdot10^4$	.
0,9	0,03	0	23,359	$0,1113\cdot10^5$	0	$-0,13861\cdot10^4$	.
0,9	0,03125	32	23,363	$0,1121\cdot10^5$	$0,2081\cdot10^4$	$-0,13864\cdot10^4$	.
		0	23,640	$0,1174\cdot10^5$	0	$-0,14221\cdot10^4$	Есть (3)
		32	23,645	$0,1183\cdot10^5$	$0,2167\cdot10^4$	$-0,14224\cdot10^4$	.
0,9	0,05	0	30,420	$0,2477\cdot10^5$	0	$-0,23591\cdot10^4$	.
		10	30,420	$0,2478\cdot10^5$	$0,9960\cdot10^3$	$-0,23591\cdot10^4$	.
		25	30,423	$0,2483\cdot10^5$	$0,2489\cdot10^4$	$-0,23595\cdot10^4$	. (4)
0,98	0,006	150	115,21	$0,1567\cdot10^7$	$0,2553\cdot10^6$	$-0,40995\cdot10^5$	Нет
0,98	0,00(6)	0	119,11	$0,1794\cdot10^7$	0	$-0,43982\cdot10^5$	Есть (5)
		100	119,12	$0,1798\cdot10^7$	$0,1889\cdot10^6$	$-0,43986\cdot10^5$	.
		150	119,13	$0,1804\cdot10^7$	$0,2831\cdot10^6$	$-0,43991\cdot10^5$	.
0,98	0,015	80	293,06	$0,1179\cdot10^8$	$-0,3515\cdot10^6$	$-0,22166\cdot10^6$	.
0,6	0,05	0	5,7116	$0,3870\cdot10^2$	0	$-0,32037\cdot10^2$	Нет (2)
		5	5,7117	$0,3890\cdot10^2$	$0,6658\cdot10^1$	$-0,32037\cdot10^2$	.
		8	5,7118	$0,3920\cdot10^2$	$0,1063\cdot10^2$	$-0,32037\cdot10^2$	.
0,6	0,125	7	6,4231	$0,1102\cdot10^3$	$0,2351\cdot10^2$	$-0,41918\cdot10^2$	.
0,6	0,13	7	6,5252	$0,1178\cdot10^3$	$0,2280\cdot10^2$	$-0,44160\cdot10^2$	Есть (5)
0,6	0,25	0	10,482	$0,3819\cdot10^3$	0	$-0,11180\cdot10^3$	.
		3	10,482	$0,3819\cdot10^3$	$0,1354\cdot10^2$	$-0,11181\cdot10^3$	.
		5	10,480	$0,3820\cdot10^3$	$0,2259\cdot10^2$	$-0,11194\cdot10^3$	.

Key: (1). Recurrent flow. (2). No. (3). There is.

Page 99.

For explaining this phenomenon, let us note that the parity in Φ of the terms of series (4) coincides with the parity of their reference numbers, and the variable part of hydrodynamic pressure

(12) has opposite parity. From (13) it follows that the odd terms of series (4) affect that comprise F_y and exert no effect on M and F_x.

From the formula of Green and from (6) it is easy to obtain the equality

$$\iint_S (\Psi_0 \Delta H_\rho^{-2} \Delta \Psi_{2k+1} - \Psi_{2k+1} \Delta H_\rho^{-2} \Delta \Psi_0)\, ds = -\int_{\Gamma_0} (V_0 H_\rho^{-1} \Delta \Psi_{2k+1} - V_{2k+1} H_\rho^{-1} \Delta \Psi_0)\, dl.$$

The first three integrals in this equality are equal to zero according to observation about parity. Consequently, $V_{2k+1} = 0$.

Thus, in first (relative to Re) approach/approximation of value of V, M and F_x they are not changed, their disturbance/perturbations have second orders of smallness $O(Re^2 h^2)$. This same it is explained (calculations this confirm) the fact that F_y increases directly proportional to Re **number**, i.e.

$$F_y = c(r, e)\, \mathrm{Re}\, [1 + O(\mathrm{Re}^2 h^2)],$$

where c(r, e) - the **constant, which depends** on the geometry of range and which does not depend on Re number.

Work [1] gives an example of the appearance of a zone of recurrent flow in the diffuser part of the bearing, about motionless wall, near the outermost from pin point. As can be seen from table, the emergence of recurrent flow does not depend on Re number. With small h it appears in the case when $\frac{e}{1-r} > 0.3$, which will agree well

with the conclusions of the works [6].

In Fig. 2 for case of r = 0.9, e = 0.05, Re = 25, are plotted to the line of level ψ and the components F_x and F_y, that balance the directed down load on pin - F.

At the end of table, gives the results of calculation for the case when a difference in the radii is equal to 0.4. From them it is evident that all observations relative to the effect of Re number on values V_θ, F_x, F_y and M and relative to the presence of the zone of recurrent flow are valid and in this case, although the clearance between the surfaces of cylinders sufficiently great.

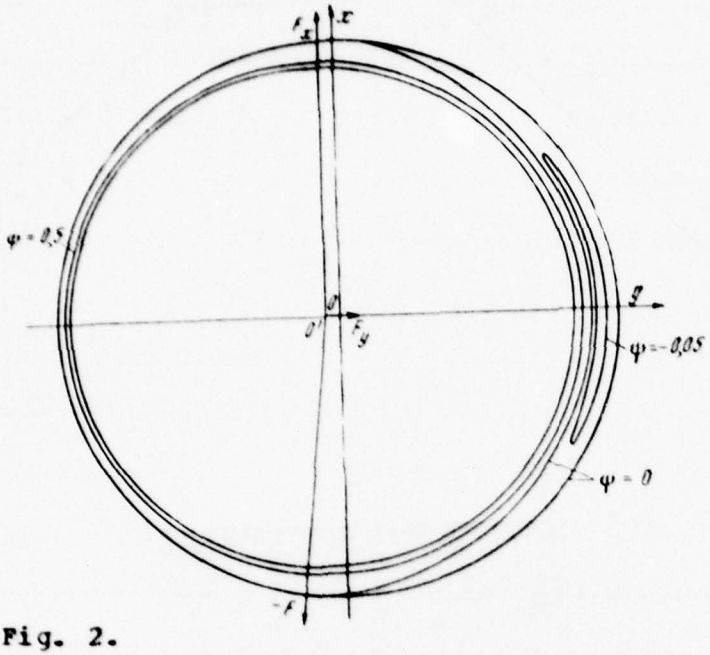


Fig. 2.

Page 100.

REFERENCES

1. E. N. Sarmin. On one numerical method of the solution of the particular problem of the hydrodynamic theory of lubrication. Transactions of section according to numerical methods in gas dynamics of the second international examination on gas dynamics of explosion and reacting systems. Novosibirsk, August, 1969. Vol. I. M., Izd. by the VTs of the AS USSR, 1971.

2. E. N. Sarmin. Method of the splitting/fission of boundary conditions for a task of the motion of the liquid between two noncoaxial cylinders. "scientific notes of TsAGI", Vol. III, No 5, 1972.

3. B. V. Pal'tsev. On the decomposition of the Dirichlet problem and mixed problem for biharmonic equation in a series for the solutions of the decomposing problems. "i. of comp. math. and math. physics", Vol. 6 No 1, 1966.

4. B. V. Pal'tsev. On the convergence of the method of successive approximations with the splitting/fission of boundary conditions during the solution of boundary-value problem for Navier-Stokes equation. "i. of comp. math. and mat. physics", Vol. 10, No 3, 1970.

5. N. Ye. Kochin, I. A. Kibel', I. V. Roze. Theoretical hydromechanics. Part II, M., Fizmatgiz, 1963.

6. Hydrodynamic theory of lubrication. Edited by A. S. Leybenzon. M., Gostekhteorizdat, 1934.

Received 28 June 1972

Page 105.

EXPERIMENTAL INVESTIGATION OF THE EFFECT OF RE NUMBER ON THE NATURE OF FLOW AROUND AXIALLY SYMMETRICAL BODIES INDENTED IN NOSE SECTION.

V. I. Shustov.

Is investigated the effect of Re numbers, M and of the form of leading edge on the character of the flow around axially symmetrical body with spherical indentation in nose section. Experiments are carried out with Mach numbers $\approx$ 6 and 5 in the range of Re numbers approximately $(0.035\text{-}0.6)\cdot10^6$. The character of the flow around the nose section of the model was determined from the direct-shadow images, obtained at different moment of time. It is shown, that the instability of the flow around bodies with indentations in nose section depends on Re number and the geometric special feature/peculiarities of the leading edge of model. The maximum departure/withdrawal of the shock wave before the axially symmetrical body throated three times approximately exceeds the departure/withdrawal of shock wave from the circular end/face, streamlined with flow with the same Mach number.

1. Flow in shock layer about dull bodies in super and hypersonic flow in majority of cases stable and does not lead to change in forces, which act on body during steady flight. However, there are forms of the bodies for which stable flow not always can be realized. So, in work [1] were examined dull bodies with indentations in the nose section about which the flow at the hypersonic speeds of the flow of gas was unstable. According to these investigations the flow instability, apparently, is caused by the formation/education of eddy/vortices within indentation. The developing within indentation eddy/vortices at the specific stage are discarded from it. The various forms of indentations to dissimilar degree contribute to the formation/education of eddy/vortices. In work [2] was undertaken the attempt to explain the character of the instability of the flow around concave cavities without duct on the basis of the numerical solutions of axisymmetric inviscid flow. However, the examination of inviscid flows, apparently, cannot give the complete explanation to flow instability near bodies with indentations. This is confirmed by the fact that along with flow instability about bodies with indenatations in nose section it was observed and the stable (or sufficiently close to stable) flow around them of the supersonic flow of gas.

That presented indicates the need for parameter determination of the supersonic flow and the fundamental geometric characteristics of

body, which cause the realization of unstable flow about the bodies, notched. The indentations of different form can appear in connection with the combustion loss of body with the passage of the dense layers of the atmosphere, and they are sometimes the design features of body. This work is dedicated to the study of the effect of Mach numbers and Re and of the geometric parameters of the leading edge of body on the character of flow of the supersonic flow about the axially symmetrical body throated in nose section.

2. Investigated model represented by itself body of revolution of ogival form with spherical indentation in nose section. The flow around model was studied with three versions of the edge of the nose section: acute/sharp, circular and by plane.

Page 106.

During a change in the form of edge, the depth of indentation a little changed. The geometric dimensions of model are given to Fig. 1. Model was installed in wind-tunnel test section on tailed bracket. During experiments was record/fixed the shadow flow pattern of model. The time of exhibition was approximately 6 μs. The photographing of flow pattern was conducted after the establishment of flow conditions in wind tunnel. (Dark spots in the given photographs are caused by some heterogeneities of the surface of glass of the window of the

test section of the duct).

Investigations are carried out with Mach numbers ≈ 5 and 6 in the range of Re numbers approximately $(0.035\text{-}0.6)\cdot 10^6$. During the calculation of Re number the characteristic linear dimension, is undertaken the diameter of nose section ($d = 0.016$ m). Re number was varied by changing the total pressure in settling chamber of wind tunnel.

3. Results of experimental studies of flow by supersonic flow of axially symmetrical bodies with indentations in nose section are represented in the form of shadowgraphs with different Re numbers.

Fig. 2, gives the flow patterns of model with flat/plane edge at $M = 6$ and some values of Re. Visual observations during experiments and the photographs obtained showed that fluctuations in the primary shock wave occurred with numbers $Re > 0.12 \cdot 10^6$. The maximum value of the departure/withdrawal of shock wave 2.4 times approximately exceeded the obtained by calculation [3] value of the departure/withdrawal of shock wave Δ_∞ for a circular end/face during the steady flow of it of flow with Mach number = 6. With Re number $\approx 0.58\cdot 10^6$, the maximum value of the departure/withdrawal of shock wave decreased and it was close to Δ_∞. With Re numbers $\lesssim 0.12\cdot 10^6$ of the oscillation of the shock wave before the model with spherical indentation and flat/plane leading edge they were not observed.

In the case of the flow around model with round leading edge on the basis of visual observations and the shadowgraphs, it is possible to conclude that with Re number $\approx 0.07 \cdot 10^6$ the flow around model is close to stationary. In this case, was observed the weakly-noticeable oscillation of shock wave. The value of the departure/withdrawal of shock wave was the in effect equal to the value of departure/withdrawal Δ before the circular end/face. An increase in Re number caused the noticeable instability of shock wave. The maximum value of its departure/withdrawal from the nose section of the model increased approximately to 2.8 Δ. This maximum departure/withdrawal during the oscillations of shock wave occurred up to Re number $\approx 0.58 \cdot 10^6$. Transition to Mach number = 5 (see Fig. 4c) significantly changed the character of the flow around model with spherical indentation and round edge. The frequency of shock wave considerably decreased, decreased the value of its maximum departure/withdrawal from body. In this case during the asymmetric flow around the model (angle of attack $\alpha \neq 0$) of the oscillation of shock wave in the time interval of visual observation (~50 s) they were absent. Fig. 3, gives the photograph of the picture of flow about this model at $\alpha = 10°$. For determining the flow pattern about bodies with indentations with other Mach numbers and $\alpha \neq 0$ are necessary supplementary experimental investigations.

Some photographs of the picture of flow about model with

spherical indentation and sharp edge are represented in Fig. 4b with M ≈ 6. In this case the oscillations of the leading shock wave were observed in all investigated range of Re numbers. The maximum value of the departure/withdrawal of shock wave was the same as of the models, having the flat/plane and round edges of nose section. With Re number ≈ $0.58 \cdot 10^6$, the maximum value of the departure/withdrawal of shock wave decreased almost to value $\varepsilon_{0.}$ the process of oscillations became weakly-noticeable.

Typical configurations of shock waves, obtained during the flow around models with spherical indentations in nose section at different moment of time, represented in Fig. 4. In this case, they occurred as the asymmetric (see Fig. 4a), so also almost symmetrical (see Fig. 4b) oscillations of shock wave, and also oscillation with the restoration/reduction of the position of shock wave, close to steady flow circular end/face (see Fig. 4c).

Fig. 5 gives the dependences of the maximum departure/withdrawal of shock wave (during its oscillation) $\varepsilon_{max} = \frac{\Delta_{max}}{d}$ from Re number for the investigated models. From these dependences it is evident that the maximum value of the departure/withdrawal of shock wave from body depends on Re number and the form of the edge of nose section. On this same figure is compared the maximum departure/withdrawal of shock wave from model throated during unstable flow with the value of

the departure/withdrawal of shock wave from circular end/face with Mach numbers = 5 and 6, obtained in work [3] with calculation. Comparison shows that the departure/withdrawal of the fluctuating shock wave is considerably more than departure/withdrawal during steady flow.

Page 107.

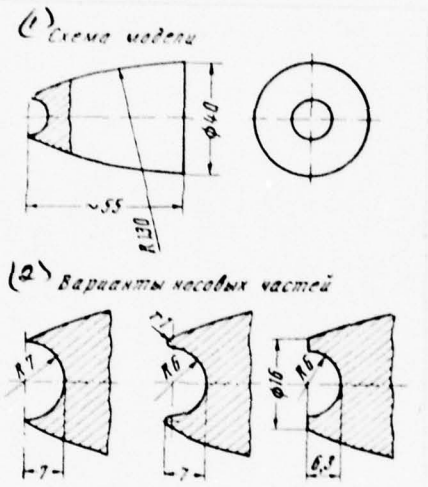


Fig. 1.

Key: (1). Schematic of model. (2). Versions of nose sections.

M~ 6; α = 0; flat/plane edge.

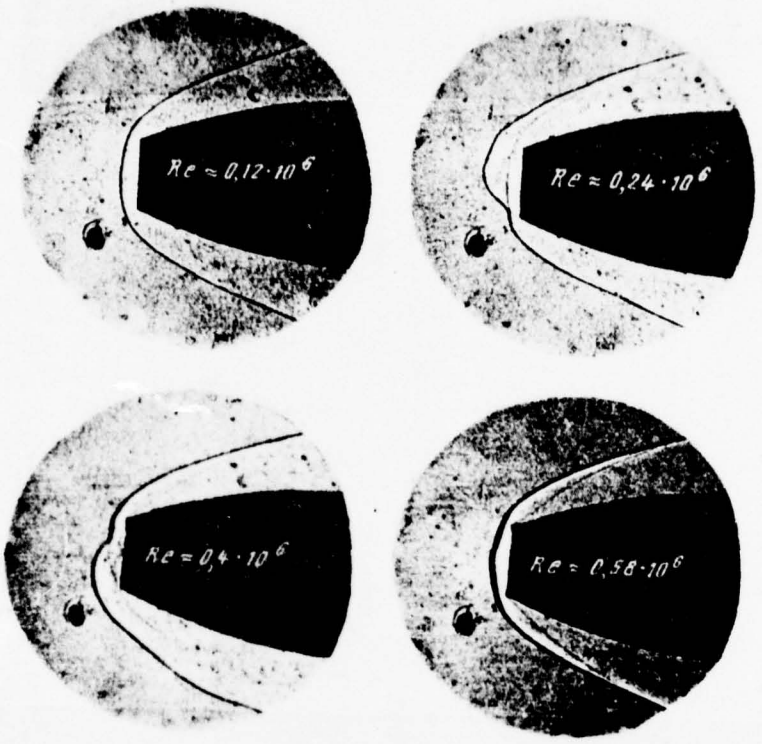


Fig. 2.

$M \sim 5$; $Re \sim 0.32 \cdot 10^6$; $\alpha = 10$, round edge.

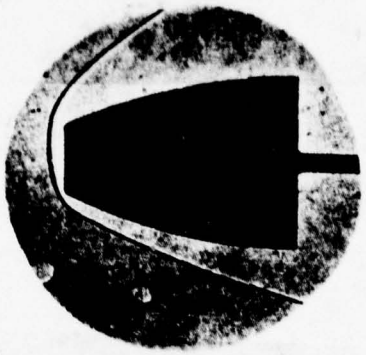


Fig. 3.

Page 108.

Fig. 6 shows ranges with the greatest and small amplitudes of the oscillations of the shock wave before the body with spherical indentation during a change in the radius of curvature of leading edge. The given curve/graph has qualitative character, since it is constructed on the basis of data, obtained only for three versions of the radius of curvature of edges, and boundaries of the region according to Re numbers are those approximated.

Investigations showed that the instability of the flow around

bodies with indentations in nose section depends on Re numbers, M, and also on the form of the leading edge of model. The maximum value of the departure/withdrawal of shock wave from body comprises approximately 3.3 °.

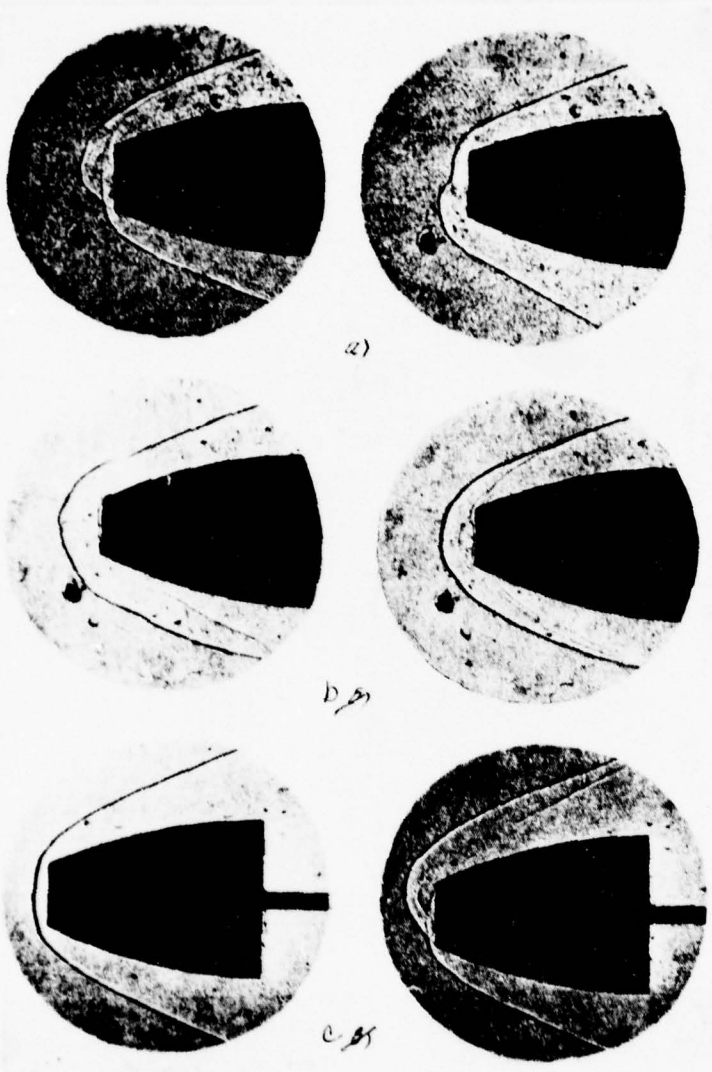
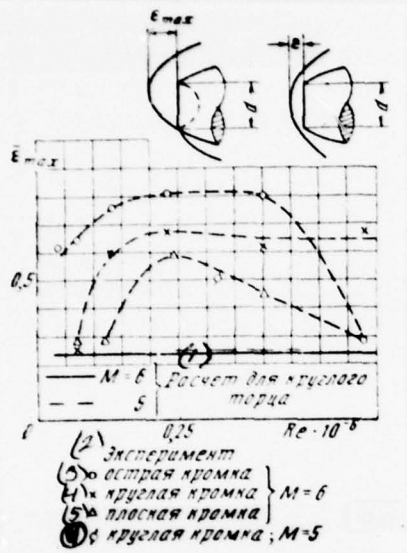


Fig. 4. (a) flat/plane edge, M ≈ 6, Re ≈ 0.24•10⁶; (b) sharp edge, M ≈ 6, Re ≈ 0.4•10⁶; (c) round edge, M = 5, Re ≈ 0.32•10⁶.

Page 109.

These special feature/peculiarities of the flow around bodies with indentations can affect aerodynamics of body; therefore must be considered them during the determination of the aerodynamic forces, which act on body in flight with super-and hypersonic speeds. The described phenomenon also it is necessary to keep in mind during the construction of the aerometric instruments, notched in nose section (for example, such, as Pitot tube for measuring the total pressure after the shock wave, etc.).



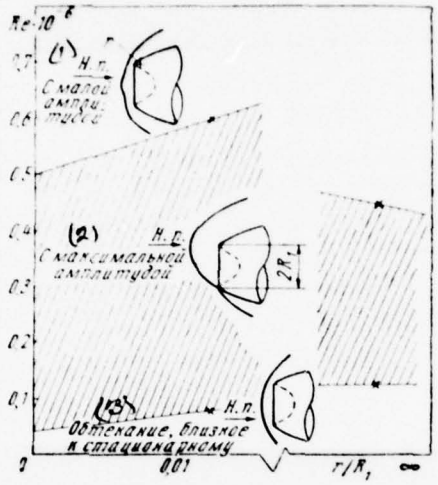


Fig. 6.

Fig. 5.

Key: (1). Calculation for a circular end/face. (2). Experiment. (3). sharp edge. (4). round edge. (5). flat/plane edge.

Fig. 6.

Key: (1). With small amplitude. (2). With maximum amplitude. (3). Flow, close to stationary.

~~REFERENCES~~

References

1. R. H. Johnson. Instability in hypersonic flow about blunt bodies. The Physics of Fluids, Vol. 2, No 5, 1959.

2. R. A. Bastianon. Unsteady solution of the flowfield over concave bodies. AIAA J, 1969, No 3.

3. A. N. Minaylos. Similarity parameters and approximating dependences at the ellipsoid flow of the supersonic flow. "Bull. of the AS USSR - MZhG", 1973, No 3.

Received 25/V 1972.

APPLICATION OF A METHOD OF INSTANTANEOUS FREEZING IN FLOWS WITH VIBRATIONAL RELAXATION.

V. L. Men'shikova, O. Yu. Polyanskiy.

Is investigated the effect of the basic dimensionless parameters on relaxation process in flows with the excited vibrational degrees of freedom. It is shown, that only during certain combination of these parameters are realized the flows in which the asymptotic values of vibrational energy will considerably differ from the values of vibrational energy, determined by the method of instantaneous freezing. Are given examples of calculation.

1. In gas Dynamics of nonequilibrium flows wide acceptance obtained method of instantaneous freezing [1, 2]. Both theoretical and experimental investigations as a whole they confirmed the sufficiently high accuracy/precision of this method in appendix to such relaxation processes as oscillations, dissociation and chemical reactions [2, 3]. However, in work [4] by Blythe, who investigated the process of vibrational relaxation in nozzles and obtained asymptotic expressions for the level of the frozen energy, the

conclusion is made that the method of instantaneous freezing is wrong in the case of small energy capacity of fluctuating degrees, when parameter $\frac{e_к}{RT} \ll 1$ ($e_к$ - vibrational energy, R - universal gas constant, T - temperature of forward/progressive degrees of freedom). This derivation was sufficient not expected, since it contradicted the accumlated facts. In work [5] Blyth and Shih having abandoned the supposition that $\frac{e_к}{RT} \ll 1$ and specifying the temperature dependence, relaxation time

$$(\rho\tau)^{-1} = f(T)\exp[-A(T^{-1/3}-1)], \quad A > 1,$$

where ρ - density, f(T) - certain function of temperature, A - constant, they showed the validity of the method of instantaneous freezing for this case. Despite the fact that in this case by the authors of work [5] substantially it was utilized condition $A \gg 1$, they its conclusion about the validity of the method of instantaneous freezing was explained first of all by failure of the assumption that $\frac{e_к}{RT} \ll 1$. However, strict substantiation of this position in work [5] is not contained, and a question concerning the reasons for the disturbance/breakdown of the validity of the method of instantaneous freezing remained opened.

In the set-forth here work was undertaken an attempt at the numerical investigation of the asymptotic behavior of vibrational energy in the case of a small energy content of vibrational degrees of freedom when the equations of gas dynamics and the equation of kinetics in the first approximation, were not connected.

In this case, were placed two tasks: first, to investigate the effect of different dimensionless parameters on the pattern of nonequilibrium flows in nozzles, and, in the second place, to explain that were possible in practice the conditions/modes when is disrupted the validity of the method of instantaneous freezing.

2. Let us examine flow of relaxing gas with excited vibrational degrees of freedom in hyperbolic nozzle whose form is described by equation

$$\frac{F}{F_*} = 1 + \frac{x^2}{r_*^2 \operatorname{tg}^2 \varphi}, \qquad (1)$$

where F - area of nozzle, F_* and r_* - respectively area and radius of critical section, φ - half-angle of asymptotic cone.

The equations of gas dynamics and relaxation equation take the form

$$\left.\begin{aligned} &\rho u F = \text{const}, \quad u\frac{du}{dx} + \frac{1}{\rho}\frac{dp}{dx} = 0, \\ &\frac{u^2}{2} + c_p T + e_\kappa = h_0 = \text{const}, \quad p = \rho T, \end{aligned}\right\} \qquad (2)$$

$$\frac{de_\kappa}{dx} = \frac{e_{\kappa e} - e_\kappa}{u\tau}, \qquad (3)$$

where p - pressure, u - velocity, h - enthalpy, c_p - heat capacity of active degrees of freedom.

Equilibrium value of oscillatory energy $e_{\kappa e}$ and relaxation time τ are assigned in the form (model of harmonic oscillator)

$$e_{\kappa e} = \frac{R\Theta}{\exp\frac{\Theta}{T} - 1}, \tag{4}$$

$$\tau p = B\exp(AT^{-1/3}), \tag{5}$$

where Θ - characteristic temperature of oscillations, B - constant. In the case $\frac{e_\kappa}{RT} \ll 1$ in the equation of energy, it is possible to disregard value e_κ, and in the first approximation, system of equations (2), (3) decomposes into system (2) and equation (3), system (2) not depending on equation (3). The solution of system (2) it is possible to consider known: this usual solution for the isentropic quasi-unidimensional flow of ideal gas with constant specific heat ratio $\varkappa$. Thus, during the solution of equation (3) of function p, T, u, $e_{\kappa e}$ let us consider known.

After passing to the dimensionless variables

$$\left.\begin{aligned} \bar{p} = \frac{p}{p_0},\ \bar{u} = \frac{u}{a_0},\ \bar{T} = \frac{T}{T_0},\ \bar{\Theta} = \frac{\Theta}{T_0}, \\ \bar{e}_\kappa = \frac{e_\kappa}{e_{\kappa 0}},\ \bar{e}_{\kappa e} = \frac{e_{\kappa e}}{e_{\kappa e 0}}\ \ (e_{\kappa e 0} = e_{\kappa 0}), \\ \bar{x} = \frac{x}{r_*/\mathrm{tg}\,\varphi}, \end{aligned}\right| \tag{6}$$

let us write equation (3) in the form

$$\frac{d\bar{e}_\kappa}{d\bar{x}} = \frac{\lambda\bar{p}}{\bar{u}\exp[K(\bar{T}^{-1/3} - 1)]}(\bar{e}_{\kappa e} - \bar{e}_\kappa). \tag{7}$$

Equation (4) in this case will take the form

$$\bar{e}_{\kappa e} = \frac{\exp\bar{\Theta} - 1}{\exp\frac{\bar{\Theta}}{\bar{T}} - 1}. \tag{8}$$

Thus, the solution of equation (7) depends not only on $\varkappa$, but

also from three more dimensionless parameters - $\bar{\theta}$, λ, K:

$$\bar{\theta} = \frac{\theta}{T_0}, \quad \lambda = \frac{p_0 r_* / \operatorname{tg}\varphi}{a_0 B \exp(A T_0^{-1/3})}, \quad K = A T_0^{-1/3} \tag{9}$$

Parameters K and θ depend on the thermodynamic and kinetic characteristics of gas and on initial data (conditions in precombustion chamber), the parameter λ includes also the geometric characteristics of nozzle.

Page 112.

Equation (7) with boundary condition $\bar{e}_к = 1$ with $\bar{x}$ = -- was solved numerically. The parameters λ, $\bar{\theta}$, and K were varied in the ranges

$$\left.\begin{array}{l} 0{,}01 \leqslant \lambda \leqslant 10\,000, \\ 1 \leqslant \bar{\theta} \leqslant 200, \\ 0{,}015 \leqslant K \leqslant 200. \end{array}\right| \tag{10}$$

In all cases was observed the freezing of vibrational energy, i.e., activation, by which, beginning with certain section of nozzle, the value of vibrational energy is not virtually changed.

In the method of instantaneous freezing value $e_{кf}$ - the frozen value of vibrational energy - usually is determined on the basis of the condition that the freezing occurs in the section where begins noticeable deviation $e_к$ from $e_{кe}$. This section is characterized by

the fact that the relaxation time τ in it is equal to the characteristic time t (for example, see [2]):

$$\tau = t_* \equiv \left(\frac{1}{e_{\kappa e}} \frac{de_{\kappa e}}{dt} \right)^{-1} \qquad (11)$$

[$e_{\kappa f}$ in work [2]
$e_{\kappa e}$ - to solution of equation (11)].

For value $\zeta = e_{\kappa\infty}/e_{\kappa f}$ in work [4] under the assumption $N > 1$ $(N = \bar{\theta}/\bar{T}_f)$ was obtained the formula

$$\zeta = [2\pi/G'(1)]^{1/2} [N^{1/2} + O(N^{-1/2})] \exp\left[-N \int_1^{\infty} G(\xi)\, d\xi \right], \qquad (12)$$

where

$$G(\xi) = \frac{F(\bar{T})}{F(\bar{T}_f)}, \quad \xi = \frac{T_f}{T}, \quad F(\bar{T}) = \frac{1}{\bar{u}(\bar{T})\,\bar{\tau}(\bar{T})} \left(\frac{d(1/\bar{T})}{d\bar{x}} \right)^{-1}, \quad \bar{\tau} = \frac{\tau}{\tau_0}.$$

FOOTNOTE 1. Work (4) used another condition for determining value $e_{\kappa f}$. However, it is possible to show that the criterion of Blyth is identical to criterion (11). ENDFOOTNOTE.

FOOTNOTE 2. The form of the function $G(\xi)$ in work [4] it is not defined concretely. Was only made assumption about that which in the vicinity of point of freezing $G(\xi)$ can be represented in the form of series $G(\xi) = 1 + \sum_{n=1}^{\infty} a_n (\xi - 1)^n$ and with $\xi \to \infty$ $G(\xi) \to 0$. ENDFOOTNOTE.

Table 1. $\theta = 20$

$\lambda = 1$			$\lambda = 10$			$\lambda = 100$		
N	N/K	ζ	N	N/K	ζ	N	N/K	ζ
20,46	0,10	1,17	20,8	0,10	1,23	21,2	0,10	1,26
20,8	1,04	1,02	22,2	1,11	0,80	25,0	1,25	0,56
20,8	10,4	0,78	22,4	11,2	0,22	29,6	14,8	$0,12 \cdot 10^{-1}$
20,8	104	0,72	23,2	116	0,14	30,8	154	$0,16 \cdot 10^{-2}$
20,8	1040	0,72	23,2	1160	0,13	31,0	1550	$0,12 \cdot 10^{-2}$

Table 2. $\theta = 1.5$; $K = 0,015$

λ	N	ζ
1	1,75	1,07
10	2,40	0,97
10^2	4,11	0,65
10^3	7,83	0,23
10^4	15,48	0,15

Table 3. N = 200.

λ	(1) Величины ζ при N/K, равных		
	0,1	1	10
1	1,21	0,79	0,32
10	1,25	0,66	$0,14 \cdot 10^{-1}$
100	1,26	0,49	$0,79 \cdot 10^{-4}$

Key: (1). Values ζ with N/K, equal.

Page 113.

On the basis of formula (12) in work [4] the conclusion was made that with $N \gg 1$ asymptotic value $e_{K\infty}$ there will not compulsorily be of the same order as as value e_{Kf}.

Calculations showed (see Table 1-3 and Fig. 1 and 2, to which are given some results of calculations) that really at sufficiently high values of N it is possible to observe the noticeable difference for value $\zeta = \frac{e_{K\infty}}{e_{Kf}}$ from unity, but only under condition $N/K \geqslant 1$ and is sufficient large λ (in the range of the parameters being investigated). It is necessary to note that the deviation ζ from unity noticeable increases with increase $n = \frac{\bar{\theta}}{K}$ and λ (see tables), high values $N = \bar{\theta}/T_f$ (sufficient for obtaining $\zeta \ll 1$) can be provided not only with the large $\bar{\theta}$ ($\bar{\theta} \gg 1$, when $e_K/RT \ll 1$), but also at high values $1/T_f$, what it is possible to achieve, increasing n and λ (see Table 2).

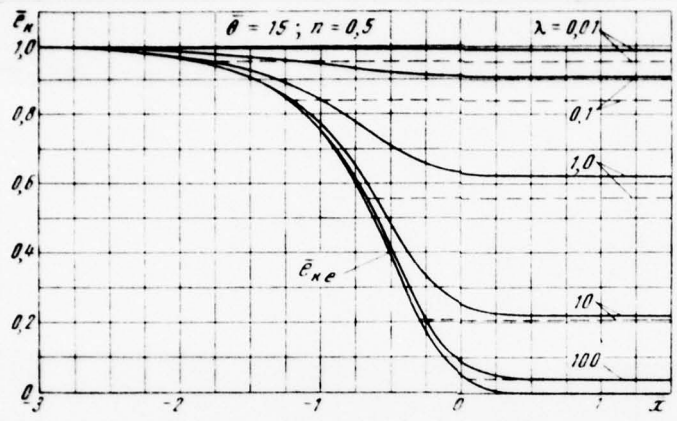


Fig. 1.

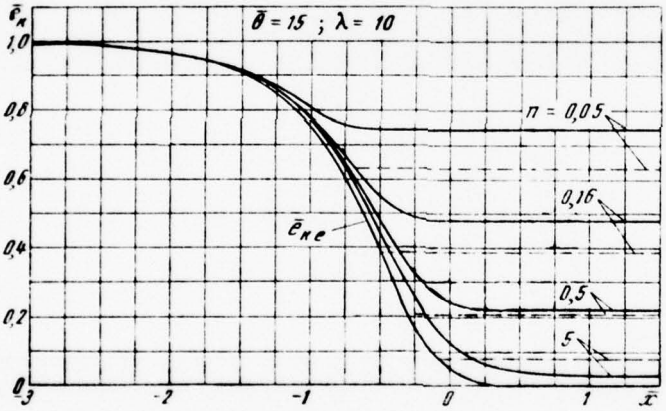


Fig. 2.

Page 114.

3. Real ranges of change in parameters are only small range of

ranges (10). Thus, for instance, for nitrogen by real ranges during change T_0 from 200 to 2000 K and pressure from 10^4 to 10^8 Pa they are $1{,}65 \leqslant \theta \leqslant 16{,}5$, $15 \leqslant K \leqslant 30$, $10^{-7} \leqslant \lambda \leqslant 10$ for $r_*/tg\phi = 1$ cm. Fig. 1 and 2 as an example, give corrected values e_x depending on x for some values of the parameters λ, θ and $n = \frac{\theta}{K}$ from these ranges. Broken lines plotted/applied the sclutions, obtained according to the method of instantaneous freezing with the application/use of condition (11). The calculations, carried out for the flows of nitrogen, show that in the in practice interesting cases it is not possible to simultaneously ensure such values θ, K and λ, which lead to large difference ζ from unity.

Thus, the result, obtained in work [4], can be considered as mathematical limit in $N \longrightarrow \infty$ and some communication/connections, superimposed on the remaining parameters. In actuality assignment to physical model of the medium gives the dependence between these parameters, which one must take into account during the investigation of solution.

REFERENCES

1. K. N. C. Bray. Simplified sudden-freezing anlysis in nonequilibrium nozzle flows. ARS J, Vol. 31, No 6, 1961.

2. V. P. Agafonov, V. K. Vertushkin, A. A. Gladkov, O. Yu. Polyasnskiy. Nonequilibrium physicochemical processes in aerodynamics. M., "machine-building", using 1972.

3. J. L. Stollery, J. E. Smith. A ncte on the variation of vibrational temperature along a nozzle. J Fluid Mech., Vol. 13, No 2, 1962.

4. P. A. Blythe. Asymptotic solutions in nonequilibrium nozzle flow. J Fluid Mech., Vol. 20, No 2, 1964.

5. C. J. Shih, P. A. Blythe. On the sudden freeze approximation in vibrationally relaxing gas. Eight Internaticnal Shock Tube Symposium, London, 1971.

Received 30/VI 1972.

Page 115.

CLIMB OF SHOCK WAVE ON WEDGE STREAMLINED BY A SUPERSONIC FLOW.

Yu. F. Makovskiy, F. V. Shygayev.

Is contained the description of the experimental investigation of an incidence in the shock wave on wedge with the half-angle of solution/opening of 5°, that is located in the supersonic flow, with Mach number of flow M_1 = 1.46 and of the incident shock wave M_2 = 1.51. Corrected values of gas density in different ranges of flow, obtained with the aid of interferometer.

The task of interaction of shock wave with the wedge, streamlined with the supersonic flow of gas, in linear approach/approximation was examined in works [1] (infinitely fox tail) and [2] (weak compression wave, falling/incident to wedge). In article [3] is given numerical solution of task for the case when the incident shock wave experience/tests regular reflection from the surface of wedge.

In the described here work experimentally was investigated climb of shock wave to wedge with the half-angle of solution/opening of 5°, streamlined with the supersonic flow. The direction of the motion of wave coincided with direction of the flow, flowing around wedge. In this case, the incident shock wave experience/tested Mach reflection from the surface of wedge. Experiments are carried out in the two-diaphragm shock tube in which appeared two shock waves. Flow behind the first shock wave created the supersonic flow around wedge, after which on it fell the second shock wave. Time interval between the arrival of the first and second shock waves into working section was 50-150 μs. As working gas served nitrogen. Mach number of the flow, which flows around wedge, $M_1 = 1.46$, Mach number of the wave, falling/incident to wedge, $M_2 = 1.51$. The velocities of shock waves were measured with the aid of piezoelectric pickups. For density measurement of gas, was applied makh - Tsender's interferometer. As the source of light of interferometer served pulse ruby laser with the q-switching. Were obtained also the shadowgraphs of process.

Typical interferogram, taken through 4.9 μs after the collision of the incident shock wave with the leading edge/nose of wedge, given to Fig. 1. Here 1 - initial wave on wedge; 2 - incident shock wave; 3, 4 - shock waves after interaction; 5 - shock wave, which is formed during the steady flow around wedge of the flow of gas behind the second shock wave. As a result of processing experimental data, was

determined the position of shock waves after interaction and is obtained the value of density in different zones of flow. Density was calculated from formula $\Delta\rho = \lambda\delta/(kL)$. Here λ - wavelength of the world/light, emitted by lasers (λ = 6943 Å), k - constant gladstona - Deyla, L - path length of ray/beam, δ - shift of interference fringe.

Experiments showed that gas density in plug behind the first and second shock waves is in effect constant. The observed about wedge picture of flow is close to self-similar.

Fig. 2, gives the shadowgraph of process and is shown the position of shock waves near wedge.

Page 116.

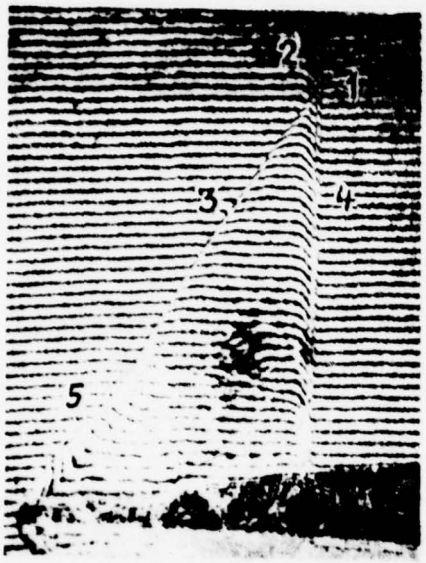
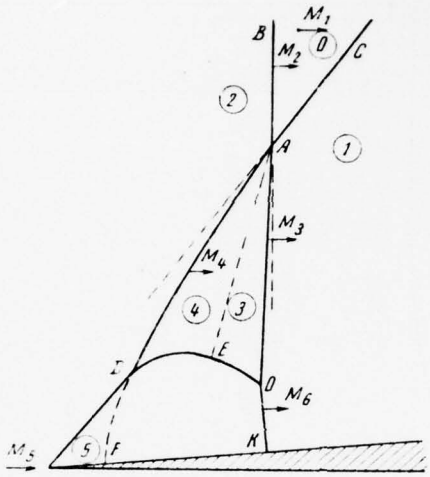


Fig. 1.

kinetics in the first approximation, [illegible]





$M_1 = 1,46$; $M_2 = 1,51$; $M_5 = 1,9$; $M_6 = 1,6$

Отношение плотностей (1)	Расчет (2)	Эксперимент (3)
ρ_1/ρ_0	1,31	1,3
ρ_2/ρ_0	1,88	1,8
ρ_3/ρ_0	2,36	2,2
ρ_4/ρ_0	2,91	2,6
ρ_K/ρ_0	—	2,5

Fig. 2.

Key: (1). Density ratio. (2). Calculation. (3). Experiment.

Page 117.

Here corrected values of density in the different ranges of flow and value of mach numbers of shock waves. As a result of cooperating the

incident shock wave AB with leading wave AC, are formed two new shock waves AD and AO, between which appears the contact surface AE. Under our conditions of gas density behind the shock waves AD and AO, they virtually coincide, and contact surface on photographs is not noticeable. The disturbed range OEDFK, the parameters of flow in which are alternating/variable, limited from above by the shock wave, which proceeds from point O. Range 5 corresponds to the flow around wedge of the supersonic flow with new Mach number. The calculated and experimental values of density in ranges 1-5 will agree well. Calculation is related to ideal gas with $\gamma = 1.4$. In the disturbed range OEDFK, gas density decreases in direction from carrying wedge downstream. Near the surface of wedge, this decrease comprises approximately 10o/o. Experiments show that the number M_6 of the leg of the Mach configuration OK exceeds number M_2 of the incident shock wave. Wave velocity OK in the laboratory coordinate system is smaller than the velocity of incident wave AB ($v_{OK} = 0{,}95\, v_{AB}$).

REFERENCES

1. Smyrl J. L. The impact of a shock wave on a thin two-dimensional aerofoil moving at supersonic speed. J. Fl. Mech., vol. 15, 1963.

2. S. M. Ter-Minasyants. Problem of the diffraction of plane wave on the wedge, driving/moving with supersonic speed. Reports of the AS USSR, Vol. 155, No 4, 1964.

3. R. Ya. Tugazakov. Interaction of shock wave with the wedge, driving/moving with supersonic speed. "scientific notes of TsAGI", Vol. II, No 2, 1971.

Received 24/VII 1972.

BREAKAWAY OF TURBULENT BOUNDARY LAYER DURING ITS INTERACTION WITH SHOCK WAVE IN AN ACCELERATED SUPERSONIC FLOW.

A. I. Tolmanov, V. V. Filatov.

Are given the results of the experimental study of interaction of shock waves with turbulent boundary layer. Is examined the effect of pressure gradients on the values of maximum pressure differentials in the jumps, calling boundary-layer separation. It is shown, that in the case of accelerating the "external" flow the limiting values of pressure differential in jumps grow/rise in comparison with the case of the breakaway of turbulent boundary layer by flat/plane plate. In experiments are used the expanded conical nozzles, working medium/propellant - air.

One of the basic questions, sclved in the tasks of cooperating the boundary layer with shock waves, is the determination of maximum pressure increase which is maintain/withstood by boundary layer until breakaway. The obtained at the present time dependences, as a rule, are related to the cases of the gradient-free flow before the place of breakaway; however, frequently them they spread to the classes of

the flows, in which the flow before the jump is accelerated. The analysis of some theoretical and experimental examinations [1, 2] forces to doubt the fact that for all models of flow must exist the single ratio of pressure in the jumps, calling boundary-layer separation. For obtaining the quantitative evaluations of the effect of initial pressure gradients in the case of cooperating the shock wave with turbulent boundary layer, were carried out pressure measurements in the range of flow breakaway from the walls of the expanded conical nozzles.

Fig. 1 gives for the comparison two circuits of flow with boundary-layer separation, and also shows the character of pressure distribution in each case. The most common/general/total sign/criteria, which are inherent in different models, are rapid pressure rise in the range of breakaway and the presence of the following characteristic points: 1 - point at which the boundary layer experience/tests initial compression; S - separation point; 2 - point of elevated pressure, determined in the pressures plateau. Among the distinguishing features of the presented circuits most essential is the acceleration of the flow before the shock wave in the case of breakaway in nozzle. Shock wave is form/shaped within the limits of boundary layer, beginning from sonic line, so that its intensity in viscous layer is variable. A maximum pressure differential on shock wave in the range, which adjoins the breakaway

zone, it will correspond to certain point e (see fig., 1b), arrange/located on the boundary of the disturbed boundary layer. If for the step, streamlined with the steady flow, number $M_e = M_1$, then for a nozzle as a result of the expansion of the undisturbed flow at the length of the zone of interaction of jump with boundary layer (Δx_2) $p_e < p_1$ and $M_e > M_1$.

Page 119.

Therefore, considering critical the pressure differential on shock wave in the undisturbed zone of flow, which adjoins the breakaway zone, we must establish/install dependence for ratio $p_2/p_e = f(M)$, if we examine flow with pressure gradients before the shock wave. In the case of breakaway on plate, this jump/drop is determined by the relation of pressures p_2/p_1 and for a turbulent boundary layer in essence depends on numbers M_1 of flow. In the experiments conducted was placed the task additionally to explain that in which measure the acceleration of the flow before the jump affects the value of a critical jump/drop in the pressures p_2/p_e.

For experiments were selected conical nozzles with different half-angles of the solution/opening (α = 9°, 11°, 15°, 25°) and exit mach numbers within limits M_a = 2.86-4.18; critical throat diameter comprised approximately 14 mm. A change in the location of the

breakaway of flow relative to walls and, therefore, the initial parameters of interaction was achieved by the variation of the total pressure at the nozzle entry (discharge occurred into the environment with the pressure, equal atmospheric).

The usual draining of nozzle liners does not make it possible to construct reliable pressure profiles in the vicinity of breakaway; therefore for measurements was used the fine/thin cylindrical nozzle of static pressure (0.8 x 0.5 mm) with skew shear of leading edge/nose. Nozzle is establish/installed on coordinate equipment/device which was run up/turned to the angle, equal to the half-angle of the solution/opening of nozzle, thanks to which introduced into breakaway zone from the side of the section/shear of cap/fillings it slipped on the forming wall. Static-pressure probe was located at a distance by 8 mm from carrying nozzle and it was directed to the side of nozzle liner. The escape of nozzle relative to bracket was 80 mm. Position of intake on forming the nozzles was determined with the aid of the indicator of the linear displacements of coordinate spacer apparatus with accuracy/precision 0.1 mm. Pressure was recorded with the aid of instrument GRM-2 through 1 mm of the course of nozzle, and also via the oscillography of signals from the pressure sensors MDD-780-220, ensuring accuracy/precision with $\pm$2o/o ($\pm$11.2 mm Hg), at the rate of the displacement of nozzle of approximately 0.05 mm/s.

For each of the nozzles, it was realized on 6-8 stable operations of flow breakaway and carried out measurement in the interaction region of jump with boundary layer on the basis of which were constructed the curve/graphs of pressure distribution along the length of supersonic part of the nozzles, analogous presented in Fig. 1b.

Prior to the beginning of the interaction region of jump with boundary layer, the results of measurements coincide sufficiently well with the values of the pressures, obtained by calculation according to relationship/ratios for one-dimensional isentropic flows. Point 1 (see Fig. 1b), in which pressure curve will move away for the first time from the calculated, it was accepted for the beginning of breakaway zone.

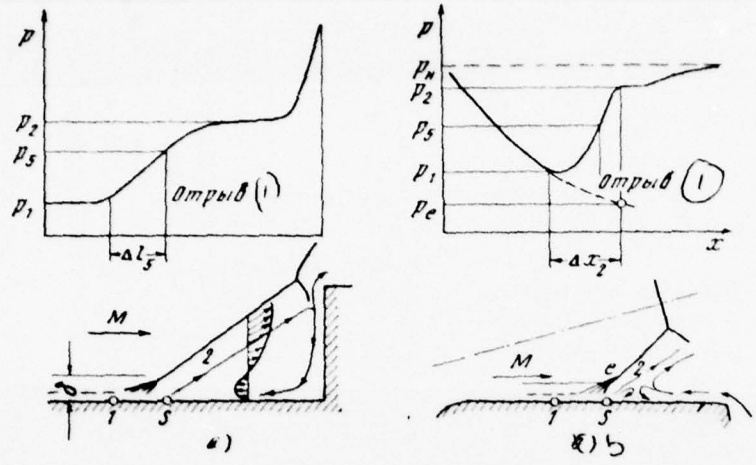


Fig. 1. a) - the breakaway before the direct/straight step; b) - breakaway in conical nozzle.

Key: (1). Breakaway.

Page 120.

Since within the limits of the range of breakaway in boundary layer due to the presence of compression waves are transverse pressure gradients $\left(\frac{\partial p}{\partial y} \neq 0\right)$, the direct measurement of value p_e is not represented possible. For its determination were conducted preliminary blasting during nonseparable flow on an entire part of the nozzle and was establish/installed the function of pressure $p/p_0 = \pi(M)$. On the specific from experiment geometry of the zone of breakaway and known for each nozzle function $\pi(M)$ were located

pressure values at point e, which corresponds to the undisturbed flow in the beginning of the pressures plateau (see Fig. 1b).

The obtained experimental data are represented on Fig. 2a in the form of the dependence of the critical sense of pressures p_2/p_e on number M_e before the shock wave. With the relatively small scatter of experimental points for nozzles with identical aperture angle, is observed a noticeable difference in the results within the limits of entire selected range of aperture angles. Here for a comparison is given analogous dependence for flat/plane detached flows [3], that generalizes the experimental data of a number of different authors. With identical numbers M_e is noted clear tendency toward an increase in the maximum shock-wave intensity with an increase in the expansion angles of nozzles or absolute values of pressure gradients.

Findings were generalized in form, indicated in work [1], and were represented in Fig. 2b. The effect of pressure gradient is here taken into account by coefficient $c = 1 - \frac{\xi_e}{\xi_{пл}}$, where ξ_e, $\xi_{пл}$ - the dimensionless parameters, determined respectively for the nozzle liner and flat/plane turbulent flow at the identical values of the gas-dynamic parameters in the beginning of interaction region:

$$\xi_e = \frac{p'_{xe}\Delta x_2}{p_e u_e^2}; \quad \xi_{пл} = \frac{p'_{x\,пл}\Delta l_S}{\rho_1 u_1^2}.$$

Here $p'_{xe} = \left(\frac{dp}{dx}\right)_e$ - pressure gradient before the shock wave, calling flow breakaway in nozzle; $p'_{x\,пл} = \left(\frac{dp}{dx}\right)_{пл}$ - maximum value of pressure gradient

on wall in the breakaway zone the flat/plane turbulent flow before the step.

Value p'_{xe} was determined by calculation with the known from experiments geometric characteristics of the range of flow breakaway in nozzle. Derivative p'_x can be written as $\frac{dp}{dx} = \frac{dp}{dM}\frac{dM}{dx}$.

Since point e lie/rests at the region of inviscid flow, the derivative dp/dM is determined from the function of pressure for the isentropic flow:

$$\left.\begin{aligned} \frac{p}{p_0} &= \left(1 + \frac{\varkappa - 1}{2} M^2\right)^{-\frac{\varkappa}{\varkappa - 1}} = \pi(M); \\ \frac{dp}{dM} &= -\frac{\varkappa p_0 \pi(M) M}{1 + \frac{\varkappa - 1}{2} M^2}. \end{aligned}\right\} \qquad (1)$$

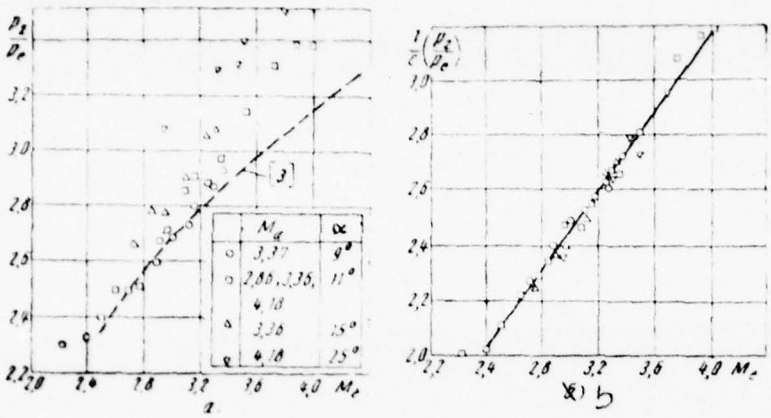


Fig. 2.

Page 121.

For flows in conical nozzle, it is possible to consider valid of relationship/ratio for a supersonic source, therefore, the velocity gradient in arbitrary point can be determined from the expression:

$$\left(\frac{x}{x_{кр}}\right)^2 = \frac{1}{M}\left(\frac{1+\frac{\varkappa-1}{2}M^2}{\frac{\varkappa+1}{2}}\right)^{\frac{\varkappa+1}{2(\varkappa-1)}} = q(M),$$

where x, $x_{кр}$ - respectively distance from the point in question and the point, which corresponds to the transonic speed, of the pole for which can be accepted the point of intersection of generatrices of conical nozzle.

Differentiating this relationship/ratio, we obtain

$$\frac{dM}{dx} = \frac{2}{x}\left(1+\frac{\varkappa-1}{2}M^2\right)\frac{M}{M^2-1}. \qquad (2)$$

Utilizing relationship/ratios (1) and (2), we can write for pressure gradient at point e the following expression:

$$p'_{xe} = -\frac{2}{x_e}\frac{p_0 M_e^2 \pi(M_e)}{M_e^2 - 1}. \qquad (3)$$

The values p'_{xe}, calculated according to formula (3) with the use of experimental values of the parameters, entering the right side of the expression, they varied within the limits (-0.08)-(-0.29) (kg/cm³)/cm.

It is experimentally establish/installed [3] that the maximum values of gradients $p'_{x\,max}$ in pressure profiles near separation point can be approximately determined by the dependence

$$p'_{x\,max} = \frac{1}{2}\frac{p_2 - p_1}{\delta_1}.$$

The values of critical jump/drops in pressures p_2/p_1 for the flat/plane case were accepted on experimental data [3], and boundary layer thickness δ_1 was determined by calculation according to the parameters at point 1. Numbers Re_1 were calculated from data in the beginning of the interaction region of jump with the boundary layer of nozzle, in this case, for characteristic linear dimension, was accepted the distance from point 1 to pole. The range of a change in numbers Re_1 comprised $(2.43-12.5)\cdot 10^6$.

In the parameters ξ_e, ξ_{max} enter also the characteristic linear dimensions: Δx_2 - for a nozzle and Δl_s - for the flat/plane breakaway before the step. The selection of precisely these parameters is

caused by the fact that the values Δx_2 sufficiently accurately are establish/installed along experimental pressure profiles in the breakaway zone of flow, but the dimensionless length of the range of lifting the pressure is above with flow from separation point before the step $\frac{\Delta l_s}{\delta_1}$, as it follows from the experimental data [3], does not depend on numbers Re_1 and M_1 and comprises $\frac{\Delta l_s}{\delta_1} = 2{,}25 \div 2{,}75$ During processing of experimental data, it was assumed that $\Delta l_s = 2{,}5\,\delta_1$.

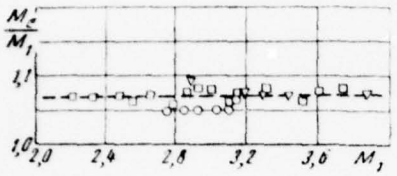


Fig. 3. Designations the same as in Fig. 2.

Page 122.

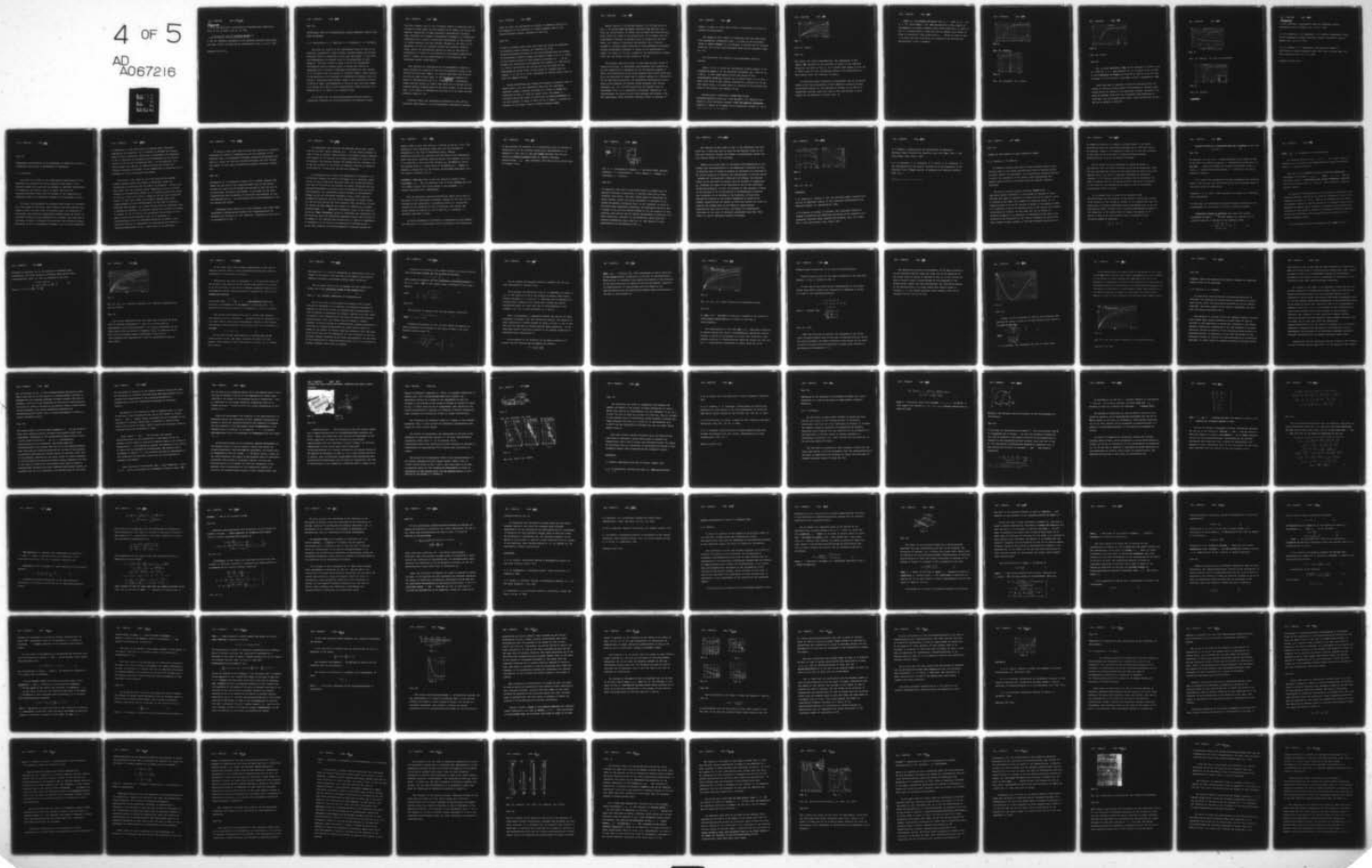
As concerns the determination of the extent of the interaction region of jump with boundary layer in conical nozzle, on the basis of experimental data (Fig. 3) it is possible tc count that for the investigated range of numbers M_1 and of the half-angles α of value Δx_2 they correspond to a change of relation M_2/M_1 within limits of 1.05-1.08. In experiment these values were 3.5-12 mm.

That presented makes it possible to make the conclusion that the disregard of the effect of pressure gradients before the jump, calling boundary-layer separation in the accelerated flow, can lead sometimes to essential errors during determining of the characteristics of breakaway. To the presented in Fig. 2b, results of processing experimental data correspond the values of parameter c = 1.04-1.30.

~~REFERENCES~~

AD-A067 216 FOREIGN TECHNOLOGY DIV WRIGHT-PATTERSON AFB OHIO F/G 20/4
SCIENTIFIC NOTES OF CENTRAL INSTITUTE OF AEROHYDRO DYNAMICS (SE--ETC(U)
JUN 78 A S FONAREV, A G ZAKHAROV
UNCLASSIFIED FTD-ID(RS)T-0679-78 NL

4 OF 5
AD A067216



References

1. G. M. Bam-Zelikovich. Calculation of boundary-layer separation. "Izv. of the AS USSR", OTN, No 12, 1954.

2. Herbert M. V., Herd R. J. Boundary-layer separation in supersonic propelling nossles. Reports and Memoranda, No 3421, 1964.

3. Ye. Ye. Zukoskya. Breakaway of the turbulent boundary layer before the step. "rocket engineering and astronautics", Vol. 5, No 10, 1967.

Received 16/VI 1972.

Page 123.

EXPERIMENTAL STUDY OF AXISYMMETRICALLY SHAPED SUPERSONIC NOZZLES WITH SMALL RE NUMBERs.

L. I. Kudryavtseva, I. I. Mezhirov, S. P. Ponomarev, V. L. Yakusheva.

Are given the results of the experimental study of flow in two supersonic axisymmetric shaped nozzles, designed taking into account viscosity effect on obtaining of flow with Mach number = 6 and which are distinguished by computed value of the temperature of wall. Number Re_L for both nozzles is equal $9.3 \cdot 10^3$, the displacement thickness of laminar boundary layer in nozzle exit section is comparable with a radius of isentropic duct/contour or even exceeds it. It is shown, that the account of viscosity effect, which consists of the addition of the thickness of tightening of boundary layer to a radius of isentropic duct/contour, leads to the satisfactory result: in spite of small size/dimensions of inviscid flow core, Mach number in it within the limits of exit characteristic rhomb virtually it is constant and it is equal to its computed value.

It is known that the ductility/toughness/viscosity exerts a substantial influence on the characteristics of supersonic nozzle

flow (for example, see [1, 2]). Viscosity effect is amplified with an increase in Mach number and the decrease of Re number, and during the specific combination of these parameters characteristic boundary layer thickness (for example, displacement thickness) can render/show comparable with a radius of isentropic duct/contour or even exceed it. Arises question, can such nozzles, designed on the basis of the separation of flow into inviscid nucleus and classical boundary layer, ensure the satisfactory quality of flow, or they must be calculated as a result of the solution of the complete equations of nav'ye - Stokes. For an answer/response to this question, was undertaken present investigation.

Were designed the coordinates of two axisymmetric nozzles of those intended for creation in the exit characteristic rhomb of the uniform flow with Mach number = 6. Initial isentropic duct/contour, one and the same in both cases, it was designed on computers by method of characteristics by V. K. Solodkin (Solodkin). This - axisymmetric nozzle with the section of radial flow which will be joined with the leveling section. Maximum value of the slope tangent of duct/contour $tg\theta_0 = 0.25$. Nozzle is designed for the flow in it of ideal gas with adiabatic index $\chi = 1.4$.

Viscosity effect was considered by addition to radii of the isentropic duct/contour r of the displacement thickness of boundary

layer δ^*, which was determined as a result of numerical solution on the computers of the equations of laminar boundary layer by the finite-difference method, presented in work [3].

Page 124.

As data on boundary layer edge, were taken the values of parameters on isentropic nozzle contour, the coefficient of the ductility/toughness/viscosity of air was calculated from the formula of Southerland, Prandtl's number was taken as equal to 0.71. A radius of the critical section of both nozzles is accepted r_*= 2.5 mm, pressure and temperature of stagnation with respect p_0 = 5000 Pa and T_0 = 450 K. Calculations are carried out for two values of the temperature of nozzle liner (in both cases of constant over its length) $T_w = 290$ and 80 K, which corresponds to cooling nozzle liner by water and liquid nitrogen.

During calculations was assumed the absence of boundary layer in nozzle throat. Slip and temperature jump were not considered (Knudsen's number, designed according to a radius of nozzle and conditions on wall, it does not exceed 0.03). The number Re_L, calculated along the length of nozzle and the static parameters in its exit section, is equal to 9300. So low a value Re_L confirms the presence on the nozzle liners of laminar boundary layer.

Nozzle contours 1 ($T_w = 290$ K) and nozzles 2 ($T_w = 80$ K) are given to Fig. 1. On curve/graphs are shown isentropic r(x) and real r(x) + δ*(x) the duct/contours. By dotted line is shown the characteristic, which limits the rhomb of the uniform flow. It is evident that the displacement thickness of boundary layer in nozzles has the same order, as a radius of isentropic duct/contour, but in nozzle 1 exceeds it. Boundary layer thickness in these parameters noticeably exceeds displacement thickness. A radius of the output/yield of nozzle 1 is equal to 41.2 mm, a radius of the output/yield of nozzle 2-28.7 mm, the length of both nozzles is 178 mm.

The nozzles, depicted on Fig. 1, were made and were tested in vacuum wind tunnel. In experiments were measured total pressure p_0 and the temperature of stagnation T_0 (in the settling chamber of duct), the distribution of the total pressure after normal shock wave p_0' on the axle/axis of nozzle and in primary section at a distance of 150 mm from critical section, the temperature distribution on wall. Value p_0 was measured by U-shaped liquid manometer with dibutyl phthalate, p_0' - by a hot-wire gauge with the maximum error of measurement 3o/o, N. I. Lyapunovoy's developed, temperature - by thermocouples. The nozzle of the total pressure had diameter 5 mm. The coefficient, which considers viscosity effect on readings of

nozzle, is equal to ~0.99, which leads to corrections in limits of accuracy of measurements.

The values of Mach numbers in isentropic core were determined from relation p_0'/p_∞ in boundary layer - in terms of the calculated values of static pressure on the boundary of nucleus and the measured values p_0'. Air in this case considered ideal gas the adiabatic index $\varkappa = 1.4$.

Are given below the results of the experimental study of nozzles.

Nozzle 1. Fig. 2, gives the distribution of Mach numbers to the axle/axis of nozzle 1 in the calculated parameters (p_0 = 5000 Pa; T_0 = 450 K; $T_w = 290$ K). Mach numbers within the limits of exit characteristic rhomb are constant and in effect equal to 6. On Fig. 3 shown cross field of Mach numbers, measured at a distance of 150 mm from nozzle throat. In nozzle there is a nucleus of the uniform flow, which in this section has diameter 15 mm.

Boundary-layer calculations showed that at the assigned/prescribed values p_0 = 5000 Pa and $T_w = 290$ K value δ^* with change T_0 is not virtually changed, since the opposite influences, caused by a change in Re number and in temperature factor T_w/T_∞ it is compensated for one by another.

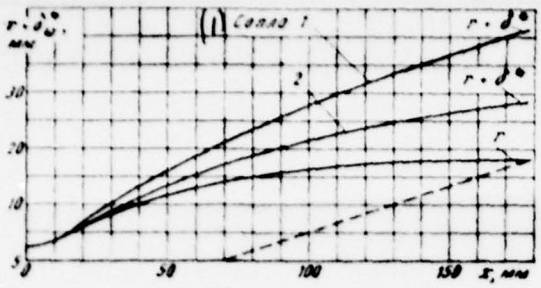


Fig. 1.

Key: (1). Nozzles.

Page 125.

This result was tested experimentally. The dependences of Mach numbers (M), measured on the axle/axis of nozzle at the different values T_0, are given to Fig. 4. It is evident that change T_0 from 300 to 1000 K does not have considerable effect on the distribution of Mach numbers along the axle/axis of nozzle.

If deviations under conditions of experiments lead to noticeable change in δ^*, the distribution of Mach numbers in inviscid nucleus can strongly change. So, the decrease of pressure p_0 to 2500 Pa or temperature contrast along wall lead to the high gradient of Mach numbers on the axle/axis of nozzle (Fig. 5).

Nozzles 2. This nozzle was tested with p_0 = 5000 Pa, T_0 = 450 K, $T_w = 90$ K (calculated $T_w = 80$ K). The distribution of Mach numbers on the axle/axis of nozzle, measured under these conditions, is given to Fig. 2. In characteristic rhomb the flow is uniform, mach number is close to calculated. Cross field with x = 150 mm is shown on Fig. 3. In this case here also there is a nucleus of the uniform flow approximately 15 mm in diameter.

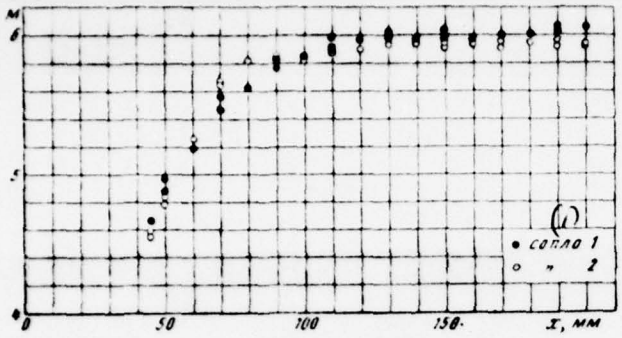


Fig. 2.

Key: (1). Nozzles.

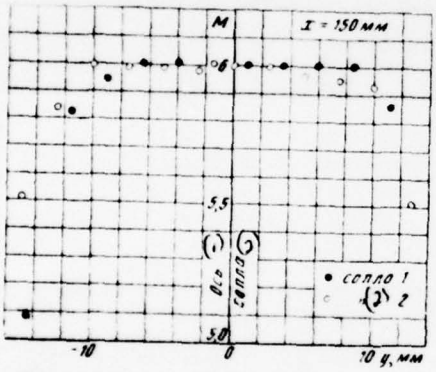


Fig. 3.

Key: (1). Axle/axis. (2). nozzle.

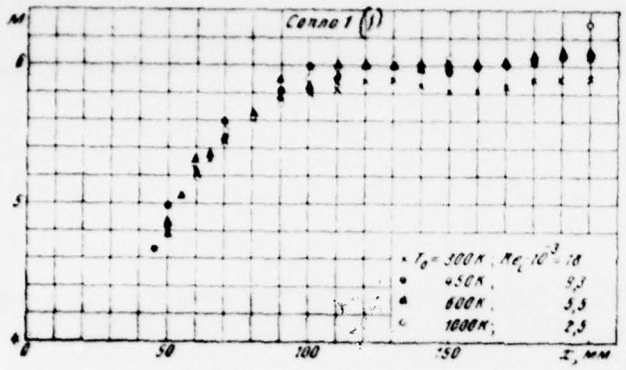


Fig. 4.

Key: (1). Nozzle.

Fig. 6, gives dependences M(x) on the axle/axis of nozzle 2 with p_0 = 5000 Pa, T_w = 90 K and different T_0. It is evident that a change in the temperature of stagnation from 450 tc 1000 K, as in the case of nozzle 1, did not cause a noticeable change in dependences M (x).

Given data make it possible to draw the conclusion that the account of viscosity effect within the framework of boundary-layer theory during the design of the supersonic nozzles, designed on the small Re numbers, with which the transverse size/dimensions of isentropic core are comparatively small, gives satisfactory results and can be applied in practice.

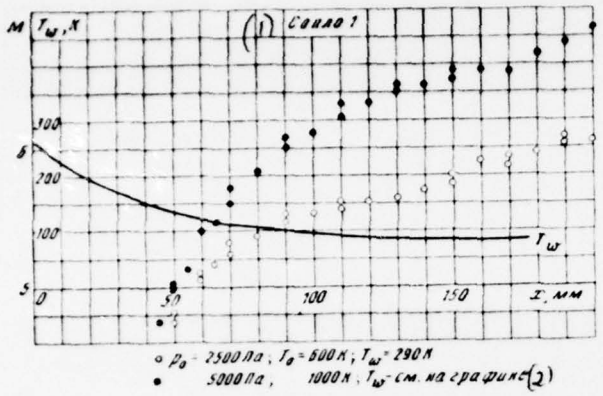


Fig. 5.

Key: (1). Nozzles. (2). see on curve/graph.

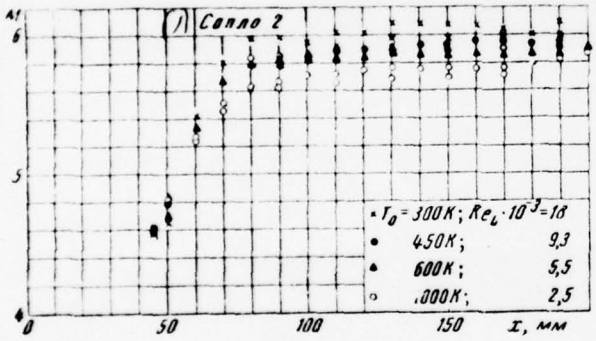


Fig. 6.

Key: (1). Nozzles.

[redacted]ES

References

1. G. M. Ryabinkov. Experimental study of supersonic nozzles. "scientific notes of TsAGI", Vol. 1, No 1, 1970.

2. I. I. Mezhirov, T. A. Timofeyev, S. I. Chistov. Experimental study of the axisymmetric shaped hypersonic nozzles. "scientific notes of TsAGI", Vol. II, No 6, 1971.

3. A. P. Byrkin, V. V. Shchennikov. One numerical method of calculation of laminar boundary layer. The "jour. of comp. math. and math. physics", Vol. 10, No 1, 1970.

Received 31/VIII 1972.

EXPERIMENTAL DETERMINATION OF THE DEPENDENCE OF INTENSITY OF FLOW IN A MOLECULAR WIND TUNNEL ON TEMPERATURE OF STAGNATION.

I. D. Vershinin.

Are given the results of the experimental determination of the dependence of intensity of flow in molecular wind tunnel on the distance between the nozzle and the skimmer at different temperatures of stagnation (293-1033 K) and it is shown, that with the constant/invariable nozzle flow an increase in the temperature of stagnation leads to an essential increase in the intensity of flow.

The basic flow parameters in molecular wind tunnel are intensity (i.e. the number of molecules, which intersect the unit surface area, normal to flow, per unit time) and average speed. Is accumulated at the present time extensive experimental material about the effect of different factors on these parameters [1]. However, the large part of the works, in which is obtained this material, was fulfilled without preheating of gas in precombustion chamber, i.e., at room temperature

of stagnation. At the same time it is obvious that, increasing temperature of stagnation, it is possible to increase the average speed of flow in molecular wind tunnel. Furthermore, the preheating of gas is necessary for preventing the condensation on the initial section of the circuit of molecular duct - in the supersonic jet, which escapes into vacuum. In connection with this arises the question concerning the effect of the temperature of stagnation T_0 on intensity of flow in molecular wind tunnel.

The effect of the value of T_0 on the value of the optimum distance between nozzle and skimmer of molecular tunnel was investigated in work [2], but its effect on intensity - in work [3], where given data on intensity change depending on T_0 at a constant pressure in precombustion chamber p_0. It should be noted that change T_0 with p_0 = const will entail a change in the gas flow through the nozzle. In this case, change the pressure residual gas in the camera/chambers of duct ("background") and the flow of molecule, reflected from skimmer, i.e., those factors which by themselves exert a substantial influence on intensity. Taking into account the absence at present of the methods of the calculation of the effect of the named factors on the molecular flow, it is necessary to state/establish that the development/detection of effect on the intensity strictly of temperature T_0 according to the results of intensity measurements at p_0 = const proves to be difficult.

In order to avoid side effects during the solution of a question concerning the effect of temperature T_0 on the intensity of the molecular flow, is represented advisable conducting measurements not with p_0 = const, but with the constant/invariable gas flow through the nozzle. In this case, is reached the pressure constancy residual gas.

Page 128.

Furthermore, it is possible to expect that in effect constant will remain the gas flow in jet cross-sectionals area on the section between the nozzle and the skimmer and because of this the flow of the molecules, reflected from skimmer. On the basis of the given considerations when conducting of this work, the intensity of flow was measured with T_0 = var and constant flow rate/consumption of the gas through the nozzle.

Experiments were carried out in the molecular wind tunnel whose diagrammatic representation together with equipment/device for measuring the intensity of flow (detector), described in work [4], it is represented in Fig. 1.

In experiments were utilized the becoming narrow sonic nozzle with the critical throat diameter d_0 = 1.1 mm, conical skimmer of inlet 2.9 mm in diameter whose external and internal angles comprised with respect to 70° and 50°, and ccnical collimator of inlet 2.7 mm in diameter. The distance between the skimmer and the collimator was 47 mm. The entrance of the nozzle of detector (0.76 mm in diameter) was located at a distance by 290 mm frcm ccllimator.

In experiments were defined the dependences of intensity J on the distance between the nozzle and skimmer x_{01} at different values T_0 and, as has already been indicated that the constant/invariable flow rate of the working gas through the nozzle. Virtually this was realize/accomplished as follows. With off preheater with the aid of flow regulator, was established certain pressure in precombustion chamber p_0 and was determined dependence $J(x_{01})$. After this was included the preheater and was raised temperature to certain value T_0. The gas flow through the flow regulator (and, therefore, through the nozzle) in this case, did not change, but pressure p_0 increased proportionally $\sqrt{T_0}$. Determined dependence $J(x_{01})$ at new values of T_0 and p_0. Then, increasing current in preheater, was established the new value T_0, again was determined dependence $J(x_{01})$ and so forth. As an example of the obtained thus results Fig. 2, gives the dependences of intensity J of the flow of the molecules of nitrogen on $\bar{x}_{01} = x_{01}/d_0$ with constant flow rate/consumption of the gas through the

nozzle, equal to flow rate with $p_0 = 2.67 \cdot 10^4$ Pa and $T_0 = 293$ K. The analysis of these dependences shows that with the increase of temperature T_0 the form of dependences $J(x_{01})$ remains constant/invariable and coincides with the form of such dependences, which were being repeatedly observed earlier (for example, see [1]). It is possible to note also that distance x_{01}, at which is reached the maximum (with T_0 = const) value of intensity J_{max}, weakly it depends on temperature T_0. This result qualitatively will agree with the results, obtained in [2][1].

FOOTNOTE [1]. From the given in work [2] empirical formula, which determines $x_{01\,opt}$ for the molecular flow of argon, follows that with the constant nozzle flow during change T_0 the distance $x_{01\,opt}$ changes insignificantly. ENDFOOTNOTE.

Most the important conclusion/derivation, which can be made on the basis of the experiments conducted, consists of the fact that an increase in the temperature of stagnation leads to a considerable increase of the intensity of flow in molecular wind tunnel. So, during change T_0 from 293 to 1033 K (see Fig. 2) intensity J_{max} increases more than 4 times.

So strong dependence of intensity on temperature T_0 was somewhat not expected. It is real/actual, with an increase in the temperature,

T_0 was somewhat not expected. It is real/actual, with an increase in temperature T_0 at the constant nozzle flow, approximately it is possible to count that in each jet cross-sectional area the gas velocity increases proportionally $\sqrt{T_0}$ density decreases proportionally $\frac{1}{\sqrt{T_0}}$ and, therefore, flow rate in this section does not depend on T_0.

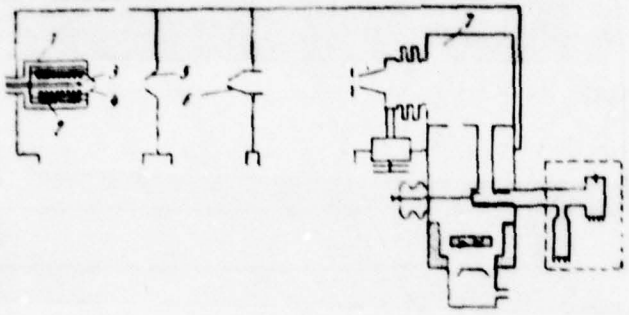


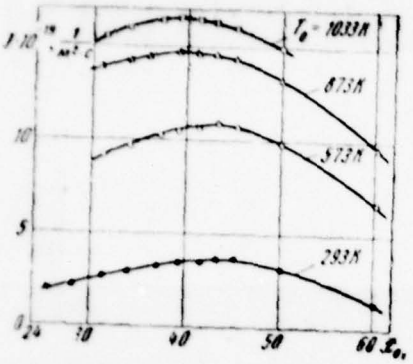
Fig. 1. 1 - precombustion chamber; 2 - multishirt ohmic Nichrome preheater; 3 - thermocouple; 4 - sonic nozzle; 5 - skimmer; 6 - collimator; 7 - detector.

Page 129.

In connection with this it would seem natural to assume that the measured intensity, proportional to specific flow rate at large distances from nozzle, also must weakly depend on temperature T_0. Since, however, occurs the strong dependence of intensity on T_0, arises the question concerning that, is not connected, in spite of the given above elementary reasonings, the dependence indicated with a change in the gas flow through skimmer $\dot{N}$. For the solution of this question, were carried out the special measurements of flow rate of $\dot{N}$ under conditions, identical to the conditions, under which were obtained dependences $J(\bar{x}_{01})$ (see Fig. 2). The results of these measurements are represented in Fig. 3.

The analysis of data given to Fig. 3, and comparison them with given Fig. 2 they show that on value T_0 the relative change in the flow rate depending through the skimmer is significantly lesser than the relative change in the intensity.

Taking into account that in conformity with establishing at the present time representations [1] the weakening of intensity of flow in molecular duct is caused in essence by scattering the molecules of jet on the molecules of residual gas ("background") on section nozzle - skimmer and the molecules, reflected from skimmer, the obtained result can be explained as follows. With an increase in temperature T_0, increases the speed of the molecules of jet of the relatively scattering molecules. In turn, an increase in this velocity it leads to the decrease of the cross section of intermolecular collisions and, therefore, to an increase in the intensity. In this case, because the relation of the angular dimensions of detector and skimmer (characterized the angles, at which are visible the inlets of detector and skimmer made of the center of nozzle throat) substantially less than the unit, the effect of intermolecular collisions on the value of intensity considerably more than their effect on rate of discharge through the skimmer.



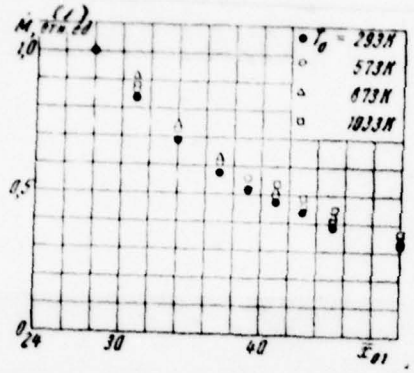


Fig. 2.

Fig. 3.

Key: (1). rel. un.

REFERENCES

1. D. Anderson, R. Andres, D. Fen. The molecular beams, obtained with the aid of supersonic nozzle. In the collection "investigation with molecular beams". M., "peace/world", 1969.

2. T. R. Govers, R. L. LeRoy, J. M. Deckers. The concurrent effects of skimmer interactions and background scattering cn the intersity of a supersonic molecular beam. Rarefied Gas Dynamics, Proc. 6-th Symp., Vol. 2. New York-London, Acad. Press, 1969.

3. K Schugerl. Investigations and applications of supersonic molecular beams. Rarefied Gas Dynamics, Pros. 6-th Symp., Vol. 2. New York-London, Acad. Press, 1969.

4. I. S. Borovkov, I. D. Vershinin, E. P. Pavlov, V. M. Sankovich. To the determination of the partial intensities of the components of the molecular flow. "Journal applied of mechanics and technical physics", 1968, No. 5.

Manuscript received 9 June 1972

CONTROL OF SOFT LANDING OF SPACE VEHICLE ON PLANET.

E. V. Gaushus, S. N. Maksimov.

Is examined steering the center of mass of space vehicle along vertical line in the uniform gravitational field in landing process on planet without the atmosphere. It is proposed as steering function to select the polynomial of the square, which approximates the nominal phase trajectory of descent with the smallest quadratic deviation.

The use of on-board digital computers (**BTsVM** [БЦВМ - high-speed digital computer]) in the systems of steering of space vehicles (KA) makes it possible to realize the law of control, close to optimum in any sense, for example for operating speed. So, in landing process of KA on the surface of planet in the memory of BTsVM it is possible to store the necessary data on the nominal and current trajectories of descent. In this case, the law of control of actuating elements it is expedient to form/shape in the form of the function of the deviations of the current parameters of motion from their nominal values. However, on the small descent vehicles not it

is always profitable, for example in weight sense, to set BTsVM. Nevertheless when the disturbance/perturbations of different nature are present, always it is required to carry out a safe and economical in the sense of the flow rates of working medium/propellant landing/fitting of KA on the surface of planet.

Let us assume that the atmosphere of planet is absent or rarefied so, that its effect on motion of KA can be disregarded. Then the main perturbation sources are the deviations of initial data from nominal values, the error of measuring equipment and actuating elements. It is logical, appears the problem: how to form/shape the laws of steering such KA in landing process. This work is dedicated to the study of this problem during motion of KA in the uniform gravitational field of planet.

It is assumed that on board KA is equipment, with height/altitude and the velocity of the motion of the center of mass of KA relative to the surface of planet. It is accepted also that the brake motor is fasten/strengthened along longitudinal axis of KA, and steering the center of mass of KA is realize/accomplished by means of the regulating of the thrust level of engine. The motion of the center of mass of KA along vertical line is described by the following system of equations:

$$\ddot{x} = \frac{P}{m} - g, \quad \dot{m} = -\frac{P}{c}. \tag{1}$$

Softness condition of landing/fitting let us present in the form

$$x(T) = \dot{x}(T) = 0. \qquad (2)$$

Page 131.

In equations (1) and (2); x - height/altitude of the center of mass of KA above the surface of planet, P - thrust/rod of brake motor, m - mass KA, c - effective exhaust gas velocity from engine nozzle, c = const, g - gravitational acceleration, T - duration of the active section of braking.

It is known[1] that optimum for the fuel consumption and operating speed is the circuit with one active section at the maximum value of the thrust level of brake motor.

FOOTNOTE [1]. A. M. Letov. flight dynamics and control. M., Fizmatgiz, 1969. ENDFOOTNOTE.

In this case, the termination of powered flight corresponds to the torque/moment of the contact of KA of the surface of planet.

Integrating system of equations (1) taking into account conditions (2) when $P = P_{\text{п}} = \text{const}$, we will obtain the equations of the nominal trajectory of descent in the parametric form:

$$\left.\begin{aligned} \dot{x}_{\text{п}} &= c\ln(1-kT) + gT, \\ x_{\text{п}} &= -\frac{c}{k}\ln(1-kT) - cT - \frac{gT^2}{2}, \\ m_{\text{п}} &= m_0(1-kT), \end{aligned}\right| \qquad (3)$$

where $k = \frac{P_н}{m_0 c}$, T - a duration of active section.

In controlled motion of KA $P = P_н + \delta P$. $\delta P = f(u)$, where δP - deviation of the values of the thrust level of engine from nominal value, u - steering function.

The laws of the controls in which the control signals are form/shaped in the form $u = \varphi(x_н, x_н)$, where $x_н = x - x_н$, let us call/name controls in deviations from nominal trajectory, while the laws of the controls which $u = \theta(\dot{x}, x)$ - with controls in absolute measured values.

An essential deficiency/lack in the controls in deviations from nominal trajectory consists of the need for "locking" to time for the formation of values χ_{cc} and $\dot{\chi}_{cc}$, what is the steady source of errors. Furthermore, during the control prccess it is required by any form to memorize the nominal phase trajectory of descent, which without the presence on board BTsVM to fulfill is completely difficult. Therefore we will be restricted to the examination only of control in the absolute measured values.

Let the engine thrust be regulated in the range $[P_{max}, P_{min}]$.

According to equations (3) of the equation of boundary phase trajectories, the which isolate on the phase plane the $\dot{x}x$ "zone controllability" (Fig. 1), will be rewritten in the form

$$\left.\begin{aligned} \dot{x}_j &= c\ln(1-k_jT_j)+gT_j, \\ x_j &= -\frac{c}{k}\ln(1-k_jT_j)-cT_j-\frac{gT_j^2}{2}. \end{aligned}\right\} \tag{4}$$

where $j = 1, 2,\ k_1=\frac{P_{\min}}{m_0 c},\ k_2=\frac{P_{\max}}{m_0 c}$.

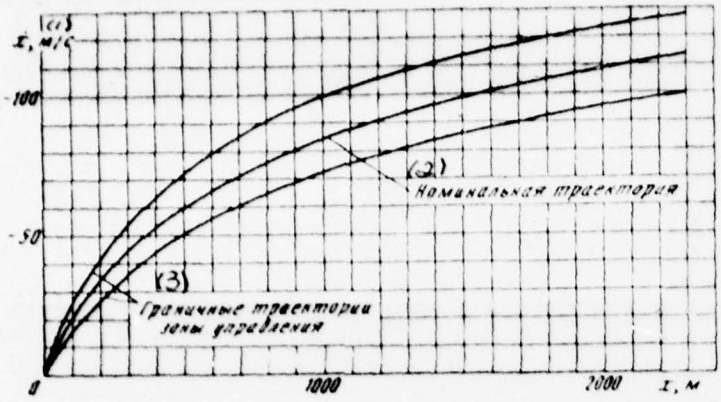


Fig. 1.

Key: (1). m/s. (2). Nominal trajectory. (3). Limiting trajectories of zone of control.

Page 132.

Let us note immediately that the linear law of control of thrust level on absolute coordinates $u = a_0\dot{x} + a_1 x$ in this case is unacceptable, since direct/straight $u = 0$ (line of changeover) on the phase plane $x\dot{x}$ at any values of parameters a_0 and a_1 in vicinity zero it will cross the boundary phase trajectories of the zone of controllability and compulsorily it will hit uncontrolled range of phase plane.

On the other hand, the excessive complication of the form of steering function leads to large difficulties during the technical realization of this method of control.

Therefore as the line of changeover u = 0 on the phase plane $x\dot{x}$, let us select the function of the second order relative to x and $\dot{x}$, it is most accurate in the sense of smallest quadratic deviation the approximating nominal phase trajectory of descent. For this, let us examine the function

$$F(T) = \frac{\dot{x}_n^2}{x_n}. \qquad (5)$$

Let us note that $|\dot{x}_n(T)|$ and $x_n(T)$ - monotonically increasing functions of parameter T. It is possible to show that F(T) - the monotonically increasing function of parameter T, close to constant.

From second relationship/ratio (3) it follows that between x (for simplicity let us designate x_n through x) and the parameter T($T \geq 0$) there exists one-to-one correspondence. Because of this taking into account relationship/ratio (4) function F(T) can be presented in the form

$$F(T) = \frac{\dot{x}(T)}{x(T)} = p(x). \qquad (6)$$

Let us find the best approximation of function p(x) by the linear function $\Im_1(x) = \alpha_0 + \alpha_1 x$, applying the method of least squares. After selecting thus coefficients α_0 and α_1, let us examine the function

$$\delta = \alpha_0 + \alpha_1 x - \frac{\dot{x}^2}{x}. \qquad (7)$$

The curve of u = 0 (line of changeover) on phase plane of all the curved second order in the best way in the sense of the smallest quadratic deviation approximates nominal phase trajectory.

Let us select function (7) as manager and will examine the linear law of the regulating values of the engine thrust:

$$P = P_0 + \delta P, \quad \delta P = -au, \tag{8}$$

where a - the constant coefficient of intensification.

Let us note that in the process of descent of KA to planet without the atmosphere it is possible to isolate two sections of braking. On the first section is conducted the "extinguishing" of rate of descent to relatively low values. Steering KA in this stage is reduced to the orientation of the vector of brake motor against velocity vector. With this thrust level of engine it remains constant. On second section of landing/fitting, examine/considered in this work, is realize/accomplished the thrust vector control of engine at the signals of on-board metering equipment. With this mass of KA by the force of the "smallness" of rate of descent it does not virtually change. Therefore in the first approximation, for the study of the trajectories of controlled motion mass of KA it is possible to consider constant which below is assumed.

Control of the motion of the center of mass of KA along vertical line taking into account (8) let us write in the form

$$\ddot{x} = \frac{P_u - a\left(a_0 + a_1 x - \frac{x^2}{x}\right)}{m} - g. \tag{9}$$

After making in equation (9) the replacement alternating/variable $v = \dot{x}^2$, $v' = dv/dx = 2\ddot{x}$, we will obtain linear differential first-order equation

$$v' + \varphi(x)\, v = \psi(x), \tag{10}$$

where $\varphi(x) = -\frac{\gamma_1}{x}$, $\psi(x) = -\gamma_2 x - \gamma_3$,

$$\gamma_1 = \frac{2a}{m}, \quad \gamma_2 = \frac{2a a_1}{m}, \quad \gamma_3 = 2\left(\frac{P_u - a a_0}{m} - g\right).$$

Page 133.

The solution of equation (10) will be written in the form

$$v = e^{-F}\left(\eta_1 + \int \psi(x)\, e^{F}\, dx\right), \tag{11}$$

where $F = \int \varphi(x)\, dx$, $\eta_1 = \text{const}$.

Producing integration in (11), we will obtain the equation of phase trajectory of the motion of the center of mass of KA along vertical during control (7)

$$\dot{x}^2 = \eta_1 x^{\gamma_1} + b_1 x + b_2 x^2, \tag{12}$$

where

$$\left.\begin{aligned} \eta_1 &= \left(\dot{x}_0^2 - b_1 x_0 - b_2 x_0^2\right) x_0^{-\gamma_1}, \\ b_1 &= -2\,\frac{P_u - \frac{\gamma_1 m}{2} - gm}{m(\gamma_1 - 1)}, \quad b_2 = \frac{a_1 \gamma_1}{\gamma_1 - 2}, \\ \gamma &= \frac{m\gamma_1}{2} \end{aligned}\right\} \tag{13}$$

Let us examine the negative branch of parabola (12) ($\dot{x} \leq 0$), that corresponds to descent of KA.

For realizing the reduction of KA, it is necessary, in order to $\gamma_1 > 0$. The velocity of KA in the process of descent takes finite values; therefore $\gamma_1 \neq 1$ and $\gamma_1 \neq 2$. Selecting now the parameter γ_1, so that phase trajectory (12) taking into account the initial disturbances would not leave the zone of controllability, from formulas (13), let us find parameters a, b_1 and b_2.

Thus, the parameter γ_1 completely defines the type of the phase trajectory of descent (12). The qualitative picture, the behavior of phase trajectory in landing process of image a in Fig. 2. Let us note that with the decrease of height/altitude phase trajectory of the controlled descent oscillates relative to the nominal trajectory of landing/fitting, approaching it.

As the measure of the deviation of the phase trajectory of motion from the nominal, let us examine the function

$$\Delta(x) = \frac{a_0 + a_1 x - p_H(x)}{|p_{rp}(x) - p_H(x)|}.$$

where $p_{rp}(x)$ - function (6), which corresponds to motion along one of the boundary phase trajectories of the zone of controllability. Function $\Delta(x)$ is convenient that besides the measure of the deviation of the phase trajectory of motion of KA from the nominal trajectory of landing/fitting it characterizes even the degree of its removal/distance from the appropriate boundary phase trajectories of the zone of controllability.

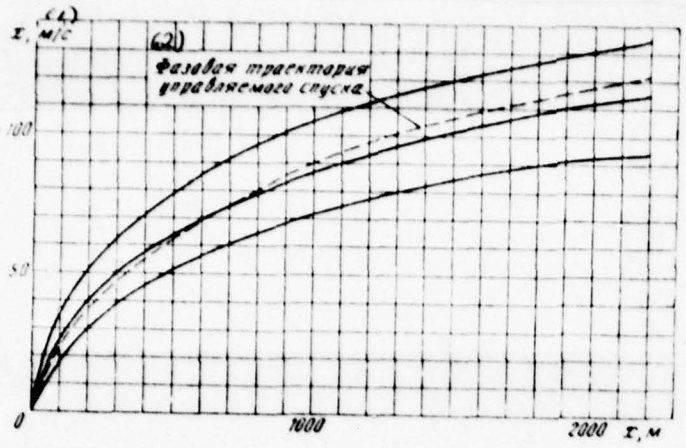


Fig. 2.

Key: (1). m/s. (2). Phase trajectory of controlled descent.

Page 134.

So, when $|\Delta(x)|<1$ the phase trajectory of descent in the process of entire control approximately is located in the zone of controllability.

The torque/moments of the time when $|\Delta(x)|>1$, the phase trajectory of descent emerges the zone of controllability, and further landing process, in spite of the presence of control (8), proceeds so that softness condition of landing/fitting cannot be carried out. The case $\Delta(x) = 1$ approximately corresponds to motion along one of the

boundary phase trajectories of the zone of controllability.

Plotted function $\Delta(x)$ for the phase trajectory of the controlled descent, to Fig. 2, depicts on Fig. 3.

In the case of the relay control characteristic of the engine thrust from control signal, the integration of equations of motion (1) leads to the relationship/ratios:

$$\dot{x} = \dot{x}_0 - c \ln(1 - \bar{k}t) - gt,$$

$$x = x_0 + \dot{x}_0 t + \frac{c}{\bar{k}}[(1 - \bar{k}t)\ln(1 - \bar{k}t) + \bar{k}t] - \frac{gt^2}{2},$$

$$m = m_0(1 - \bar{k}t),$$

where t - current time,

$$\bar{k} = \begin{cases} \frac{P_{\min}}{m_0 c} & \text{(1) при } u > 0, \\ \frac{P_{\text{н}}}{m_0 c} & \text{при } u = 0, \\ \frac{P_{\max}}{m_0 c} & \text{при } u < 0. \end{cases}$$

Key: (1). with.

Under the relay law of control, the regulating of the thrust level of engine depends only on the sign of steering function. During the control process, the phase trajectory of the motion of the center of mass of KA along vertical oscillates on phase plane relative to the function of changeover u = 0.

The qualitative picture of the behavior of the phase trajectory of the controlled descent under the relay law of the regulating of the thrust level of engine is depicted on Fig. 4. In the vicinity of zero of control signal u during delays in the changeover of the engine thrust, appear the auto-oscillations. For oscillation damping of the characteristic of a power change from control signal in vicinity u = 0, one should introduce linear section. This can be realized with the aid of law (8).

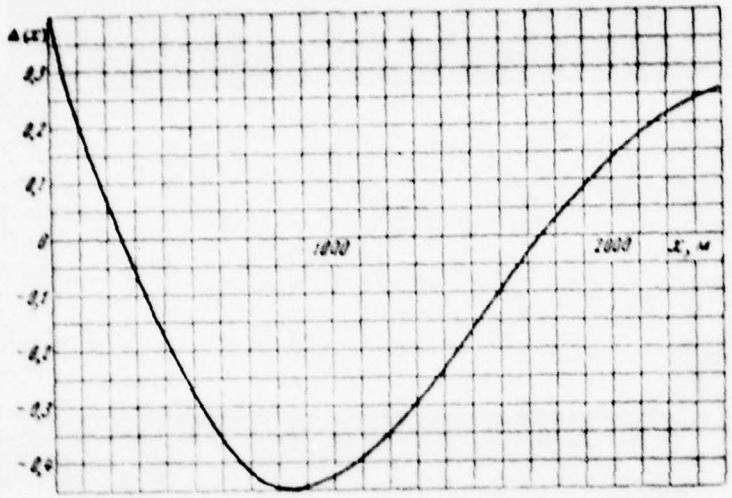


Fig. 3.

Page 135.

Summing up that presented, we come to the conclusion that steering the center of mass of KA along vertical line should be selected in the form:

$$\left.\begin{array}{l} P = P_u + \delta P, \\ \delta P = \begin{cases} -\Delta_1 \operatorname{sign} u & u > \xi, \\ -\alpha u \operatorname{sign} u & |u| \leqslant \xi, \\ \Delta_2 \operatorname{sign} u & u < -\xi, \end{cases} \end{array}\right\} \qquad (14)$$

where

$$u = a_0 + a_1 x - \frac{\dot{x}^2}{x},$$

$$\Delta_1 = P_u - P_{\min},$$

$$\Delta_2 = P_{\max} - P_u,$$

$$\alpha = \text{const},$$

ξ - is constant, that determines the size of linear zone.

The proposed method of control (14) of the motion of the center of mass KA along vertical line permits implemention of a soft landing on the surface of planet without the atmosphere. The law of the regulating of magnitude of vector of the thrust/rod of brake motor is form/shaped directly from readings of on-board metering equipment and its technical realization is sufficiently simple. The parameters of the phase trajectory of motion in the process of descent do not emerge the zone of controllability and approach their nominal values.

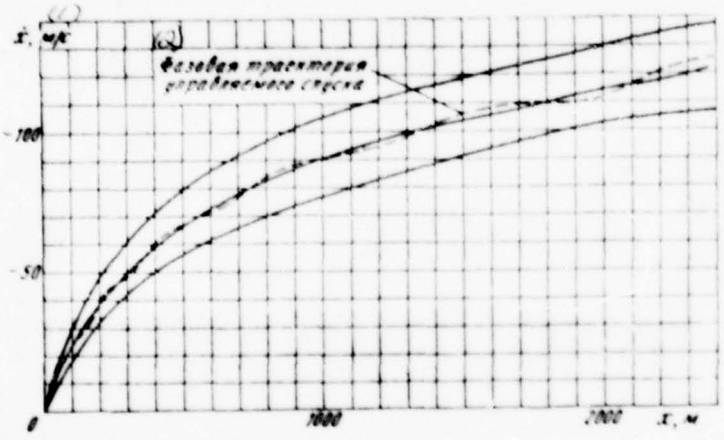


Fig. 4.

Key: (1). m/s. (2). Phase trajectory of controlled descent.

Received 19/V 1972.

Page 136.

AUTOMATIC DEVICE FOR MEASURING THE FORCE OF ADHESION OF CONTACTING HEATED SOLIDS AT LOW PRESSURES.

A. N. Petunin, A. L. Stasenko.

Are described construction and the operating principle of instrument for measuring the normal force of interaction of heated solid bodies, which are periodically contacted at the low ambient pressures. Are given results of the tests of instrument, and also some preliminary measurement data.

The emergence of cohesive forces (or adhesion) between contacted solid bodies under normal conditions is noted long [1]. With an increase in the temperature of bodies and a decrease of the ambient pressure (conditions, characteristic for some elements of airframe structure) surface interaction of the contacting bodies strongly is promote/activated. In monograph [2] are given the results of the systematic studies of friction and cohesion/coupling at low absolute pressures. Is widely known the diffusion welding of strongly heated

solid bodies in the vacuum when the time of process is sufficient so that the average depth of diffusion would achieve many atomic layers. In works [3] and [4] it is described a series of the settings, intended for the study of forces of periphery of interaction of the contacted bodies under quasi-staticnary conditions.

In a series of the cases, it is necessary to know the force of surface interaction of heated solid bodies, which are contacted in vacuum during short time [5, 6]. This unsteady process can be simulated by contact under the action of the normal compressive force of P of two bodies, heated until temperature T and maintain/withstood in the state of contact for a period of time t. It is necessary to determine force F(P, T, t, ...), necessary for the dissociation of these bodies through time t, which depends on the parameters indicated and, possibly, on some others (for example, surface condition and nature of the contacted bodies, ambient pressure p and so forth). Let us note that during the arbitrarily assigned/prescribed set of the values of arguments it is previously difficult to evaluate even the order of this magnitude. For the experimental investigation of the functional dependence indicated developed multiple-contact programmed automatic device (PAU).

Construction and the operating principle of device. PAU consists of nine identical contact pairs (Fig. 1). The diagram of one contact

pair is depicted on Fig. 2. The arranged/located from above movable disk A with the aid of leaf spring B is pressed against cylinder C, equipped with the tungsten preheater of direct current. The time of pressing t and force P are determined by the form of cam/catch/jaw E. The latter is given in rotation by the electric motor, working during entire experiment, that allows repeatedly (virtually any assigned/prescribed number once) to realize/accomplish a process of contact interaction vapor.

Page 137.

The movable disks A have the small thickness a = 0.5 mm, thanks to which after pressing against cylinders they rapidly accept their temperature. Estimation of the characteristic warm-up time of disk $\tau = \rho c a^2/\lambda$ gives 0.003-0.05 s (ρ, c, λ - thermophysical characteristics of its substance). The mobile disks are isolate/insulated from springs with the aid of the alundum bushings which with gaps are establish/installed on the ends of the springs. Gap provides plane-parallel surface contact of contacts. After time of the pressing, greatest for all pairs, begins to rotate framework J, which stretches the measuring helical spring, connected with disk A. The angle of rotation of the framework with value of which is unambiguously connected the force, developed with helical spring, is measured with the aid of rheostat K. At certain value of this angle

(at the moment of equality of the tensile stress of spring and force of interaction of contacts) the disk blows away from cylinder and is recorded the torque/moment of the disconnection/cutoff of voltage/stress from the corresponding terminals of electrical circuit.

The phases of the rotation of cams are selected that, in order to the ends of all intervals of the time of the contact of contact pairs t_i ($i \leqslant 9$ - number vapors) coincided with the beginning of the elongation of springs, which makes it possible to exclude "dead time", during which the disks, "which fixed" with cylinders, would be contacted after the elimination of load.

Thus, values P_i and t_i for each pair are rigidly assign/prescribed by the construction of instrument and by the average on cycle speed of rotation of electric motor ω; the values of temperatures T_i are assigned by position the rheostat of the circuit of heater and are measured by thermocouples. The signals, which correspond to values ω, T_i, F_i, are recorded directly by experimenter or are transmitted by electrical system and are record/written by automatic instruments.

Basic the data of the devices: mass - 3 kg, dimensions - 0.36 x 0.13 x 0.13 m, the supply of the heaters of electric motor 27 V,

1A, the time of one operating cycle -12 s, the pressing force 7-18 H, the time of pressing -0.8-6.6 s, the temperature of contact pair - 300-1000 K, the amount of the measured forces of interaction - 0-0.3 H. Conditions of the normal operation: temperature from -30 to +150°C, pressure - $1.3 \cdot 10^5$-$1.3 \cdot 10^{-6}$ Pa, linear acceleration to 25 g during 0.1 s.

Errors of measurement. The stability of the characteristics of measuring springs was determined by their repeated calibrations in process of which was establish/installed the linearity of response and was estimated a root-mean-square error of measurement in the cohesive force of contacts. It is equal to $\gamma_F^0 = \pm 3\%$. A relative root-mean-square error of measurement of temperature does not exceed $\gamma_T^0 = \pm 5\%$.

As show the results of the repeatedly repeated measurements of the cohesive force of certain selected contact pair during the constant/invariable conditions/mode of experiment, the random error in determining F does not exceed $\gamma_F = \pm$ 20-30o/o. During a change in the conditions/mode, the spread of the measured force of interaction grow/rises. This spread is connected, however, not with the characteristics of instrument, but with the instability of the measured value (nonrecurrence of the consecutive contacts of contacts, the uncontrollable changes in their surfaces after each

contact and other random phenomena, connected with quite contact surface).

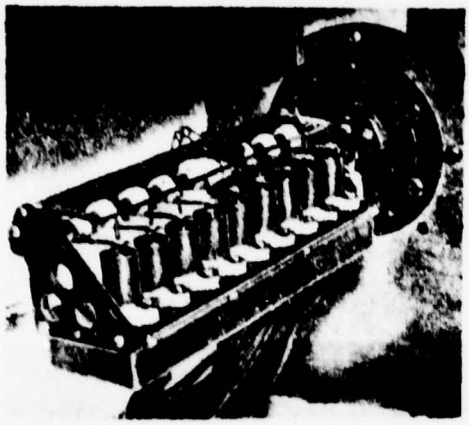


Fig. 1.

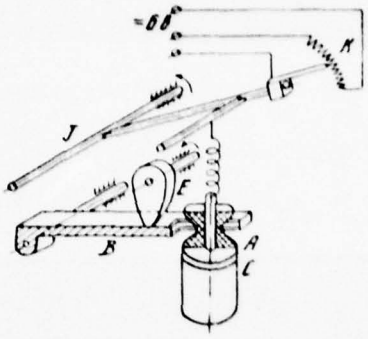


Fig. 2.

[B - V]

Page 138.

Laboratory tests. PAU was placed so that the contact system was in gaseous medium with the assigned/prescribed pressure, and drive - under room conditions. (For the work of instrument in real flight experiment for drive is provided for the airtight camera/chamber with the conditions, close to normal). At different temperatures of the contact pairs whose values were establish/installed by a stepped variation in the supply voltage of the heaters of cylinders, to time t_1 = 60 s, was included the drive of device, also, on electronic potentiometer and oscillograph were record/written temperatures and the forces of interaction. The time of output/yield to new temperature conditions after a change in the

stress of preheaters comprised t_2 = 600 s. At constant temperature of contact pair, were realize/accomplished five contacts. the qualitative picture of a change in the temperature of disk and cylinder in the process of one series of closing of contacts is given to Fig. 3. Before each new set of experiments, were carried out the control calibrations of springs, the dressing of contact surfaces by rouge sandpaper and flushing by alcohol or carbon tetrachloride.

For estimating the operating ranges of a change in the recorded parameters (Fig. 4) were carried out laboratory investigations with copper and steel contact vapors.

The results of measurements are represented in the form of the dependence of dimensionless quantity $\phi = F/P$ from reverse/inverse temperature $10^3/T$, where T - in the Kelvins. It is establish/installed that interaction of steel surfaces is detected at temperatures, by approximately 400 K greater than interaction of copper.

The results of the systematic tests of two specimen/samples of the device, equipped only with copper contact vapors, with $p \approx 1.3 \cdot 10^{-3}$ Pa are given to Fig. 5 and 6. Here each point is the mean arithmetical value for five consecutive measurements of force of interaction of each contact pair; for one specimen/sample of PAU t = 0.8-3.5 s, for another t = 0.8-6.6 s.

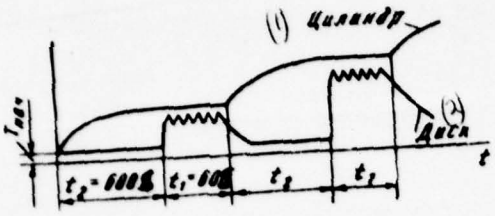


Fig. 3.

Key: (1). Cylinder. (2). Disk.

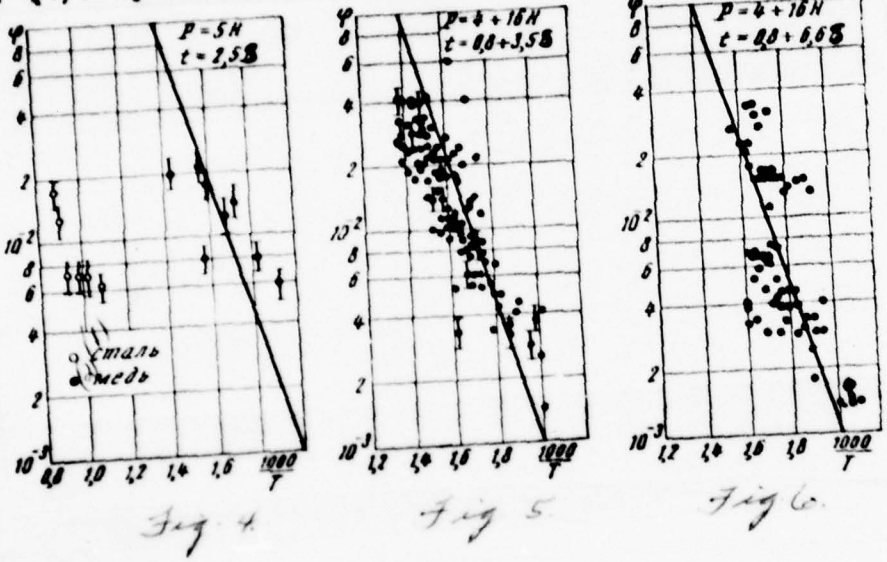


Fig. 4 Fig 5 Fig 6.

Fig. 4.

Key: (1). steel. (2). copper.

Page 139.

For explaining the effect of composition and pressure the ambient gas medium on the process of power interaction of contact pairs, were carried out measurements F in the atmosphere of air ($p \approx 1.3 \cdot 10^{-3}$ Pa) and of argon ($p \approx 1.3 \cdot 10^{-3}$–$1.3 \cdot 10^{4}$ Pa). With an increase in the pressure argon of interacting, forces decrease, although they remain measured even with $p \approx 1.3 \cdot 10^{4}$ Pa. At low pressures ($p \approx 1.3 \cdot 10^{-3}$ Pa) the composition of residual gas (air or argon) barely affects value F.

The given results confirm efficiency under the high-altitude conditions of described a device which makes it possible for comparatively short time to obtain vast information about the amount of the normal force of interaction of contacted solid bodies in wide parametric domain, which characterize the process of contact.

REFERENCES.

1. C. Beilby. Aggregation and flow of solids. London, 1921.

2. I. V. Kragel'skiy. Friction and wear. M., "Machine-building", using 1968.

3. N. A. Golego. Wear and fight with it Kiev, "Scientific Thought", 1966.

4. A. P. Semenov, V. V. Pozdnyakov. Investigation of antifriction properties of solid bodies at the high temperatures in vacuum and some gaseous media. Reports of the AS USSR, Vol. 160, No. 4, 1965.

5. R. C. Weatherston, W. E. Smith. A method of heat rejection from space powerplants. ARS, Vol. 30, No. 3, 1960.

6. A. L. Stasenko. Characteristics of strip radiator taking into account self-emission and real contact. "Thermophysics of high temperatures", 1966, No. 1.

Received 24/VII 1972.

DERIVATION OF THE EQUATIONS OF THE METHOD OF FORCES FOR A PLATE REINFORCED BY A BEAM ON THE BASIS OF CASTIGLIANO'S VARIATION PRINCIPLE.

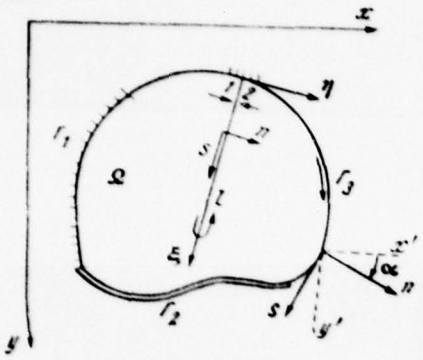
Yu. F. Yaremchuk.

For the elastic system, which consists of lamina and beam, without the account of the voltage/stresses of transverse shift/shear, with the aid of the functional of Reissner is obtained the complete system of equations of equilibrium and boundary conditions which together with the condition of the extremality of the functional of internal energy of system correspond to Castigliano's principle, i.e., they coincide with the equations of the so-called method of forces.

For the elastic construction, which consists of plate and the tanks (see figure), under the assumption that the sagging/deflections are small in comparison with thickness of plate, the functional of complete potential energy it takes the form

$$\Pi = \iint_{\Omega} \left\{ D \left\{ (\Delta w)^2 - 2(1-\nu) \left[\frac{\partial^2 w}{\partial x^2} \frac{\partial^2 w}{\partial y^2} - \left(\frac{\partial^2 w}{\partial x \partial y} \right)^2 \right] \right\} - 2qw \right\} dx\, dy +$$
$$+ \int_{\gamma} \left[EI \left(\frac{\partial^2 w}{\partial \xi^2} \right)^2 + GI_p \left(\frac{\partial^2 w}{\partial \xi \partial \eta} \right)^2 - 2pw \right] d\xi, \qquad (1)$$

where Ω - flat/plane region with boundary $\Gamma = \Gamma_1 + \Gamma_2 + \Gamma_3$ and l, l - a line segment with boundary $\gamma = \gamma_1 + \gamma_2 + \gamma_3$, occupied respectively by plate and beam.



Through s the martedly positive direction of the circuit/bypass of duct/contour.

Page 141.

To the point of intersection of boundary Γ from the straight line τ it corresponds one of values γ_i. So that the extremum of functional (1) would correspond to real state of strain of the construction in question in the assigned/prescribed external loads $p(\xi)$ and to $q(x, y)$, the continuously differentiated function of instrument $w(x, y)$ must satisfy on the parts of boundary Γ_1 and γ_i the boundary conditions:

$$\left.\begin{aligned} w|_{\Gamma_1} = \left.\frac{\partial w}{\partial n}\right|_{\Gamma_1} = w|_{\gamma_1} = \left.\frac{\partial w}{\partial \xi}\right|_{\gamma_1} = \left.\frac{\partial w}{\partial \eta}\right|_{\gamma_1} = 0 \quad &\text{(заделка);}\\ w|_{\Gamma_2} = w|_{\gamma_2} = 0 \quad &\text{(опора);}\\ \Gamma_3,\ \gamma_3 \text{ соответствуют свободному краю.} & \end{aligned}\right\} \qquad (2)$$

(1). (2). (3).

Key: (1). (stopping up). (2). (support). (3). they correspond to free edge.

In expressions (1) and (2) n - external standard to duct/contour Γ, D(x, y) - the flexural rigidity of plate, EI(ξ) and $GI_{p}(\xi)$ - hardness of beam for curvature and twisting, ν - Poisson ratio.

The minimum of functional (1) and the state of strain of the system in question can be approximately determined with the aid of Ritz's method in the class of functions w, which satisfy conditions (2) [1-3]. This approach can be considered as application/use of a method of displacement/movements to the solution of problems for plates.

In order to formulate the variational problem with unknown internal power factors, which corresponds to the so-called method of forces, let us use to functional (1) the transformation of Friedrichs [1, 3]. In the case in question it expresses the known conditions of the consistency of strains, which relate the characteristics that deformed and stressed of the states of construction [2]:

$$\left.\begin{aligned}
&\frac{M_x - \nu M_y}{D(1-\nu^2)} + \frac{\partial^2 w}{\partial x^2} = 0;\\
&\frac{M_y - \nu M_x}{D(1-\nu^2)} + \frac{\partial^2 w}{\partial y^2} = 0;\\
&\frac{M_{xy}}{D(1-\nu)} - \frac{\partial^2 w}{\partial x\,\partial y} = 0;\\
&\frac{M}{EI} + \frac{\partial^2 w}{\partial \xi^2} = 0;\\
&\frac{M_{kp}}{GI_p} + \frac{\partial^2 w}{\partial \xi\,\partial \eta} = 0.
\end{aligned}\right| \qquad (3)$$

Here M_x, M_y and M_{xy} - bending and that turn moments in plate, M and M_{kp} - bending and torsional moments in beam.

We will use method of Lagrange's factors. Multiplying equations (3) and (2) to the factors of Lagrange μ_i and α_i let us integrate them with respect to region Ω and boundary Γ. ξ, γ, where equations (3) and (2) are assign/prescribed. Store/adding up the obtained expressions with functional (1), in which the derivatives w are replaced by their expressions from (3), we will obtain the functional which sometimes they are related to the name Reissner [4-6]:

$$R = \iint_{\Omega} \left\{ \frac{1}{D(1-\nu^2)} [M_x^2 + M_y^2 - 2\nu M_x M_y + 2(1+\nu) M_{xy}^2] - 2q\omega \right\} dx\,dy +$$
$$+ \iint_{\Omega} \left\{ \mu_1 \left[\frac{M_x - \nu M_y}{D(1-\nu^2)} + \frac{\partial^2 \omega}{\partial x^2} \right] + \mu_2 \left[\frac{M_y - \nu M_x}{D(1-\nu^2)} + \frac{\partial^2 \omega}{\partial y^2} \right] + \mu_3 \left[\frac{M_{xy}}{D(1-\nu)} - \frac{\partial^2 \omega}{\partial x\,\partial y} \right] \right\} dx\,dy +$$
$$+ \int_{l} \left(\frac{M^2}{EI} + \frac{M_{kp}^2}{GI_p} - 2p\omega \right) d\xi + \int_{l} \left[\mu_4 \left(\frac{M}{EI} + \frac{\partial^2 \omega}{\partial \xi^2} \right) + \mu_5 \left(\frac{M_{kp}}{GI_p} + \frac{\partial^2 \omega}{\partial \xi\,\partial \eta} \right) \right] d\xi +$$
$$+ \int_{\Gamma_1 + \Gamma_3} \alpha_1 \omega\, ds + \int_{\Gamma_1} \alpha_2 \frac{\partial \omega}{\partial n}\, ds + \alpha_3 \omega|_{\gamma_1 + \gamma_3} + \alpha_4 \left. \frac{\partial \omega}{\partial \xi} \right|_{\gamma_1} + \alpha_5 \left. \frac{\partial \omega}{\partial \eta} \right|_{\gamma_1} \qquad (4)$$

Page 142.

For the unknown stress-strain state of structure, functional (4) takes steady-state value ($\delta R = 0$), since for this state functional (1) also takes steady-state value, and the coefficients when μ_i and α_i turn into zero on the basis of conditions (2) and (3):

$$\delta R = \iint_{\Omega} \left\{ \frac{1}{D(1-\nu^2)} [2M_x \delta M_x + 2M_y \delta M_y - 2\nu(M_x \delta M_y + M_y \delta M_x) + 4(1+\nu) M_{xy} \delta M_{xy}] - \right.$$
$$\left. - 2q\delta\omega \right\} dx\,dy + \iint_{\Omega} \left\{ \delta\mu_1 \left[\frac{M_x - \nu M_y}{D(1-\nu^2)} + \frac{\partial^2 \omega}{\partial x^2} \right] + \delta\mu_2 \left[\frac{M_y - \nu M_x}{D(1-\nu^2)} + \frac{\partial^2 \omega}{\partial y^2} \right] + \right.$$
$$\left. + \delta\mu_3 \left[\frac{M_{xy}}{D(1-\nu)} - \frac{\partial^2 \omega}{\partial x\,\partial y} \right] \right\} dx\,dy + \iint_{\Omega} \left\{ \mu_1 \left[\frac{\delta M_x - \nu \delta M_y}{D(1-\nu^2)} + \frac{\partial^2 \delta\omega}{\partial x^2} \right] + \right.$$
$$\left. + \mu_2 \left[\frac{\delta M_y - \nu \delta M_x}{D(1-\nu^2)} + \frac{\partial^2 \delta\omega}{\partial y^2} \right] + \mu_3 \left[\frac{\delta M_{xy}}{D(1-\nu)} - \frac{\partial^2 \delta\omega}{\partial x\,\partial y} \right] \right\} dx\,dy +$$
$$+ \int_{l} \left(\frac{2M\delta M}{EI} + \frac{2M_{kp}\delta M_{kp}}{GI_p} - 2p\delta\omega \right) d\xi + \int_{l} \left[\delta\mu_4 \left(\frac{M}{EI} + \frac{\partial^2 \omega}{\partial \xi^2} \right) + \delta\mu_5 \left(\frac{M_{kp}}{GI_p} + \frac{\partial^2 \omega}{\partial \xi\,\partial \eta} \right) \right] d\xi +$$
$$+ \int_{l} \left[\mu_4 \left(\frac{\delta M}{EI} + \frac{\partial^2 \delta\omega}{\partial \xi^2} \right) + \mu_5 \left(\frac{\delta M_{kp}}{GI_p} + \frac{\partial^2 \delta\omega}{\partial \xi\,\partial \eta} \right) \right] a\xi + \int_{\Gamma_1 + \Gamma_3} \delta\alpha_1 \omega\, ds + \int_{\Gamma_1} \delta\alpha_2 \frac{\partial \omega}{\partial n}\, ds +$$
$$+ \int_{\Gamma_1 + \Gamma_3} \alpha_1 \delta\omega\, ds + \int_{\Gamma_1} \alpha_2 \frac{\partial \delta\omega}{\partial n}\, ds + \delta\alpha_3 \omega|_{\gamma_1 + \gamma_3} + \delta\alpha_4 \left. \frac{\partial \omega}{\partial \xi} \right|_{\gamma_1} + \delta\alpha_5 \left. \frac{\partial \omega}{\partial \eta} \right|_{\gamma_1} +$$
$$+ \alpha_3 \delta\omega|_{\gamma_1 + \gamma_3} + \alpha_4 \left. \frac{\partial \delta\omega}{\partial \xi} \right|_{\gamma_1} + \alpha_5 \left. \frac{\partial \delta\omega}{\partial \eta} \right|_{\gamma_1} = 0. \qquad (5)$$

The requirement of equality zero coefficients of variations $\delta\mu_i$ and $\delta\chi_i$ leads to satisfaction of the conditions of the consistency of strains (3) and of boundary conditions (2).

Expressions with variations δM_i give conditions for determining factors μ_i:

$$\left.\begin{array}{l} \mu_1 = -2M_x;\ \mu_2 = -2M_y;\ \mu_3 = -4M_{xy};\\ \mu_4 = -2M;\ \mu_5 = -2M_{kp}. \end{array}\right\} \qquad (6)$$

Integrating in parts expressions in (5), the containing derivatives of variation δw, with the aid of Gauss-Ostrogradskiy's formula

$$\iint_{\Omega} \mu_1 \frac{\partial^2 \delta w}{\partial x^2}\, dx\, dy = \iint_{\Omega} \frac{\partial^2 \mu_1}{\partial x^2}\, \delta w\, dx\, dy + \int_{\Gamma+l_1+l_2} \mu_1 \frac{\partial \delta w}{\partial n} \cos^2 \alpha\, ds -$$
$$- \int_{\Gamma+l_1+l_2} \mu_1 \frac{\partial \delta w}{\partial s} \sin\alpha \cos\alpha\, ds - \int_{\Gamma+l_1+l_2} \frac{\partial \mu_1}{\partial x}\, \delta w \cos\alpha\, ds$$

[here index "1" with ξ means that the integration is conducted by circuit/bypass ξ to the right, if we move to the side of increase ξ (see figure), "2" - respectively to the left], taking into account (6), introducing designations [2]:

$$M_x \cos^2\alpha + M_y \sin^2\alpha - 2M_{xy} \sin\alpha \cos\alpha = M_n,$$
$$(M_x - M_y) \sin\alpha \cos\alpha + M_{xy} (\cos^2\alpha - \sin^2\alpha) = M_{ns},$$
$$\left(\frac{\partial M_x}{\partial x} - \frac{\partial M_{xy}}{\partial y}\right) \cos\alpha + \left(\frac{\partial M_y}{\partial y} - \frac{\partial M_{xy}}{\partial x}\right) \sin\alpha = Q_n,$$

and accumulating in (5) similar terms with variations δw and it derivatives, we will obtain

$$\delta R = -2 \iint_{\Omega} \left(\frac{\partial^2 M_x}{\partial x^2} + \frac{\partial^2 M_y}{\partial y^2} - 2\frac{\partial^2 M_{xy}}{\partial x\, \partial y} + q\right) \delta w\, dx\, dy + \int_{\Gamma_1} (\alpha_2 - 2M_n) \frac{\partial \delta w}{\partial n}\, ds -$$
$$- 2 \int_{\Gamma_1+\Gamma_2} M_n \frac{\partial \delta w}{\partial n}\, ds - 2 \int_{\gamma} \left(M_{n1} - M_{n2} - \frac{\partial M_{np}}{\partial \xi}\right) \frac{\partial \delta w}{\partial \eta}\, d\xi +$$
$$+ \int_{\Gamma_1+\Gamma_2} \left[\alpha_1 + 2\left(Q_n - \frac{\partial M_{ns}}{\partial s}\right)\right] \delta w\, ds + 2 \int_{\Gamma_2} \left(Q_n - \frac{\partial M_{ns}}{\partial s}\right) \delta w\, ds +$$
$$+ 2 (M_{ns1} - M_{ns2}) \delta w|_{\Gamma_1} + 2 \int_{\gamma} \left[\left(Q_n - \frac{\partial M_{ns}}{\partial s}\right)_1 + \left(Q_n - \frac{\partial M_{ns}}{\partial s}\right)_2 - \frac{\partial^2 M}{\partial \xi^2} - P\right] \delta w\, d\xi +$$
$$+ \left[\alpha_3 + 2\left(M_{ns1} - M_{ns2} + \frac{\partial M}{\partial \xi}\right)\right] \delta w|_{\Gamma_1+\Gamma_2} + 2\left(M_{ns1} - M_{ns2} + \frac{\partial M}{\partial \xi}\right) \delta w|_{\Gamma_2} +$$
$$+ (\alpha_4 - 2M) \frac{\partial \delta w}{\partial \xi}\bigg|_{\Gamma_1} - 2M \frac{\partial \delta w}{\partial \xi}\bigg|_{\Gamma_2+\Gamma_3} + (\alpha_5 - 2M_{np}) \frac{\partial \delta w}{\partial \eta}\bigg|_{\Gamma_1} - 2M_{np} \frac{\partial \delta w}{\partial \eta}\bigg|_{\Gamma_2+\Gamma_3} = 0$$

(here indices "1" and "2" again mean that the values are taken to the right and to the left of beam; Γ_i - the point of intersection of

boundary Γ and of the straight line t).

Page 143.

Equalizing zero expressions with variations, we will obtain the values of factors α_i, which represent by themselves the doubled values of bearing reactions and stopping up:

$$\left.\begin{gathered}\alpha_1 + 2\left(Q_n - \frac{\partial M_{ns}}{\partial s}\right)\Big|_{\Gamma_1+\Gamma_2} = 0; \quad \alpha_2 - 2M_n|_{\Gamma_1} = 0;\\ \alpha_3 + 2\left(M_{ns\,1} - M_{ns\,2} + \frac{\partial M}{\partial \xi}\right) + \left\{\begin{matrix}2(M_{ns\,1} - M_{ns\,2})|_{\Gamma_l}, & \text{если} \quad \Gamma_l = \gamma_1 + \gamma_2\\ 0, & \text{если} \quad \Gamma_l = \gamma_3\end{matrix}\right\}\Big|_{\gamma_1+\gamma_2} = 0;\\ \alpha_4 - 2M|_{\gamma_1} = 0; \quad \alpha_5 - 2M_{\kappa p}|_{\gamma_1} = 0.\end{gathered}\right\} \quad (7)$$

Key: (1). if.

Furthermore, we will obtain the conditions by which they must satisfy M_i and which represent by themselves the known equations of equilibrium and the natural boundary conditions:

$$\left.\begin{gathered}\frac{\partial^2 M_x}{\partial x^2} + \frac{\partial^2 M_y}{\partial y^2} + 2\frac{\partial^2 M_{xy}}{\partial x \partial y} + q = 0;\\ M_n|_{\Gamma_2+\Gamma_3} = 0; \quad Q_n - \frac{\partial M_{ns}}{\partial s}\Big|_{\Gamma_3} = 0;\\ M_{n1} - M_{n2} - \frac{\partial M_{\kappa p}}{\partial \xi}\Big|_l = 0; \left(Q_n - \frac{\partial M_{ns}}{\partial s}\right)_1 + \left(Q_n - \frac{\partial M_{ns}}{\partial s}\right)_2 - \frac{\partial^2 M}{\partial \xi^2} - p\Big|_t = 0;\\ M|_{\Gamma_2+\Gamma_3} = 0; \quad M_{\kappa p}|_{\Gamma_2+\Gamma_3} = 0;\\ M_{ns\,1} - M_{ns\,2} + \frac{\partial M}{\partial \xi} + \left\{\begin{matrix}(M_{ns\,1} - M_{ns\,2})|_{\Gamma_l}, & \text{если} \quad \Gamma_l = \gamma_3\\ 0, & \text{если} \quad \Gamma_l = \gamma_1 + \gamma_2\end{matrix}\right\}\Big|_{\gamma_3} = 0.\end{gathered}\right\} \quad (8)$$

Key: (1). if.

To such, by form, the requirement of the stability of the functional of Reissner gives the conditions of the consistency of strains, equation of equilibrium and boundary conditions, i.e., it corresponds to the solution of the problem of determining the stress-strain state of construction [4] being investigated.

The physical sense of the members of functional (4), that contain factors P_i consists of following. let us visualize "everywhere cut" on structure, then in view (6) term in question values are proportional to the work of voltage/stresses, it is compulsory not satisfying the conditions of equilibrium, during the displacement/movements, which arose as a result of the disturbance of the conditions of the consistency of strains.

If we require so that functional (4) it would reach extremum under supplementary conditions (3) and (2), then we come to the initial task of finding the extremum of functional (1) and obtain the virtual work principle: among the possible states of strain of construction, which satisfy the condition of the consistency of strains (3) and geometric boundary conditions (2), the state of strain, which satisfies the conditions of equilibrium (8), supply/delivers to functional (1) steady-state value.

If we as preliminary conditions during finding of extremum (4) require satisfaction of conditions (8), then, substituting (6)-(8) in (4), after some transformations we come to task - to find the extremum of the functional

$$U = -\left\{\iint_{\Omega} \frac{1}{D(1-\nu^2)}\left[M_x^2 + M_y^2 - 2\nu M_x M_y + 2(1+\nu)M_{xy}^2\right]dxdy + \right.$$
$$\left. + \int_{\gamma}\left(\frac{M^2}{EI} + \frac{M_{kp}^2}{GI_p}\right)d\gamma\right\} \qquad (9)$$

under additional conditions (8) - and obtain Castiglianos's principle: among the possible stressed states of construction, which satisfy the conditions of equilibrium (8), the stressed state, which satisfies the conditions of the consistency of strains (3) and (2), supply/delivers steady-state value to functional (9).

Thus, the functional of Reissner (4) makes it possible to obtain the basic of the equation for both principles of structural mechanics and theory of elasticity. Furthermore, functional R can be used for the approximate determination of the stress-strain state, if we in it substitute values μ_i and $\varkappa_i$ from (6) and (7). In this case, is required the satisfaction of no conditions, except the condition of

differentiability w(x, y).

In comparison with the method of single force and the purely physical approach, with which are presented more stringent requirements for the idealization of construction and it is necessary to construct the "self-balanced" systems (what is difficult task), the formulated in expressions (8), (9) analytical approach to the method of forces makes it possible to more effective find the classes of the functions, which satisfy uniform (p = q = 0) system (8), for sufficiently complex constructions.

REFERENCES.

1. S. G. Mikhlin. Variational methods of mathematical physics. M., the State Technical Press, 1957.

2. S. P. Timoshenko, S. Voynovskiy-Kriger. Plates and shells. M., Fizmatgiz, 1963.

3. R. Kurant, D. Gil'bert. Methods of mathematical physics. T. 1, M., the State Technical Press, 1951.

4. E. Reissner. On a variational theorem in elasticity. J Math. and Phys., 29, No. 2, 1950.

5. E. Reissner. On a variational theorem for finite elastic deformations. J Math. and Phys., 32, No. 2-3, 1953.

6. Yu. A. Amenzade. Theory of elasticity. M., "higher school", 1971.

7. J. H. Argyris. Contemporary methods of calculation of the complex statically indeterminable systems. Coll. of article edited by Prof. A. P. Filin, L., Sudpromgiz, 1961.

Received 12/VI 1972.

RATIONAL DISTRIBUTION OF RIBS IN A MONOCOQUE WING.

V. N. Semenov.

Is given the solution of the problem of the rational number of ribs and their optimum weight span distribution caisson high-aspect-ratio wing with the observance of the stability condition of the compressed panels. Are given the results of calculation.

The optimization of the load-carrying structure of aircraft is conducted in essence in two directions: the optimization of structural cell/elements from the point of local strength and the optimization of the structural load-bearing diagram from the position of common/general/total strength and aeroelasticity. It is logical that the possibilities, discovered by the optimization of the structural load-bearing diagram, can be realized in that case, if they do not contradict the requirements of local strength and, in particular, to the requirements of the stability of the compressed panels.

In this article is proposed one of the possible methods of the

optimization of the construction of caisson simultaneously according to the conditions of common/general/total strength and the stability conditions of the compressed panels.

Let us examine the compressed panel of the section of the monocoque wing, included between ribs k, k + 1 (Fig. 1), which has the parameters: $l_{пл}$ - length of the panel of section (space of ribs); B(z) - the width of caisson; b(z) - wing chord; $\bar{c}(z)$ - wing chord ratio; α - distance ratio between the center of gravity of upper and lower panels to the maximum altitude of wing in this section. The flow of normal stresses in section z let us determine according to the formula

$$q(z) = \frac{n_p M_{изг}(z)}{\alpha c(z) B(z) b(z)} = \frac{n_p \int_L^z p_p(z) b(z) dz}{\alpha c(z) B(z) b(z)}, \qquad (1)$$

where n_p - calculated overload, $p_p(z)$ - calculated distributed load, L - value of semirange.

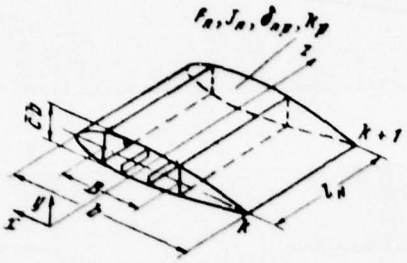


Fig. 1.

Page 146.

The effect of the torsional moment for a direct/straight monocoque wing less substantially and here is not examined. The estimation of maximum, i.e., critical, the stress level overall loss of stability for the assigned/prescribed characteristics of material, airfoil/profile of panel and loading conditions is obtained on the formula of Shenli [1] [formula (2.15)], presented in the form

$$\sigma_{кр} = \left(\frac{\pi^2 E_t k_p^2 c}{1-\mu^2}\right)^{1/3} \left(\frac{q}{l_н}\right)^{2/3}, \qquad (2)$$

where k_p - factor of the form of panel, E_t - tangential modulus of elasticity, μ - Poisson ratio c - the coefficient of sealing off of the panel which is located experimentally and for real panels is equal to 1.5-2.0.

Accordingly (2) the level of allowable voltages is limited by

the value of the breaking stresses of loss of stability $\sigma_{кр}$ and depends, on the parameter of the intensity/strength of panel $\left(\frac{q}{l_н}\right)^{2/3}$.

In the end zone of wing, according to formula (1), the flow of normal stresses substantially decreases; therefore for obtaining more high voltages, it is necessary to decrease the value $l_н$. in this case, is equalized the stress level in panels along wing. On the other hand, the decrease of the space of ribs leads to an increase in their quantity and, therefore, the weight. It is assumed that the weight of longerons and cell/elements of wing out of caisson remains constant; therefore the process of optimization is reduced to the determination of the number of ribs and this span distribution by which the total weight of longitudinal and lateral power assembly takes minimum value.

The given thickness of panel $\delta_{пр}$ is defined as

$$\delta_{пр}(z) = \frac{F_п(z)}{B(z)}, \tag{3}$$

where $F_п$ - the cross-sectional area of panel, connected with $\sigma_{кр}$, E_t and $k_р$ the following system of transcendental equations:

$$\left.\begin{aligned}
&\sigma_{кр}(z) = \left[\frac{c^{1/2}\pi n_р M_{изг}(z)}{(1-\mu^2)\, l_{н_t}^2 c(z)\, B(z)\, b(z)}\right]^{2/3} [E_t(z)]^{1/3} [k_р(z)]^{2/3} = \\
&\qquad = A_1(z)\,[E_t(z)]^{1/3}\,[k_р(z)]^{2/3};\\
&\delta_{пр}(z) = \frac{q(z)}{\sigma_{кр}(z)} = \frac{n_р M_{изг}(z)}{c(z)\, B(z)\, b(z)} \frac{1}{\sigma_{кр}(z)} = A_2(z) \frac{1}{\sigma_{кр}(z)};\\
&k_р(z) = \sqrt{\frac{J_п}{F_п \delta_{пр}^2}} = \sqrt{\frac{\psi_1(\delta_{пр})}{\psi_2(\delta_{пр})\,\delta_{пр}^2}} = [\psi(\delta_{пр})]^{1/2};\\
&E_t(z) = \frac{27E}{4\sigma_в^3}\,\sigma_{кр}(z)\,[\sigma_в - \sigma_{кр}(z)]^2 = A_3\,\sigma_{кр}(z)\,[\sigma_в - \sigma_{кр}(z)]^2.
\end{aligned}\right\} \tag{4}$$

where $J_п$ - the moment of the inertia of panel, $\sigma_в$ - ultimate strength, E - modulus of elasticity.

The first equation of system (4) is obtained via the substitution of formula (1) into formula (2); the second follows from the determination of the flow of stresses $q = \delta\sigma$, which is solved relatively δ and into which is substituted expression q(z) from formula (1); the third corresponds to the determination of the factor of the form of panel. The last/latter equation of system is undertaken from work [2] [formula (13)], where a change of the modulus of elasticity in the zone of nonlinear strains is assign/prescribed by empirical dependence. When $\sigma_{кр} \leq \frac{\sigma_в}{3}$ (in elastic zone) $E_t = E$.

To the parameters of system (4) is superimposed a series of the limitations:

$$\delta_{пр} \geqslant \delta_{min} \qquad (5)$$

(structural/design limitation, caused by technological and operating requirements);

$$0{,}288 \leqslant k_{\text{p}} \leqslant k_{\max} \tag{6}$$

(limitation to the factor of the form of panel; value $k_{\text{p}} = 0{,}288$ corresponds to smooth skin, $k_{\max}$ is determined by the radii of inertia of real panels);

$$\sigma_{\text{A}} \leqslant \left[\min\left(\sigma_{\text{Aon}}, \frac{\sigma_{\text{kp}}}{1+\xi}\right)\right] \tag{7}$$

(limitation to the effective stresses σ_{A}, which must not exceed permissible normal stresses σ_{Aon} and the permissible breaking stresses σ_{kp}; ξ - safety factor in the criterion of overall stability).

Page 147.

System of equations (4) for different sections of wing is solved differently. The common/general/total tendency of the optimization of caisson from the point of common/general/total and local strength is expressed in the tendency to build up effective stresses of up to the level of permissible normal stresses with of conditions of the sufficient high level breaking stresses of loss of stability:

$$\sigma_{\text{A}} \to \sigma_{\text{Aon}}; \tag{8}$$

$$\sigma_{\text{kp}} \to \sigma_{\text{A}}(1+\xi). \tag{9}$$

In root zone can been satisfied the condition

$$\sigma_{\text{д}} = \sigma_{\text{доп}} = \sigma_{\text{кр}}/(1+\varepsilon) \tag{10}$$

and the solution of system (4) on this section is reduced to calculation $\delta_{\text{пр}}(z)$ and $k_{\text{р}}(z)$ on the formulas:

$$\delta_{\text{пр}}(z) = \frac{A_2(z)}{\sigma_{\text{доп}}}; \tag{11}$$

$$k_{\text{р}}(z) = \left[\frac{\sigma_{\text{доп}}}{A_1(z)\, E_t(\sigma_{\text{доп}})}\right]^{3/2}. \tag{12}$$

Value $k_{\text{р}}$ is calculated for a check of the execution of limitation (6) and gives information about the required form of the airfoil/profile of panel.

In end sections the breaking stresses will be less than permissible, and system (4) is permitted relatively $\delta_{\text{пр}}$ with the aid of the iterative formula

$$[\delta_{\text{пр}}(z)]_j = \frac{A_2(z)}{A_1(z)\,(E_{t,\,j-1})^{1/3}\,[\psi(\delta_{\text{пр}\,j-1}(z))]^{1/3}}. \tag{13}$$

satisfaction of the condition

$$\left|\left(\frac{A_2\,[\psi(\delta_{\text{пр}})]^{1/3}}{A_1\,E_t^{1/3}}\right)'\right| = \left|\frac{A_2}{3A_1\,E_t^{1/3}}\,\frac{\psi'(\delta_{\text{пр}})}{[\psi(\delta_{\text{пр}})]^{4/3}}\right| \leqslant 1 \tag{14}$$

in the region

$$R = \{|\delta_{\text{к}} - \delta_0| \leqslant 0{,}2\,\delta_0\} \tag{15}$$

provides the convergence of iterative process. (Indices have the value: "0" - the initial value of the parameter, j - a number of iteration, κ - maximum deviation of the parameter from original value).

In each space of iteration on $\delta_j(z)$ is included the iterative loop for the correction of values $\sigma_{кр}$ and E_t on the formula, which ensues from expressions (4):

$$\sigma_{кр\,j} = A_1 A_3^{1/3} k_p^{2/3} [\sigma_{кр\,j-1} (\sigma_в - \sigma_{кр\,j-1})^2]^{1/3}. \qquad (16)$$

The corresponding to value $\sigma_{кр}$ value E_{tj} is utilized in iteration j + 1 on formula (13) as constant.

For the constant within the limits of section values of the parameters k_p and $\delta_{пр}$ the panel is calculated from condition $\sigma_д \leqslant \sigma_{доп}$ in tail piece of the section and according to condition $\sigma_{кр} \geqslant \sigma_д(1+\xi)$ in the center of section. The found thus thickness of the panel $\delta_{пр\,j}$ of section i, which satisfies both limitations, it is utilized for its determination weighing:

$$G_j = 1{,}9\gamma\left(1 + \zeta\frac{N_{var}}{N_c}\frac{G_{п\,0}}{G_{п\,j-1}}\right)\sum_{i=1}^{N}\delta_{пр\,i}\,l_{н\,i}\,\frac{B_i + B_{i+1}}{2}. \qquad (17)$$

Here G_j the weight of panels and ribs at the j space of calculation; ζ - statistical coefficient, which evaluates the weight of ribs with respect to the weight of panels of the number of ribs N_c; N_{var} -

varied number of ribs; G_{n0} - initial weight of panels; G_{nj-1} - weight of panels at the previous space of calculation; γ - the specific gravity/weight of material.

The ratio of the weight of the panels, tensile, to the weight of the panels, compression, is accepted equal to 0.9 according to recommendations [2].

The first stage of the optimization of construction represents by itself the task of integral programming for number determination of ribs. On the basis of formulas (4)-(17) is comprised the program in language FORTRAN, and to besm-6 are produced the calculations of the minimum structural weight during the even distribution of ribs according to the wingspan.

Page 148.

In the second stage of search, was placed the task of finding the optimum for weight design parameters with the variable space of ribs at their fixed/recorded number. Let us present purposeful weighing function as sum of the weights of the separate sections:

$$G_j = \sum_{i=1}^{N} [F(P_{ji}, l_{ni})]_i \qquad (18)$$

where N - the number of sections, which coincides with the number of

ribs P_β - the parameters on which depends the weight of section - load, geometric dimensions so forth:

$$P_\beta = P_1, P_2, P_3, \ldots = M_{изг}(z), b(z), \bar{c}(z), \ldots$$

The optimization of weight is conducted consecutively for different pairs of adjacent sections. The algorithm of optimization is comprised on the basis of gauss - Zaydel's method [3]. Let us isolate two adjacent sections (see 1 in Fig. 2) from their common/general/total sequence (18):

$$\sum_{i=1}^{N} [F(P_\beta, l_н)] = [F(P_\beta, l_н)]_{k-1} + [F(P_\beta, l_н)]_k + \sum_{i=1}^{k-2} F(P_\beta, l_н) + \sum_{i=k+1}^{N} F(P_\beta, l_н). \quad (19)$$

During one passage on the wingspan, it is considered that a variation in the position of rib k within the limits of the pair of sections $(k-1, k+1)$, changes only the value of the first two terms of expansion (19). Complete sorting the possible positions of rib k showed that the dependence of the weight of the pair of adjacent sections on the position of rib has one strict minimum; therefore the optimum position of rib k* is located by the method of steepest descent. Position k* let us fix as next approach/approximation to the optimum position of k*½. Further we pass to the following pair of sections (II) with a variation in rib k-1 within limits $(k-2, k^*)$ and find its local optimum: (k-1)*. To sorting we subject consecutively all the pairs of sections, in this case, are possible two issues:

1) all ribs preserved their position, i.e., initial distribution was optimum;

2) at least one rib occupied the new position that it led to a reduction in the weight:

$$\sum_{i=1}^{N} |F(P_{\beta}, l_n)|_i^* < \sum_{i=1}^{N} |F(P_{\beta}, l_n)|_i.$$

The obtained distribution l_{n}^{*} is utilized as initial for the following space of optimization.

The process of iterations is repeated to the convergence, by which

$$\frac{G_j - G_{j-1}}{G_j} \leqslant \varepsilon,$$

where ε - low value, determined by the accuracy/precision of calculation.

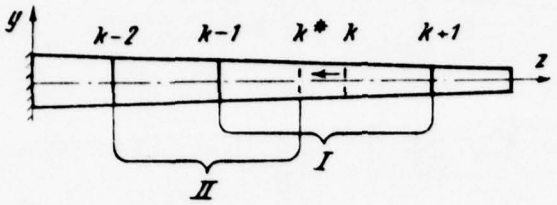


Fig. 2.

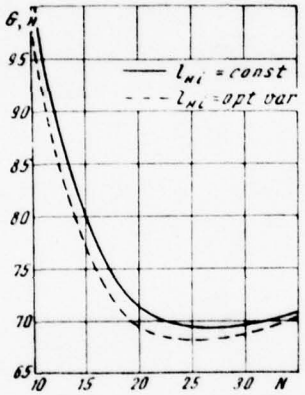


Fig. 3.

Page 149.

The finally obtained distribution l_{ni}^{**} is considered optimum. For the investigation of a question concerning that, is the obtained solution the global or local minimum of weight, was carried out calculated experiment. The problem of finding the optimum distribution of the assigned/prescribed number of ribs according to

spread/scope was solved several times, moreover as the initial distribution of ribs, besides uniform, consecutively were taken distributions with the increase in the number of ribs in root, central and wing tip, furthermore, was varied the way of search. The final distribution of ribs in all cases coincided and gave one and the same value of weighing function. Even small deviations any of the ribs from their optimum position increased weight. Thus, on the basis of the results of calculated experiment it was shown, that the comprised algorithm led to optimum solution, moreover to solution only. This makes it possible to draw the conclusion that within the framework of the assumptions accepted and limitations the obtained distribution of ribs realizes the global optimum of the weight of caisson.

When conducting of calculations, it turned out that the number of ribs by which the construction from uniform by their distribution has a minimum of weight, coincides with the number of ribs which provides the minimum of the structural weight with their variable space on spread/scope. This fact makes it possible to reduce the process of the determination of optimum construction.

Figures 3 shows a change in the weighing function with different number evenly to ($l_{n\,i} = \text{const}$) and is optimal ($l_{n\,i} = \text{opt var}$) the distributed on spread/scope ribs. It is evident that there is range of rational

(close to optimum) on the criterion of the weight of the number of ribs. In Fig. 4-7 in the same designations, is illustrated the obtained gain in weight during the redistribution of ribs in the cases of their insufficient, optimum and abundant number.

From physical 5 it is evident that as a result of small flows of normal stresses (1), and also of the action of structural/design limitations (5) in all cases the breaking stresses in end zone considerably exceed those act, and therefore the space of ribs in this zone can be increased, that it will not lead to the loss of stability of construction.

An increase in the space of ribs is expedient also in the zone of the root section when $\sigma_{кр} > \sigma_{доп}$ (see Fig. 5). The decrease of the space of ribs is conducted in the zones where normal stresses can be built up to the level permissible, in particular, in root section with a deficiency/lack in the ribs (see Fig. 4 and 5).

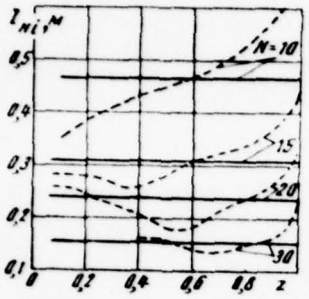


Fig. 4.

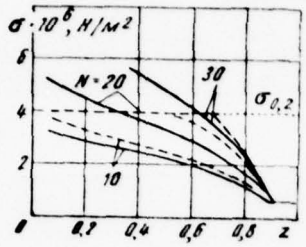


Fig. 5.

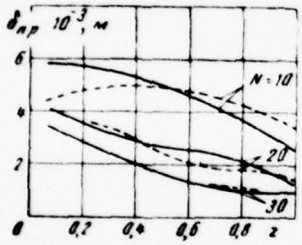


Fig. 6.

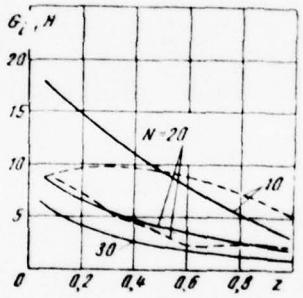


Fig. 7.

Page 150.

With an increase in the number of ribs, the minimum of function (Fig. 8)

$$f(N, z/L) = \frac{l_{\text{п opt}}(N, z/L)}{l_{\text{п const}}(N)}$$

is shift/sheared into the end region of wing, which attests to the fact that in end zone are realized higher normal stresses (see Fig.

5). During approach/approximation f(N, z/L) to unity in absolute value the level of acting in panels normal stresses is equalized on spread/scope and construction is close to uniformly strong, but this distribution of ribs does not correspond to the construction, optimum for weight.

With the insufficient and optimum number of ribs, it is required so that the type of panels would provide high value factor of form $[k_p(z) = k_{p\max}]$ for all extent/elongation of wing, with the exception/elimination of its end. Of the abundant number of ribs, the factor of the form of panel (12) can be decreased.

Fig. 3, shows that the construction with the abundant number of ribs is more preferable, from the point of weight, construction with the number of ribs smaller than optimum. If the number of ribs is selected by close to optimum, then the weight of the structure of caisson with the optimum space of ribs is smaller than the structural weight with the constant space of ribs with their the same number of altogether only to 2-3o/o. This occurs because the weight of longitudinal assembly, decreased as a result of the approach/approximation of construction to uniform strength on spread/scope, must be summarized with weight continually of the increasing number of supplementary ribs.

In real construction in view arrangement/position in the wing of chassis/landing gear, aggregate/units, fuel tanks and the like only to 30-40o/o of spread/scope of wing are superimposed the limitations to the position of ribs; therefore in each specific case it is necessary to evaluate, is sufficient gain in weight, so that it would cost to complicate the construction, transfer/converting to the variable space of ribs, or it is possible tc stop at the selection of rational constant space.

Let us note that the given results and derivations are obtained for concrete/specific/actual wing construction with the following basic parameters: L = of 5.9 m, p_p = 5000 N/m². The calculation of other constructions can lead to the derivations, which differ somewhat from those presented.

The author expresses appreciation to V. M. frolov for the valuable recommendations, obtained during the execution of work.

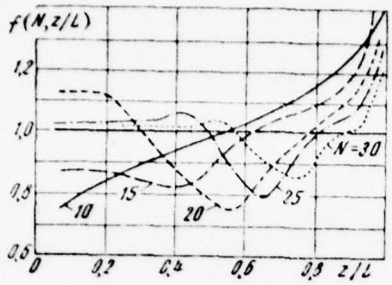


Fig. 8.

REFERENCES

1. F. R. Shenli. Analysis of weight and strength of aircraft constructions. M., Oborongiz, 1957.

2. V. F. Sinitsyn. Optimization and gravimetric analysis of some aircraft constructions. Transactions of TsAGI [99sp04 - Central Institute of Aerohydrodynamics im. N. Ye Zhukovskiy, iss. 1262, 1970.

3. L. A. Rastrigin. Statistical methods of search. M., "science", 1968.

Received 4/IV 1972.

EXPERIENCE IN SIMULATION OF AUTO-OSCILLATIONS OF TALL STRUCTURES IN WIND TUNNELS.

A. N. Lugovtsov, G. M. Fomin.

Are examined questions of simulation in the wind tunnels of wind resonance and galloping high constructions. Based on the examples of the simulation of the oscillation/vibrations of four obelisks, is investigated the effect of different parameters on the process of oscillation/vibrations and they are given to recommendation regarding the elimination of dangerous oscillation/vibrations by the setting up of damping devices and execution of through channels.

Model tests in wind tunnels are one of the basic methods of obtaining different characteristics of the aircraft and other flight vehicles. Ever more wide acceptance finds this method, also, during the investigation of the effect of the wind on construction constructions (tower, high-altitude buildings, bridges, industrial structures). The attention, given to the study of the effect of the wind on constructions, grew considerably because of contemporary

tendency to construct the very high constructions, possessing often great flexibility and the low value of structural oscillation damping.

The action of the wind can be presented in the form of the combination of the static and dynamic loads of construction [1]. Dynamic effect can be divided into the gust effect and pressure fluctuation in trace from adjacent structures (forced oscillation) and the separation effect of flow from the surface of construction, which leads to the excitation of auto-oscillations. Most frequently are observed auto-oscillations from vortex/eddy excitation (wind resonance) and auto-oscillation as a result of aeroelastic instability (galloping and stalled flutter).

However,, until now, there are no calculation methods, which make it possible with sufficient reliability to determine the critical speeds of auto-oscillations and to obtain the values of the amplitudes of limiting cycles; therefore for the investigation of the character of auto-oscillations in the majority of the cases, they resort to testings of the aeroelastic models of construction in wind tunnels.

During the simulation of the dynamic phenomena of aeroelasticity which include the auto-oscillations of constructions in airflow, it

is necessary to maintain/withstand the similarity of aerodynamic flows and the similarity of the characteristics of construction. For this, the model, first of all, must be geometrically similar to nature, i.e., exterior forms of model in all basic parts must be similar to the form of prototype. It is necessary to also observe the identity of the direction of the incident flow (angles of attack and downwash) and to maintain similarity criterion according to Mach numbers, Re and μ. Mach number characterizes change air density because of compressibility. At wind velocities to 50-60 m/s this change can be disregarded; therefore model tests can be carried out with any, sufficiently small Mach number.

Page 152.

During model tests of construction constructions, it is very important to observe a similar to nature boundary-layer development, since the state of boundary layer determines character and the place of flow separation from body surface. The forms of the bodies, investigated in industrial aerodynamics, are usually such, that from their surface occurs flow separation. These disruption/separations must be reproduced on test models as possible more closely to nature. The similarity of boundary layers is provided, when Reynolds numbers for nature and model are equal to:

$$Re_н = \frac{V_н d_н}{\nu_н} = Re_м = \frac{V_м d_м}{\nu_м},$$

where V - velocity of flow; d - characteristic linear dimension; ν - the kinematic modulus of viscosity of air.

Equality Reynolds numbers has special importance for constructions with "smooth" cross section profiles (circle, ellipse, section with the filleted corners). During the flow around such airfoil/profiles in the specific range of Reynolds numbers during the transition of laminar boundary layer into turbulent, occurs a sharp incidence/drop in the value of drag coefficient c_x - it begins the crisis of drag. With this separation point it is displaced back/ago along flow, the width of cocurrent trace decreases, sharply changes the character of the formation/education of eddy/vortices after airfoil/profile.

For airfoil/profiles with points of inflection (square, rhomb, astroid, etc.), which are separation points, critical region of reynolds number it is not observed. This makes it possible to assume that flow separation from such airfoil/profiles - phenomenon self-similar according to Re number.

During the simulation of the fluctuations of elastic construction in airflow, must be preserved the ratio of wavelength to

linear dimensions and is maintained equality the relations of elastic and aerodynamic forces. This is realized with equality for nature and the model of Strouhal numbers Sh, of Cauchy Ca* and of number μ:

$$\mathrm{Sh}_{\text{н}} = \frac{f_{\text{н}} d_{\text{н}}}{V_{\text{н}}} = \mathrm{Sh}_{\text{м}} = \frac{f_{\text{м}} d_{\text{м}}}{V_{\text{м}}};$$

$$\mathrm{Ca}^{*}_{\text{н}} = \frac{(EI)_{\text{н}}}{\rho_{\text{н}} V^{2}_{\text{н}} d^{4}_{\text{н}}} = \mathrm{Ca}^{*}_{\text{м}} = \frac{(EI)_{\text{м}}}{\rho_{\text{м}} V^{2}_{\text{м}} d^{4}_{\text{м}}};$$

$$\mu_{\text{н}} = \frac{m_{\text{н}}}{\rho_{\text{н}} d^{3}_{\text{н}}} = \mu_{\text{м}} = \frac{m_{\text{м}}}{\rho_{\text{м}} d^{3}_{\text{м}}},$$

where f - frequency; EI - rigidity of structure; ρ - air density; m - mass of construction.

Experiment shows [2] that the character of the auto-oscillations of construction, caused by the action of the wind, can qualitatively change depending on the value of structural attenuation, characterized by the logarithmic decrement of fluctuations δ. Therefore it is necessary to approach that so that the decrements of the fluctuations of nature and model would be identical. However, to determine value δ of nature is possible only after the erection of construction, and in connection with this during model tests it is completely desirable to vary value δ with the fact in order to have a dependence of characteristics of fluctuations on this parameter.

Model tests can solve a question not only concerning the character of fluctuations and the value of the appearing in this case

dynamic torque/moments, but also concerning the stresses in the elements of construction. For this, the model must be to structurally similar nature, i.e., repeat all the basic design features of construction and make itself from the same materials. Simultaneous satisfaction to the conditions of similarity Re, Sh, Ca* and μ is impossible in ducts with the open test section; in these cases it is necessary to carry out model tests in wind tunnel with the increased density of working medium. Without dwelling in detail on the special feature/peculiarities of simulation in ducts with the increased density, let us note only that and in this case appears a series of difficulties during the execution of the model, which corresponds to similarity conditions, and it proves to be necessary to apply the special methods of simulation.

Most frequently is applied the principle of the approximate simulation with failure of the observance of some conditions of similarity.

Page 153.

With failure of the observance of some criteria, their effect can be corrected by the introduction of corrections. In the practice of aviation investigations, the methods of the introduction of such corrections in many instances are developed in sufficient detail,

while in industrial aerodynamics of this experiment, it is much less [3].

In this sense a definite interest represents that experiment which is realized during wird tunnel tests of the models of high obelisks - pedestal, sword, bayonet and Stella. General view and the basic dimensions of these obelisks are given to Fig. 1. They all have great lengthening, i.e., the high value of the ratio of height/altitude to characteristic transverse dimension, a small structural attenuation (small δ) and bluff forms of cross section. The low values of structural attenuation are explained by the fact that these constructions are made made of steel, and as the basic method of the connections of cell/elements, is used welding. The forms of cross sections are such, that from them occurs flow separation with the formation/education of the eddy/vortices which can lead to the auto-oscillations of construction, called wind resonance; furthermore, the aerodynamic forces, which act on such airfoil/profiles, depend on the direction of the incident flow, i.e., on angle of attack α. For the airfoil/profiles of the mentioned obelisks, there are ranges of angles of attack in which it is possible to expect the emergence of galloping. These facts forced with thoroughness to match up the study of the character of the fluctuations of obelisks in airflow by testing their models in wind tunnels.

Most schematic was the model of pedestal, representing by itself the tetrahedral frustum with a height/altitude approximately 2 m with alternating/variable section in the form of trapezoid; the thickness of the walls, prepared from steel, 1 mm. The basic geometric dimensions of pedestal were reproduced to scale 1:20. Unlike nature, internal structural cell/elements - the diaphragm of staircase and so forth - of model were not made. Similarly, according to numbers Ca*, Re and μ was not maintain/withstood, it is possible to speak only about the observance of similarity according to number Sh.

The frequency of the natural flexural vibrations of model on the first tone was equal to 21 Hz, and to number SH = 0.14-0.15, characteristic for the wind resonance of constructions with square and the close to it forms of sections, it had to correspond to the velocity of flow V = of 25-26 m/s. It is real/actual, with v = of 26 m/s (number Sh = 0.14) is visible clearly expressed it is by no the amplitude of oscillations (Fig. 2), which, obviously, corresponds to wind resonance.

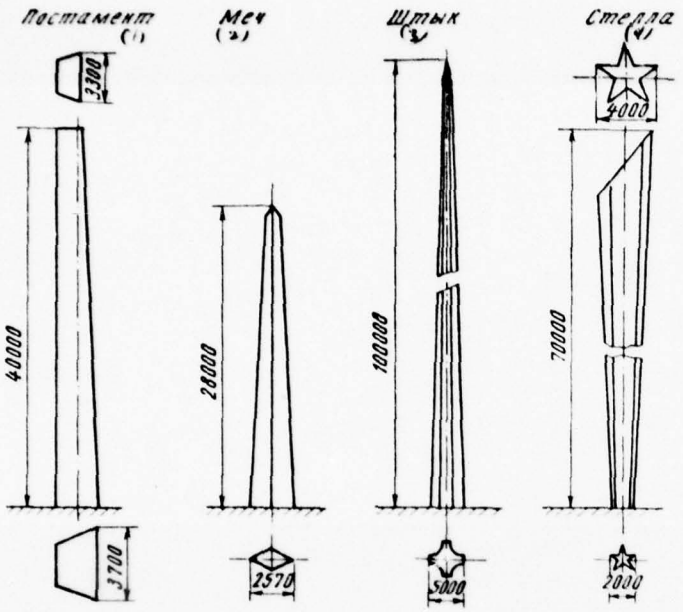


Fig. 1.

Key: (1). Pedestal. (2). Sword. (3). Bayonet. (4). Stella.

Page 154.

With an increase in the velocity of the flow of the amplitude of these stable intense oscillations, somewhat they decrease, and then again grow/rise. It is probable that the repeated rapid increase of amplitudes is connected with galloping. As a result of testings, it was establish/installed that the intense auto-oscillations of model appear only in two comparatively narrow ranges of angles of attack

(Fig. 2).

The detailed study of oscillations was carried out during testings two small and large of the models of sword. The first small model it was possible to fulfill dynamically similar nature; however, the rigid characteristics of this model render/showed understated, in connection with which was not maintained the similarity in the natural frequencies of oscillation ($Sh_M < Sh_H$) and according to numbers Ca*. Similarity according to numbers μ and Re was observed. Last/latter criterion it was possible to maintain because of the fact that model tests were conducted in wind tunnel with the increased density of working medium (air).

For a model were selected the following three basic scales: linear dimensions $k_L = L_M/L_H = 1/10$; the densities of working medium $k_\rho = \rho_M/\rho_H = 5$ and the moduli of elasticity of material $k_E = E_M/E_H = 1$ (nature and model were made made of steel). Remaining scales taking into account similarity from Re numbers, Sh and μ were determined through basic. For example, the scale of the velocities of flow $k_V = 2$. linear masses $k_m = 1/20$. frequencies $k_f = 20$. The frequency of the natural flexural vibrations of model in the direction of a small diagonal of rhomb render/showed equal to 18 Hz, i.e., approximately 1.5 times it is less than it would follow the scale of frequencies. Decrement of the natural flexural vibrations of the first tone $\delta \approx 0.05$.

The results of the tests of this model of sword (Fig. 3) show that the most intense oscillations of model in the direction of a small diagonal of rhomb appeared with velocities of flow $\forall$ = of 16-18 m/s (number Sh $\approx$ 0.15). Oscillations occur without deep play (Fig. 4), frequency and form correspond to frequency and the form of the natural oscillations of the first tone. These auto-oscillations - of wind resonance when the frequency of the forming after body eddy/vortices is close to frequency of its natural. It is completely important that the wind resonance in this case was observed with full-scale Reynolds numbers (Re $\approx 1.05 \cdot 10^6$).

The second small model had the same graphic scale $k_L = 1/10$, but was tested at normal air density ($k_\rho = 1$). In this case, was maintained the similarity according to numbers Sh, Ca* and μ, but Re numbers were 10 times less than full-scale.

In connection with this let us pause at the results, which characterize the effect of Re number. It was above noted that for airfoil/profiles with points of inflection, which include the cross section profiles of all investigated by us obelisks, is not observed critical region of reynolds number, connected with the transition of laminar boundary layer into turbulent; does not in effect depend on Re number the character of the auto-oscillations of the constructions, which have sharp flank edges.

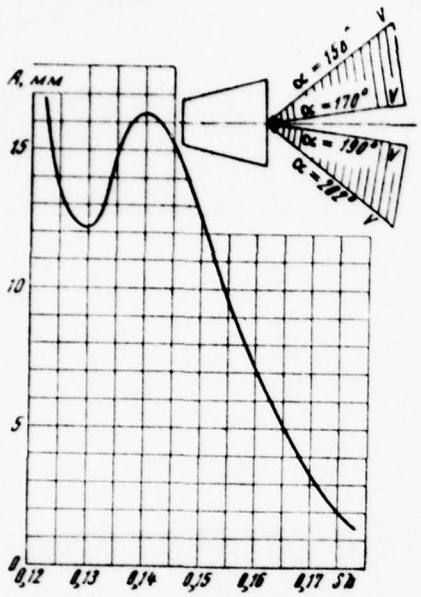


Fig. 2.

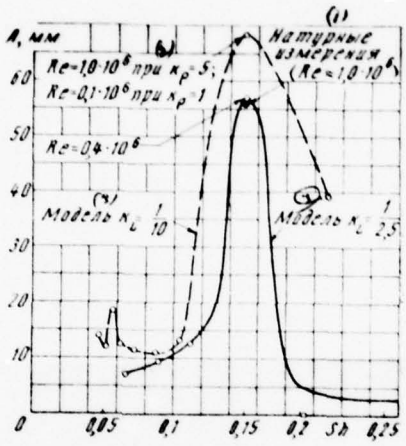


Fig. 3.

Key: (1). Full-scale measurements. (2). with. (3). Model.

Page 155.

Fig. 3 gives the results of the tests[1] of small models, large model and full-scale sword whose comparison shows that a change in Re number 10 times does not in practice affect character and value of the maximum of the amplitudes of oscillations in the presence of wind resonance.

FOOTNOTE [1]. Amplitudes are given in recalculation to nature. Conditions/mode of the testings $\alpha = 0$. ENDFOOTNOTE.

Hence it is possible to draw a conclusion about the self-similarity of this phenomenon according to Re number for constructions with the cross section profiles, which have points of inflection. The possibility of nonobservance in these cases of similarity according to Re number considerably facilitates the problem of developing of models and conducting their testings (there is no need for utilizing ducts with the increased air pressure).

On the small models of sword, were not sufficiently accurately modelled some most important characteristics of nature. It was not impossible to also thoroughly test on it and the effectiveness of means the extinguishing of auto-oscillations. In connection with this it was solved to prepare a constructionally/structurally-such/similar to nature model of sword to scale 1:2.5 and to test it in large industrial wind tunnel. This model in the form of the frustum with rhombic cross section represents by itself shell of supporting steel sheathing whose thickness gradually was changed on the height/altitude of model; sheathing/skin was welded to the longitudinal carrying belt/zones whose thickness was changed from 7 mm below to 4 mm above of model. Were establish/installed also the diaphragms and the stiffening ribs, ensuring the stability of

construction. For the investigation of the effect of structural attenuation on the character of auto-oscillations, was provided for the installation within the model of the damping device, consisting of mass, air piston dampers and the springs, connected both with the mass and with the shell of model. The value of attenuation could vary itself because of a change in air gap between piston and cylinder of damper. For this model the similarity according to numbers Sh, Ca* and μ is made when $k_0 = 1$ automatically. The velocity of flow in wind tunnel corresponded to full-scale wind velocities. Re number for a model was 2.5 times less than in nature.

Frequencies and the forms of the natural flexural vibrations of model were obtained by conducting special resonance testings. The frequencies of the first and second tones of flexural vibrations in the direction of a small diagonal of rhomb comprised with respect to 3.2 and 14.8 Hz, but for the first tone of oscillations in the direction of the large diagonal of rhomb 3.6 Hz. For the first tone decrement $\delta \approx 0.035$.

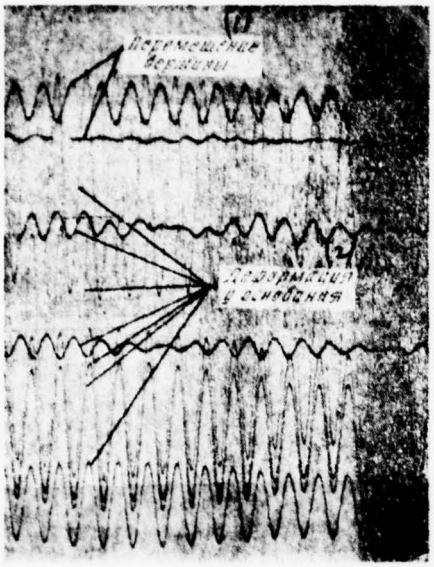


Fig. 4.

Key: (1). Displacement of apex/vertex. (2). Strain of basis/base.

Page 156.

Model tests in wind tunnel were carried out at the velocities of flow V = of 7.5-30 m/s in different directions of the incident in model flow (at different angles of attack α relative to larger diagonal). The greatest amplitudes of oscillations in the direction of a small diagonal of rhomb were observed at α = 0 and 180°. The sharply pronounced maximum of amplitudes is obtained with V = of 10 m/s. At these angles of attack and at this velocity of flow the model

accomplished stable very intense oscillations across flow with the frequency and the form, corresponding to the first tone of natural oscillations. During this conditions/mode number Sh = 0.15.

Since the flow in wind tunnel was "smooth", i.e., without pulsations and gusts, but amplitude and frequency they were determined by the parameters of most oscillatory system, these oscillations one should relate to auto-oscillations.

The character of amplitude change in velocity, truth, the typical for this conditions/mode value of number Sh = 0.15 attest to the fact that these auto-oscillations the essence is wind resonance.

The greatest measured during testings dynamic stresses σ > of $\pm$5 daN/mm^2 significantly exceed the stresses, permissible according to the conditions of fatigue structural strength (σ = 1-1.5 daN/mm^2), and therefore the decrease of the intensity of the auto-oscillations of sword render/showed completely necessary.

As one of the means the extinguishing of auto-oscillations, was utilized damping device indicated above. The selection of its parameters was carried out by calculations, and the final testing of its effectiveness was realize/accomplished by model tests with damping device. As a result were selected the parameters of the

device, which made it possible to increase the decrement of the natural oscillations of the first tone more than four times (with σ = 0.035 to δ = 0.15). Under conditions of the most intense oscillations, the damping device decreases the amplitudes of oscillations 5-8 times (Fig. 5), moreover dynamic stresses were less than $\pm$1.5 daN/mm^2 [4].

Another tested means a reduction in the intensity of auto-oscillations were the through slit-shaped channels (sluices), gashed near longitudinal carrying belt/zones (Fig. 6). These channels change the character of the flow around construction, decreasing the intensity of the broken away from it eddy/vortices. The amplitudes of the auto-oscillations of model with slit-shaped channels were lowered in the most dangerous conditions/modes more than two times [5].

The comparison of the results of the tests of small and large of models with the results of measuring the oscillations of full-scale sword shows that and on the zones of the most dangerous angles of attack, and in the values of the critical speeds of flow, and in the values of the amplitudes of auto-oscillations and appearing in construction dynamic stresses, and according to the evaluation of the effectiveness of means the extinguishing of auto-oscillations is obtained their very satisfactory conformity to each other. For example, before application/use on the full-scale sword of means the

AD-A067 216 FOREIGN TECHNOLOGY DIV WRIGHT-PATTERSON AFB OHIO F/G 20/4
SCIENTIFIC NOTES OF CENTRAL INSTITUTE OF AEROHYDRO DYNAMICS (SE--ETC(U)
JUN 78 A S FONAREV, A G ZAKHAROV
UNCLASSIFIED FTD-ID(RS)T-0679-78 NL

5 OF 5
AD A067216



END
DATE FILMED
6-79
DDC

extinguishing of oscillations most dangerous were wind velocities 8-12 m/s and in its most adverse directions of the amplitude of oscillations of the apex/vertex of sword they reached 150 mm. On testings of large model, the critical speed of wind resonance render/showed 10 m/h, and the maximum measured amplitude of oscillations was 55 mm, which in recalculation to nature gives the amplitude approximately 140 mm.

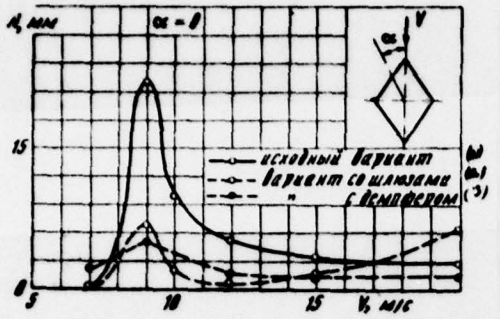


Fig. 5.

(1). initial version. (2). version with sluices. (3). with damper.

Page 157.

Experiment, obtained during the investigation of the auto-oscillations of sword, it was used for the design of a bayonet-obelisk for the memorial complex of Brest strength. Bayonet-obelisk is a vertically arranged/located welded construction made of steel. Its height/altitude 100 m, cross section takes the form of astroid with the blunt angles. In initial version the ratio of its height/altitude to the diagonal of average cross section was accepted equal to 30. Structurally bayonet it was possible to fulfill in the form of carrying conical duct with the welded-on to it outside four T-shaped stiffening ribs. Through every 6 m were provided for the transverse septa. To T-shaped fin/edges is fastened the metal

covering, which creates the external enclosures of bayonet. Since the bayonet was designed as all-welded steel construction, it was to be expected that the value of structural attenuation will render/show small ($\delta < 0.05$). At the same time the form of cross section and the size/dimensions of construction are such, which one ought not to have feared the onset of its intense oscillations at wind velocities, real for the wind area in which was arrange/located Brest. In connection with this were carried out the wind tunnel tests of a constructionally/structurally-such/similar model, made to scale 1:10. Model was geometrically similar to nature, was observed also similarity according to numbers Sh, Ca* and μ. Similarity according to Re number could not be maintained. Scale factors, from which were determined all the characteristics of model, were following: linear $k_l = 1/10$; velocities $k_v = 1$; air density $k_\rho = 1$; hardnesses $k_{EI} = 10^{-4}$; linear masses $k_m = 10^{-2}$; frequencies $k_f = 10$. Model had frequency of natural flexural vibrations of the first tone f_1 = of 2.8 Hz; the second tone f_2 = of 15.4 Hz; the logarithmic decrement of the oscillations of the first tone δ = 0.02.

Testings showed that in the range of the velocities of flow from 7 to 20 m/s of oscillation they occur with frequency and form of the first tone, but at high velocities on these oscillations, are superimposed oscillations with frequency and form of the second tone. Noted powerful effect of angle of attack: at α = 35° and 55° with an increase in flutter speed they became so intense that testing.

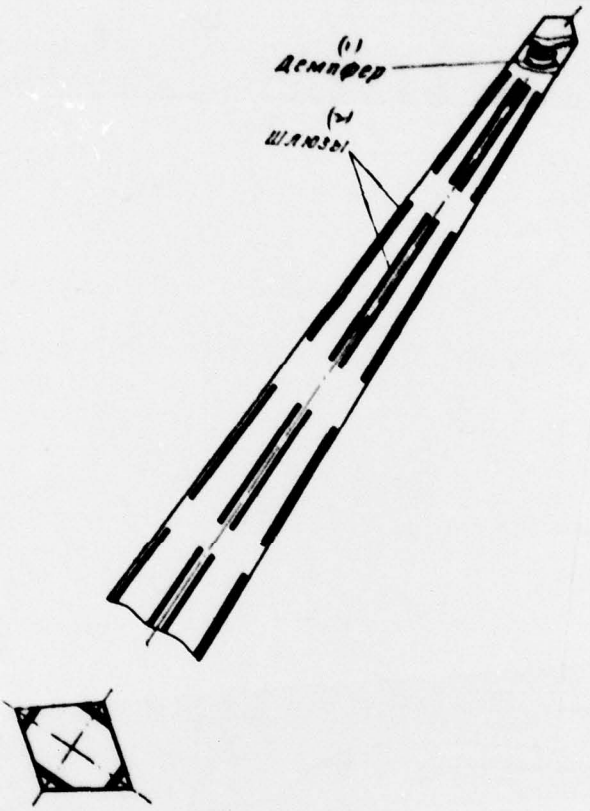


Fig. 6.

Key: (1). Damper. (2). Sluices.

DISTRIBUTION LIST

DISTRIBUTION DIRECT TO RECIPIENT

ORGANIZATION		MICROFICHE
A205	DMATC	1
A210	DMAAC	2
B344	DIA/RDS-3C	8
C043	USAMIIA	1
C509	BALLISTIC RES LABS	1
C510	AIR MOBILITY R&D LAB/FIO	1
C513	PICATINNY ARSENAL	1
C535	AVIATION SYS COMD	1
C591	FSTC	5
C619	MIA REDSTONE	1
D008	NISC	1
H300	USAICE (USAREUR)	1
P005	ERDA	1
P005	CIA/CRS/ADB/SD	1
NAVORDSTA (50L)		1
NASA/KSI		1
AFIT/LD		1

ORGANIZATION		MICROFICHE
E053	AF/INAKA	1
E017	AF/RDXTR-W	1
E403	AFSC/INA	1
E404	AEDC	1
E408	AFWL	1
E410	ADTC	1
E413	ESD	2
	FTD	
	CCN	1
	ASD/FTD/NICD	3
	NIA/PHS	1
	NICD	2